High Scale Boundary Conditions in Extensions of the Standard Model

John McDowall

Supervised by Dr. David Miller and Dr. Christoph Englert

Submitted in fulfillment of the requirements for the degree of
Doctor of Philosophy

October 2018

The University of Glasgow
College of Science and Engineering

High Scale Boundary Conditions in Extensions of the Standard Model

Abstract: The recent discovery of the Higgs boson by the ATLAS and CMS experiments and the subsequent measurements of it properties are the latest vindications of the Standard Model of particle physics. The SM has a number of well known flaws, and the continuing dearth of Beyond the Standard Model signatures from experiment has led to investigations into whether the SM is valid up to very high scales. The motivation for much of this work comes from the quartic Higgs coupling λ and its β function, which run to an extremely small values at high scales. These may be hints of new UV dynamics, in particular the Multiple Point Principle which posits the existence of a second degenerate minimum in the effective potential at the Planck scale, and Asymptotic Safety, where the dimensionless couplings of the potential run towards an interacting UV fixed point. In this work we will investigate the possibility for similar high scale boundary conditions in extensions of the Standard Model. Specifically, we look at the Real Singlet model, the Complex Singlet model, the Type-II Two Higgs Doublet Model, and the Inert Doublet Model. We will apply the relevant theoretical constraints to the parameter space of theses models, as well as experimental constraints such as those from ATLAS, CMS, LEP, the Tevatron, WMAP, Planck and LUX. Points that pass these constraints will also be investigated for their validity under a number of high scale boundary conditions on its scalar sector, and the valid parameter space will be checked for signatures in the mass spectrum that can be probed by current and future collider experiments.

Keywords: Beyond the Standard Model Physics, particle physics phenomenology, Higgs physics, dark matter physics

Declaration of originality

I declare that the research that is presented in this thesis is my original work and has not previously been presented for a degree. Citations are provided whenever other published work is presented. Chapters 2 to 4 provide an introduction to the theoretical concepts found in my research, whilst chapter 5 detail the numerical framework that underpins that research. Chapters 6 to 8 detail work that was done in collarboration with Dr David J Miller. Chapter 7 is built from our paper *High scale boundary conditions with an additional complex singlet* [1], whilst chapter 8 details work from our paper *High Scale Boundary Conditions in Models with Two Higgs Doublets* [2].

For Mum and Dad

Acknowledgments

Firstly, I'd like to thank David Miller, who has been an excellent supervisor and friend throughout the course of my PhD. I don't think I could have done this without him.

Thanks must also go to Christopher Craig and Gemma Craig, my friends and family. Your love means the world to me and for it i'll be forever thankful.

I'd also like to thank my friends and fellow PhD students: Euan Mclean, Dan Smaranda, Dan Hatton, Stephen Brown, Will Breadon Madden, as well as Liam Moore, Sven-Patrik Hallsjö, Stephen Ogilvy, Gavin Kirby and all those that have shared this journey with me.

Special mention goes to Karl Nordstrom, Sarah Karodia and Andres Luna. I've had to deal with some extremely difficult times during the course of my PhD, times that were made easier by your unwavering support and friendship. I will cherish this time we have had together and I'll never forget what all of you have done for me.

Taylor, your kindness and understanding has made this last portion of my PhD some of the happiest times of my life. I love you so much.

Lastly, my Mum and Dad. You both were with me during the some worst days of my life, caring for me and supporting me without question. You are the best parents anybody could ask for and I don't know if I could have got through all of this without your love. Thank you.

Contents

Chapter 1

Introduction

The Standard Model of particle Physics [3–5] is an enormously successful description of the strong and electroweak interactions, that has been verified by experimental tests to an incredibly high precision. Arguably the most significant verification of the Standard Model (SM) is the recent confirmation of the existence of the Higgs boson by the ATLAS and CMS collaborations at the LHC [6, 7].

The numerous successes of the SM are impressive, but there are a number of experimental and theoretical issues that it is not able to explain. One of the most glaring omissions is its lack of gravitational interactions. It also lacks a mechanism to explain the small but non-zero masses of the neutrinos. Neither does it provide a valid candidate for Dark Matter or Dark Energy, a solution to the strong CP problem nor an explanation for the observed matter antimatter asymmetry. From a theoretical point of view, the SM has 19 free parameters (the quark and lepton masses, Higgs mass, CKM mixing angles and phases, the gauge coupling constants, and the vacuum expectation value) that have to be determined from experiment and plugged into the model. Even some fundamental issues, such as the quantisation of electric charge or why the electron and proton have equal but opposite charge, have no explanation with the SM.

The combined ATLAS and CMS determination of the Higgs mass $m_h = 125 \pm 0.23\,\text{GeV}$ [8] is in a phenomenologically difficult range for many of the most popular frameworks for Beyond the Standard Model (BSM) physics, which try to address the SM's problems. Unlike the other particles of the SM, the mass of the Higgs is not protected from the effect of radiative corrections by a symmetry, so it should be sensitive to new physics at higher mass scales Λ_{UV}. In principle this scale could be as large as the Planck mass $M_{Pl} = 2.4 \times 10^{18}\,\text{GeV}$, the energy scale at which gravitational contributions become significant, but its experimentally verified mass is much lighter. This seems to require an extremely precise fine-tuning of mass parameter to rectify, a problem that is known as the *Hierarchy Problem* [9–11]. Supersymmetric models (SUSY) [12–14] add a symmetry between fermions and

bosons which introduces new loop corrections that go towards cancelling out the loop corrections, quadratic in Λ_{UV}, that would increase the Higgs mass. These models can provide a Higgs with a mass that is compatible with experiment but it often requires some residual fine tuning or the introduction of non-minimal field content [14–16] to evade increasingly strong collider constraints on the parameter space.

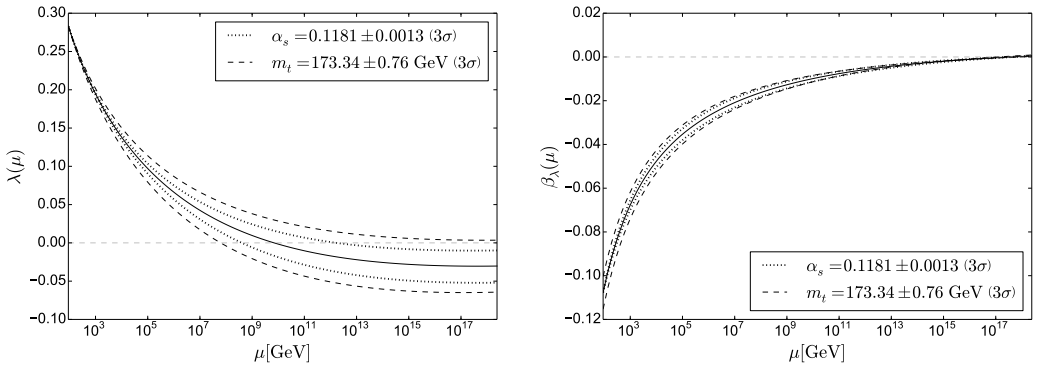

(a) (b)

Figure 1.1: Three-loop running of (a) the SM Higgs quartic coupling λ and (b) its β function with $3\,\sigma$ uncertainties from the top pole mass m_t (dashed) and the strong coupling constant α_s (dotted). Calculated using SARAH 4.9.3 [17] and FlexibleSUSY 1.6.1 [18–21].

The current lack of experimental evidence for phyics beyond the Standard Model has left open the possibility that the SM is valid up to very high scales, such as the Grand Unification (GUT) scale $M_{GUT} \approx 10^{16}\,\text{GeV}$ or even the Planck scale. For the SM to be a viable model up to a scale such as M_{Pl} it is desirable, but not required, that the dimensionless couplings of the model, for example the gauge couplings, Yukawa couplings, or the Higgs quartic coupling λ, remain perturbative to that scale. In the case of λ this means $\lambda \leq 4\pi$ at all scales. The SM potential must be either completely stable, which requires $\lambda > 0$ for all scales, or metastable with a lifetime much longer than the age of the universe [22]. Figure 1.1a shows that using the central experimental value of the top pole mass m_t and the strong coupling constant $\alpha_S(M_Z)$ results in λ turning negative at around $10^{10}\,\text{GeV}$. If we insist upon an absolutely stable vacuum in the SM up to the Planck scale then the bounds upon the top mass become [15],

$$m_t < 171.36 \pm 0.46\,\text{GeV}, \tag{1.1}$$

which is now in tension with the experimental value of m_t by around 2.6σ. This suggests that the SM has a metastable electroweak vacuum, but it could also be an indication that there are unknown degrees of freedom which alter the running of the couplings and stabilise the potential.

Figure 1.1a highlights another interesting feature of the SM Higgs quartic coupling, namely the very small values of λ at high scales. This is even more remarkable given the feature shown in figure 1.1b, that the running of λ flattens out at the same high scales e.g $\beta_\lambda(M_{Pl}) \approx 0$. This has led to a number of investigations into whether they are boundary conditions that are enforced by some high scale dynamics at M_{Pl} [23–29].

We are primarily interested in two possibilties for the existence of high scale boundary conditions: the *Multiple Point Principle* (MPP), which posits the existence of a second minimum in the effective potential that is degenerate with the electroweak minimum [30], and *Asymptotic Safety*, where the couplings of the model run toward a UV interacting fixed point [31]. Both of these force the β functions of the quartic couplings to run to zero at M_{Pl}, whilst the MPP also requires λ to be zero at M_{Pl}. The MPP hypothesis has been used in the SM to predict a Higgs mass of $m_h = 129 \pm 1.5\,\text{GeV}$ [15], and a model with asymptotic safety in the SM due to gravitational contributions gave a predicted Higgs mass range of $126 < m_h < 174\,\text{GeV}$. Whilst both of these are now very much in tension with experiment they are both close enough to warrant further investigation.

Grand Unification Theories (GUTs) are another set of extensions of the SM that is motivated by the high energy behaviour of couplings. Specifically, these models are motivated by the running of the SM gauge couplings, shown in figure 1.2. The strong, weak and electromagnetic couplings approach each other at around $10^{15}\,\text{GeV}$. One interpretation of this feature is that the SM is an effective field theory of some larger model. In this scenario the SM gauge group $SU(3)_C \times U(2)_L \times U(1)_Y$ is embedded into a larger gauge group $\mathcal{G}$, under which the gauge couplings of the SM g_1, g_2, g_3 are unified under one coupling constant g_{GUT} at some high scale M_{GUT}.

GUTs can provide answers to a number of the problems encountered by the SM. The quantisation of electric charge and the parity of the proton and electron charges arises naturally from embedding the quarks and leptons into a representation of a larger group such as $SU(5)$ or $SO(10)$ [32]. Many GUT models include a heavy right

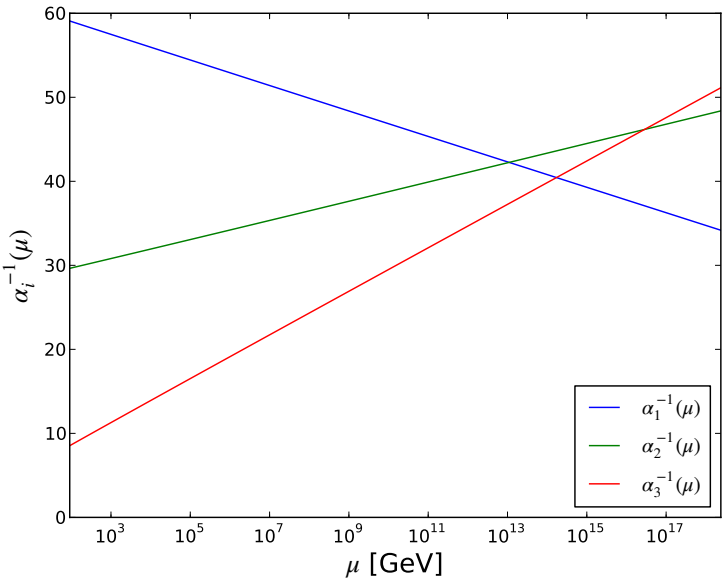

Figure 1.2: Three loop running of the Standard Model gauge coupling constants $\alpha_i = g_i^2/4\pi$ with renormalisation scale μ.

handed neutrino that can be used to generate non-zero neutrino masses via a seesaw mechanism [33,34]. GUTs also predict the existence of magnetic monopoles [35] and the decay of the proton [36], both of which can be verified experimentally.

In this thesis we will investigate simple extensions to the Standard Model, focusing on their compatability with various high scale boundary conditions that can arise from the MPP, asymptotic safety, and gauge coupling unification. We will also investigate whether these scenarios are viable under a number of theoretical and experimental constraints, such as those from collider and dark matter experiments. In Chapter 2 we will begin by summarising the Standard Model and reflecting on its various problems and inadequacies. In Chapter 3 we will detail our investigation into high scale boundary conditions in the SM, whilst Chapter 4 will review a particular type of high scale boundary condition: gauge coupling unification and Grand Unification Theories. In Chapter 5 we will outline our general approach to the parameter space scans that make up much of our model investigations. Our results for the Real Singlet model will be discussed in Chapter 6, the Complex Singlet model in Chapter 7 and the Two Higgs Doublet Model in Chapter 8. Chapter 9 will summarise our findings.

Chapter 2

The Standard Model

Contents

2.1 Introduction to the Standard Model

The Standard Model (SM) is our most successful description of the strong, weak and electromagnetic fundamental forces. The particle content on the SM is split into two classes: *fermions*, which obey the Pauli Exclusion Principle, and *bosons*, which do not. Fermions are further grouped into three generations of quarks and leptons. Quark interactions are mediated by both the strong and electroweak forces, whilst leptons do not interact via the strong force.

Both the quarks and the leptons have up and down types. The up type (u, c, t) quarks have electric charges of $2/3e$, where $e = 1.602 \times 10^{-19} C$ is the electron charge,

while the down type (d, s, b) quarks each have $-1/3e$ charge. The neutrinos, which interact only via the weak force and as such have zero electric charge, comprise the up type leptons whilst the down type (e, μ, τ) leptons have $-e$ charge.

The boson sector is mostly comprised of the spin-1 vector gauge bosons that mediate the interactions of the SM. The photon γ is the mediator of the electromagnetic force, the charged $W^{\pm}$ and neutral Z bosons are the force carriers of the weak force, and the gluons g mediate the strong force. The spin-0 Higgs boson is a neutral scalar boson that is associated with the generation of mass. The massive particles of the SM get their mass through the Higgs mechanism, which we shall discuss in more detail in section 2.3.2.

2.2 Symmetries of the Standard Model

The Lagrangian of the Standard Model $\mathcal{L}_{SM}$ is an object that encodes the model's structure and interactions. The observed physical symmetries of the SM are represented by symmetries of the Lagrangian under transformations of its field content. Symmetries can be classified in a number of different ways. For example, *discrete symmetries* are those which take specific values, such as the discrete rotational symmetry of a triangle. The Standard Model exhibits a number of discrete symmetries, such as parity **P**, the reversal of the spatial coordinates of a field. Charge conjugation **C** describes the symmetry of interactions when particles are changed to anti-particles, or vice versa. Interactions are symmetric under time reversal **T** if they remain unchanged when the direction of time is flipped. All of the observables of the SM are invariant under the product of all three of these transformations, namely **CPT**, however weak interactions violate both **C** and **P** and in some cases the product **CP**, and therefore **T**.

Transformations that can take any value, such as a rotational symmetry parameterised by a rotation angle, are called *continous symmetries*. These can be further categorised as *global* transformations, which do not depend on space-time coordinates, and *local* transformations which do depend on them. For example, a field $\phi = (\phi_1, \dots \phi_n)$ could be invariant under the infinitesimal global transformation,

$$\phi \to \phi' = \phi + \delta\phi. \tag{2.1}$$

This symmetry can be described by a *Lie group* G which has the following properties,

- if g_1 and g_2 are elements of the group G, then $h = g_1 g_2$ is also an element of the group.
- if g_1, g_2, g_3 are elements of G, then $g_1 (g_2 g_3) = (g_1 g_2) g_3$.
- there is an identity element e of G which satisfies $g_i e = g_i$ for all elements g_i of G.
- for every element g_i in G, there is another element h_i such that $g_i h_i = e$.

A Lie group has an infinite number of elements and as such can be used to describe continuous symmetries. The infinitessimal global transformation $\delta\phi$ can be parameterised by,

$$\delta\phi_i = i\varepsilon^a \Omega^a_{ij} \phi_j, \tag{2.2}$$

where a ranges over the number of transformations, and the parameters ε^a are not dependent on space-time coordinates. Ω^a_{ij} are called the *generators* of the group G. These generators are represented as $n \times n$ matrices (we will discuss representations further in Chapter 4). The Lie algebra of G describes such an infinitesimal global transformation under G and is defined by its Lie bracket, a commutation relation between its generators,

$$\left[\Omega^a, \Omega^b\right] = i f^{abc} \Omega^c. \tag{2.3}$$

If the structure constant f^{abc} is zero then the group is *Abelian*, otherwise it is *non-Abelian*.

Under local transformations the parameters ε are dependent on space-time coordinates x, and the infinitesimal transformation becomes,

$$\delta\phi = i\varepsilon^a (x) \Omega^a \phi. \tag{2.4}$$

Models whose Lagrangian is invariant under local transformations are known as gauge theories. The Standard Model falls under this catagory and is invariant under a number of gauge transformations, each of which describes a fundamental class of interactions of the model. In section 2.3 we will discuss the gauge structure of the SM further by looking in detail at its Lagrangian and its invariance under the SM gauge transformations.

The particles of the Standard Model are also associated with representations of the *Poincaré group*, a non-Abelian Lie group that describes the model's symmetry

under both the Lorentz transformations and four-dimensional space-time translations. The Lorentz group $SU(2) \oplus SU(2)$ of symmetries under rotations and boosts is therefore a subgroup of the Poincaré group and the various particles of the SM provide different representations under this group. The spin-0 particles are under the scalar representation $(0, 0)$, which describes the Higgs field in the SM and transforms trivially under Lorentz transformations. The spin-1 vector bosons are the $(1/2, 1/2)$ representation of the Lorentz group. The spin-$1/2$ fermions are the left-handed and right-handed Weyl spinor representations $\psi_L \to (1/2, 0)$ and $\psi_R \to (0, 1/2)$, which have two degrees of freedom each. These representations are not equal, meaning that transformations between left and right-handed Weyl spinors are not invariant. Theories that can be built from these spinors, such as the SM, are therefore known as *chiral theories*. Weyl spinors on their own are useful objects for describing massless fermions, however if we try to build mass terms for charged fermions we introduce mixing between left and right spinors. The massive fermions of the SM are Dirac spinors, which transform under $(1/2, 0) \oplus (0, 1/2)$, a combination of Weyl spinors with four degrees of freedom. The *Dirac γ matrices* are a useful tool when working with Dirac spinors, and are defined via the Clifford algebra anti-commutation relation $\{\gamma_\mu, \gamma_\nu\} = 2g_{\mu\nu}$, where $g_{\mu\nu} = \text{diag}\,(-1, 1, 1, 1)$ is the Minkowski metric. They can be built in the Weyl basis from the Pauli spin matrices σ^i,

$$\sigma^1 = \begin{pmatrix} 0 & 1 \\ 1 & 0 \end{pmatrix}, \quad \sigma^2 = \begin{pmatrix} 0 & -i \\ i & 0 \end{pmatrix}, \quad \sigma^3 = \begin{pmatrix} 1 & 0 \\ 0 & -1 \end{pmatrix}, \tag{2.5}$$

using $\sigma^\mu = \left(1, \sigma^i\right)$ and $\bar{\sigma}^\mu = \left(1, -\sigma^i\right)$, resulting in,

$$\gamma^\mu = \begin{pmatrix} 0 & \sigma^\mu \\ \bar{\sigma}^\mu & 0 \end{pmatrix}. \tag{2.6}$$

In this work we will often discuss the massive fermions of the SM using Weyl spinors, which we can project out of Dirac spinors using a projection operator made from these matrices,

$$P_{L,R} = \frac{1}{2}\left(\mathbb{I} \pm i\gamma^0\gamma^1\gamma^2\gamma^3\right) = \frac{1}{2}\left(\mathbb{I} \pm \gamma^5\right). \tag{2.7}$$

2.2.1 Quantum Electrodynamics

Quantum Electrodynamics (QED) is a useful example of the local gauge invariance principle. We begin by looking at the Lagrangian for a free Dirac spinor ψ,

$$\mathcal{L} = i\overline{\psi}\gamma^{\mu}\partial_{\mu}\psi - m\overline{\psi}\psi, \tag{2.8}$$

where $\overline{\psi} = \psi^{\dagger}\gamma^{0}$ is the adjoint Dirac spinor. The symmetry tranformations for ψ and $\overline{\psi}$ are $\delta\psi = i\alpha\psi$ and $\delta\overline{\psi} = -i\alpha\overline{\psi}$ respectively. If α is independent of space-time coordinates then the Lagrangian is invariant under these tranformations and the theory is said to be globally $U(1)$ symmetric. However, if $\alpha = \alpha(x)$ depends on space-time coordinates then the Lagrangian is no longer invariant under these transformations. Invariance is restored by promoting the partial derivative to a covariant derivative of the form,

$$D_{\mu} = \partial + igA_{\mu}, \tag{2.9}$$

which transforms as $\delta D_{\mu}\psi = i\alpha(x)D_{\mu}\psi$. Here we have introduced a gauge field A_{μ} that transforms as $\delta A_{\mu} = \frac{1}{g}\partial_{\mu}\alpha$ and couples to the Dirac field as,

$$\mathcal{L}_{A} = g\overline{\psi}\gamma^{\mu}\psi A_{\mu}. \tag{2.10}$$

The introduction of the gauge field also necessitates an extra term that describes the propagation of A_{μ}, which in QED is the photon. This term is constructed from the field strength tensor,

$$F_{\mu\nu} = \partial_{\mu}A_{\nu} - \partial_{\nu}A_{\mu} = [D_{\mu}, D_{\nu}], \tag{2.11}$$

which is manifestly gauge invariant. The full, locally gauge invariant QED Lagrangian is given by,

$$\mathcal{L}_{QED} = -\frac{1}{4}F_{\mu\nu}F^{\mu\nu} + i\overline{\psi}\gamma^{\mu}D_{\mu}\psi - m\overline{\psi}\psi. \tag{2.12}$$

Expanding this Lagrangian highlights that the requirement of local gauge invariance results in an interaction term between the fermionic field ψ and the gauge field A_{μ}. QED is a locally gauge invariant $U(1)$ theory with an associated electromagnetic charge Q. Mass terms for photons of the form $m_{A}^{2}A_{\mu}A^{\mu}$ are forbidden by gauge invariance, and since $U(1)$ is an Abelian group, so are interactions between photons.

2.2.2 Non-Abelian Theories

The previous discussion of local gauge invariance in an Abelian $U(1)$ theory such as QED can be extended to non-Abelian theories, such as the $SU(3)_{C}$ and $SU(2)_{L}$

gauge symmetries that describe the strong and weak interactions of the SM. We begin by considering the Lagrangian for a field Ψ_i which is a vector of dimension n,

$$\mathcal{L} = \overline{\Psi}_i \left(i(\gamma^\mu)_{ij} \partial_\mu - m\delta_{ij} \right) \Psi_j, \tag{2.13}$$

where δ_{ij} is the Kronecker delta. The field Ψ_i and its adjoint $\overline{\Psi}_i$ transform under a non-Abelian $SU(N)$ symmetry as $\delta\Psi_i = i\varepsilon^a(x)\Omega^a_{ij}\Psi_j$ and $\delta\overline{\Psi}_i = -i\varepsilon^a(x)\Omega^a_{ij}\overline{\Psi}_j$, where Ω_{ij} are the group generators. Since the transformations in question are non-Abelian, their associated Lie algebra is defined by a Lie bracket with a non-zero structure constant f^{abc}.

As in the abelian case, we need to introduce a covariant derivative to ensure local gauge invariance. It takes the form,

$$(D_\mu)_{ij} = \partial_\mu \delta_{ij} + ig \left(\Omega^a\right)_{ij} A^a_\mu. \tag{2.14}$$

In QED the gauge field was the photon, but in the non-Abelian case there are m gauge fields A^a_μ, $a = (1, \dots m)$. Local gauge invariance requires that the covariant derivative transform as $\delta\left(D_\mu\Psi\right) = i\varepsilon^a(x)\Omega^a D_\mu\Psi$. The commutator of the covariant derivative is,

$$[D_\mu, D_\nu] = ig\left(\partial_\mu A^a_\nu \Omega^a - \partial_\nu A^a_\mu \Omega^a + ig\left[\Omega^b, \Omega^c\right] A^b_\mu A^c_\nu\right), \tag{2.15}$$

from which we can calculate the non-Abelian field strength tensor,

$$F^a_{\mu\nu} = \partial_\mu A^a_\nu - \partial_\nu A^a_\mu + g f^{abc} A^b_\mu A^c_\nu. \tag{2.16}$$

The field strength tensor of non-Abelian theories differs further in that it must transform like Ψ to maintain local gauge invariance, specifically $\delta F^a_{\mu\nu} = -f^{abc}\varepsilon^b F^c_{\mu\nu}$. We now have all of the pieces we need to write the full locally gauge invariant non-Abelian Lagrangian,

$$\mathcal{L} = \overline{\Psi}_i \left(i(\gamma^\mu)_{ij} D_\mu - m\delta_{ij} \right) \Psi_j - \frac{1}{4} F^a_{\mu\nu} F^{a\mu\nu}. \tag{2.17}$$

Crucially, this Lagrangian includes terms such as $g f^{abc} \partial_\mu A^a_\nu A^{\mu b} A^{\nu c}$ that are not present in the QED Lagrangian, meaning that the gauge fields carry their own charge and interactions between them are allowed under a non-Abelian symmetry.

2.3 The Lagrangian of the Standard Model

The SM is a renormalizable quantum field theory built upon the gauge groups,

$$SU(3)_C \otimes SU(2)_L \otimes U(1)_Y, \tag{2.18}$$

where $SU(3)_C$ describes the strong interactions and $SU(2)_L \times U(1)_Y$ describes the electroweak interactions. The Lagrangian of the SM is made up of all of the allowed renormalizable operators with this symmetry and can be conveniently split into four parts:

$$\mathcal{L}_{SM} = \mathcal{L}_g + \mathcal{L}_f + \mathcal{L}_Y + \mathcal{L}_H. \tag{2.19}$$

We will now look at each of these terms in more detail.

2.3.1 The Gauge Sector $\mathcal{L}_g$

The gauge sector of the SM Lagrangian describes the gauge bosons that are associated with the interactions of the SM symmetry groups,

$$\mathcal{L}_g = -\frac{1}{4} G^{\alpha}_{\mu\nu} G^{\mu\nu}_{\alpha} - \frac{1}{4} W^{\alpha}_{\mu\nu} W^{\mu\nu}_{\alpha} - \frac{1}{4} B_{\mu\nu} B^{\mu\nu}, \tag{2.20}$$

where $G^{\alpha}_{\mu\nu}$, $W^{\alpha}_{\mu\nu}$ and $B_{\mu\nu}$ are the $SU(3)_C$, $SU(2)_L$ and $U(1)_Y$ field strength tensors. G^a_μ is the gluon field that describes the 8 gauge bosons of the strong $SU(3)_C$ interactions, the W^i_μ field describes the 3 weak $SU(2)_L$ bosons, and B_μ is the hypercharge $U(1)_Y$ boson field. They transform under the gauge symmetries as,

$$\begin{aligned} \delta G^a_\mu &= \frac{1}{g_3}\partial_\mu \gamma^a + i f^{abc} \gamma^b G^c_\mu \\ \delta W^i_\mu &= \frac{1}{g_2}\partial_\mu \omega^i + i \varepsilon^{ijk} \omega^j W^k_\mu \\ \delta W^i_\mu &= \frac{1}{g_1}\partial_\mu \beta, \end{aligned} \tag{2.21}$$

where g_3, g_2 and g_1 are the coupling constants that determine the strength of the $SU(3)_C$, $SU(2)_L$ and $U(1)_Y$ interactions respectively, ε^{ijk} is the $SU(2)_L$ structure constants, and γ^a, ω^i and β are the $SU(3)_C$, $SU(2)_L$ and $U(1)_Y$ infinitesimal transformations.

The fermions ψ_f of the SM transform under the fundamental or trivial representations of the SM groups, and are coupled to the gauge bosons via,

	$SU(3)_C$	$SU(2)_L$	$U(1)_Y$
q_L	**3**	**2**	$1/6$
l_L	**1**	**2**	$-1/2$
u_R	**3**	**1**	$2/3$
d_R	**3**	**1**	$-1/3$
e_R	**1**	**1**	-1

Table 2.1: Standard Model matter content and their representations under $SU(3)_C$ and $SU(2)_L$, as well as their $U(1)_Y$ hypercharge. $q_L = (u_L, d_L)$ and $l_L = (\nu_L, e_L)$ are the left-handed quarks and leptons, u_R is the right-handed up quarks, d_R the right-handed down quarks, and e_R the right-handed electron. These representations are identical for each the three generations of matter.

$$\mathcal{L}_f = \sum_f i\bar{\psi}_f \gamma^\mu D_\mu \psi_f. \tag{2.22}$$

The covariant derivative,

$$D_\mu = \partial_\mu - ig_3 T^a_{\alpha\beta} G^a_\mu - ig_2 \tau^i_{jk} W^i_\mu - ig_1 Y B_\mu, \tag{2.23}$$

extends the partial derivative to ensure local invariance under the SM gauge symmetries by adding interactions with their respective field strength tensors. $T^a = (1/2)\lambda^a$ and $\tau^i = (1/2)\sigma^i$ are the generators of the fermion's representation under $SU(3)$ and $SU(2)$, where λ^a and σ^i are the Gell-Mann* and Pauli matrices, and Y is its $U(1)$ hypercharge. As we have discussed previously, left-handed and right-handed fermions behave diferently in electroweak processes. The SM represents this by having the left-handed fermions transform under the fundamental representation of $SU(2)_L$ whilst right-handed fermions are trivial under this symmetry. The fermion sector is further complicated by the existence of three generations which are identical to each other in their interactions except for their masses. The representations of the SM matter content under $SU(3)_C \times SU(2)_L \times U(1)_Y$ are summarised in Table 2.1

*The Gell-Mann matrices for $SU(5)$ are given in Appendix A

2.3.2 The Higgs Sector $\mathcal{L}_H$

The symmetries of nature are rarely exact. For example, the isospin symmetry between the proton and neutron is broken, as evidenced by the mass difference between them. The gauge symmetry of the SM is preserved only if all of its fields are massless. For example, a simple mass term for gauge bosons of the type $W^a_\mu M_{ab} W^{\mu b}$ would break gauge symmetry. The problem is that this goes against current experimental observations, as we have extremely precise measurements of the masses of the $W^\pm$ and Z bosons as well as all of the SM fermions [37].

We rectify this problem in the theory by spontaneously breaking the SM gauge symmetry down to a smaller subgroup, giving masses to the W and Z bosons in the process. The specific symmetry breaking chain is,

$$SU(3)_C \times SU(2)_L \times U(1)_Y \longrightarrow SU(3)_C \times U(1)_Q, \tag{2.24}$$

where $U(1)_Q$ is the QED symmetry associated with electromagnetic charge Q. The *Higgs Mechanism* breaks the electroweak symmetry by introducing a complex scalar field H in the $(\mathbf{2}, 1/2)$ representation of $SU(2)_L \times U(1)_Y$. [38–40]. The Lagrangian for the Higgs field is given by,

$$\mathcal{L}_H = |D_\mu H|^2 - V(H), \tag{2.25}$$

where the scalar potential is,

$$V(H) = -\frac{\mu^2}{2} H^\dagger H + \frac{\lambda}{4}\left(H^\dagger H\right)^2. \tag{2.26}$$

The Higgs field develops a non-zero vacuum expectation value (vev) $\langle H \rangle = \mu/\sqrt{\lambda} \approx 174\,\text{GeV}$ if the mass term μ^2 is positive, breaking the electroweak symmetry down to $U(1)_Q$. We can expand H around the vev v,

$$H = \begin{pmatrix} \chi^- \\ (v + h + i\sigma)/\sqrt{2} \end{pmatrix}, \quad v = \sqrt{\frac{\mu^2}{\lambda}}. \tag{2.27}$$

The massless Nambu-Goldstone bosons χ^-, σ become the longitudinal components of the $W^\pm$ and Z bosons. The full kinetic term in the scalar potential is given by,

$$D_\mu H = \partial_\mu H - \frac{i}{2} g_2 \tau^j W^j_\mu H - i g_1 Y B_\mu H. \tag{2.28}$$

After spontaneous symmetry breaking $\mathcal{L}_H$ contains mass terms for $W^\pm$ and Z,

$$\mathcal{L}_H \supset \frac{v^2}{8}\left[g_2^2 W_\mu^1 W^{1\mu} + g_2^2 W_\mu^2 W^{2\mu} + \left(g_2 W_\mu^3 - g_1 B_\mu\right)\left(g_2 W^{3\mu} - g_1 B^\mu\right)\right]. \quad (2.29)$$

We now have two massive vector bosons,

$$W_\mu^\pm = \frac{1}{\sqrt{2}}\left(W_\mu^1 \mp i W_\mu^2\right), \quad Z_\mu = \frac{1}{\sqrt{g_2^2 + g_1^2}}\left(g_2 W_\mu^3 - g_1 B_\mu\right), \quad (2.30)$$

with tree-level masses,

$$M_W = \frac{g_2 v}{2}, \quad M_Z = \frac{\sqrt{g_2^2 + g_1^2}v}{2} = \frac{M_W}{\cos\theta_W}, \quad (2.31)$$

where $\tan\theta_W = g_1/g_2$ is the weak mixing angle, and the massless gauge boson of $U(1)_Q$,

$$A_\mu = \frac{1}{\sqrt{g_2^2 + g_1^2}}\left(g_2 W_\mu^3 + g_1 B_\mu,\right) \quad (2.32)$$

which we identify as the photon. The $U(1)_Q$ electromagnetic charge operator Q is given by a linear combination of the weak isospin I_3 and the hypercharge Y,

$$Q = \frac{1}{2}Y + I_3. \quad (2.33)$$

The final degree of freedom left after spontaneous symmetry breaking is associated with fluctuations around the vev v, which manifests as a real scalar boson h with a tree-level mass of $m_h = \sqrt{2\lambda}v$. We call this the *Higgs boson*. The observation of a scalar resonance at a mass of $m_h = 125\,\text{GeV}$ by the ATLAS and CMS collaborations at the LHC is used to fix the mass of the Higgs, which is a free parameter in the SM.

2.3.3 The Yukawa Sector $\mathcal{L}_Y$

A mass term for fermions of the type $\bar{\psi}_L M \psi_R$ would break the $SU(2)_L \times U(1)_Y$ electroweak symmetry, much in the same way as mass terms for gauge bosons. The SM's solution to this problem is also the same; to couple the fermions to the Higgs field. The Yukawa sector of the SM Lagrangian consists of all of the allowed gauge invariant operators that couple the SM fermions to the Higgs field,

$$\mathcal{L}_Y = \frac{1}{\sqrt{2}}\sum_{i,j} Y_u^{ij}\bar{q}_L^i H^c u_R^j + Y_d^{ij}\bar{q}_L^i H d_R^j + Y_e^{ij}\bar{l}_L^i H^c e_R^j + h.c, \quad (2.34)$$

where $i = 1, 2, 3$ are the generation indices of the SM fermions and the Higgs conjugate term is $H^c = i\sigma^2 H^*$. Y_u^{ij}, Y_d^{ij} and Y_e^{ij} are the 3×3 Yukawa matrices of the up quarks, down quarks and leptons respectively, which determine the strength of interactions between these fermions and the Higgs field. After electroweak symmetry breaking $\mathcal{L}_Y$ contains the terms,

$$\mathcal{L}_Y = -\frac{v}{\sqrt{2}}\bar{u}_L^i Y_u^{ij} u_R^j - \frac{v}{\sqrt{2}}\bar{d}_L^i Y_d^{ij} d_R^j - \frac{v}{\sqrt{2}}\bar{e}_L^i Y_e^{ij} e_R^j + h.c + \dots. \tag{2.35}$$

We need to diagonalise the quark mass matrices to get the mass eigenstates of the three generations (u, d), (c, s) and (b, t). We do this by exploiting the fact that there exists diagonal mass matrices such as M_u, M_d, as well as corresponding unitary matrices U_u, U_d such that,

$$Y_u Y_u^\dagger = U_u M_u^2 U_u^\dagger, \quad Y_d Y_d^\dagger = U_d M_d^2 U_d^\dagger. \tag{2.36}$$

We then end up with quark mass terms of the form,

$$\mathcal{L}_{Y,\text{ mass}} = -m_j^u \bar{u}_L^j u_R^j - m_j^d \bar{d}_L^j d_R^j + h.c + \dots, \tag{2.37}$$

where m_j^u and m_j^d are the diagonal elements of $\frac{v}{\sqrt{2}}M_u$ and $\frac{v}{\sqrt{2}}M_d$. The rotation matrix between these mass eigenstates and the weak eigenstates is known as the Cabbibo-Kobayashi-Maskawa matrix [41, 42],

$$V_{CKM} = U_u^\dagger U_D = \begin{pmatrix} V_{ud} & V_{us} & V_{ub} \\ V_{cd} & V_{cs} & V_{cb} \\ V_{td} & V_{ts} & V_{tb}. \end{pmatrix} \tag{2.38}$$

We can paramaterise this matrix using three mixing angles θ_{12}, θ_{13}, and θ_{23}, as well as a complex phase δ,

$$V_{CKM} = \begin{pmatrix} c_{12}c_{13} & s_{12}c_{13} & s_{13}e^{-i\delta} \\ -s_{12}c_{23} - c_{12}s_{23}s_{13}e^{i\delta} & c_{12}c_{23} - s_{12}s_{23}s_{13}e^{i\delta} & s_{23}c_{13} \\ s_{12}c_{23} - c_{12}s_{23}s_{13}e^{i\delta} & -c_{12}c_{23} - s_{12}s_{23}s_{13}e^{i\delta} & c_{23}c_{13}. \end{pmatrix} \tag{2.39}$$

This parametrisation makes clear that the potentially complex nature of these mixing effects can be a source of CP violation within the SM.

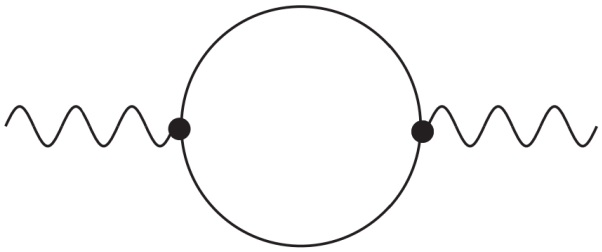

Figure 2.1: Examples of a one-loop Feynman diagram.

2.4 Renormalization in the Standard Model

The Standard Model is an interacting quantum field theory, which means that analytical calculations for observables are, in general, not possible. Instead, we calculate observables using perturbative expansions in the various couplings of the model. These calculations are made easier using Feynman diagrams that represent the various terms in the expansion and can be converted into the corresponding integrals using the appropriate Feynman rules. These calculations include the tree-level diagrams as well as loop diagrams, such as the one shown in figure 2.1, that depict the emission and absorbption of virtual particles. These loop calculations involve divergent loop momenta integrals that are dependent on the momentum scale, such as,

$$\int^{q_{\max}} \frac{d^4q}{(2\pi)^4} \frac{1}{q^2\,(q-p)^2} \simeq \int^{q_{\max}} \frac{q^3 dq}{(2\pi)^4} \frac{1}{q^4} \sim \int^{q_{\max}} \frac{dq}{q} \sim \log \frac{q_{\max}}{Q}, \tag{2.40}$$

where q is the internal momentum in the loop. The process of *renormalization* deals with these divergent terms in a model by absorbing the divergences into its bare parameters, leaving behind finite terms that correpsond to physical observables. The precise way in which the divergent terms are cancelled and collected is known as the *renormalization scheme*. We can implement this approach in the SM by rewriting the Lagrangian in terms of the physical parameters and collecting up the bare parameters into counterterms. We can then rewrite the bare couplings of the Lagrangian g_0 in terms of the renormalized coupling g_R and its counterterm δ_g,

$$g_0 = (1 + \delta_g(\mu))\, g_R(\mu) = Z_g(\mu)\, g_R(\mu)\,. \tag{2.41}$$

QED is an instructive example of the use of counterterms: the bare fields ψ and A_μ are related to the renormalized fields by,

$$\psi = \sqrt{Z_2}\psi_R, \quad A_\mu = \sqrt{Z_3}A_{\mu,R}, \tag{2.42}$$

where $Z_i = 1 + \delta_i$. The bare mass m is written as,

$$m = Z_m m_R, \tag{2.43}$$

and the bare electric charge e is written as,

$$e = Z_e e_R. \tag{2.44}$$

We can now rewrite the Lagrangian in terms of the physical, renormalized parameters and their counterterms, omitting the renormalized subscript and using $Z_1 = Z_e Z_2 \sqrt{Z_3}$,

$$\begin{aligned} \mathcal{L}_{QED} &= -\frac{1}{4}F_{\mu\nu}F^{\mu\nu} + i\overline{\psi}\gamma^\mu\partial_\mu\psi - m_R\overline{\psi}\psi - e_R\overline{\psi}\gamma^\mu A_\mu\psi \\ &\quad -\frac{1}{4}\delta_3 F_{\mu\nu}F^{\mu\nu} + i\delta_2\overline{\psi}\gamma^\mu\partial_\mu\psi - (\delta_m + \delta_2)\, m_R\overline{\psi}\psi - e_R\delta_1\overline{\psi}\gamma^\mu A_\mu\psi. \end{aligned} \tag{2.45}$$

Now, as long as we include the Feynman diagrams for the counterterms, any calculation that we do using this renormalized Lagrangian will have finite results.

After renormalization the parameters of the SM depend on the renormalization scale μ. We can capture how these paramters evolve with energy by exploiting the fact that the bare parameters do not depend on μ,

$$\mu\frac{d}{d\mu}g_0 = \mu\frac{d}{d\mu}\left(Z_g\left(\mu\right)g_R\left(\mu\right)\right) = 0. \tag{2.46}$$

We build the *Callan-Symanzik equations* by applying this princple to a bare n point Green's funtion G_0^n, resulting in [43],

$$\left(\mu\frac{\partial}{\partial\mu} + \frac{n}{2}\gamma_A + \beta\left(g_R\right)\frac{\partial}{\partial g_R}\right)G_R^n = 0, \tag{2.47}$$

where γ_A is the *anomalous dimension*, which describes the scale dependence of dimensionful objects, and $\beta\left(g_R\right)$ is the β *function*, which describes the evolution with energy of dimensionless parameters,

$$\gamma_A = \frac{\mu}{Z_A}\frac{dZ_A}{d\mu}, \quad \beta\left(g_R\right) = \mu\frac{dg_R\left(\mu\right)}{d\mu}. \tag{2.48}$$

The complete set of β functions that describe the scale dependence of all of the dimensionless parameters of a model is called the *Renormalization Group Equations*

(RGEs). In this work we will use the RGEs of the SM, as well as those of other models, to investigate their behaviour at scales that cannot currently be probed experimentally.

2.5 Problems with the Standard Model

The Standard Model is an extremely successful model of three of the four fundamental interactions of nature. Most notably, the SM cannot describe gravity because there is no renormalisable quantum field theory formulation of gravitational interactions. Beyond this omission, there are a number of theoretical and experimental issues with the SM that we will discuss in more detail here.

2.5.1 The Free Parameters and Structure of the Standard Model

The SM has 19 free parameters, detailed in Table 2.2. The values of these free parameters are determined by experiment and have no theoretical motivation under the current structures of the SM. Neither does the SM have an explanation for the quantisation of electric charges nor a mechanism to explain why the proton and electron have equal and opposite charges. Countless models have been developed that try to put these problems onto a more solid theoretical footing, one class of which is GUT models that embed the SM within a larger gauge group such as $SU(5)$ or $SO(10)$. We will discuss these models later.

2.5.2 The Hierarchy Problem

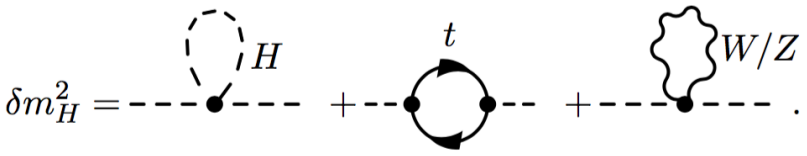

Figure 2.2: Examples of one-loop corrections to the squared Higgs mass δm_H^2 from (left to right) Higgs self interactions, the top quark, and the W, Z gauge bosons.

One issue of the Standard Model in particular has driven much of the research into beyond the standard model physics, namely; why is the scale associated with the weak bosons $M_W \approx 100\,\text{GeV}$ so low compared to other fundamental mass scales such as the Planck scale $M_{Pl} = 2.4 \times 10^{18}\,\text{GeV}$? This is known as the *Hierarchy*

Input Parameter	Measured Value
$m_u^{\overline{\text{MS}}}\,(\mu = 2\,\text{GeV})$	$2.2^{+0.6}_{-0.4}\,\text{MeV}$
$m_d^{\overline{\text{MS}}}\,(\mu = 2\,\text{GeV})$	$4.7^{+0.4}_{-0.4}\,\text{MeV}$
$m_c^{\overline{\text{MS}}}\,(m_c)$	$1.28 \pm 0.03\,\text{GeV}$
$m_s^{\overline{\text{MS}}}\,(\mu = 2\,\text{GeV})$	$96^{+8}_{-4}\,\text{MeV}$
$m_b^{\overline{\text{MS}}}\,(m_b)$	$4.18^{+0.04}_{-0.03}\,\text{GeV}$
m_t (Pole Mass)	$173.1 \pm 0.6\,\text{GeV}$
m_e (Pole Mass)	$0.511\,\text{MeV}$
m_μ (Pole Mass)	$105\,\text{MeV}$
m_τ (Pole Mass)	$1.78\,\text{GeV}$
m_H (Pole Mass)	$125.09 \pm 0.24\,\text{GeV}$
v	$246.2\,\text{GeV}$
$g_1\,(M_Z)$	0.356
$g_2\,(M_Z)$	0.649
$g_3\,(M_Z)$	1.218 ± 0.006
θ_{12}	$13.02 \pm 0.04^\circ$
θ_{13}	$2.36 \pm 0.08^\circ$
θ_{23}	$0.20 \pm 0.02^\circ$
$\bar{\theta}$	≈ 0

Table 2.2: The current values and uncertainties of the free parameters of the Standard Model, taken from the PDG [37]. $\bar{\theta}$ is the coefficient of the strong CP term allowed by the symmetries of the SM.

Problem and the recent observation of a scalar with a mass of 125 GeV has only added to the focus on this issue.

The hierarchy problem is usually formulated as a quadratic dependence of the Higgs mass on any new physics scales up to and including the Planck scale. The fermions and massive gauge bosons are protected by symmetries of the SM, inasmuch as they are proportional to the vev and the masses go to zero when these symmetries are unbroken. The mass of the Higgs m_H is not protected by any such symmetry. To illustrate this problem let's consider a fermion f that couples to the Higgs. Calculating the one-loop corrections to m_h results in an unphysical ultraviolet divergence. One way to deal with this is to introduce a large ultraviolet cutoff scale Λ_{UV} that regulates the divergence. the correction becomes [44],

$$m_H^2 = m_{H_0}^2 - \frac{|y_f| N_c}{8\pi^2}\Lambda_{UV}^2 + \dots . \tag{2.49}$$

Here y_f is the Yukawa coupling for the fermion and N_c is the number of colours. Figure 2.2 shows some examples of one loop contributions to the squared Higgs mass, including one from the top quark that contributes the most due to its large Yukawa coupling. Regulating UV divergences using a cutoff like this is a useful way to visualise the problem, but in practice it breaks both gauge and Lorentz invariance. For most applications *dimensional regularisation* is used instead; loop integrals are calculated in $d = 4 - 2\varepsilon$ dimensions and the divergences manifest themselves as $1/\varepsilon$ poles in the limit $\varepsilon \to 0$. The $1/\varepsilon$ poles are then subtracted away using counterterms. In this work we will use the $\overline{\text{MS}}$ renormalization scheme, under which the counterterms subtract away a rescaled pole $1/\bar{\varepsilon} = 1/\varepsilon + \gamma^E + \log(4\pi)$, where γ^E is the Euler-Mascheroni constant.

The heart of the hierarchy problem is that one must fine tune the bare mass m_{H_0} to an extremely high degree to counter such loop corrections and to bring the physical Higgs mass down to 125 GeV. This fundamental fine tuning problem of the physical Higgs mass is present regardless of how you choose to regularise the theory. Potential solutions to this problem usually introduce new fields or symmetries with the aim of cancelling out the offending loop corrections. One of the most popular approaches is to invoke *Supersymmetry* (SUSY), which relates bosons and fermions by a symmetry [12, 44]. The SM spin 1/2 fermions are embedded within chiral supermultiplets alongside their spin 1 partners, known as sfermions, whilst the gauge bosons of the SM are embedded within gauge supermultiplets with their spin 1/2 SUSY partners, called gauginos. These new SUSY fields introduce loops that help to

cancel out the SM UV loops and bring the Higgs mass down towards its experimental value.

If supersymmetry were an exact, unbroken symmetry of nature then the masses of the SM particles and their SUSY partners would be degenerate. The fact that we haven't observed any evidence of the existence of SUSY partners suggests that supersymmetry, if it is realised in nature, must be broken, with a characteristic breaking scale M_{SUSY}.

SUSY was investigated for other reasons before its utility as a solution to the hierarchy problem was understood [45]. The supersymmetric algebra is the maximal extension of the Poincarè algebra of spacetime transformations that extends the traditional spacetime degrees of freedom to include fermionic degrees of freedom. It could be argued that the largest possible spacetime symmetry would be the one that best describes nature, therefore supersymmetry should be realised in some way. However, this argument is somewhat aesthetic and is often overlooked as a motivator of SUSY in favour of the model's obvious phenomenological power.

Unfortunately, despite the numerous compelling theoretical arguments in its favour, the fact remains that there has been no experimental observation of evidence of supersymmetry [16]. The SUSY model space has been gradually narrowed by results from LEP, the Tevatron, and the ATLAS and CMS experiments at the LHC, and although it is still possible for SUSY models to evade the tightening constraints from these experiments it often requires the introduction of non-minimal field content or a fine-tuning of parameters [14–16]. In this work we focus on non-supersymmetric extensions of the SM, and until strong experimental evidence makes a clear case for the existence of supersymmetry it is important to investigate if these models can also account for what is currently known about low energy phenomena.

2.5.3 Experimental and Cosmological Observations and The Standard Model

As we discussed previously, the SM's enduring experimental success is impressive, but it has ran into difficulty with some recent observations. Most notably is the observation of neutrino oscillations which suggest that neutrinos have extremely small masses [46–48]. Neutrinos are massless in the SM, but one can extend it with a right handed neutrino which can either be a Dirac or Majorana fermion. In the Majorana case the mass term for the neutrinos looks like,

$$\mathcal{L}_\nu = \begin{pmatrix} \nu_L & \nu_R \end{pmatrix} \begin{pmatrix} 0 & m \\ m & M/2 \end{pmatrix} \begin{pmatrix} \nu_L \\ \nu_R \end{pmatrix}, \tag{2.50}$$

where M is the Majorana mass. Diagonalising the mass matrix gives the eigenvalues $\approx (m^2/M, M)$. If we associate M with a large mass scale such as M_{GUT} or M_{Pl} then we get one light mass eigenstate that is predominantly the left-handed neutrino and one very heavy right handed neutrino. This is known as the *seesaw mechanism*. This can be added to the SM, but an intermediate scale that can facilitate this mechanism arises naturally from $SO(10)$ GUT models, which we will discuss later.

There are a number of cosmological observations that the SM is unable to explain, which suggests the existence of physics beyond the Standard Model. Most notably, the SM has no mechanism to explain the various experimental evidence for the existence of large amounts of dark matter in the universe [49]. In this work we will investigate a number of models that attack this problem by introducing new scalar field content.

Another weakness of the SM is that the amount of $\mathcal{CP}$ violation that can occur in the CKM matrix is not sufficient to explain the observation that the universe is dominated by baryons and not anti-baryons [50]. The Sakharov conditions [51] are those that must exist in the early universe to generate an appropriate baryon anti-baryon asymmetry. Specifically, baryon number, $\mathcal{C}$, and $\mathcal{CP}$ must be violated in the early universe, and there must be interactions that are out of thermal equilibrium. In this work we will look at the complex singlet extension of the SM, which introduces new sources of $\mathcal{CP}$ violation in its Higgs sector that can account for the baryon anti-baryon asymmetry.

Chapter 3

High Scale Boundary Conditions in the Standard Model

Contents

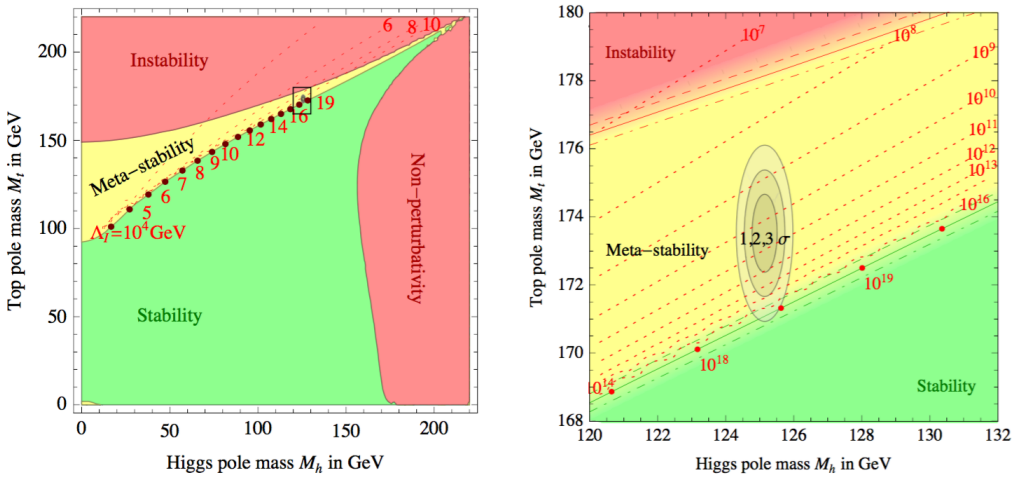

Figure 3.1: Vacuum stability for the SM in the $M_h - M_t$ plane, taken from [15]. The right plot expands the rectangular region highlighted in the left plot. The dotted lines are contours that show the scale up to which the vacuum remains stable, and the ellipses show the $1, 2, 3\sigma$ experimental regions for M_h, M_t.

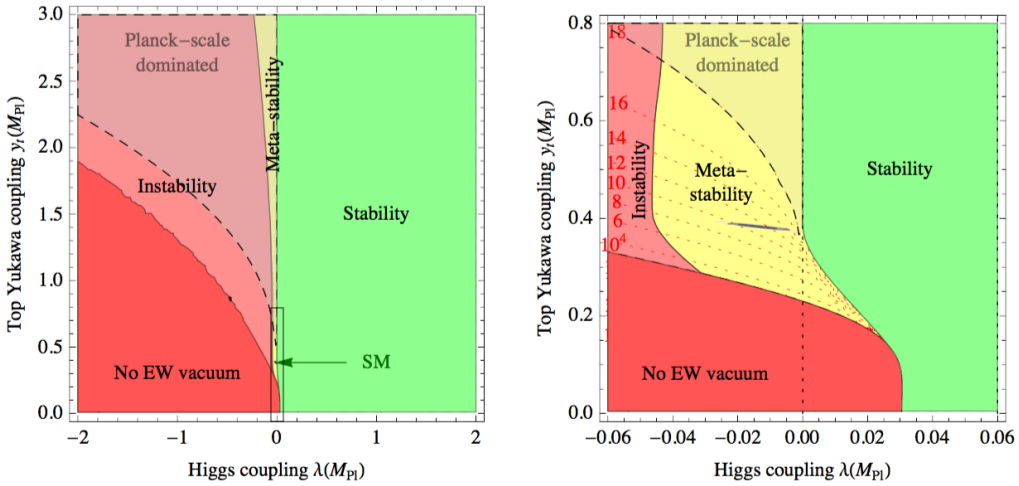

Figure 3.2: Vacuum stability for the SM in the $\lambda(M_{Pl}) - y_t(M_{Pl})$ plane, taken from [15]. The right plot expands the rectangular region highlighted in the left plot. The dotted lines are contours The dotted lines are contours that show the scale up to which the vacuum remains stable, and the thin ellipses near the centre of the plot show the $1, 2, 3\sigma$ regions for $\lambda(M_{Pl}), y_t(M_{Pl})$ that correspond to the central experimental values of M_h, M_t.

3.1 High Scale Behaviour of the Standard Model

As we discussed in the introduction, the experimentally measured mass of the Higgs boson, and its seemingly very SM-like nature [8, 52–54], makes life difficult for some of the most popular extensions of the SM. The Higgs mass determination also places the SM potential in an interesting position in terms of vacuum stability. Figure 3.1 shows that the experimentally measured Higgs and top quark pole masses suggest the universe lies in a critical metastable region near the boundary of stability with a lifetime that is much longer than the age of the universe [15], which the Planck Collaboration estimates to be $13.813 \pm 0.038 \times 10^9$ years old [55]. Figure 3.2 is a vacuum stability plot, focussing on the values of the Higgs quartic coupling λ and the top quark Yukawa y_t at the Planck scale. The current situation leaves us with a very small, negative value of $\lambda(M_{Pl})$.

Any instability of the SM potential is sometimes interpreted as a sign that some new physics must come into play at intermediate scales, stabilising the potential. However, the same properties of the SM Higgs sector have also encouraged exploration into whether it could be the fundamental description of nature up to energies

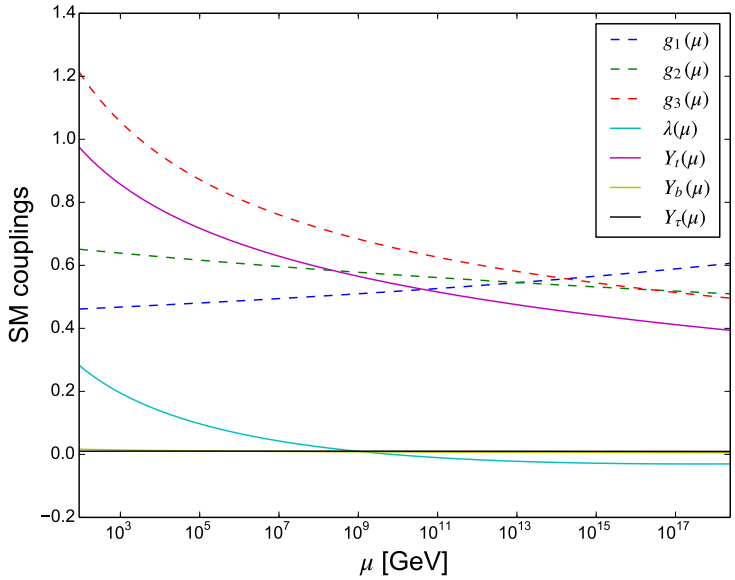

Figure 3.3: Three loop running of the Standard Model couplings with renormalisation scale μ. Here g_i are the gauge couplings, λ is the Higgs quartic coupling and Y_i are the Yukawa couplings of the top and bottom quarks, as well as the τ lepton.

such as the Planck scale. To investigate this possibility we need to compute the changes in all of the SM couplings from low scales such as M_Z all the way up to M_{Pl}. To that end we utilise the RGEs of the Standard Model at three-loop accuracy. We provide the two-loop RGEs in Appendix B [56–59].

The running of the SM couplings shown in Figure 3.3 hide some intriguing hints of potential new dynamics at high energy scales. Not only does λ run to a very small value at M_{Pl}, but its β function runs flat at high scales. This has led to a number of investigations into whether these features are boundary conditions that are a consequence of new physics at the Planck scale [23–29].

As far as the Standard Model is concerned, we are primarily interested in the following possible boundary condidions,

$$\lambda\left(M_{Pl}\right) = 0, \tag{3.1}$$

$$\beta_\lambda\left(M_{Pl}\right) = 0. \tag{3.2}$$

There are a number of possible models for how these boundary conditions on the Higgs sector can come about. We will discuss two of them in more detail in the following sections; the *Multiple Point Principle* (MPP) and *Asymptotic Safety* (AS).

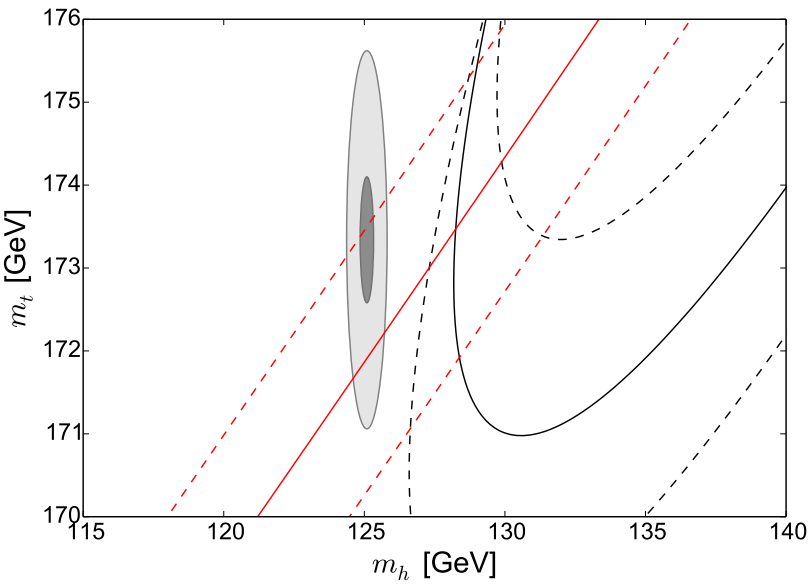

Figure 3.4: $\lambda(M_{Pl}) = 0$ (red) and $\beta_\lambda(M_{Pl}) = 0$ (black) in the $m_h - m_t$ plane. The dashed lines show 3σ variations in $\alpha_S(M_Z) = 0.1181 \pm 0.0013$. Ellipses show the experimentally allowed values of m_t and m_h with 1σ (dark grey) and 3σ (light grey) uncertainty.

Figure 3.4 shows contours corresponding to the boundary conditions 3.2 in the $m_h - m_t$ plane, indicating that, assuming the central values of m_t and α_S, a heavier Higgs than experimentally observed is needed to satisfy both conditions. These contours were calculated using SARAH 4.9.3 [17] and FlexibleSUSY 1.6.1 [18–21], and use the three-loop RGEs of the SM to run between M_Z and M_{Pl}. FlexibleSUSY calculates the Higgs mass to two-loop order, whilst the top pole mass includes three-loop QCD corrections. This plot broadly agrees with a similar plot in [23], however we use a different value of the uncertainty in $\alpha_S(M_Z) = 0.1181 \pm 0.0013$ that reflects a recent change in its estimation [60]. The authors of [23] also use the Planck scale, $m_{Pl} = \sqrt{\frac{\hbar c}{G}} = 1.22 \times 10^{19}\,\text{GeV}$, as their high scale where the boundary conditions are checked, wheras we use the reduced Planck scale, $M_{pl} = \sqrt{\frac{\hbar c}{8\pi G}} = 2.4 \times 10^{18}\,\text{GeV}$, where the additional factor of $1/8\pi$ is a convention that is used to simplify the Einstein field equations. Figure 3.4 shows that it is possible to get $\lambda(M_{pl}) = 0$ using a value of m_h within 3σ and a top pole mass $171 < m_t < 174\,\text{GeV}$, whilst also getting a value of β_λ that is extremely small.

It is possible that the mechanisms that may be fixing our boundary conditions

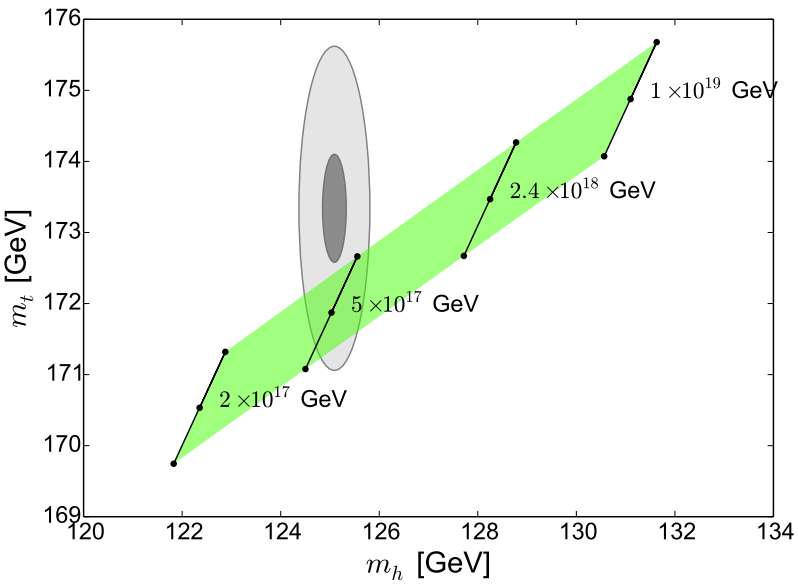

Figure 3.5: Mass values that satisfy $\lambda(M_{UV}) = \beta_\lambda(M_{UV}) = 0$ at various UV scales M_{UV}. The green region corresponds to a 1σ uncertainty in α_S. Ellipses show the experimentally allowed values of m_t and m_h with 1σ (dark grey) and 3σ (light grey) uncertainty.

can become significant at scales lower than M_{Pl}. Figure 3.5 shows points on the $m_h - m_t$ plane that give $\lambda = \beta_\lambda = 0$, within 1σ uncertainty, simultaneously at different high scales M_{UV}. It is possible to obtain points that meet both conditions and provide an experimentally viable Higgs mass at around $M_{UV} \approx 5 \times 10^{17}$. It is interesting to note that this is a scale that arises in string scenarios [61, 62].

3.2 The Multiple Point Principle

The effective potential of the SM includes quantum contributions that can modify its shape from the classical case. It is given by [63–65],

$$V_{eff}(\phi) = \frac{1}{2}m^2(\phi)\phi^2 + \frac{1}{4}\lambda(\phi)\phi^4 + \frac{1}{16\pi}V_1 + \dots. \tag{3.3}$$

Here we show the one-loop effective terms V_1 that, using the $\overline{\text{MS}}$ renormalisation scheme, takes the form,

$$V_1(\phi) = \frac{n_i}{4}M_i^4(\phi)\left[\ln\left(\frac{M_i^2}{\mu^2}\right) - C_i\right], \tag{3.4}$$

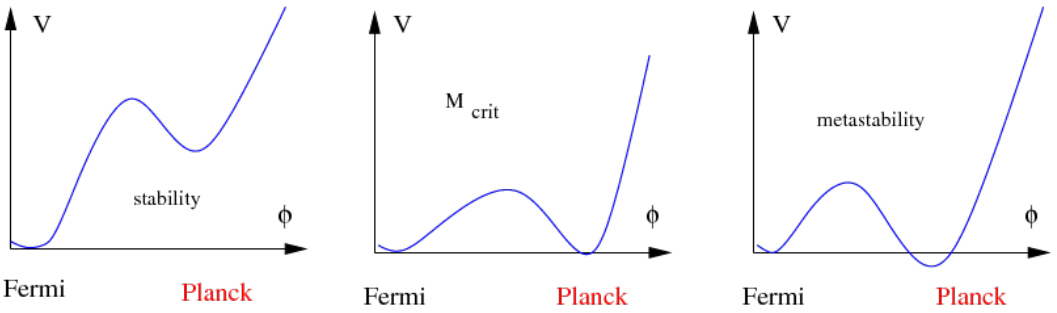

Figure 3.6: Illustration of some of the possible shapes of the effective potential that the Standard Model can accomodate, taken from [65]. The left plot shows a stable vacuum and the right plot shows a metastable configuration. The middle vacuum configuration has two degenerate minima, one at the Fermi scale and one at the Planck scale. This is a hallmark of the Multiple Point Principle. These are for illustrative purposes only, they are not to scale.

where M_i is the scale at which the corrections become significant, μ^2 is the $\overline{\text{MS}}$ renormalisation scale, and n_i and C_i are numerical constants. The loop-corrected mass term m^2 and quartic coupling λ both depend on the value of the Higgs field ϕ.

It is possible for the SM effective potential to have more than one minimum, as shown in figure 3.6. The premise of the MPP assumes that nature would prefer the configuration illustrated by the middle plot: a potential configuration where there are two degenerate minima, one at the electroweak scale and one at a much higher scale such as M_{Pl} [30]. This scenario would result in a vacuum on the cusp of stability, just as we see in figures 3.1 and 3.2.

The MPP argues that the Higgs potential parameters should be fixed to allow for different phases to coexist, much like ice, water and vapour can exist for specific values of temperature and pressure. In the language of thermodynamics, couplings such as λ and the top Yukawa y_t would correspond to intensive variables such as temperature and pressure, whilst variables such as $\langle|\phi|^2\rangle$ would be extensive. By fixing the values of the extensive variables we often reach a situation where the intensive variables take specific values, such as those that correspond to the triple point of water. The transition between two phases, represented by the two minima, may be strongly first order, so that the range of extensive variable values that result in the existence of two degenerate minima should be large. To put this analogy into more concrete terms we consider the Feynman path integral that describes the

behaviour of the SM [30],

$$\int \mathcal{D}A\mathcal{D}\psi\mathcal{D}\phi \, \exp\left(iS\left[A,\psi,\phi\right]\right), \tag{3.5}$$

where A represents the gauge fields, ψ the fermions and ϕ the Higgs field. $S\left[A,\psi,\phi\right]$ is the action. In our triple point analogy this would correspond to the statistical mechanics canonical partition function with fixed intensive parameters such as temperature. Fixed extensive parameters would correspond to a microcanonical ensemble with fixed energy, and the analogous path integral would look like,

$$\int \mathcal{D}A\mathcal{D}\psi\mathcal{D}\phi\delta\left(I\left[A,\psi,\phi\right]-I_0\right), \tag{3.6}$$

where $\delta\left(I\left[A,\psi,\phi\right]-I_0\right)$ are delta functions and,

$$I\left[A,\psi,\phi\right]=\int d^4x\mathcal{L}\left(x\right), \tag{3.7}$$

is the extensive variable that is fixed to I_0. We are also free to insert the exponentiated SM action as a factor, which gives us,

$$\int \mathcal{D}A\mathcal{D}\psi\mathcal{D}\phi \, \exp\left(iS\left[A,\psi,\phi\right]\right)\delta\left(I\left[A,\psi,\phi\right]-I_0\right). \tag{3.8}$$

We can approximate the microcanonical ensemble with a canonical one by Fourier transforming the delta function,

$$\delta\left(I-I_0\right)=\frac{1}{2\pi}\int d\left(m_{Hl}^2\right) \, \exp\left(im_H^2\left(I-I_0\right)\right). \tag{3.9}$$

We find that when we use this delta function in our path integral the result is dominated by a small range of the bare Higgs mass squared m_H^2. This lets us use just the dominant value of m_H^2, as long as we ensure that it gives the correct average value of $\langle I\rangle = I_0$ by adjusting the parameters of the SM, such as λ and y_t. This very often results in an effective potential that has two minima, and the correct average value of I will only occur if the two of them have very similar energy densities. If the differences in the average densities of the Higgs field $\langle|\phi|^2\rangle$ at the two phases is small then the degenerate vacua situation is very unlikely to occur. Therefore the difference $\langle|\phi|^2\rangle_2-\langle|\phi|^2\rangle_1$ must be of the order M_{Pl}^2 to be at all likely.

We want the first vacuum at the electroweak symmetry breaking scale $\langle|\phi|\rangle_1\approx 246\,\mathrm{GeV}$ and the second vacuum to exist at $\langle|\phi|\rangle_2\approx M_{Pl}$. At the scale of the second vacuum the effective potential is dominated by the quartic $V_{eff}\approx\frac{1}{16}\lambda\left(\phi\right)\phi^4$, the derivative of which is,

$$\frac{dV_{eff}}{d\phi}|_{\langle\phi\rangle_2} = \frac{1}{4}\lambda\left(\phi\right)\phi^3 + \frac{1}{16}\beta_\lambda\phi^4. \tag{3.10}$$

The existence of the second degenerate minima at M_{Pl} requires that $V_{eff}\left(M_{Pl}\right) = \frac{dV_{eff}}{d\phi}\left(M_{Pl}\right) = 0$, which means that both conditions of Equation 3.2 must be satisfied.

An analysis of the MPP hypothesis, using one-loop RGEs, gave an early prediction of the Higgs mass of $m_h = 135 \pm 9\,\text{GeV}$ [30]. A more recent calculation using two-loop RGEs and an up to date value of the top pole mass gave a prediction of $m_h = 129 \pm 1.5\,\text{GeV}$ [15]. Unfortunately this is no longer compatible with the very precise combined ATLAS and CMS determination of the Higgs mass but it is close enough to warrant further investigation. These have usually taken the approach of extending the SM field content with the aim of altering the running of λ enough to satisfy both of the MPP boundary conditions, as well as providing a valid mass spectrum [66–72].

3.3 Asymptotic Safety

As we discussed in chapter 2, one of the primary motivators of research into BSM physics has been the sensitivity of the Higgs mass to quadratic corrections from new physics scales up to and including the Planck scale. One approach to tackle this has been to look for models that extend the SM and its gauge group such that the model is valid up to infinite energies. Such a model would mitigate any quadratic corrections and would remain well behaved up to any energy scale we may be interested in.

The principle behind asymptotic safety is that models remain not only well behaved and predictive, but interacting up to very high scales [73,74]. In renormalisation group terms, this means that running couplings run towards an interacting UV fixed point. Recently there has been a burst of interest in Totally Asymptotically Safe (TAS) models, in which all of the dimensionless couplings run to interacting UV fixed points [75–82].

TAS should not be confused with Total Asymptotic Freedom (TAF), which requires that all of the couplings run to zero at high scales. This is another class of models that are valid up to infinite energies, but in this case the UV fixed point is non-interacting. TAF models run into a problem with the SM $U(1)_Y$ hypercharge coupling, which is known to run towards a Landau pole at extremely high energy scales. One way to fix this problem is to embed the hypercharge gauge group into a

larger non-abelian group, such as a Pati-Salam $SU(4)_C \times SU(2)_L \times SU(2)_R$ group or a Trinification model that uses the $SU(3)_C \times SU(3)_L \times SU(3)_R$ group [83–86].

We will illustrate the principles of TAS models using an example outlined in [78]. Consider a gauge coupling $\alpha_g = g^2/16\pi^2$ and a Yukawa coupling $\alpha_y = y^2/16\pi^2$. The one-loop β functions for these couplings are,

$$\beta_g = \frac{d\alpha_g}{d\ln\mu} = (-B + C\alpha_g - D\alpha_y)\,\alpha_g^2, \tag{3.11}$$

$$\beta_y = \frac{d\alpha_y}{d\ln\mu} = (E\alpha_y - F\alpha_g)\,\alpha_y, \tag{3.12}$$

where the coefficients B, C, D, E, F are model dependent. D, E and F are greater than zero regardless of the matter content of the model, and the Yukawa coupling α_y always negatively contributes to the running of the gauge coupling α_g. We want $\beta_g = \beta_y = 0$, which can arise at a number of fixed points. The Gaussian fixed point,

$$(\alpha_g, \alpha_y) = (0, 0)\,, \tag{3.13}$$

is the simplest of these, and is an asymptotically free UV fixed point if $B > 0$. An interacting fixed point for the gauge coupling is,

$$(\alpha_g, \alpha_y) = (B/C, 0)\,. \tag{3.14}$$

This is the Caswell-Banks-Zak fixed point [87, 88] and it requires $BC > 0$ and $B/C \ll 1$ to be physically valid. It is impossible to get a UV Caswell-Banks-Zak fixed point because it has been shown that if $B < 0$ then $C > 0$ [77], so BC is always negative in the UV case.

If we want $\beta_g = \beta_y = 0$ as well as a non-zero gauge and Yukawa coupling we end up with a relationship between the gauge and Yukawa couplings of the form $\alpha_y = \frac{F}{E}\alpha_g$. Substituting this into the gauge β function gives,

$$\beta_g = \left(-B + C'\alpha_g\right)\alpha_g^2, \quad C' = C - D\frac{F}{E}. \tag{3.15}$$

The fixed point is now,

$$(\alpha_g, \alpha_y) = \left(\frac{B}{C'}, \frac{B}{C'}\frac{F}{E}\right). \tag{3.16}$$

We can now get the interacting UV fixed point of the asymptotic safety scenario by requiring $B < 0, C' < 0$. Much of the research into TAS models has investigated

whether this condition can be met in extensions of the SM. These models usually introduce a large amount of new field content, such as new scalars or new vector-like fermions, in a variety of different representations of the SM gauge group.

In this work we are primarily interested in asymptotically safe quartic couplings in the Higgs sector, so the models we will look at are somewhat simpler than TAF or TAS models. A possible source of a UV fixed point in the potential of the SM is the contribution to the running of λ from gravitational interactions at very high scales [31,89–92]. In this scenario the running of the quartic coupling β_λ^{SM} is altered by additional terms β_λ^{grav} that become significant at scales above some transition scale such as M_{Pl},

$$\mu\frac{d\lambda}{d\mu} = \beta_\lambda^{SM} + \beta_\lambda^{grav} = \beta_\lambda^{SM} + \frac{a}{8\pi}\frac{\mu^2}{M_{Pl}^2}\lambda. \tag{3.17}$$

Here the coefficient a is dependent on the exact model used to describe high scale behaviour, and its value and sign determines the nature of the gravitational contribution to the running. It is now possible for λ to run towards an interacting UV fixed point. The approach outlined in [31] predicts a range of possible values for the Higgs mass $126 < m_h < 174\,\text{GeV}$, where the lower limit is achieved when $\lambda\left(M_{Pl}\right) = \beta_\lambda\left(M_{Pl}\right) = 0$. Once again we are left with an intriguing prediction that is close enough to the experimental results to be worthy of further investigation.

Chapter 4

Grand Unification Theories

Contents

4.1 Introduction to Grand Unification Theories

The Standard Model gauge group $SU(3)_C \times SU(2)_L \times U(1)_Y$ does not describe the very different properties of the weak and electromagnetic interactions that we see at low energies. As we discussed in chapter 2, at those scales the electroweak $SU(2)_L \times U(1)_Y$ symmetry is spontaneously broken to the electromagnetic $U(1)_Q$ group via the Higgs mechanism, a process that gives masses to the weak W and Z gauge bosons, as well as the masses of the SM fermions via Yukawa interactions. This is an example of a gauge symmetry arising from the breaking of a larger symmetry at a higher energy scale, a theoretically attractive idea that has been a powerful motivator of particle physics research in the past, and one that drives much of the current theoretical and experimental research into BSM models.

One class of models that continues this trend are *Grand Unification Theories.* (GUTs), which posit that the SM is a subgroup of a larger theory under which the strong and electroweak interactions are unified at some high scale M_{GUT}. The SM gauge group is a very successful description of much of what we observe at experiments, however from a theoretical point of view its gauge structure appears as a

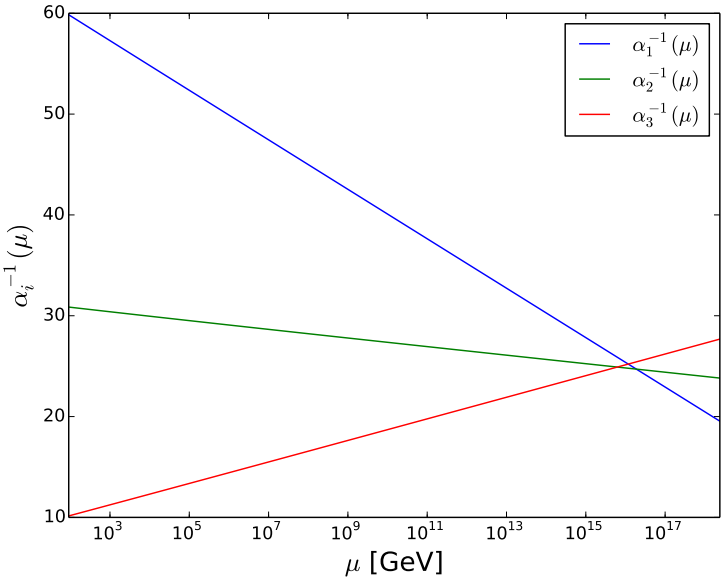

Figure 4.1: Two loop running of the Minimal Supersymmetric Standard Model gauge coupling constants $\alpha_i = g_i^2/4\pi$ with renormalisation scale μ.

somewhat arbitrary choice by nature. Our understanding of the origins of the symmetries of the SM would be on a firmer footing if we discovered some experimental evidence that the SM gauge group naturally arose via spontaneous symmetry breaking from a larger gauge group, one which also provides an explanation for some of the unanswered questions of the SM. This is the central idea behind GUTs, and in this chapter we will discuss some of the motivations for these models as well as the model building techniques used to construct them. We will then discuss in detail two of the most common gauge groups used to construct GUT models: $SU(5)$ and $SO(10)$.

4.1.1 Gauge Coupling Unification

We've already discussed the main physical motivator for GUTs; the hints of gauge coupling unification shown in Figure 1.2. Running the SM up to high energies suggests that all three of the gauge couplings may be unified to a single coupling at a high scale of $M_{GUT} \approx 10^{15}$ GeV, however it is important to note that a unified gauge coupling constant can be defined in a variety of ways. For example, we could argue that the couplings are unified when $\alpha_1(M_{GUT}) = \alpha_2(M_{GUT}) = \alpha_3(M_{GUT}) = \alpha_{GUT}$, where $\alpha_i = g_i^2/4\pi$, or we could define some combination of the couplings g_i

and designate g_{GUT} to be the scale at which this combination are minimised. These are just some of any number of arbitrary definitions that can be used to determine whether the gauge couplings unify at high energies.

Definitions such as the ones we have discussed are often used to argue that the SM couplings do not unify at a high scale unlike supersymmetric models, such as the Minimal Supersymmetric Standard Model (MSSM) shown in Figure 4.1, which seems much closer to unification at around $M_{GUT} \approx 2 \times 10^{16}\,\text{GeV}$. However, as is made clear in [93], these arguments are oversimplifications. It makes more physical sense to consider a matching between the GUT coupling and the SM (or MSSM) couplings that accounts for the heavy fields that are integrated out in the low energy EFT.

To illustrate this, let's consider the two-loop renormalisation group equations for the SM coupling constants g_i, where $i = 1, 2, 3$ corresponds to the $U(1)_Y$, $SU(2)_L$ and $SU(3)_C$ gauge groups, and we use the $SU(5)$ GUT normalisation $g_1 = \sqrt{3/5}g'$. They are [58],

$$\frac{dg_i}{dt} = \beta_i^{(1)} + \beta_i^{(2)} = \frac{b_i g_i^3}{(4\pi)^2} + \frac{g_i^3}{(4\pi)^4}\left[\sum_{j=1}^{3} B_{ij} g_j^3 + \sum_{a=u,d,e} C_i^a \text{Tr}\left(Y_a^\dagger Y_a\right)\right] \tag{4.1}$$

where $t = \ln \mu$ for renormalisation scale μ and Y_a are the Yukawa matrices for the quarks and leptons. The coefficients of the one-loop $\beta_i^{(1)}$ and the two-loop $\beta_i^{(2)}$ functions are b_i, B_{ij} and C_i^a. They depend on group theoretic factors of the field content, such as the quadratic Casimir operators and indices of their representations [57]. Near M_{GUT} the one-loop coupling at low energy g_i and the coupling at the GUT scale g_{GUT} are related by threshold corrections $\lambda_i\left(M_{GUT}\right)$ that account for the increasing significance on the running of heavy fields at high energies,

$$g_i^{-2}\left(M_{GUT}\right) = g_{GUT}^{-2}\left(M_{GUT}\right) - \frac{\lambda_i\left(M_{GUT}\right)}{48\pi^2} \tag{4.2}$$

where [94],

$$\lambda_i\left(M_{GUT}\right) = l_i^{V_n} - 21 l_i^{V_n} \ln\left(\frac{M_{V_n}}{M_{GUT}}\right) + l_i^{S_n} \ln\left(\frac{M_{S_n}}{M_{GUT}}\right) + 8 l_i^{F_n} \ln\left(\frac{M_{F_n}}{M_{GUT}}\right) \tag{4.3}$$

depends on a sum over the n heavy fermions F_n, vector bosons V_n and scalars S_n as well as the indices l_i of their representations in the SM group i. The difference between each gauge group's threshold corrections, $\Delta\lambda_{ij} = \lambda_i - \lambda_j$, allows us to

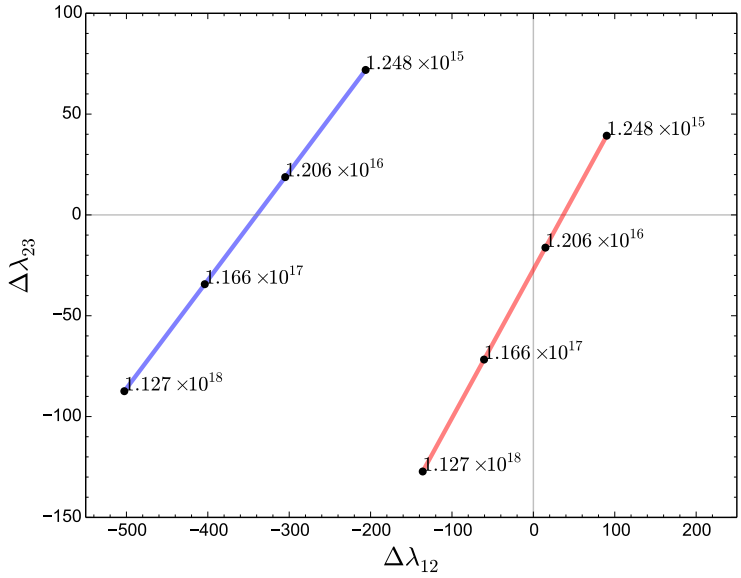

Figure 4.2: Comparison of $\Delta\lambda_{23}$ against $\Delta\lambda_{12}$ for the Standard Model (SM) in blue and the Minimal Supersymmetric Standard Model (MSSM) in red. The black dots indicate the value of M_{GUT} in GeV at which gauge coupling unification occurs, whilst the distance from the origin shows the size of the corrections required to achieve unification

.

visualise the size of the corrections needed to achieve coupling unification in a model independent way. We now have a simple relation between $\Delta\lambda_{ij}$ and the gauge couplings $g_{i,j}$,

$$\frac{\Delta\lambda_{ij}\left(M_{GUT}\right)}{48\pi^2} = g_i^{-2}\left(M_{GUT}\right) - g_j^{-2}\left(M_{GUT}\right). \tag{4.4}$$

Figure 4.2 shows $\Delta\lambda$ plots for the SM and the MSSM. The distance from the origin indicates the size of the threshold corrections a GUT model would have to provide to achieve gauge coupling unification. With plots like these we can check if SM coupling unification is possible within a given GUT scenario by matching the SM thresholds to the values of λ_i we calculate for the GUT model in question, which requires knowledge of the heavy spectrum of the GUT that is integrated out in the low energy EFT description.

The contribution of threshold corrections to the running of the gauge couplings is something that is often neglected in GUT model building. Comparing the cor-

rections that arise from the running of the couplings in the low energy EFT to the threshold corrections that the heavy field content of a GUT model provides is a more robust method of determining whether or not the model is compatible with gauge coupling unification.

4.1.2 GUT Model Building

Like any gauge theory, GUT models describe physical symmetries via infinitesimal transformations, and as such are built from representations of Lie Algebras. As we discussed in chapter 2, the generators of a Lie Algebra g satisfy the commutation relation,

$$[T_i, T_j] = f_{ijk} T_k, \tag{4.5}$$

where f_{ijk} are the structure constants. The representation of a Lie algebra is a map of the group of linear transformations onto a vector space V that preserves the commutation relation of the algebra. The dimension of the representation is equal to the dimension of the V. The direct sum of two representations is given by,

$$D_1(g) \oplus D_2(g) = \begin{pmatrix} D_1(g) & 0 \\ 0 & D_2(g) \end{pmatrix} \tag{4.6}$$

which can be generalised to a sum of n representations. A representation that cannot be decomposed in this way is called an irreducible representation (or irrep), and any reducible representation can be decomposed into a direct sum of irreps. It is also possible to build a higher dimensional representation from the tensor product of two or more representations $D_1(g) \otimes D_2(g)$.

These days the construction of representations and the calculation of their irreps is usually offloaded to publically available codes, such as LieART [95]. The decomposition of representations can be visualised using a pictorial tool, called Young's tableaux, that visualises representations of groups such as $SU(N)$ as a series of boxes. For example, in $SU(3)$ the fundamental representation **3** is given by,

$$\mathbf{3} = \ydiagram{1}, \tag{4.7}$$

whilst the conjugate $\overline{\mathbf{3}}$ is

$$\bar{\mathbf{3}} = \ydiagram{1,1}. \tag{4.8}$$

There are a number of rules for manipulating these diagrams. An $SU(N)$ representation can have at most $N-1$ boxes in any column and each row must be shorter than the row above, so diagrams such as $\begin{array}{|c|c|}\hline \\\hline \\\hline\end{array}$ are invalid. To decompose tensor products we begin by putting letters $(a, b, \dots)$ etc into the 1st, 2nd etc rows of the 2nd diagram, e.g for $\mathbf{3} \otimes \bar{\mathbf{3}}$,

$$\square \otimes \begin{array}{|c|}\hline a\\\hline b\\\hline\end{array}.$$

The decomposition begins by taking the first row boxes and attaching it to the right of the first diagram to build and sum all possible legal diagrams that contain no duplicate letters in the same column. The process is continued for the next letter with the stipulation that, from right to left reading downwards, the letters must be organised alphabetically. Looking at our $\mathbf{3} \otimes \bar{\mathbf{3}}$ example,

$$\square \otimes \begin{array}{|c|}\hline a\\\hline b\\\hline\end{array} = \begin{array}{|c|c|}\hline & a\\\hline b\\\cline{1-1}\end{array} \oplus \begin{array}{|c|}\hline \\\hline a\\\hline b\\\hline\end{array}. \tag{4.9}$$

The representations that remain after this process are the irreducible representations of the original tensor product. Their dimensions can be calculated by first putting N, for $SU(N)$, in the top left box then counting up along the top row and down each column. These numbers are then multiplied together. Next we fill the boxes again by counting the number of boxes to the right of a box in the same row, plus below in the same column, then adding one to the result. These numbers are then multiplied. The ratio of the results gives the dimension of the representation. This process is best illustrated by examples,

$$\begin{array}{|c|c|}\hline 3 & 4\\\hline 2\\\cline{1-1}\end{array} \Big/ \begin{array}{|c|c|}\hline 3 & 1\\\hline 1\\\cline{1-1}\end{array} = \frac{2 \times 3 \times 4}{3} = 8, \tag{4.10}$$

$$\begin{array}{|c|}\hline 3\\\hline 2\\\hline 1\\\hline\end{array} \Big/ \begin{array}{|c|}\hline 3\\\hline 2\\\hline 1\\\hline\end{array} = 1. \tag{4.11}$$

These rules allow for the calculation of the irreducible representations for a tensor product of $SU(N)$ representations, catagorised by their dimension. The result for our previous example in $SU(3)$ is therefore,

$$\mathbf{3} \otimes \bar{\mathbf{3}} = \mathbf{8} \oplus \mathbf{1}. \tag{4.12}$$

Irreducible representations are of particular importance in gauge theories as the creation operators of a particle are given by their irreducible representations in the

Poincaré group (the group of translations, boosts and rotations in Minkowski space) as well as its internal SM gauge symmetries, such as $SU(3)_C$.

4.2 $SU(5)$ GUT Models

GUT model building starts with a search for a gauge group $\mathcal{G}$ that has the SM gauge group as a subgroup, one from which we can construct representations that can accommodate the SM field content. The larger symmetry must also have the same or higher rank as the SM group, which is rank 4, and must also allow complex representations to accomodate the chiral structure of the SM fields. The simplest simple Lie group that meets these requirements is $SU(5)$, which was first investigated as a potential GUT model by Georgi and Glashow [32]. The generators of $SU(5)$ are related to 24 generalised Gell-Mann matrices λ_a,

$$T_a = \frac{\lambda_a}{2}, \quad a = 1...24. \tag{4.13}$$

These generalised Gell-Mann matrices are given in Appendix A. Since $SU(5)$ has the SM group as a subgroup, its generators can be constructed from the $SU(3)_C$ and $SU(2)_L$ generators. The $SU(3)_C$ generators T_a^C are the 8 λ matrices that have non-zero entries in the first three rows and columns, whilst the $SU(2)_L$ generators T_a^L are the 3 combinations of the λ matrices which have non-zero entries in the last two rows and columns, i.e

$$\left[T_a^C\right]_{ij} = \left[\frac{\lambda_a}{2}\right]_{ij}, \quad a = 1...8 \tag{4.14}$$

$$\left[T_1^L\right]_{ij} = \left[\frac{\lambda_{22}}{2}\right]_{ij}, \quad \left[T_2^L\right]_{ij} = \left[\frac{\lambda_{23}}{2}\right]_{ij}, \quad \left[T_3^L\right]_{ij} = \left[\frac{\sqrt{10}\lambda_{24} - \sqrt{6}\lambda_{15}}{8}\right]_{ij}, \tag{4.15}$$

where $i, j = \{1, 2, 3\}$. The remaining generators are representations of new gauge bosons which mediate interactions that violate the conservation of baryon number. All of the above generators commute with the $U(1)_Y$ hypercharge generator.

The left handed quarks and leptons are embedded into the conjugate fundamental $\bar{\mathbf{5}}$ representation Ψ_L and a **10** representation χ_L,

$$\Psi_L = \begin{pmatrix} d_1^c \\ d_2^c \\ d_3^c \\ e \\ -\nu \end{pmatrix}_L , \quad \chi_L = \begin{pmatrix} 0 & u_3^c & -u_2^c & u_1 & d_1 \\ -u_3^c & 0 & u_1^c & u_2 & d_2 \\ u_2^c & -u_1^c & 0 & u_3 & d_3 \\ -u_1 & -u_2 & u_3 & 0 & e^c \\ -d_1 & -d_2 & d_3 & -e^c & 0 \end{pmatrix}_L \tag{4.16}$$

where the superscript c denotes the charge conjugate of the field. One of the advantages of embedding the SM fields in this way is that their correct charges arise naturally, which we can illustrate by building the $\bar{\mathbf{5}}$ and **10** charge operators. The charge operator for the **5** representation is constructed from the sum of the third $SU(2)_L$ generator and the weak hypercharge generator,

$$Q_{\mathbf{5}} = T_3^L + Y = -\sqrt{\frac{2}{3}}\lambda_{15}. \tag{4.17}$$

In matrix form this is,

$$Q_{\mathbf{5}} = \begin{pmatrix} -\frac{1}{3} & 0 & 0 & 0 & 0 \\ 0 & -\frac{1}{3} & 0 & 0 & 0 \\ 0 & 0 & -\frac{1}{3} & 0 & 0 \\ 0 & 0 & 0 & 1 & 0 \\ 0 & 0 & 0 & 0 & 0 \end{pmatrix}, \tag{4.18}$$

which is related to the charge operator for the $\bar{\mathbf{5}}$ by complex conjugation. The action of $Q_{\bar{\mathbf{5}}}$ gives the correct charges for the anti-down quark, electron and electron neutrino. To build the charge operator for the **10** representation we exploit the fact that it can be written as the antisymmetric tensor product of two **5** representations, e.g,

$$\mathbf{10} \oplus \mathbf{15} = \mathbf{5} \otimes \mathbf{5}. \tag{4.19}$$

We can then build the generators of the **10** from the generators of the **5**,

$$\tilde{T}_a = \frac{\lambda_a}{2} \otimes 1 + 1 \otimes \frac{\lambda_a}{2}. \tag{4.20}$$

So the charge operator for the **10** is given by,

$$Q_{\mathbf{10}} = -\sqrt{\frac{2}{3}}\left[\frac{\lambda_{15}}{2} \otimes 1 + 1 \otimes \frac{\lambda_{15}}{2}\right]. \tag{4.21}$$

The action of this charge generator gives the correct charges for embedded quarks and leptons. To see this, take the row and column values for a particular particle in **10** and add up the corresponding diagonal terms in $Q_{\mathbf{5}}$. For example, the u_3^c is at row 1, column 2 of the **10** representation. Adding the 1st and 2nd diagonal terms of $Q_{\bar{\mathbf{5}}}$ gives $-\frac{1}{3} + (-\frac{1}{3}) = -\frac{2}{3}$, the correct charge of the anti-up quark.

By embedding the Standard Model groups into $SU(5)$ we also gain a natural explanation as to the fractional nature of the quark charges. The generators of an $SU(N)$ group must be traceless, so the charge operator for the fundamental **5** representation of $SU(5)$ must also be traceless,

$$3Q_{d^c} + Q_{e^+} = 0 \quad i.e \quad Q_{e^c} = \frac{Q_{d^c}}{3}. \tag{4.22}$$

A similar relation holds for the **10** representation. This property means that the Georgi-Glashow Model also predicts the equality of the proton and electron charges, something that has no explanation in the Standard Model.

4.2.1 The $SU(5)$ Lagrangian

Much like we did with the SM, The $SU(5)$ Lagrangian can be split into four sectors,

$$\mathcal{L} = \mathcal{L}^{fermion} + \mathcal{L}^{gauge} + \mathcal{L}^{Higgs} + \mathcal{L}^{Yuk}. \tag{4.23}$$

In order to ensure local gauge invariance, covariant derivatives are required for both Ψ_L and χ_L,

$$D_\mu \Psi = \partial_\mu \Psi - igA_\mu \Psi \tag{4.24}$$

$$D_\mu \chi = \partial_\mu \chi + 2igA_\mu \chi. \tag{4.25}$$

The action of these covariant derivatives on ψ_L and χ_L allows for interactions between fermions and gauge fields, which in the Georgi-Glashow model are embedded within a **24** adjoint representation A_μ,

$$A_\mu = \begin{pmatrix} G_\mu & \frac{X_\mu}{\sqrt{2}}, \frac{Y_\mu}{\sqrt{2}} \\ \frac{\bar{X}_\mu}{\sqrt{2}}, \frac{\bar{Y}_\mu}{\sqrt{2}} & \frac{W_\mu}{2} \end{pmatrix} + \sqrt{\frac{3}{5}} B_\mu \begin{pmatrix} -\frac{\mathbb{I}_3}{3} & 0 \\ 0 & \frac{\mathbb{I}_2}{2} \end{pmatrix}, \tag{4.26}$$

where $\mathbb{I}_3$ and $\mathbb{I}_2$ are the 3×3 and 2×2 identity matrices. This representation is given in block form to make clear that it embeds the SM gluon and electroweak

gauge fields G_μ, W_μ and B_μ, but it also includes exotic coloured gauge fields X_μ and Y_μ.

The kinetic term for the gauge fields is the standard $SU(N)$ kinetic Lagrangian,

$$\mathcal{L}^{gauge} = -\frac{1}{2}\mathrm{Tr}(A^{\mu\nu}A_{\mu\nu}), \tag{4.27}$$

where $A_{\mu\nu}$ is the gauge field tensor,

$$A_{\mu\nu} = \partial_\mu A_\nu - \partial_\nu A_\mu + ig[A_\mu, A_\nu]. \tag{4.28}$$

The fermion sector of the $SU(5)$ Lagrangian is,

$$\begin{aligned} \mathcal{L}^{fermion} &= i\bar{\Psi}\gamma^\mu D_\mu \Psi + \frac{i}{2}\mathrm{Tr}(\bar{\chi}\gamma^\mu D_\mu \chi) \\ &= i\bar{\Psi}\gamma^\mu \partial_\mu \Psi + \frac{i}{2}\mathrm{Tr}(\bar{\chi}\gamma^\mu \partial_\mu \chi) + \mathcal{L}^{fermion}_{int}. \end{aligned} \tag{4.29}$$

The covariant derivatives bring about the interaction terms,

$$\mathcal{L}^{fermion}_{int} = g\bar{\Psi}\gamma^\mu A_\mu \Psi - g\mathrm{Tr}(\bar{\chi}\gamma^\mu A_\mu \chi). \tag{4.30}$$

Expanding this out makes explicit the interactions between fermions and gauge fields,

$$\begin{aligned} \mathcal{L}^{fermion}_{int} = &- g\left[\bar{u}\gamma^\mu G_\mu u + \bar{d}\gamma^\mu G_\mu d\right] \\ &- g\left[\overline{\psi}_L\gamma^\mu W_\mu \psi_L + \bar{l}_L\gamma^\mu W_\mu l_L\right] \\ &- \sqrt{\frac{3}{5}}g[-\frac{1}{2}(\bar{\nu}_L\gamma^\mu B_\mu \nu_L + \bar{e}_L\gamma^\mu B_\mu e_L) \\ &+ \frac{1}{6}(\bar{u}_L\gamma^\mu B_\mu u_L + \bar{d}_L\gamma^\mu B_\mu d_L) + \frac{2}{3}\bar{u}_R\gamma^\mu B_\mu u_R \\ &- \frac{1}{3}\bar{d}_R\gamma^\mu B_\mu d_R - \bar{e}_R\gamma^\mu B_\mu e_R] + \frac{g}{\sqrt{2}}[\bar{d}_R\gamma^\mu X_\mu e_R \\ &+ \bar{d}_L\gamma^\mu X_\mu e_L + \bar{u}_L\gamma^\mu X_\mu u_L] + \frac{g}{\sqrt{2}}[-\bar{\nu}_R\gamma^\mu Y_\mu d_R \\ &+ \bar{u}_L\gamma^\mu Y_\mu e_L + \bar{u}_L\gamma^\mu Y_\mu d_L] + h.c, \end{aligned} \tag{4.31}$$

where ψ_L and l_L are the left handed quark and lepton doublets. The majority of the terms above are analogous to SM interactions, however the X and Y bosons mediate baryon number violating interactions that result in proton decay (see section 4.2.3).

4.2.2 Spontaneous Symmetry Breaking

Spontaneous symmetry breaking in the Georgi-Glashow Model takes place in two stages. The overall breaking scheme is,

$$SU(5) \xrightarrow{\Sigma} SU(3)_C \otimes SU(2)_L \otimes U(1)_Y \xrightarrow{\Phi} SU(3)_C \otimes U(1)_Q. \tag{4.32}$$

Firstly, a Higgs field Σ in the adjoint **24** representation, breaks $SU(5)$ to the SM group $SU(3)_C \otimes SU(2)_L \otimes U(1)_Y$. Electroweak symmetry breaking is handled in a similar way to the SM and is mediated by Φ, in the fundamental **5** representation, which contains both the SM electroweak Higgs doublet and a new scalar Higgs triplet,

$$\Phi = \begin{pmatrix} H_1 \\ H_2 \\ H_3 \\ \phi^+ \\ \phi^0 \end{pmatrix}. \tag{4.33}$$

The potential for Σ is,

$$V_\Sigma = -\frac{\mu^2}{2}\mathrm{Tr}(\Sigma^2) + \frac{a}{4}\mathrm{Tr}(\Sigma^2)^2 + \frac{b}{4}\mathrm{Tr}(\Sigma^4). \tag{4.34}$$

The vacuum expectation value of Σ breaks the $SU(5)$ symmetry in the hypercharge direction and can be written as,

$$\langle\Sigma\rangle = \frac{v_\Sigma}{\sqrt{30}}\,\mathrm{Diag}(2,2,2,-3,-3). \tag{4.35}$$

The full Higgs potential describes both the adjoint field and the fundamental **5** field Φ, as well as mixed terms containing both Higgs fields.

$$\begin{aligned} V_{\Phi\Sigma} = \quad & -\frac{\mu^2}{2}\mathrm{Tr}(\Sigma^2) + \frac{a}{4}\mathrm{Tr}(\Sigma^2)^2 + \frac{b}{4}\mathrm{Tr}(\Sigma^4) \\ & -\frac{\mu_\Phi}{2}\Phi^\dagger\Phi + \frac{\lambda}{4}\left(\Phi^\dagger\Phi\right)^2 + \alpha\Phi^\dagger\Phi\mathrm{Tr}(\Sigma^2) - \beta\Phi^\dagger\Sigma^2\Phi. \end{aligned} \tag{4.36}$$

The second Higgs field Φ gains a vev of the type,

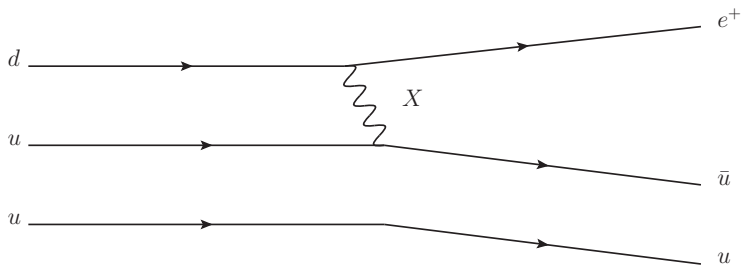

Figure 4.3: An example of proton decay via an X boson to a positron and π^0

$$\langle \Phi \rangle = \frac{v_\Phi}{\sqrt{2}} \begin{pmatrix} 0 \\ 0 \\ 0 \\ 0 \\ 1 \end{pmatrix}, \tag{4.37}$$

which spontaneously breaks the SM group down to $SU(3)_C \otimes U(1)_Q$, analogous to the SM Higgs mechanism. The Yukawa sector of the $SU(5)$ Lagranigan is given by,

$$\begin{aligned} \mathcal{L}^{Yuk} &= Y_d \bar{\Psi}_R \chi_L \Phi^\dagger + Y_u \chi_L^T C \chi_L \Phi + h.c \\ &= Y_d \bar{\Psi}_{Ri} \chi^{ij} \Phi_j^\dagger + Y_u \varepsilon_{ijklm} (\chi^T)^{ij} C \chi^{kl} \Phi^m + h.c, \end{aligned} \tag{4.38}$$

where Y_d and Y_u are Yukawa interaction matrices, C is the conjugation matrix, and ε is the anti-symmetric Levi-Civita tensor. The Yukawa Lagrangian includes interactions between the fermions and the coloured Higgs triplet $H = (H_1, H_2, H_3)$,

$$\begin{aligned} \mathcal{L}_H^{Yuk} &= Y_d \bar{\Psi}_{Ri} \chi^{i\alpha} H_\alpha + Y_u \varepsilon_{ijkl\alpha} (\chi^T)^{ij} C \chi^{kl} H^\alpha \\ &= Y_d (\bar{u}_L d_R + \bar{u}_L e_R^+ + \bar{d}_L \nu_R^C) H + Y_u (\bar{u}_R d_L + \bar{u}_R e_L^+) H. \end{aligned} \tag{4.39}$$

These interactions break baryon number conservation in a similar manner to the coloured X and Y gauge fields, introducing another mediator for proton decay.

4.2.3 Problems with the Georgi-Glashow Model

As we have seen, the running of the couplings suggests some sort of unification of the Standard Model interactions under a larger internal symmetry. Georgi-Glashow

$SU(5)$ unification is the minimal model for this process, nevertheless it leads to some impressive results such as an explanation for the quantisation of electric charge and the fractional charges of the quarks. The Standard Model has no explanation for this property, and yet the simplest GUT predicts it as a direct consequence of the structure of its generators.

However, there are a number of issues with this model in its simplest form. Quarks and leptons share representations in all GUT models, leading to proton decay that is mediated by the X and Y fields, an example of which is shown in figure 4.3. Since QCD is non-perturbative at the mass scale of the proton, calculations of the proton decay are extremely difficult and computationally expensive, and are usually done using lattice QCD techniques [96]. However, we can approximate these interactions in analogy with the weak decay of the muon, which can be written as [97],

$$\Gamma\left(\mu^- \to e^+ \bar{\nu}_e \nu_\mu\right) = \frac{g_2^4}{192\pi^3} \frac{m_\mu^5}{M_W^4}, \tag{4.40}$$

where the decay is suppressed by the fourth power of electroweak scale M_W. The proton width estimation looks like,

$$\Gamma\left(p \to e^+ \mu^0\right) \approx \frac{3}{400\pi^3} \frac{m_p^5}{M_{GUT}^4}, \tag{4.41}$$

where $M_{GUT} \approx M_X$ is the mass of the proton decay mediator. Unfortunately, $SU(5)$ GUTs with no modifications predict a proton lifetime of $\tau_p \approx 10^{24}$ years, much shorter than the current experimental lower limits of $\tau_p \approx 10^{34}$ years [98].

$SU(5)$ GUT models also introduce a doublet-triplet splitting problem in the Higgs sector. The problem is that we have an experimentally verified light scalar, the SM Higgs, sharing a representation with a Higgs Triplet that has to be of the order M_{GUT} so as not to get an extremely short proton lifetime. The model needs a very large fine tuning to accomodate this hierarchy. Non-minimal solutions to this problem usually introduce new field content and symmetries [99–103]. The Yukawa interactions in $SU(5)$ also predict a relationship between quark and lepton masses at the GUT scale, specifically,

$$\begin{aligned} m_b\left(M_{GUT}\right) &= m_\tau\left(M_{GUT}\right), \\ m_s\left(M_{GUT}\right) &= m_\mu\left(M_{GUT}\right), \\ m_d\left(M_{GUT}\right) &= m_e\left(M_{GUT}\right) \end{aligned} \tag{4.42}$$

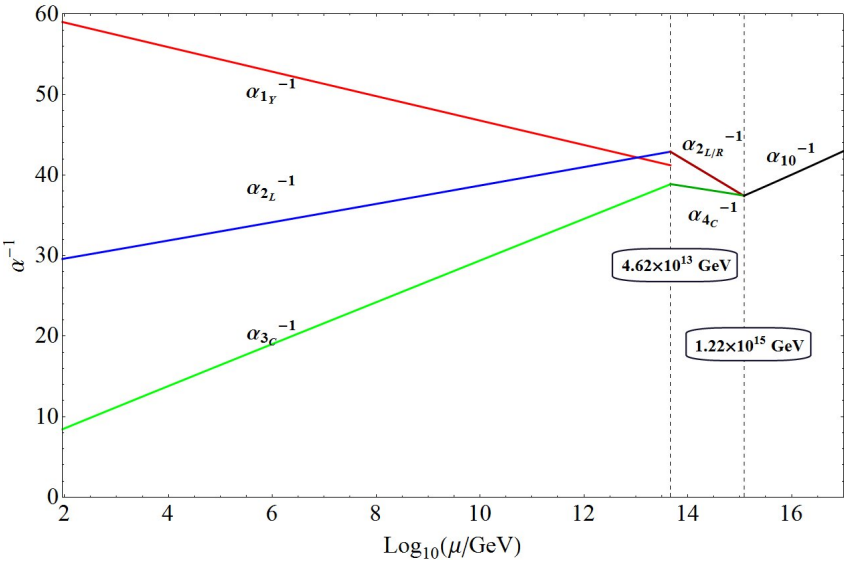

Figure 4.4: Example of the two-loop RGE running of the gauge coupling constants in an $SO(10)$ model with an intermediate Pati-Salam scale, taken from [106].

These relations cannot be made to agree with experiment in a simple Georgi-Glashow model. A possible solution is to introduce a **45** Higgs representation that Yukawa couples to the fermions and adjusts the GUT scale mass relations [104]. Like the SM, the Georgi-Glashow model in its minimal form does not incorporate neutrino masses. It is possible to accomodate a seesaw mechanism by adding new fields in the **15** representation of $SU(5)$ [105].

Its clear that the minimal non-supersymmetric $SU(5)$ GUT is experimentally excluded by proton lifetime estimates and quark-lepton mass relations. Whilst we have discussed non-minimal extensions to the model that can help ameliorate some of these issues, there are other avenues towards grand unification that we can explore. One such avenue is $SO(10)$ GUTs, which we will discuss in more detail in the next section.

4.3 $SO(10)$ Grand Unification

$SO(10)$ GUTs embed the Standard Model field content into the spinor **16** representation [107],

$$\mathbf{16} = (u_1^c, d_1^c, d_1, u_1, \nu^c, e^c, d_2, u_2, u_2^c, d_2^c, d_3, u_3, u_3^c, d_3^c, e, \nu)_L \,. \tag{4.43}$$

One of the most appealing properties of $SO(10)$ models is that not only does the **16** embed all of the SM fields, but the remaining field has the SM quantum numbers of a right handed neutrino. Combine this with the fact that breaking the Rank 5 $SO(10)$ group down to the Rank 4 SM group requires a rank reducing intermediate step, then it's clear that this class of models can naturally accomodate neutrino masses and oscillations via a Type-I or Type-II seesaw mechanism [108].

An intermediate scale also allows for a much more convincing form of gauge coupling unification in $SO(10)$ without the need for supersymmetry, an example of which is shown in Figure 4.4. Notice that the gap between the SM $U(1)_Y$ and the $SU(2)_{L/R}$ couplings at the intermediate scale gives an indication of the size of threshold corrections required for such a unification.

$SO(10)$ models usually have a grand unification scale of the order $M_{GUT} \approx 10^{16}\,\text{GeV}$, somewhat higher than for $SU(5)$, which can help to ensure a proton lifetime estimate that is experimentally valid. The intermediate scale M_R in non-supersymmetric $SO(10)$ models is usually quite distant from the GUT scale, unlike their SUSY counterparts which often have intermediate scales that are much closer to M_{GUT}. This causes difficulties in generating neutrino masses of the correct order [109]. This problem with SUSY $SO(10)$ models can be addressed by additions to the Higgs sector [34] or by invoking split supersymmetry [110].

It is instructive to investigate $SO(10)$ by looking at two of its maximal subgroups; firstly there is $SU(5) \times U(1)$, under which the spinor representation decomposes to the $SU(5)$ representation $\bar{\mathbf{5}}$, **10** and a singlet,

$$\mathbf{16} = \bar{\mathbf{5}} \oplus \mathbf{10} \oplus \mathbf{1}. \tag{4.44}$$

Secondly, $SO(10)$ can be spontaneously broken to a Pati-Salam (PS) subgroup $SU(4)_C \otimes SU(2)_L \otimes SU(2)_R$. PS models treat the SM as an effective field theory of a left-right symmetric model that treats lepton number as a fourth colour [111]. The SM fields are embedded within the $Q = (4, 2, 1)$ and $Q^c = (\bar{4}, 1, 2)$ under $(SU(4)_C, SU(2)_L, SU(2)_R)$,

$$Q = \begin{pmatrix} u_1 & u_2 & u_3 & e^- \\ d_1 & d_2 & d_3 & \nu_e \end{pmatrix}, \quad Q^c = \begin{pmatrix} u_1^c & u_2^c & u_3^c & e^+ \\ d_1^c & d_2^c & d_3^c & \nu_e^c \end{pmatrix}. \tag{4.45}$$

$SO(10)$ differs from $SU(5)$ GUT models in that there are a number of different mechanisms to break $SO(10)$ down to the SM. Figure 4.5 shows the myriad different ways that the $SO(10)$ group can be broken to the SM group [112]. Here we will

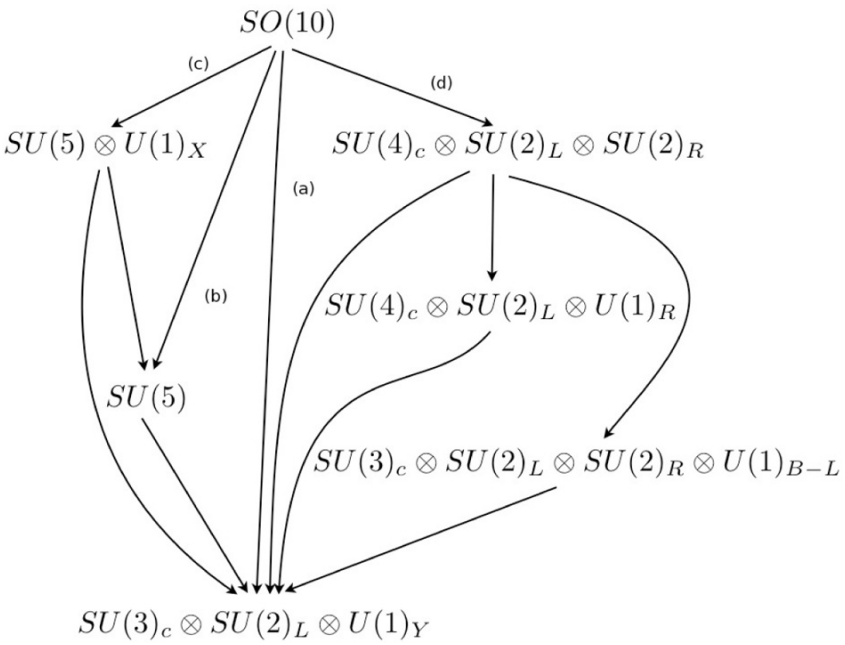

Figure 4.5: Illustration of the various $SO(10)$ breaking schemes, taken from [112].

discuss just one of these breaking schemes, that of [113]. In it $SO(10)$ is broken down to the PS group which in turn is broken to the SM group at an intermediate scale M_R. The breaking scheme is,

$$SO(10) \xrightarrow{210} PS \xrightarrow{126,45} SM \xrightarrow{10} SU(3)_C \otimes U(1)_Q, \tag{4.46}$$

where the numbers above the arrows are the dimensions of the Higgs representations that spontaneously break each symmetry. The **10** representation is responsible for electroweak symmetry breaking, as it contains two scalars $H_u = (1, 2, 1/2)$ and $H_d = (1, 2, -1/2)$ of the type found in Two Higgs Doublet Models. They have different couplings to the SM fermions in such models, but if we wish to break to the SM we require $H_u^* = H_d$. However, if **10** is a real representation then the VEVs of the two doublets are equal, which ultimately leads to the prediction $m_t/m_b = 1$ [114]. This is well known to be incorrect. So we require a complex **10**, with some sort of symmetry that excludes couplings that involve $\mathbf{10}^*$. If we impose a Peccei-Quinn (PQ) $U(1)_{PQ}$ symmetry [115] and give appropriate PQ charges to the **16**, **10**, **45** and $\overline{\mathbf{126}}$ then the problem with the Higgs fields is solved. Not only that, but the addition of a PQ symmetry can be used to solve the strong CP problem and provides an axion dark matter candidate [116].

The most common breaking chains used in SUSY $SO(10)$ models have $SU(5) \otimes$

$U(1)$ as an intermediate group. Unfortunately this is not a suitable candidate for non-SUSY GUT model building as it would inherit the previously discussed problems of a non-supersymmetric $SU(5)$ model, namely that the problems with gauge coupling unification and the difficulties with experimental proton lifetime estimates and quark-lepton mass relations. There are many examples of non-SUSY $SO(10)$ models that do not break to the PS group at an intermediate scale. A number of these models, with either one or two intermediate mass scales, were investigated in [117] for their ability to provide two-loop gauge coupling unification as well as for their prospects in delivering a realistic mass spectrum. It found that a number of models with a minimal Higgs sector were able to meet such criteria.

Chapter 5

Numerical Investigation Framework

Contents

In the following chapters we will investigate whether high scale boundary conditions can be realised in a number of different extensions of the Standard Model, specifically the Real Singlet, Complex Singlet and Two Higgs Doublet Models. In each of these cases we will use a number of publically available tools and codes to build each of our models and perform a numerical scan of their parameter spaces, calculating each point's mass spectrum and checking its validity under theoretical constraints such as perturbativity and vacuum stability. We are also interested in whether the points that pass the theoretical constraints are valid under the increasingly tight experimental constraints that are relevant to extensions of the SM, such as those from ATLAS and CMS or those from dark matter relic density measurements from Planck and WMAP and direct detection constraints from LUX. Finally, but most interestingly, we will investigate those points that survive for their validity under the high scale β function constraints that are a hallmark of the Multiple Point Principle and Asymptotic Safety.

In this chapter we will describe the general framework that we will use in our investigation of high scale boundary conditions in SM extensions, beginning with the calculation of the vertices, mass matrices, corrections and renormalisation group equations that we will use to build a mass spectrum for each of our models.

5.1 Building the Models Using SARAH and FlexibleSUSY

The initial step in each of our analyses is to build the model in question. SARAH [17] is a Mathematica package designed to facilitate the study of general extensions of the SM, whether they be supersymmetric or non-supersymmetric in nature. The derivation of the Lagrangian of the model is fully automated, requiring only its fundamental properties as input. Specifically, SARAH requires definitions of the model's global and gauge symmetries, the field content and their properties such as gauge quantum numbers, VEVs and mixings, as well as the model's scalar potential. From these basic properties the Lagrangian is derived, along with the vertices of the fermion, boson and scalar interactions, the tadpole equations and their one-loop corrections, mass matrices and the one-loop self energies of all particles. SARAH can also calculate the renormalisation group equations up to the two-loop level using generic formulae for both SUSY and non-SUSY models.

The output that SARAH produces can be used by a number of different tools, many of which we will discuss in due course. The most important of these tools, from the point of view of our analysis, is FlexibleSUSY [18–21], a Mathematica and C++ tool that uses the SARAH model files to create a C++ spectrum generator that numerically calculates the pole masses and couplings when given the input parameters for a point in phase space. FlexibleSUSY takes SARAH output of the tree-level mass matrices, electroweak symmetry breaking conditions, one-loop self energies and corrections to the tadpole equations, as well as the two-loop renormalisation group equations, converts them to C++ code and creates a modular spectrum generator that can be easily modified by the user. FlexibleSUSY can also incorporate some extra corrections that SARAH does not calculate, such as the two-loop corrections to the Higgs masses.

We are particularly interested in the relationship between physics at high scales such as M_{Pl} and low scale physics that can be probed by current experiments. The spectrum generators that FlexibleSUSY builds allow us to probe this relationship by iteratively running parameters up and down between scales. The user can define boundary constraints at three different scales: the low scale M_Z, the SUSY scale M_{SUSY} which is associated with the mass of SUSY particles, and a high scale such as M_{GUT} or M_{Pl}. These boundary constraints, along with the renormalisation group equations, form a boundary value problem which the spectrum generator

attempts to solve by finding the values of parameters that are consistent with all of the constraints. FlexibleSUSY does this by integrating the RGEs to a given scale using an adaptive Runge-Kutta algorithm and iterating this calculation until the constraints are met and the parameters converge. During each iteration the parameters are run to the low scale and the mass spectrum is calculated, any low scale constraints are imposed and the parameters are run up to the high scale. High scale constraints are applied, then parameters are run to the SUSY scale and the SUSY scale constraints are imposed. At this point the EWSB conditions are solved at the one loop level. This process is repeated until convergence is reached. At this point the physical mass spectrum is calculated. The model input parameters can be set at any of the defined scales, a function that we will use to set the quartic Higgs couplings at the high scale.

5.2 Parameter Space Scan

The primary aim of this work is to investigate the possibility and consequences of boundary conditions that are applied at the high scale of extensions of the SM. To do that we will perform a number of scans of those models' parameter space via a toolchain that begins with the random generation of the model input parameter space. Each point in the parameter space is defined by a set of input parameters that include the parameters of the potential, the VEVs of the model, and additional SM parameters such as the top pole mass m_t and the strong coupling constant α_S. At this stage we can apply any constraints on the input parameters at the scale at which the model is initiated, such as those that can arise from the Multiple Point Principle, or vacuum stability conditions at M_{Pl}. We generate each point in the parameter space as an SLHA input file [118] that details the input parameters as well as the SM inputs and the FlexibleSUSY model settings.

5.2.1 Theoretical Constraints

Once the input parameter space is generated, we run each point through our spectrum generator. A number of checks on the theoretical constraints of the model are performed at this point. First we determine whether the dimensionless couplings of the model point remain perturbative up to the defined high scale. This amounts to requiring that their value remains below $\sqrt{4\pi}$ at all scales, which is checked when the couplings are run to a new scale during each iteration. We calculate the mass

spectrum for the points that have remained perturbative after we achieve convergence of the couplings, and discard those that do not converge or do not remain perturbative.

Next, we check whether the parameter point can meet the requirement of a SM-like Higgs. To do this we look for scalars that have masses within the range $124.7 < m_h < 127.1\,\text{GeV}$. We use this more generous range rather than the experimental bounds $m_h = 125.09 \pm 0.23\,\text{GeV}$ to account for any theoretical uncertainty in the calculation of the mass spectrum and renormalisation group running of the model couplings. Any points that cannot meet this requirement are discarded as they cannot be reconciled with the experimental observation of the Higgs boson at the ATLAS and CMS experiments.

We also require that the potential of the model remains bounded from below at all scales up to the Planck scale. The specifics of the vacuum stability conditions that a point needs to satisfy are model dependent, and we will detail them in the the model-specific chapters that will follow. Whilst boundedness from below is a necessary condition for a stable vacuum, it does not guarantee that the electroweak symmetry breaking minimum of the effective potential is the global minimum. Additional minima can have values of the effective potential that are lower than the EWSB minimum, resulting in a metastable or unstable vacuum. We incorporate Vevacious [119] into our analysis, which constructs the one-loop effective potential, finds all of the extrema of the tree-level potential and uses them to begin minmising the one-loop potential. If the calculation discovers that multiple minima exist, Vevacious calculates the tunneling lifetime between the lowest minimum and the EWSB minimum at the one-loop level and determines whether the potential is metastable or unstable.

5.2.2 Experimental Constraints

Once we have found the points in the parameter space that satisfy the theoretical constraints of perturbativity, vacuum stability and the existence of an SM Higgs, we continue by applying to these regions a variety of experimental constraints. Arguably the most important restrictions on the Higgs sector of new physics models come from collider experiments, so in our analysis we incorporate these constraints using HiggsBounds [120] and HiggsSignals [121]. Higgsbounds compares the Higgs sector of a model from 95% C.L exclusion limits from both neutral and charged Higgs searches at LEP, the Tevatron and the LHC experiments. It requires as in-

put the model's scalar mass spectrum m_{h_i}, their total decay widths $\Gamma_{tot}(h_i)$, the branching ratios $\mathrm{BR}(h_i \to \ldots)$ and the SM normalised production cross sections $\sigma(h_i)/\sigma_{SM}(h_i)$ for all of the relevant production modes. HiggsBounds then outputs whether a parameter point is excluded at 95% C.L along with details on which analyses were most sensitive for each of the Higgs bosons of the model. HiggsSignals uses the same input to calculate a χ^2 value that quantifies how compatible the parameter point is with the SM Higgs production observed at the LHC.

If the scalar sector of the model has a possible dark matter candidate it is important that we apply constriants from a number of different dark matter experiments. We use micrOMEGAS to do this, a code that calculates the properties of a model's cold dark matter candidate. SARAH can output the model files that micrOMEGAS requires for each parameter point, which include a description of the particle content, the parameters and the relevant vertices. The code uses CalcHEP [122] to calculate the tree-level cross sections of the DM particle, which are then used to determine the relic density, indirect detection rates and scattering cross sections for direct detection experiments. In our analysis we compare the calculated value of the relic density to the combined WMAP [123] and Planck [55] result,

$$\Omega h^2 = 0.1199 \pm 0.0027. \tag{5.1}$$

We usually require that valid points satisfy $\Omega h^2 + 3\sigma$ to allow for the possibility that the stated DM candidate is not the only field in the DM sector, and that there exists some other, as yet unidentified, source of the relic density. We also apply direct detection constraints from the LUX experiment [124] by calculating the DM candidate's spin-independent nucleon scattering cross section and excluding those points with values larger than the mass-dependent constraints from LUX.

5.2.3 High Scale β Function Constraints

The final set of constraints that we apply to our data are restrictions on the value of a model's quartic Higgs coupling β functions at the Planck scale, which are a consequence of both the Multiple Point Principle and the Asymptotic Safety scenario. We are particularly interested in the scalar mass spectrum of parameter points that can pass through such constraints. In general, we require that the quartic β functions are zero at the Planck scale, but it is important to consider the uncertainties that enter into their calculation and how those uncertainties factor into our determination of $\beta(M_{Pl}) = 0$. Figure 5.1 compares the size of the loop contributions that

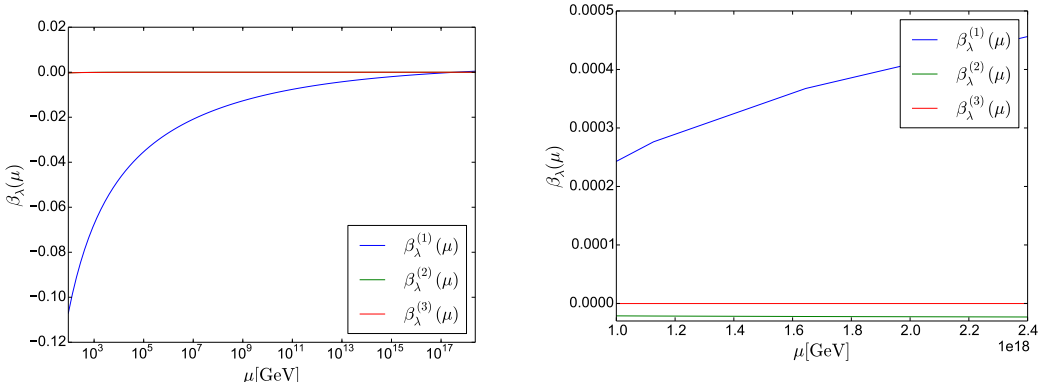

(a) (b)

Figure 5.1: Comparison of the loop contributions that make up β_λ of the Standard Model **(a)** shows the one, two and three-loop contributions, whilst **(b)** focuses the value of these terms around M_{Pl}. The green curve in **(a)** is obscured by the red curve.

make up the β funtion of the quartic Higgs coupling in the SM, β_λ. This example shows that both the two and three loop terms are, as expected, smaller than the one-loop term, and that $\beta_\lambda^{(3)}$ is much smaller than $\beta_\lambda^{(2)}$.

Our analysis uses two-loop renormalisation group equations for the Real Singlet, Complex Singlet and Two Higgs Doublet Models, so we could estimate the three-loop contribution using $\beta^{(3)}(M_{Pl}) \approx \beta^{(2)}(M_{Pl}) \times \alpha_S(M_{Pl})$. We could then use this as our zero estimation, however this constraint would be too restrictive and would not account for the range of uncertainties that enter the calculation of all of the model's coupled RGEs as well as uncertainties in the UV dynamics and mass spectrum. Therefore we will use a somewhat looser, but still very small, constraint throughout our analyses, specifically we will use the difference between the one and two-loop β function values as our zero condition. Points that provide β functions with smaller values than this error will be considered valid.

Chapter 6

The Real Singlet Extension of the Standard Model

Contents

In Chapter 3 we investigated the possibility that the SM is a valid description of physics up to very high energy scales, such as the Planck scale. We also considered whether the intruiging high scale behaviours of the Higgs quartic coupling and its β function can be explained by interpreting them as high scale boundary conditions of some new physics that makes its presence felt at M_{Pl}. We found that it is somewhat difficult for a pure Standard Model that has both $\lambda(M_{Pl}) = 0$ and $\beta_\lambda(M_{Pl}) = 0$ to be simultaneously compatible with experimental constraints on the masses of the Higgs and the top quark. The logical next step in our investigation is to extend the SM by introducing new fields with the aim of building a model that satifies some generalisation of the high scale conditions that we looked at in the SM case, but is also compatible with all of the current experimental constraints. Not only do we want a model that results in valid SM Higgs and top masses, but we also want to find regions of parameter space that are compatible with other constraints, such as those from colliders or direct and indirect dark matter detection experiments. We are particularly interested to see if applying some or all of our high scale boundary conditions can give us predictions for the allowed masses of the new scalars that are introduced in our models.

The most sensible approach to investigating the possibility of high scale boundary conditions in extensions of the SM is to begin with the minimal model. Specifically, we add a real scalar field that is a singlet under the SM gauge symmetries.

The real singlet model's scalar Lagrangian contains both the SM Higgs doublet Φ and the real scalar S [125],

$$\mathcal{L}(\phi, S) = (D^{\mu}\Phi)^{\dagger} D_{\mu}\Phi + \partial^{\mu} S \partial_{\mu} S - V(\Phi, S). \tag{6.1}$$

The most general, renormalisable scalar potential is,

$$\begin{aligned} V(\Phi, S) &= \mu^2 \Phi^{\dagger}\Phi + m_S^2 S^2 + \lambda \left(\Phi^{\dagger}\Phi\right)^2 + \lambda_S S^4 \\ &\quad + k_1 \Phi^{\dagger}\Phi S + k_2 \Phi^{\dagger}\Phi S^2 + \frac{1}{3}\kappa S^3. \end{aligned} \tag{6.2}$$

This can be simplified by imposing a Z_2 symmetry, under which the SM fields are even and the new scalar is odd, to eliminate the cubic terms in Eq 6.2. During electroweak symmetry breaking, the real singlet field can acquire a non-zero vacuum expectation value (vev) v_S alongside the SM Higgs vev $v = 246$ GeV. The scalar fields are then given by,

$$\Phi = \begin{pmatrix} 0 \\ \frac{h_1 + v}{\sqrt{2}} \end{pmatrix}, \quad S = \frac{h_2 + v_S}{\sqrt{2}}. \tag{6.3}$$

Expanding around the minimum gives us the mass matrix,

$$\mathcal{M}^2 = \begin{pmatrix} 2\lambda v^2 & k_2 v v_S \\ k_2 v v_S & 2\lambda_S v_S^2 \end{pmatrix} \tag{6.4}$$

There are two possible phases of this model. We are in the *Broken* phase if $v_S \neq 0$, the scalars are allowed to mix and the mass eigenstates h, H are given at tree level by,

$$\begin{aligned} m_h^2 &= \lambda v^2 + \lambda_S v_S^2 - \sqrt{\left(\lambda v^2 - \lambda_S v_S^2\right) + \left(k_2 v v_S\right)^2} \\ m_H^2 &= \lambda v^2 + \lambda_S v_S^2 + \sqrt{\left(\lambda v^2 - \lambda_S v_S^2\right) + \left(k_2 v v_S\right)^2}. \end{aligned} \tag{6.5}$$

They are related to the gauge eigenstates $\rho = (h_1, h_2)$ via a mixing matrix,

$$\begin{pmatrix} h \\ H \end{pmatrix} = R\rho = \begin{pmatrix} \cos\alpha & -\sin\alpha \\ \sin\alpha & \cos\alpha \end{pmatrix} \begin{pmatrix} h_1 \\ h_2 \end{pmatrix}, \tag{6.6}$$

where $-\frac{\pi}{2} \leq \alpha \leq \frac{\pi}{2}$ is the mixing angle. If $v_S = 0$ then we are in the *Dark Matter* (DM) phase, where no mixing is allowed and one of the two scalars is a possible dark matter candidate.

Broken Phase Input	
$\lambda\,(M_{Pl})$	$0.0 - 1.0$
$\lambda_S\,(M_{Pl})$	$0.0 - 1.0$
$k_2\,(M_{Pl})$	$-1.0 - 1.0$
v_S	$0.0 - 2000$ GeV

DM Phase Input	
$\lambda\,(M_{Pl})$	$0.0 - 1.0$
$\lambda_S\,(M_{Pl})$	$0.0 - 1.0$
$k_2\,(M_{Pl})$	$-1.0 - 1.0$
m_S	$0.0 - 2000$ GeV

Table 6.1: Input parameter ranges for the numerical analysis of the **(left)** Broken phase and **(right)** the Dark Matter phase of the Real Singlet Model.

Clearly the addition of just one real scalar field is enough to significantly complicate the potential, even if we employ the simplifying symmetries discussed previously. The potential is then described by 4 parameters. In the broken phase these are,

$$\lambda, \lambda_S, k_2, v_S, \tag{6.7}$$

while in the DM phase they are,

$$\lambda, \lambda_S, k_2, m_S. \tag{6.8}$$

In the broken phase the bilinear terms μ^2 and m_S^2 are fixed through the potential minimisation conditions, known as the tadpole equations,

$$\frac{\partial V}{\partial \Phi} = \mu^2 + \frac{\lambda v^2}{2} + \frac{k_2 v_S^2}{2} = 0 \tag{6.9}$$

$$\frac{\partial V}{\partial S} = m_S^2 + 2\lambda_S v_S^2 + \frac{k_2 v^2}{2} = 0, \tag{6.10}$$

whereas in the DM phase only μ^2 is fixed via its tadpole equation, since m_S is an input parameter.

6.1 Numerical Analysis and Constraints

We are interested in the effect of boundary conditions on the quartic potential parameters on the real singlet model at the Planck scale M_{Pl}. Specifically, we investigate some or all of the following conditions:

$$\lambda, \lambda_S, k_2 = 0 \tag{6.11}$$

$$\beta_\lambda, \beta_{\lambda_S}, \beta_{k_2} = 0. \tag{6.12}$$

To investigate these scenarios we fix all of the quartic scalar couplings at M_{Pl}, as well as low scale values of v_S, defining a parameter space which we scan over. For each point in this space we calculate the β functions at the two-loop level using SARAH 4.12.2 [17] to investigate their evolution with energy. SARAH also calculates the mass matrices, tadpole equations, vertices and loop corrections we need to calculate mass spectra. We use FlexibleSUSY 2.0.1 [18–21] to build the spectrum generator needed to get the mass spectrum for each point. The code runs the potential parameters between M_Z and M_{Pl} repeatedly until convergence is reached and the various outputs and pole masses can be calculated. Table 6.1 shows the input parameter ranges for both phases of the model.

For our purposes, valid points in parameter space must result in a vacuum that is bounded from below up to M_{Pl}. To that end we require that the potential couplings satisfy the following conditions at all scales:

$$\lambda, \lambda_S \geq 0 \tag{6.13}$$

$$\sqrt{\lambda\lambda_S} + k_2 \geq 0. \tag{6.14}$$

We also require that all of the dimensionless couplings remain perturbative up to M_{Pl}, which for the quartic potential couplings implies,

$$\lambda, \lambda_S, k_2 \leq \sqrt{4\pi}. \tag{6.15}$$

We further check for vacuum stability of our points using Vevacious [119] which minimises the one-loop effective potential and checks that the electroweak symmetry breaking minimum is the global minimum. Points are considered valid if the associated vacuum is stable up to M_{Pl}. We also require that one of the two scalars of the model is a valid SM Higgs candidate, with mass in the range 124.7 GeV $\leq m_{h,H} \leq$ 127.1 GeV. We allow for a wider range of Higgs masses than the experimental uncertainty as an estimate of the theoretical uncertainty associated with the calculation of the mass spectrum.

The constraints that we have outlined so far apply strong constraints which invalidate much of the parameter space. In addition to these we also apply experimental constraints from the LHC, LEP and Tevatron to investigate if parameter points which pass through our theoretical constraints are also phenomenologically viable. We employ HiggsBounds [120] and HiggsSignals [121] to do this, both of which require the following as inputs:

$$\begin{aligned} & m_{h,H}, \qquad \Gamma_{\text{total}}(h), \qquad \Gamma_{\text{total}}(H), \\ & \text{BR}(h, H \to \text{SM}), \qquad \text{BR}(h \to HH), \qquad \text{BR}(H \to hh), \qquad \frac{\sigma(h,H)}{\sigma_{\text{SM}}(h,H)}, \end{aligned} \tag{6.16}$$

i.e the masses of the two scalars, their total decay widths, their branching ratios to SM fields, their branching ratios to each other and their production cross section for all production modes, normalised with respect to the SM production rates evaluated using $m_{h,H}$. We use sHDECAY [126–128] to calculate the total widths and branching ratios for each of the parameter points that passes through our theoretical constraints. The couplings of the scalars $h(H)$ to the SM particles are modified with respect to their equivalents in the SM by the mixing matrix element $R_{11}(R_{21})$. The cross section ratios required by HiggsBounds/HiggsSignals are given by the square of these suppressing matrix elements $R_{11}^2(R_{21}^2)$. If the decay of the heavier scalar to two light scalars, e.g $H \to hh$, is kinematically allowed then it is given by [125],

$$\Gamma_{H\to hh} = \frac{|g_{Hhh}|^2}{8\pi m_H}\sqrt{1-\frac{4m_h^2}{m_H^2}}, \tag{6.17}$$

where the coupling g_{Hhh} associated with the $H \to hh$ decay is given by,

$$g_{Hhh} = -\frac{\sin\alpha}{2vv_S}(\sin\alpha v + \cos\alpha v_S)\left(m_h^2 + \frac{m_H^2}{2}\right). \tag{6.18}$$

HiggsBounds calculates 95% exclusion limits for the decay of new scalar states using analyses of LHC, LEP and Tevatron results. HiggsSignals calculates a χ^2 statistic which compares a paramater point to the observed SM Higgs production at the LHC, which we use to exclude points that do not provide a valid SM Higgs candidate.

If we are in the DM phase we must also include constraints from the dark matter relic density. To do this we use micrOMEGAS [129] to calculate the relic density for our points and compare them to the combined WMAP [123] and Planck [55] result,

$$\Omega h^2 = 0.1199 \pm 0.0027. \tag{6.19}$$

We consider a point excluded if the calculated relic density is greater than $\Omega h^2 + 3\sigma$ so as to ensure that a DM candidate does not overclose the universe, but we allow for the possibility that there may be some other contributions to the relic density which we are not taking into account here.

We also consider dark matter direct detection constraints that place limits on the spin independent cross section σ^{SI} of weakly interacting massive particles (WIMPs)

on nucleons. The strongest of those constraints comes from the LUX experiment [124]. We use micrOMEGAS again to calculate σ^{SI} for our points and exclude those with a result larger than the limits from the LUX 2016 data.

6.2 The Broken Phase

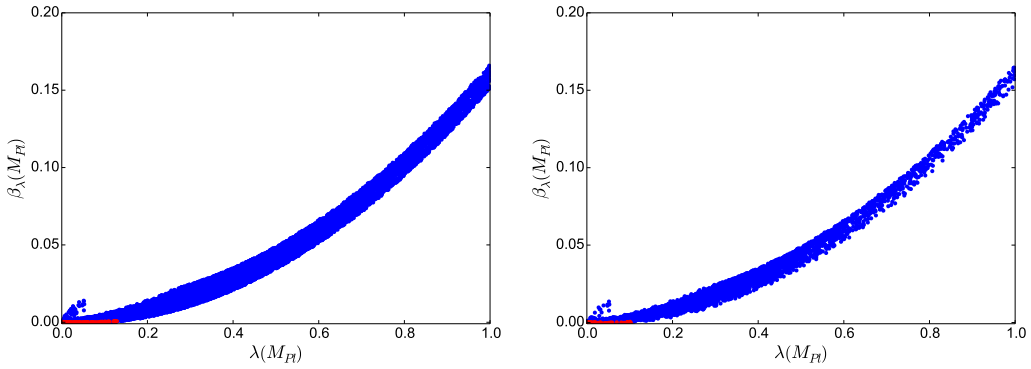

(a) (b)

Figure 6.1: Compatible values of the Higgs quartic coupling $\lambda\,(M_{\rm Pl})$ against $\beta_\lambda\,(M_{\rm Pl})$ in the broken phase. **(a)** includes points that are stable and perturbative up to M_{Pl} and include a SM Higgs candidate, whilst **(b)** also enforces all relevant experimental constraints discussed in section 6.1. Blue points obey $\beta_{\lambda,\lambda_S,k_2} < 1.0$ at M_{Pl} whilst red points obey $\beta_\lambda < 0.0009$, $\beta_{\lambda_S} < 0.019$, $\beta_{k_2} < 0.0045$ at M_{Pl}.

Here we present the results of our numerical investigation of the broken phase of the real singlet model. In this phase the two scalars are free to mix, and we want one of the mass eigenstates to be a valid SM Higgs candidate whilst the other scalar can be lighter or heavier than the SM Higgs. We apply both the theoretical and experimental constraints discussed in section 6.1 to the results of our parameter space scan. Our primary interest is the behaviour of the quartic Higgs couplings and their β functions at the Planck scale and whether they are compatible with the existence of high scale dynamics, such as the Multiple Point Principle or the Aysmptotic Safety scenarios that we discussed previously in the context of the Standard Model in chapter 3. It is important, therefore, that we clarify what it means for a β function to be zero at the Planck scale. We estimate the uncertainty in the calculation of the β functions at M_{Pl} using the difference between the one and two loop RGE calculations. We consider a β function to be zero if it is smaller than

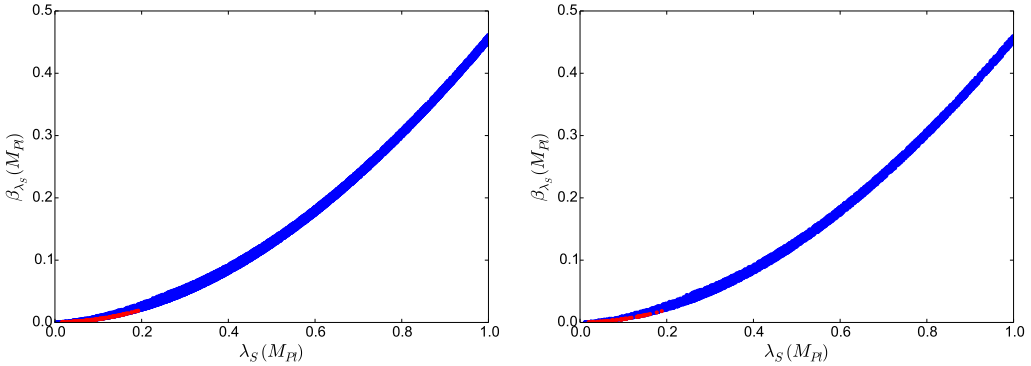

(a) (b)

Figure 6.2: Compatible values of the Higgs quartic coupling $\lambda_S(M_{\rm Pl})$ against $\beta_{\lambda_S}(M_{\rm Pl})$ in the broken phase. **(a)** includes points that are stable and perturbative up to M_{Pl} and include a SM Higgs candidate, whilst **(b)** also enforces all relevant experimental constraints discussed in section 6.1. Blue points obey $\beta_{\lambda,\lambda_S,k_2} < 1.0$ at M_{Pl} whilst red points obey $\beta_\lambda < 0.0009$, $\beta_{\lambda_S} < 0.019$, $\beta_{k_2} < 0.0045$ at M_{Pl}.

this truncation error. In the case of the real singlet model these constraints are the following,

$$\begin{aligned} \beta_\lambda(M_{Pl}) &< 0.0009 \\ \beta_{\lambda_S}(M_{Pl}) &< 0.019 \\ \beta_{k_2}(M_{Pl}) &< 0.0045. \end{aligned} \tag{6.20}$$

Figures 6.1 to 6.3 show the relationship between the Planck scale values of the quartic Higgs couplings λ, λ_S and k_2 and their β functions in our parameter space scan results. The plots on the left of each figure show those points that are compatible with the theoretical constraints discussed in section 6.1, specifically the requirement of perturbativity, a valid SM Higgs candidate, and a stable vacuum up to the Planck scale, whilst the plots on the right also include the relevant experimental constraints. The points that are compatible with all of the high scale boundary conditions of Eq. 6.20 are highlighted in red. The results suggest that it is entirely possible to find points that can accommodate our high scale boundary conditions and can also survive the very stringent constraints that arise from experiment. These points also exhibit very small values of the quartic couplings at M_{Pl}, which is consistent with

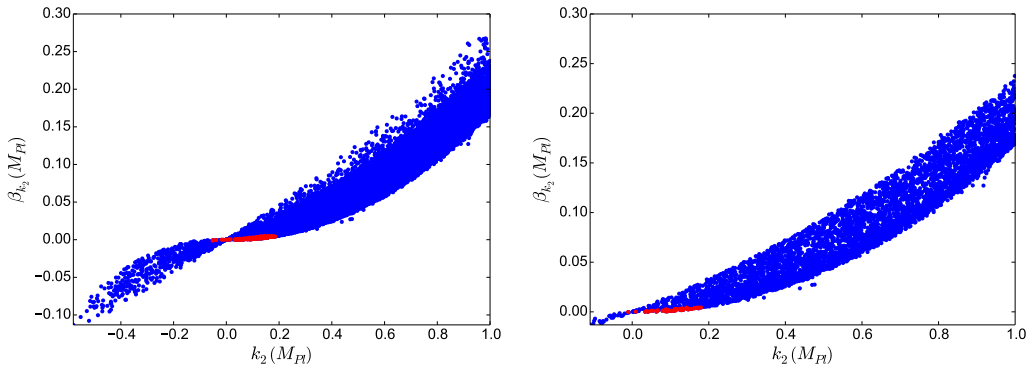

(a) (b)

Figure 6.3: Compatible values of the Higgs quartic coupling $k_2\,(M_{\rm Pl})$ against $\beta_{k_2}\,(M_{\rm Pl})$ in the broken phase. **(a)** includes points that are stable and perturbative up to M_{Pl} and include a SM Higgs candidate, whilst **(b)** also enforces all relevant experimental constraints discussed in section 6.1. Blue points obey $\beta_{\lambda,\lambda_S,k_2} < 1.0$ at M_{Pl} whilst red points obey $\beta_\lambda < 0.0009$, $\beta_{\lambda_S} < 0.019$, $\beta_{k_2} < 0.0045$ at M_{Pl}.

the asymptotic safety scenario's requirement of an interacting UV fixed point in the scalar sector.

Figures 6.4 to 6.6 show the range of allowed masses for the additional Higgs m_H against the Planck scale values of the quartic couplings. The vast majority of the points that survive the high scale boundary conditions have an additional scalar that is heavier than the SM Higgs, with a upper limit of $m_H \approx 1000\,\text{GeV}$. Additionally, the experimental constraints place a lower limit on the heavy Higgs mass of $m_H \approx 200\,\text{GeV}$. The results of our investigation of the broken phase of the real singlet model suggest that a combination of our high scale boundary conditions and the relevant experimental constraints limit the mass of the additional heavy Higgs to a range of $200 \lesssim m_H \lesssim 1000\,\text{GeV}$.

6.3 The Dark Matter Phase

There is no mixing of the scalars in the Dark Matter phase of the real singlet model, meaning that the non-SM Higgs becomes a potential dark matter candidate with mass m_{DM}. Figures 6.7 to 6.9 show the quartic Higgs couplings λ, λ_S and k_2 and their β functions, highlighting the points that can satisfy the high scale boundary conditions of Eq. 6.20 on top of the theoretical and experimental constraints dis-

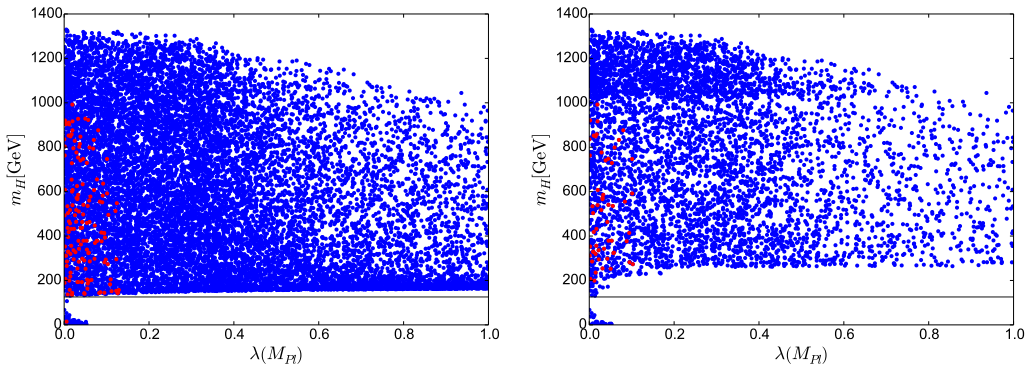

(a) (b)

Figure 6.4: Compatible values of the Higgs quartic coupling $\lambda\,(M_{\rm Pl})$ against additional Higgs mass m_H in the broken phase. **(a)** includes points that are stable and perturbative up to M_{Pl} and include a SM Higgs candidate, whilst **(b)** also enforces all relevant experimental constraints discussed in section 6.1. Blue points obey $\beta_{\lambda,\lambda_S,k_2} < 1.0$ at M_{Pl} whilst red points obey $\beta_\lambda < 0.0009$, $\beta_{\lambda_S} < 0.019$, $\beta_{k_2} < 0.0045$ at M_{Pl}.

cussed in section 6.1. As is the case in the broken phase, the valid points exhibit very smal but non-zero values of the quartic couplings, which is in keeping with the existence of an interacting fixed point at high scales that is a requirement of the Asymptotic Safety scenario in the scalar sector. Figures 6.10 to 6.12 show the possible dark matter candidate masses m_{DM} against the various quartic couplings. A small number of points survived all of our constraints with masses between the SM Higgs mass and $m_{DM} \approx 500\,\text{GeV}$. However, it is interesting to consider the possibility that new physics at or around the UV scale could alter the running of the couplings by imposing threshold corrections that would affect our calculation of the high scale boundary conditions we are using. Without knowing the exact nature of the new UV physics, we cannot precisely determine these corrections, but what we can do is estimate the implications of these threshold corrections by loosening our boundary conditions by some amount, in our case by multiplying our current values of Eq. 6.20 by ten. Figures 6.13 to 6.15 show that by relaxing our high scale boundary conditions we open up the mass range for the DM candidate, allowing for masses just below the SM Higgs mass up to around $m_{DM} \approx 1000\,\text{GeV}$.

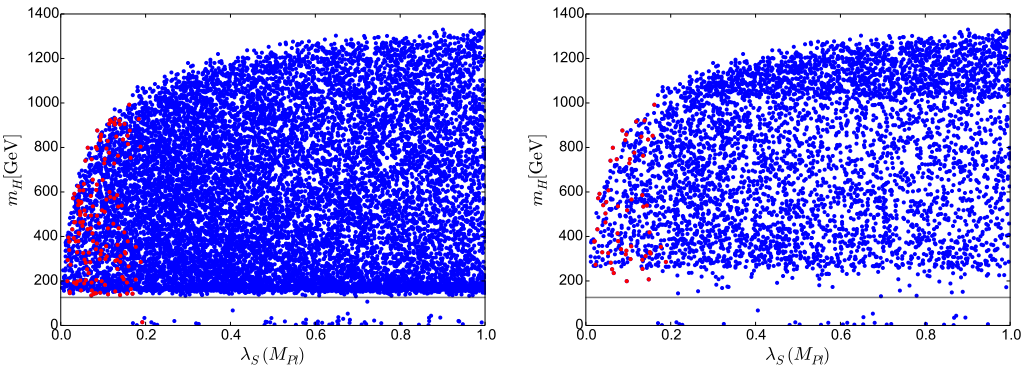

(a) (b)

Figure 6.5: Compatible values of the Higgs quartic coupling $\lambda_S(M_{\rm Pl})$ against additional Higgs mass m_H in the broken phase. **(a)** includes points that are stable and perturbative up to M_{Pl} and include a SM Higgs candidate, whilst **(b)** also enforces all relevant experimental constraints discussed in section 6.1. Blue points obey $\beta_{\lambda,\lambda_S,k_2} < 1.0$ at M_{Pl} whilst red points obey $\beta_\lambda < 0.0009$, $\beta_{\lambda_S} < 0.019$, $\beta_{k_2} < 0.0045$ at M_{Pl}.

6.4 Conclusions

We have investigated the possibility of high scale boundary conditions on the Higgs quartic couplings and their β functions in the Real Singlet Extension of the Standard Model, which can arise due to UV scale dynamics such as the Multiple Point Principle or Asymptotic Safety. Our analysis was agnostic as to which of these scenarios is responsible for high scale conditions in the β functions of the quartic couplings, and we focused on whether points that could satisfy those constraints were also compatible with the theoretical constraints of perturbativity, vacuum stability and the existence of a valid SM Higgs candidate, and with experimental constraints such as those from colliders, the dark matter relic density, as well as results from dark matter direct detection experiments. We investigated both the broken phase, in which the two scalars of the model are allowed to mix, and the Dark Matter phase, where the additional VEV is zero and one of the scalars is a potential dark matter candidate.

Our results suggest that the boundary conditions can be realised in both the broken and DM phases of the model, even after all of the theoretical and experimental constraints have been applied. In the broken phase we found that the valid region

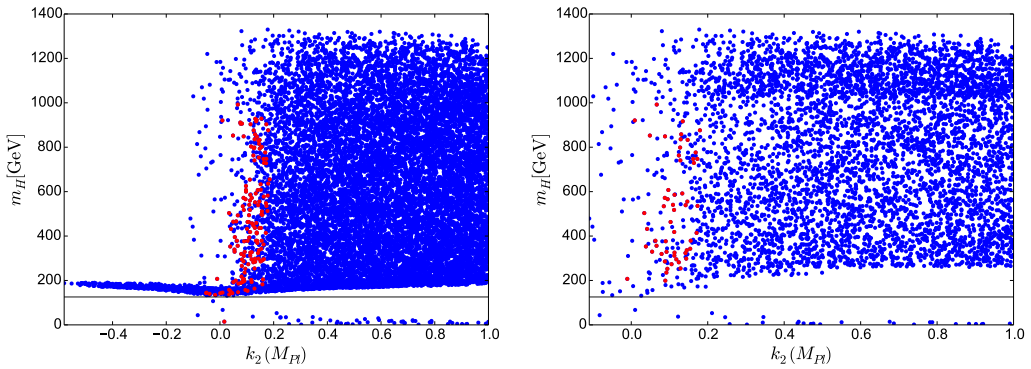

(a) (b)

Figure 6.6: Compatible values of the Higgs quartic coupling $k_2\,(M_{\rm Pl})$ against additional Higgs mass m_H in the broken phase. **(a)** includes points that are stable and perturbative up to M_{Pl} and include a SM Higgs candidate, whilst **(b)** also enforces all relevant experimental constraints discussed in section 6.1. Blue points obey $\beta_{\lambda,\lambda_S,k_2} < 1.0$ at M_{Pl} whilst red points obey $\beta_\lambda < 0.0009$, $\beta_{\lambda_S} < 0.019$, $\beta_{k_2} < 0.0045$ at M_{Pl}.

of parameter space corresponded to masses of the additional heavy Higgs within the range $200 \lesssim m_H \lesssim 1000\,\text{GeV}$. Also, the Planck scale quartic Higgs couplings of valid points were found to be very small but non-zero, which is consistent with the interacting UV fixed point that is a requirement of the Asymptotic Safety scenario. In the DM phase we found a somewhat smaller number of points that survive the strict limits placed upon the parameter space by our various constraints. Those that we did find had DM candidate masses ranging from the SM Higgs mass to $m_{DM} \approx 500\,\text{GeV}$. We loosened our high scale boundary conditions in an attempt to estimate the effect of threshold corrections that would arise from unknown UV physics, the result of which was an increase on our upper mass limit to around $m_{DM} \approx 1000\,\text{GeV}$.

In chapter 3 we investigated the potential existence of high scale boundary conditions in the SM, and in this chapter we took what we learned there and applied it to its simplest possible extension. We have found that whilst the SM cannot successfully satisfy high scale constraints in its scalar sector, the flexibility provided by even the simplest BSM model allows it to realise the conditions that are indicative of certain UV scale dynamics. In the following chapters we will continue these efforts, investigating high scale boundary scenarios in the Complex Singlet Model

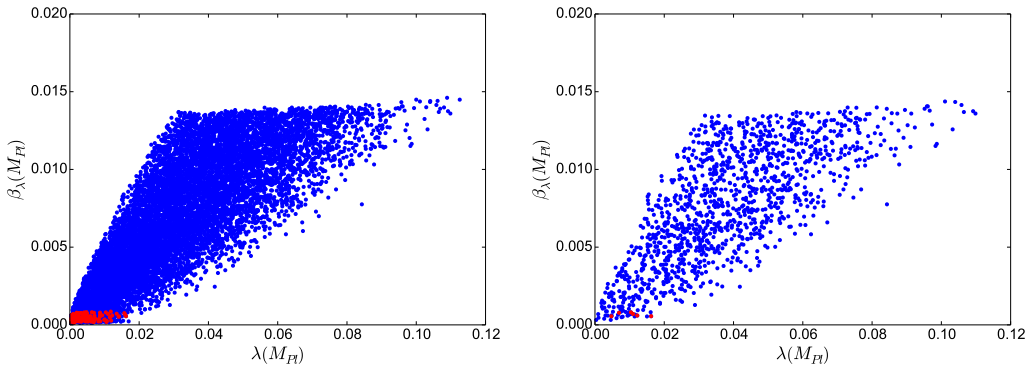

(a) (b)

Figure 6.7: Compatible values of the Higgs quartic coupling $\lambda\,(M_{\rm Pl})$ against $\beta_\lambda\,(M_{\rm Pl})$ in the DM phase. **(a)** includes points that are stable and perturbative up to M_{Pl} and include a SM Higgs candidate, whilst **(b)** also enforces all relevant experimental constraints discussed in section 6.1. Blue points obey $\beta_{\lambda,\lambda_S,k_2} < 1.0$ at M_{Pl} whilst red points obey $\beta_\lambda < 0.0009$, $\beta_{\lambda_S} < 0.019$, $\beta_{k_2} < 0.0045$ at M_{Pl}.

in chapter 7 and various Two Higgs Doublet Models in chapter 8.

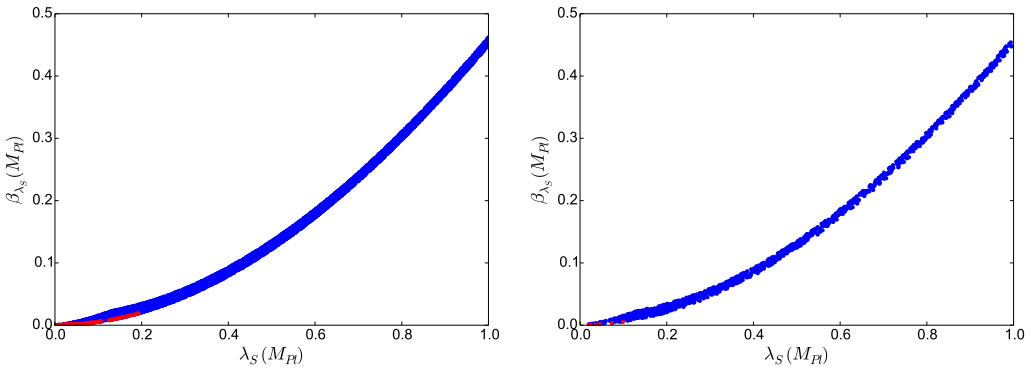

(a) (b)

Figure 6.8: Compatible values of the Higgs quartic coupling $\lambda_S(M_{\rm Pl})$ against $\beta_{\lambda_S}(M_{\rm Pl})$ in the DM phase. **(a)** includes points that are stable and perturbative up to M_{Pl} and include a SM Higgs candidate, whilst **(b)** also enforces all relevant experimental constraints discussed in section 6.1. Blue points obey $\beta_{\lambda,\lambda_S,k_2} < 1.0$ at M_{Pl} whilst red points obey $\beta_\lambda < 0.0009$, $\beta_{\lambda_S} < 0.019$, $\beta_{k_2} < 0.0045$ at M_{Pl}.

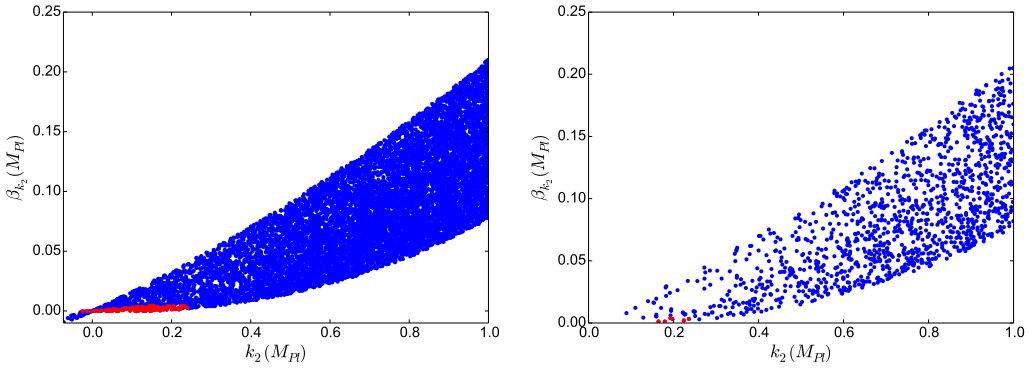

(a) (b)

Figure 6.9: Compatible values of the Higgs quartic coupling $k_2(M_{\rm Pl})$ against $\beta_{k_2}(M_{\rm Pl})$ in the DM phase. **(a)** includes points that are stable and perturbative up to M_{Pl} and include a SM Higgs candidate, whilst **(b)** also enforces all relevant experimental constraints discussed in section 6.1. Blue points obey $\beta_{\lambda,\lambda_S,k_2} < 1.0$ at M_{Pl} whilst red points obey $\beta_\lambda < 0.0009$, $\beta_{\lambda_S} < 0.019$, $\beta_{k_2} < 0.0045$ at M_{Pl}.

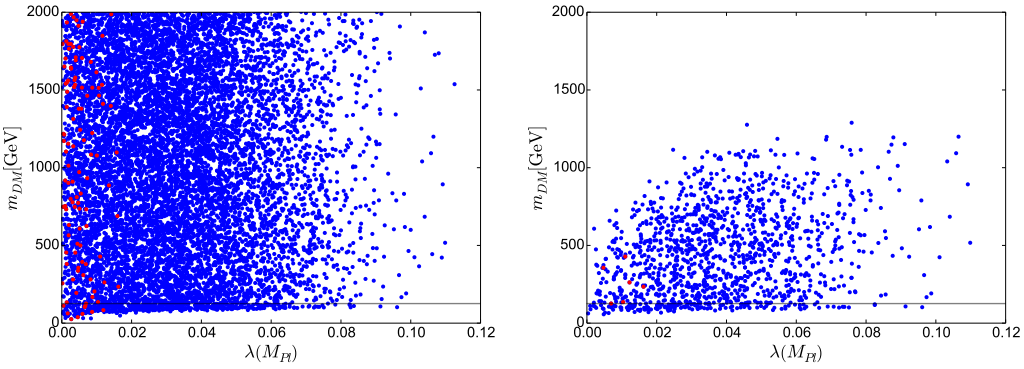

(a) (b)

Figure 6.10: Compatible values of the Higgs quartic coupling $\lambda\,(M_{\rm Pl})$ against Dark Matter candidate mass m_{DM} in the DM phase. **(a)** includes points that are stable and perturbative up to M_{Pl} and include a SM Higgs candidate, whilst **(b)** also enforces all relevant experimental constraints discussed in section 6.1. Blue points obey $\beta_{\lambda,\lambda_S,k_2} < 1.0$ at M_{Pl} whilst red points obey $\beta_\lambda < 0.0009$, $\beta_{\lambda_S} < 0.019$, $\beta_{k_2} < 0.0045$ at M_{Pl}.

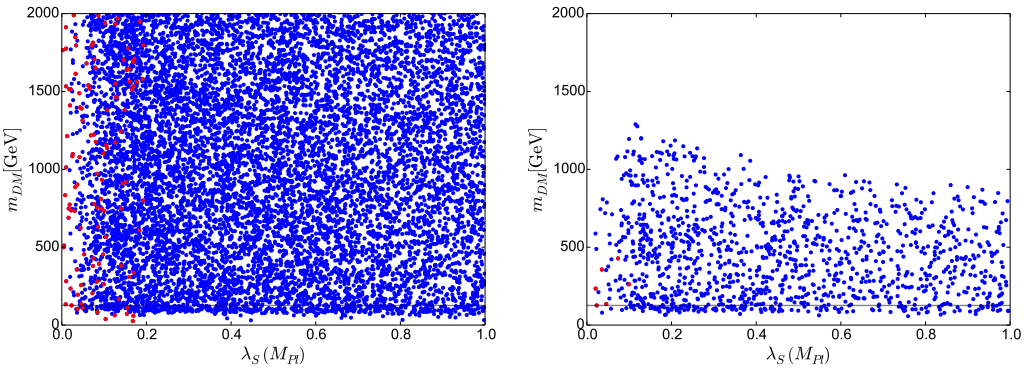

(a) (b)

Figure 6.11: Compatible values of the Higgs quartic coupling $\lambda_S\,(M_{\rm Pl})$ against Dark Matter candidate mass m_{DM} in the DM phase. **(a)** includes points that are stable and perturbative up to M_{Pl} and include a SM Higgs candidate, whilst **(b)** also enforces all relevant experimental constraints discussed in section 6.1. Blue points obey $\beta_{\lambda,\lambda_S,k_2} < 1.0$ at M_{Pl} whilst red points obey $\beta_\lambda < 0.0009$, $\beta_{\lambda_S} < 0.019$, $\beta_{k_2} < 0.0045$ at M_{Pl}.

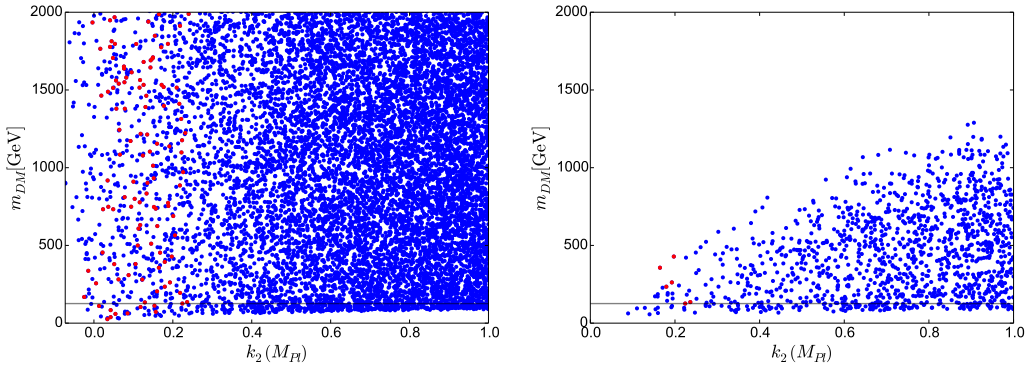

(a) (b)

Figure 6.12: Compatible values of the Higgs quartic coupling $k_2\,(M_{\rm Pl})$ against Dark Matter candidate mass m_{DM} in the DM phase. **(a)** includes points that are stable and perturbative up to M_{Pl} and include a SM Higgs candidate, whilst **(b)** also enforces all relevant experimental constraints discussed in section 6.1. Blue points obey $\beta_{\lambda,\lambda_S,k_2} < 1.0$ at M_{Pl} whilst red points obey $\beta_\lambda < 0.0009$, $\beta_{\lambda_S} < 0.019$, $\beta_{k_2} < 0.0045$ at M_{Pl}.

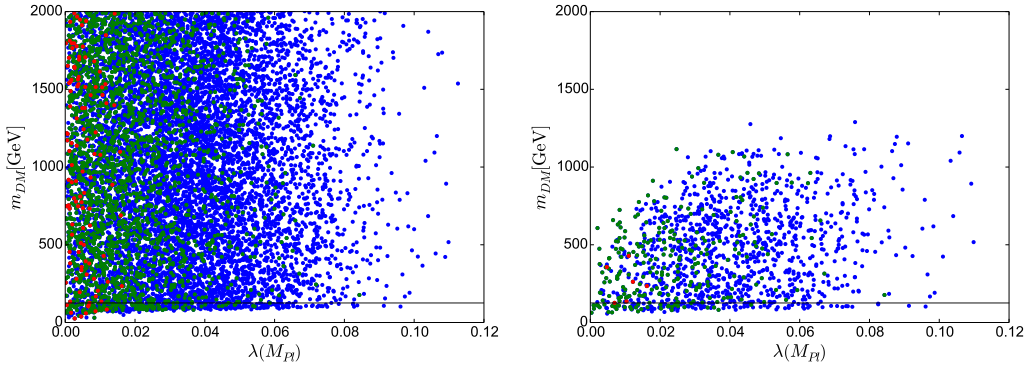

(a) (b)

Figure 6.13: Compatible values of the Higgs quartic coupling $\lambda\,(M_{\rm Pl})$ against Dark Matter candidate mass m_{DM} in the DM phase. **(a)** includes points that are stable and perturbative up to M_{Pl} and include a SM Higgs candidate, whilst **(b)** also enforces all relevant experimental constraints discussed in section 6.1. Blue points obey $\beta_{\lambda,\lambda_S,k_2} < 1.0$ at M_{Pl}, green points obey $\beta_\lambda < 0.009$, $\beta_{\lambda_S} < 0.19$, $\beta_{k_2} < 0.045$ at M_{Pl}, whilst red points obey $\beta_\lambda < 0.0009$, $\beta_{\lambda_S} < 0.019$, $\beta_{k_2} < 0.0045$ at M_{Pl}.

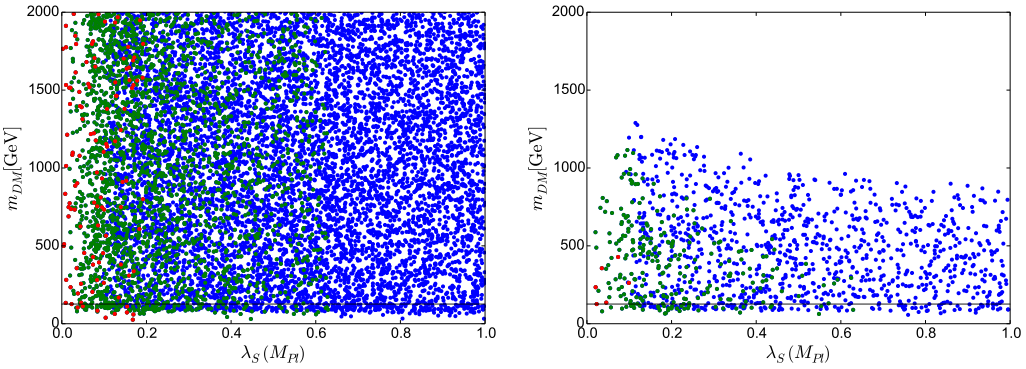

(a) (b)

Figure 6.14: Compatible values of the Higgs quartic coupling $\lambda_S\,(M_{\rm Pl})$ against Dark Matter candidate mass m_{DM} in the DM phase. **(a)** includes points that are stable and perturbative up to M_{Pl} and include a SM Higgs candidate, whilst **(b)** also enforces all relevant experimental constraints discussed in section 6.1. Blue points obey $\beta_{\lambda,\lambda_S,k_2} < 1.0$ at M_{Pl}, green points obey $\beta_\lambda < 0.009$, $\beta_{\lambda_S} < 0.19$, $\beta_{k_2} < 0.045$ at M_{Pl}, whilst red points obey $\beta_\lambda < 0.0009$, $\beta_{\lambda_S} < 0.019$, $\beta_{k_2} < 0.0045$ at M_{Pl}.

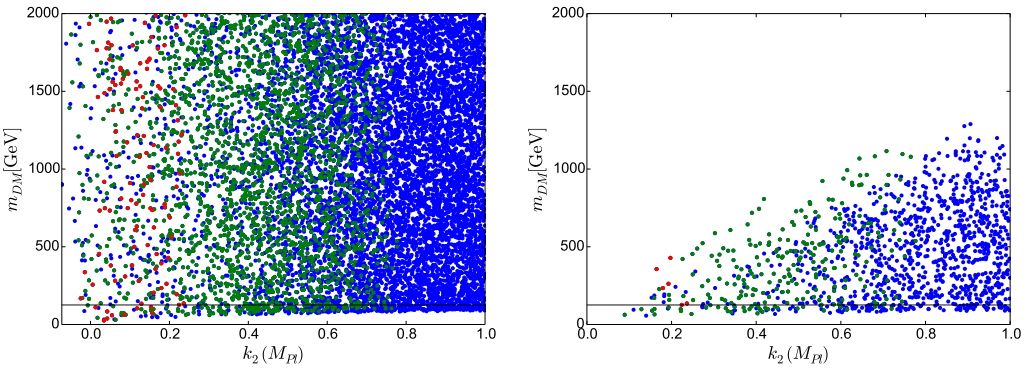

(a) (b)

Figure 6.15: Compatible values of the Higgs quartic coupling $k_2\,(M_{\rm Pl})$ against Dark Matter candidate mass m_{DM} in the DM phase. **(a)** includes points that are stable and perturbative up to M_{Pl} and include a SM Higgs candidate, whilst **(b)** also enforces all relevant experimental constraints discussed in section 6.1. Blue points obey $\beta_{\lambda,\lambda_S,k_2} < 1.0$ at M_{Pl}, green points obey $\beta_\lambda < 0.009$, $\beta_{\lambda_S} < 0.19$, $\beta_{k_2} < 0.045$ at M_{Pl}, whilst red points obey $\beta_\lambda < 0.0009$, $\beta_{\lambda_S} < 0.019$, $\beta_{k_2} < 0.0045$ at M_{Pl}.

Chapter 7

The Complex Singlet Extension of the Standard Model

Contents

We extend the SM to include a complex scalar field $\mathbb{S} = S_1 + iS_2$ which is a singlet under the SM gauge group (for other recent investigations into the phenomenology of this model see e.g [127,130,131]). The addition of $\mathbb{S}$ complicates the scalar potential and the resulting phenomenology significantly. This model contains a $\mathbb{Z}_2$ symmetry $S_2 \to -S_2$ (equivalent to $\mathbb{S} \to \mathbb{S}^*$) which is a consequence of the breaking of a global U(1) symmetry by soft terms a_1 and b_1. The potential reads [132],

$$\begin{aligned} V(H,\mathbb{S}) = \quad & \frac{\mu^2}{2}H^\dagger H + \frac{\lambda}{4}\left(H^\dagger H\right)^2 + \frac{\delta}{2}\left(H^\dagger H\right)|\mathbb{S}|^2 + \frac{b_2}{2}|\mathbb{S}|^2 + \frac{d_2}{4}|\mathbb{S}|^4 \\ & + \left(\frac{b_1}{4}\mathbb{S}^2 + a_1\mathbb{S} + c.c\right). \end{aligned} \tag{7.1}$$

This model is analogous to one with two real scalar fields S_1 and S_2 where the potential reads,

$$\begin{aligned} V(H,S_1,S_2) = \quad & \frac{\mu^2}{2}H^\dagger H + \frac{\lambda}{4}\left(H^\dagger H\right)^2 + \frac{\delta}{2}\left(H^\dagger H\right)\left(S_1^2 + S_2^2\right) \\ & + b_+ S_1^2 + b_- S_2^2 + \frac{d_2}{4}\left(S_1^4 + S_2^4 + S_1^2 S_2^2\right) + 2a_1 S_1. \end{aligned} \tag{7.2}$$

Here we simplify the billinear terms in 7.2 by defining $b_+ = \frac{1}{2}(b_2 + b_1)$ and $b_- = \frac{1}{2}(b_2 - b_1)$. Electroweak symmetry breaking occurs by expanding the Higgs and complex singlet fields around the minima,

$$H = \frac{1}{\sqrt{2}} \begin{pmatrix} G^+ \\ v + h + iG^0 \end{pmatrix}, \quad \mathbb{S} = \frac{1}{\sqrt{2}} \left[v_{s_1} + s_1 + i \left(v_{s_2} + s_2 \right) \right] \tag{7.3}$$

where v is the VEV for the SM Higgs h, and v_{s_1}, v_{s_2} are the VEVs for the real and imaginary parts of $\mathbb{S}$ respectively. The $\mathbb{Z}_2$ symmetry requires the soft parameters b_1 and a_1 to be real.

After electroweak symmetry breaking there are two phases in the model described by 7.1. These phases are categorised by the VEVs of the complex singlet. When $v_{s_2} = 0$ we find ourselves in the *dark matter phase*, where mixing is allowed between h and the real part of the complex singlet field s_1, whilst the imaginary part s_2 is a dark matter candidate. We are in the *broken phase* of the model if $v_{s_2} \neq 0$, and here all three field fluctuations can mix. The mass eigenstates $H = (h_1, h_2, h_3)$ are related to the gauge eigenstates $\rho = (h, s_1, s_2)$ by a 3x3 rotation matrix R,

$$H_i = R_{ij} \rho_j \tag{7.4}$$

$$R = \begin{pmatrix} c_1 c_2 & s_1 c_2 & s_2 \\ -(c_1 s_2 s_3 + s_1 c_3) & c_1 c_3 - s_1 s_2 s_3 & c_2 s_3 \\ -c_1 s_2 c_3 + s_1 s_3 & -(c_1 s_3 + s_1 s_2 c_3) & c_2 c_3 \end{pmatrix} \tag{7.5}$$

where $s_i \equiv \sin \alpha_i$, $c_i \equiv \cos \alpha_i$ and $|\alpha_i| \leq \frac{\pi}{2}$. The couplings of each of the scalars in the model, λ_i, to the SM particles is scaled with respect to the SM scalar couplings λ_{SM} by an element in R e.g,

$$\lambda_i = R_{i1} \lambda_{SM}. \tag{7.6}$$

The matrix R also diagonalises the mass matrix M^2, resulting in the Higgs masses m_{h_i}, $i = 1, 2, 3$:

$$R M^2 R^T = \mathrm{diag} \left(m_{h_1}, m_{h_2}, m_{h_3} \right). \tag{7.7}$$

In the broken phase, the tree-level mass matrix M takes the form,

$$M^2_{broken} = \begin{pmatrix} \frac{\mu^2}{2} + \frac{\delta v_{s_1}^2}{4} + \frac{\delta v_{s_2}^2}{4} + \frac{3\lambda v^2}{4} & \frac{\delta v v_{s_1}}{2} & \frac{\delta v v_{s_2}}{2} \\ \frac{\delta v v_{s_1}}{2} & b_+ + \frac{3 d_2 v_{s_1}^2}{4} + \frac{d_2 v_{s_2}^2}{4} + \frac{\delta v^2}{4} & \frac{d_2 v_{s_1} v_{s_2}}{4} \\ \frac{\delta v v_{s_2}}{2} & \frac{d_2 v_{s_1} v_{s_2}}{4} & b_- + \frac{d_2 v_{s_1}^2}{4} + \frac{3 d_2 v_{s_2}^2}{4} + \frac{\delta v^2}{4} \end{pmatrix} \tag{7.8}$$

whereas in the DM phase where $v_{s_2} = 0$ the mass matrix becomes,

$$M_{DM}^2 = \begin{pmatrix} \frac{\mu^2}{2} + \frac{\delta v_{s_1}^2}{4} + \frac{3\lambda v^2}{4} & \frac{\delta v v_{s_1}}{2} & 0 \\ \frac{\delta v v_{s_1}}{2} & b_+ + \frac{3 d_2 v_{s_1}^2}{4} + \frac{\delta v^2}{4} & 0 \\ 0 & 0 & b_- + \frac{d_2 v_{s_1}^2}{4} + \frac{\delta v^2}{4} \end{pmatrix}. \tag{7.9}$$

Since we are interested in the high scale behaviour of the parameters of this model, particularly the Higgs quartic couplings, its advantageous to use the following as input parameters. In the broken phase we use,

$$\lambda, \quad d_2, \quad \delta, \quad v_{s_1}, \quad v_{s_2}, \quad a_1, \tag{7.10}$$

whilst in the DM phase we use,

$$\lambda, \quad d_2, \quad \delta, \quad v_{s_1}, \quad b_-, \quad a_1. \tag{7.11}$$

The parameter space is continuous insofar as the DM phase is the limit of the broken phase when $v_{s_2} \to 0$, so the difference in the input parameters arises due to the way in which the spectrum generator that calculates the mass spectrum of each phase is built. Specifically we solve the EWSB tadpole equations for different mass parameters in each phase, and in the DM phase the mass term b_- feeds directly into the mass dark matter candidate's tree-level mass. In other circumstances it may make more sense to use the Higgs masses, VEVs and mixing angles as inputs. Its also useful to allow the top pole mass m_t and the strong coupling constant $\alpha_s(M_Z)$ to vary as input parameters by $\pm 3\sigma$ of their central values during our scans in order to take into account their contribution to the uncertainty in our results.

To investigate the RGE evolution of the scalar quartic couplings we use the β functions, as calculated at the two-loop level using SARAH. The gauge coupling β functions in this model are identical to those in the SM, whilst the running of the Yukawa couplings is only slightly modified at the two loop level from the SM case but not to an extent that impacts this work.

7.1 Numerical Analysis and Constraints

The focus of this article is the behaviour of the Higgs quartic couplings of the complex singlet potential 7.1 and their β functions at high scales, as well as the phenomenology that results. We are particularly interested in the effects of some or all of the following boundary conditions existing at M_{Pl},

Broken Phase Input	
$\lambda\,(M_Z)$	$0 - 0.5$
$d_2\,(M_{Pl})$	$0 - 0.5$
$\delta\,(M_{Pl})$	$0 - 0.5$
v_{s_1}	$0 - 2000$ GeV
v_{s_2}	$0 - 2000$ GeV
a_1	$-\left(10^8 - 0\right)$ GeV^3

DM Phase Input	
$\lambda\,(M_Z)$	$0 - 0.5$
$d_2\,(M_{Pl})$	$0 - 0.5$
$\delta\,(M_{Pl})$	$0 - 0.5$
v_{s_1}	$0 - 2000$ GeV
b_-	$0 - 10^5$ GeV^2
a_1	$-\left(10^8 - 0\right)$ GeV^3

Table 7.1: Input parameter ranges for the numerical analysis of the **(left)** broken and **(right)** DM phases.

$$\lambda, \delta, d_2 = 0, \tag{7.12}$$

$$\beta_\lambda, \beta_\delta, \beta_{d_2} = 0. \tag{7.13}$$

To investigate the possibility of this behaviour we scan the parameter space of the model and calculate the resulting mass spectrum, applying a number of phenomenological and experimental constraints to each point. The input parameter ranges are detailed in Table 7.1. We use the Mathematica package SARAH [17] to calculate the β functions at two loops for all of the model parameters. SARAH also calculates all of the mass matrices, tadpole equations, vertices and loop corrections required by spectrum generators to calculate the mass spectrum for a given point in parameter space. We use FlexibleSUSY [18], which builds a spectrum generator using the SARAH output, takes the potential parameters as inputs at various scales and outputs the mass spectrum. We scanned over a number of parameter points and ran the potential parameters between M_Z and the reduced Planck scale M_{Pl}.

Valid points must result in a vacuum that is bounded from below up to M_{Pl}. To that end the potential parameters must satisfy three conditions at all scales,

$$\begin{aligned} \lambda &> 0 \\ d_2 &> 0 \\ \delta + \sqrt{\lambda d_2} &> 0. \end{aligned} \tag{7.14}$$

We also require that all of the dimensionless couplings of our model remain perturbative up to M_{Pl}. Specifically for the Higgs quartic couplings, perturbativity at all

scales requires,

$$\lambda, \delta, d_2 < \sqrt{4\pi}. \tag{7.15}$$

We check for stability of the vacuum using Vevacious [119] which minimises the one-loop effective potential for each of our parameter space points and checks if the EWSB minimum is the global minimum. We accept points that provide a stable vacuum up to M_{Pl}. The mass spectrum of valid points must contain a SM-like Higgs candidate with mass $m_{h_{SM}} \approx 126$ GeV to explain the observed signals at the LHC.

Perturbativity of the couplings, vacuum stability and the existence of a SM Higgs candidate are strong theoretical constraints on the parameter space of this model, invalidating the vast majority of the points investigated by our numerical analysis. Our primary focus here are points that are phenomenologically compatible with current experimental constraints. Here we discuss those contraints, which we apply to those points that are theoretically valid under the theoretical conditions that we have just discussed.

Some of the strongest constraints on models that include extra scalars come from colliders such as the LHC, LEP and the Tevatron. We use HiggsBounds [120] and HiggsSignals [121] to apply these constraints. The basic input for both HiggsBounds and HiggsSignals is,

$$m_{h_i}, \quad \Gamma_{\text{total}}\left(h_i\right), \quad \text{BR}\left(h_i \to \text{SM}\right), \quad \text{BR}\left(h_i \to h_j h_k\right), \quad \frac{\sigma\left(h_i\right)}{\sigma_{\text{SM}}\left(h_i\right)} \tag{7.16}$$

i.e the scalar masses, their total decay widths, their branching ratios to SM particles and other scalars, and their production cross sections for all production modes, normalised to the SM production cross sections evaluated at m_{h_i}. We use sHDECAY [126, 128, 133] to calculate the branching ratios and total decay widths for each of our parameter space points. These inputs are used to calculate signal strengths that can be compared to the experimental analyses from colliders to apply 95% exclusion limits to our points. Since the couplings of the scalars in this model h_i to the SM particles are supressed with respect to the SM Higgs couplings by a factor R_{i1}, the signal strength is reduced to,

$$\mu_i = R_{i1}^2 \frac{R_{i1}^2 \Gamma\left(h_{SM} \to \text{SM}\right)}{R_{i1}^2 \Gamma\left(h_{SM} \to \text{SM}\right) + \sum \Gamma\left(h_i \to h_j h_k\right)} \tag{7.17}$$

which reduces further to R_{i1}^2 when decays to new scalars are forbidden. The relevant decay widths to new scalars are [127],

$$\Gamma\left(h_i \to h_j h_j\right) = \frac{g_{ijj}^2}{32\pi m_i}\sqrt{1-\frac{4m_j^2}{m_i^2}} \tag{7.18}$$

$$\Gamma\left(h_i \to h_j h_k\right) = \frac{g_{ijk}^2}{16\pi m_i}\sqrt{1-\frac{(m_j+m_k)^2}{m_i^2}}\sqrt{1-\frac{(m_j-m_k)^2}{m_i^2}} \tag{7.19}$$

where g_{ijj} and g_{ijk} are coupling strengths between the new scalars. The version of HiggsBounds used in this work (4.3.1) only includes exclusion limits from collider searches for decays to identical new scalars $h_i \to h_j h_j$ (A beta version of HiggsBounds 5 is now available which does support decays to different scalars, however there are currently no experimental results available for such signatures. We also note that HiggsBounds 4.3.1 and HiggsSignals 1.4.0 only include LHC Run-I data). For recent work on di-Higgs production with different masses see [134]. HiggsSignals uses the same input as HiggsBounds to calculate a χ^2 value which gives a quantitatively measure of a SM Higgs candidate's compatability with the signals observed at the LHC.

The Dark Matter phase of the complex singlet model includes a scalar dark matter candidate. In our numerical analysis of this case we calculate the relic density for the DM candidate of each of our parameter points using micrOMEGAS [129] and compare the results to the combined WMAP [123] and Planck [55] experimental results,

$$\Omega h^2 = 0.1199 \pm 0.0027. \tag{7.20}$$

We exclude points with results greater than $\Omega h^2 + 3\sigma$, allowing for the possibility that the scalar is not the only contribution to the dark matter relic density but ensuring that our DM candidate does not overclose the universe.

Another constraint on a potential dark matter candidate comes from direct detection experiments that place limits on the spin independent scattering cross section σ^{SI} of weakly interacting massive particles (WIMPs) off nucleons. The strongest constraints on WIMP dark matter from direct detection currently come from the LUX experiment [124] and are dependent on the mass of the DM candidate. The cross-section for a WIMP dark matter candidate off a proton can be calculated using [135],

$$\sigma^{SI} = \frac{m_p^4}{2\pi \left(m_p + m_{h_{DM}}\right)^2} \left(\frac{\delta \left(b_1 - m_{h_{DM}}^2\right)}{2 m_{h_1}^2 m_{h_2}^2} \right)^2 \left(\sum_{i=u,d,s} f_{pi} + \frac{2}{27} \left(3 f_G\right) \right)^2 \quad (7.21)$$

where m_p is the proton mass, $m_{h_{DM}}$ is the DM candidate mass, m_{h_i} are the remaining two Higgs masses, and f_{pi}, f_G are proton matrix elements [136]. In this work we use micrOMEGAS to calculate σ^{SI} off protons for each of our parameter points and exclude those that result in a σ^{SI} larger than the relevant limit from the 2016 LUX data.

7.2 The Broken Phase

We now present results of our numerical analyses of the broken phase, in which all three neutral scalars mix, applying the theoretical and experimental constraints described in section 7.1. In this phase we call the SM-like Higgs $m_{h_{SM}}$, whilst the remaining two scalars are identified as $m_{h_{\text{Light}}}$ and $m_{h_{\text{Heavy}}}$, with $m_{h_{\text{Light}}} < m_{h_{\text{Heavy}}}$. (Note that h_{Light} may still be heavier than the SM-like Higgs, and correspondingly h_{Heavy} may be lighter.)

In figure 7.1 we see $1\,\sigma$ (green) and $3\,\sigma$ (yellow) regions in the $m_{h_{SM}} - m_t$ plane of the broken phase that satisfy both boundary conditions $\lambda\left(M_{Pl}\right) = \beta_\lambda\left(M_{Pl}\right) = 0$ for different values of v_{s_1} and v_{s_2}. The soft bilinear term a_1 and the complex singlet quartic coupling d_2 are kept fixed, whilst each line corresponds to a different high scale value of the Higgs portal coupling δ. We see it is possible to satisfy the experimental constraints on the masses of both the top and the SM-like Higgs whilst meeting both high scale boundary conditions.

This compatibility is possible for a relatively large range of extra scalar masses. In Figure 7.3 we show light (a) and heavy (b) scalar masses resulting from a scan of parameters and their corresponding high scale values of λ and β_λ, once the theoretical and experimental constraints have been applied. We allowed d_2 and δ (at M_Z) to vary between 0–0.5, the vevs v_{s_1} and v_{s_2} between 0-2 TeV and a_1 between $-(464\,\text{GeV})^3$ and zero. $\lambda(M_Z)$ takes values between 0.2 and 0.43, potentially differing from the SM central value due to variation in the top mass, α_s, and the new states (Figure 7.2 shows the valid ranges of $\alpha_s\left(M_Z\right)$ and m_t from our numerical analyses). Here we are interested in the points with $\lambda = \beta_\lambda = 0$ at the Planck scale, so those in dark blue to the left of the plots. For clarity of the plots we restrict them

to only show scenarios for which $\beta_\lambda(M_{\rm Pl}), \beta_\delta(M_{\rm Pl}), \beta_{d_2}(M_{\rm Pl}) \leq 0.05$, but note that very few points exceed this value.

Before proceeding we should clarify what we really mean by a parameter, such as λ or β_λ, being zero at $M_{\rm Pl}$. At first glance one might expect that we should set these parameters to be exactly zero at the Planck scale. However, we must acknowledge that the relation between these parameters and our calculated low scale masses is necessarily perturbative. Therefore we should not restrict ourselves to keeping these parameters *exactly* zero but allow *small* values consistent with our uncertainty.

To provide an estimate on the uncertainty in our RGE evolution, we consider the difference between high scale parameters derived from the one-loop and two-loop Higgs quartic coupling RGEs (fixed at the low scale) and consider our parameters to be "zero" if they are smaller than this amount. For λ this allows relatively large values of up to 0.067, while for β_λ we have a much tighter constraint of

$$\beta_\lambda \lesssim 0.00005, \tag{7.22}$$

so only the very darkest points of Figure 7.3 satisfy $\beta_\lambda = 0$. One should not confuse this allowance with the uncertainty in λ or β_λ due to the top quark mass or α_s, which are already taken into account when applying low energy constraints.

We note that Figure 7.3 contains a significant number of scenarios where the lightest extra scalar is considerably lighter than the SM Higgs boson. Since the model only couples the new scalars to the SM Higgs doublet, these scenarios escape detection at the LHC if the mixing with the SM Higgs is very small. The relevant quantity is the mixing matrix element R_{11}^2, which we show in Fig. 7.4, demonstrating that the lightest scalar is indeed very decoupled in these scenarios.

We are in principle also interested in the high scale constraints $d_2 = \beta_{d_2} = 0$ and/or $\delta = \beta_\delta = 0$. However, we note that setting δ to zero at $M_{\rm Pl}$ decouples the extra scalars from the SM altogether, and since $\beta_\delta = 0$ for this choice, δ remains zero at all scales and the new scalars are unobservable. However, as argued above, it is not unreasonable to consider δ *small* at the Planck scale, which is anyway phenomenologically necessary to keep the observed Higgs "SM-like". For non-zero values of δ, it is also not possible to set d_2 exactly to zero at $M_{\rm Pl}$ since it is immediately driven negative by RG running and the vacuum destabilises according to Eq 7.14. Again, we are forced to only consider d_2 *small* at the Planck scale and posit some new physics that causes this small deviation.

In Figure 7.5 we show the space of allowed d_2 and δ and their high scale β functions. As before, for clarity we exclude parameter points with β functions

larger than 0.05 at $M_{\rm Pl}$. As for β_λ, the vast majority of the valid points have β_δ lower than this cutoff, but we note that β_{d_2} was able to be somewhat higher than 0.05.

As one might expect, small values of the quartic couplings correspond with small values of their respective β functions. It is also interesting to note that there exist valid scenarios that simultaneously have small values of both λ, δ, d_2 and $\beta_{\lambda,\delta,d_2}$ at the Planck scale. These results make it clear that it is possible to have a phenomenologically valid mass spectrum in the broken phase that is compatible with both the theoretical and experimental constraints whilst also allowing for the boundary conditions $\lambda = \beta_\lambda = 0$ to be at least *approximately* met.

In Figure 7.6 we demonstrate the different scalar mass hierarchies in the $m_{h_{Light}} - m_{h_{Heavy}}$ plane, for small values of λ and β_λ at the high scale. The grey bands for the SM Higgs mass cut the space into regions that have either two additional Higgs masses that are less than $m_{h_{SM}}$ (bottom-left quadrant), one less than $m_{h_{SM}}$ and one heavier (top-left), or two heavier additional scalars (top-right). The effect of the experimental constraints described in Section 7.1 can be seen by comparing Figures 7.6(a) and 7.6(b). In Figure 7.6(a) we apply only theoretical constraints (such as vacuum stability), while in 7.6(b) we also apply the experimental bounds. Irrespectively, the majority of valid points fall into the top-left or top-right quadrants. The blue points respect only the (unrestrictive) bound $\beta_\lambda < 0.05$, while red points have $\beta_\lambda < 0.00005$ and are therefore consistent with zero. The smaller cutoff excludes all of the points with two scalars lighter than $m_{h_{SM}}$ and most of the points where the SM Higgs is the lightest of the three. Indeed, the lighter additional scalar mass never exceeds about 260 GeV when the more restrictive cutoff is used. The heavier scalar never falls below ~ 140 GeV and never exceeds ~ 800 GeV.

Using the difference between one- and two-loop running to estimate what constitutes "small" for the β-functions of δ and d_2, we find the constraints,

$$\begin{aligned} \beta_\delta\left(M_{Pl}\right) &\lesssim 0.00025, \\ \beta_{d_2}\left(M_{Pl}\right) &\lesssim 0.001. \end{aligned} \tag{7.23}$$

No broken-phase parameter points survive if we include all three of the tightest β-function constraints simultaneously in addition to the experimental constraints, indicating that strictly enforcing all of these constraints is incompatible with experiment. However, if the boundary conditions are imposed by some new UV theory or principle, it may be that new physics exists at or around $M_{\rm Pl}$ that distorts the

running of the quartics as we approach. Without knowing the form of this UV completion, we don't know the size of these threshold corrections, so don't know how much deviation from zero we should allow in our boundary conditions. With this in mind we may regard these constraints as too conservative. To investigate their loosening, we somewhat arbitrarily relax our boundary condition cut-offs to ten times our previous β function constraints. We now find the points that survive and plot these in figure 7.7. Notice that this also loosens the constraint on $\beta_\lambda(M_{Pl})$ used in figure 7.6 and now a small number of points survive that have the SM Higgs as the heaviest of the three scalars.

7.3 The Dark Matter Phase

In the dark matter phase only two of the three scalars are allowed to mix, with the third becoming a dark matter candidate. We call the non-SM-like Higgs as h_{New} whilst the DM scalar is h_{DM}. Figure 7.8 shows high scale λ vs. either $m_{h_{New}}$ or $m_{h_{DM}}$, including theoretical and experimental constraints, as well as each point's corresponding value of $\beta_\lambda(M_{\text{Pl}})$. Figure 7.9 shows the valid ranges of d_2 and δ as well as their respective β-functions at M_{Pl}. These figures are analogous to Figures 7.3 and 7.5, and again for clarity we are restricting the β-functions at M_{Pl} to be smaller than 0.05.

In contrast to the broken phase, most of the valid points have a additional Higgs $m_{h_{\text{New}}}$ greater than the SM Higgs mass, illustrated by the grey horizontal band, with the majority of those points falling into a range between around $m_{h_{SM}}$ and approximately 500 GeV. It's interesting to note that the points that do result in $m_{h_{New}} < m_{h_{SM}}$ have smaller values of $\lambda(M_{\text{Pl}}) \lesssim 0.1$. As was the case in the broken phase, smaller values of the quartic couplings correspond to smaller β functions. The dark matter candidate mass $m_{h_{DM}}$ has a lower limit of about 40 GeV, as can be seen in Figure 7.8(b), which is in keeping with the results of [130]. Here, however, we point out that points at this low end of the mass range also have small values of both $\beta_\lambda(M_{Pl})$ and $\beta_\delta(M_{Pl})$.

Figure 7.10 examines the extra scalar masses when we restrict λ and β_λ to be consistent with zero. Again, for comparison, we show points with a very unrestrictive $\beta_\lambda < 0.05$ is blue before demonstrating the effect of the constraint $\beta_\lambda < 0.00005$ in red. No points with $m_{h_{New}} < m_{h_{SM}}$ survive the stronger constraint on β_λ, and the majority of the points that do survive have almost degenerate masses of $m_{h_{New}}$

and $m_{h_{DM}}$. The tree level masses of $m_{h_{New}}$ ($m_{h_{DM}}$) have a linear dependence on a_1 (b_-) which appears to dominate when both of the additional scalars are heavier than the SM Higgs. This degeneracy is visible in the parameter space where only theoretical constraints are applied but is much more pronounced when the experimental constraints are also in place, where much of the parameter space is ruled out primarily via the WMAP and Planck relic density constraint. There is a lower limit $m_{h_{New}} \gtrsim 130\,\text{GeV}$ if we include only the theoretical constraints, which rises to $\gtrsim 160\,\text{GeV}$ if we include experimental constraints. This lower limit in $m_{h_{New}}$ is similar to the lower limit on $m_{h_{Heavy}}$ in the broken phase that we discussed in Section 7.2.

Looking at figure 7.10 might suggest that small values of the β functions at the Planck scale correlates with a small mass difference $\Delta m = |m_{h_{New}} - m_{h_{DM}}|$. However, while 80% of the points that pass through the constraint $\lambda < 0.067, \beta_\lambda < 0.00005$ (red points) result in $\Delta m < 40$ GeV, so do 67% of the (blue) points that don't. This tendency towards degeneracy is a feature of all of the points that satisfy the theoretical constraints outlined in section 7.1. These points exhibit small values of the soft $U(1)$ breaking parameters a_1 and b_1, forcing a small Δm [127]. It is interesting to note that many points in the degenerate mass region can completely account for the dark matter relic density, as shown in figure 7.11. The degeneracy opens up co-annihilation channels involving both $m_{h_{DM}}$ and $m_{h_{New}}$ that enter the relic density calculation [137, 138]. These new channels help bring down the relic density to within the 3σ range.

As in the broken phase, no DM phase points survive when we strictly apply our β function constraints simultaneously with the experimental constraints. However, we see scenarios survive if we relax the constraints by a factor of 10. These scenarios are shown in Figure 7.12.

7.4 Conclusions

We have examined the Complex Singlet extension of the Standard Model with additional constraints on the model's quartic couplings at the Planck scale. These boundary conditions may arise due to high scale requirements of the potential in the Multiple Point Principle, or the evolution towards a UV fixed point, as in the Asymptotic Freedom or Asymptotic Safety scenarios. Here we have not focused on the precise mechanism by which these conditions may have arisen, but examine

the boundary conditions themselves to see if they are compatible with theoretical constraints and experimental observations.

The model exhibits multiple phases, including a "broken" phase, in which both real and imaginary parts of the extra singlet gain a vev and the three scalars all mix; and the "Dark Matter" phase, in which only the real part of the extra singlet gains a vev, only two scalars mix and the remaining scalar provides a stable dark matter candidate.

We investigate a wide range of parameter space in both phases, rejecting parameter choices that do not provide a SM-like Higgs with mass ≈ 125 GeV. We also apply theoretical constraints, such as vacuum stability and perturbativity up to the Planck scale M_{Pl}, and further experimental constraints such as Higgs production and decay rates, and where appropriate constraints on the Dark Matter relic density. We then examine the Planck scale values of the Higgs quartic couplings and their corresponding β functions.

The addition of the complex singlet gives considerable flexibility for imposition of the boundary conditions $\lambda = \beta_\lambda = 0$ at the Planck Scale. Indeed, we find regions of parameter space in both the broken and DM phases where this boundary condition is realised while maintaining compatibility with current theoretical and experimental constraints. Scenarios with *all* quartic couplings, including that of the additional scalar and the Higgs portal interaction, *exactly* zero are not possible since the Higgs portal never regenerates with RGE running once it is set to zero at $M_{\rm Pl}$. However, if some new physics theory at the high scale makes it simply *very small*, then compatibility with all low energy observations can be restored.

In the broken phase we found that the majority of valid scenarios have one additional Higgs that is lighter than the SM Higgs and one that is heavier. In contrast, in the DM phase most scenarios have additional scalars that are heavier than the SM-like Higgs and degenerate with one another. These scalars are all rather decoupled and difficult to detect, but could possibly be investigated at the high luminosity run of the LHC or at future colliders [139]. Imposing $\lambda = \beta_\lambda = 0$ requires the heaviest additional scalar in the broken phase to be lighter than about 600 GeV, with a lower upper limit of ~ 500 GeV in the DM phase. These results are in keeping with previous work on vacuum stability in the complex singlet model [130].

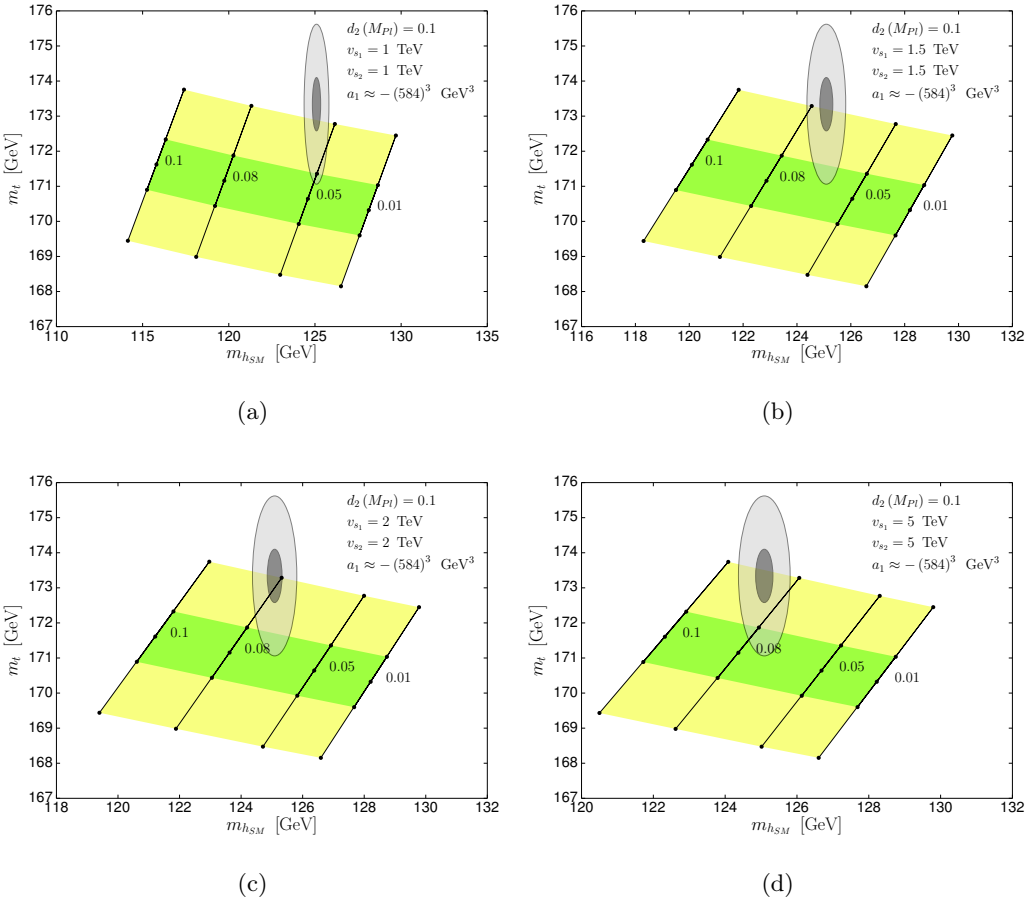

Figure 7.1: Points in the $m_{h_{SM}} - m_t$ plane that satisfy $\lambda(M_{Pl}) = \beta_\lambda(M_{Pl}) = 0$ for $\delta(M_{Pl}) = 0.1, 0.08, 0.05, 0.01$ with **(a)** $v_{s_1} = v_{s_2} = 1$ TeV **(b)** 1.5 TeV **(c)** 2 TeV and **(d)** 5 TeV. The green (yellow) region corresponds to $\pm 1\,(3)\,\sigma$ uncertainty in $\alpha_s(M_Z) = 0.1181 \pm 0.0013$, whilst the ellipses show the experimentally allowed values of m_t and $m_{h_{SM}}$ at $1\,\sigma$ (dark grey) and $3\,\sigma$ (light grey) uncertainty.

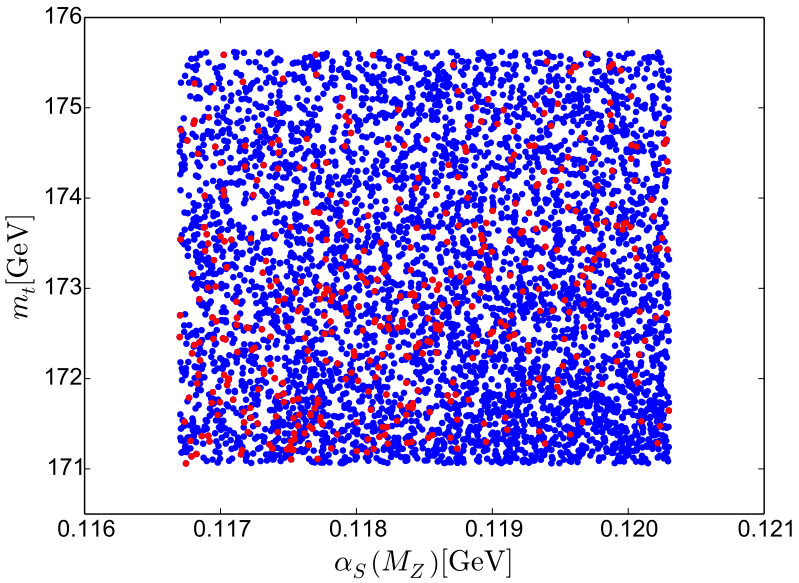

Figure 7.2: Values of $\alpha_S\,(M_Z)$ and m_t in the broken phase. Parameter points are stable and perturbative up to M_{Pl} and include a SM Higgs candidate. All points obey $\lambda < 0.067$ at $M_{\rm Pl}$. Blue points obey $\beta_\lambda < 0.05$ at $M_{\rm Pl}$ while red points obey the more restrictive condition $\beta_\lambda < 0.00005$.

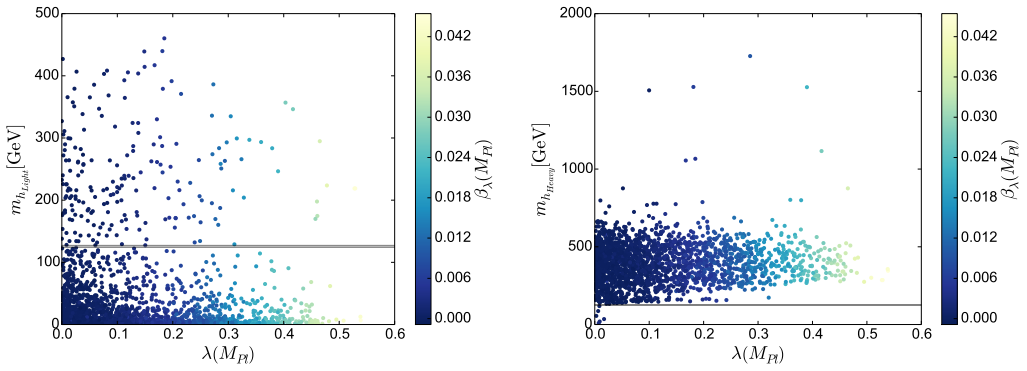

(a) (b)

Figure 7.3: Higgs quartic coupling $\lambda\,(M_{\rm Pl})$ and $\beta_\lambda\,(M_{\rm Pl})$ compared to the light additional Higgs mass $m_{h_{\rm Light}}$ or the heavy additional Higgs mass $m_{h_{\rm Heavy}}$. Parameter points pass the theoretical and experimental constraints of Section 7.1. The grey band shows the SM Higgs mass range. Only points with $\beta_\lambda(M_{\rm Pl}), \beta_\delta(M_{\rm Pl}), \beta_{d_2}(M_{\rm Pl}) \leq 0.05$ are shown.

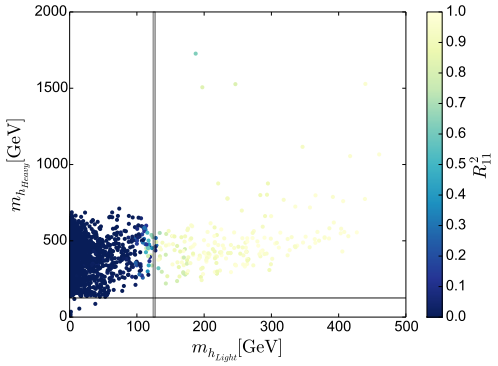

Figure 7.4: The $m_{h_{Light}} - m_{h_{Heavy}}$ plane with corresponding values of the squared Higgs mixing matrix elements R^2_{11}. All points shown pass the theoretical and experimental constraints of Section 7.1. The grey band highlights the SM Higgs mass range. Only points with $\beta_\lambda(M_{\rm Pl}), \beta_\delta(M_{\rm Pl}), \beta_{d_2}(M_{\rm Pl}) \leq 0.05$ are shown.

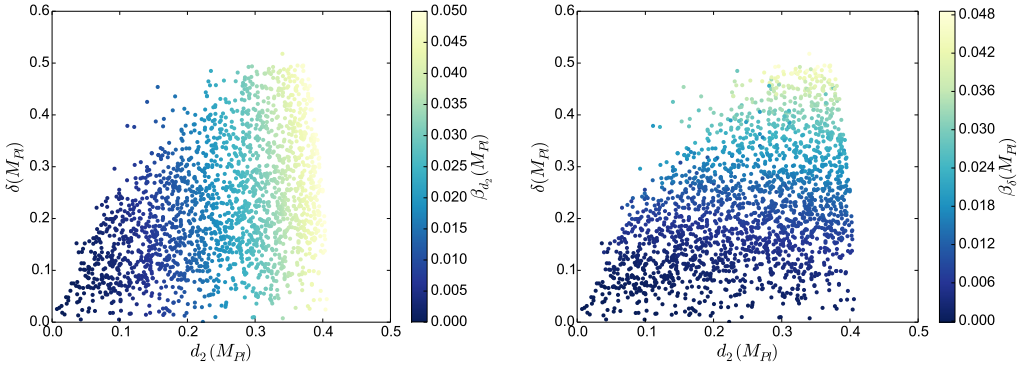

(a) (b)

Figure 7.5: High scale Higgs quartic couplings d_2 and δ with their β-functions. Parameter points pass the theoretical and experimental constraints of Section 7.1.

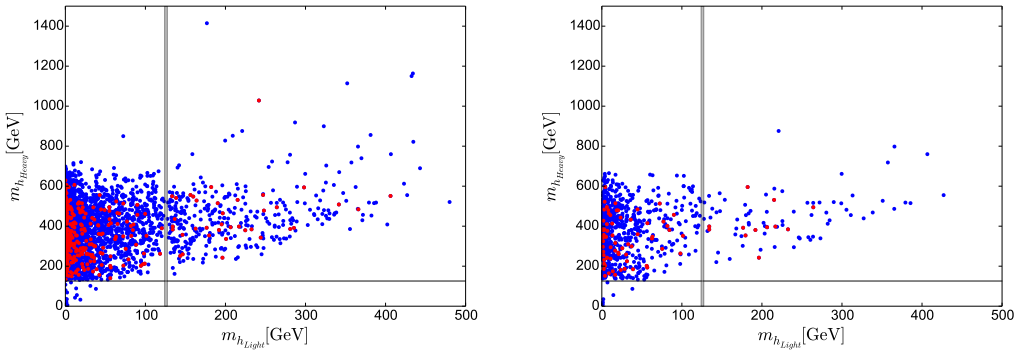

(a) (b)

Figure 7.6: Compatible values of $m_{h_{Light}}$ and $m_{h_{Heavy}}$ in the broken phase for different high scale β_λ constraints. **(a)** includes points that are stable and perturbative up to M_{Pl} and include a SM Higgs candidate, whilst **(b)** also enforces all experimental constraints. All points obey $\lambda < 0.067$ at $M_{\rm Pl}$. Blue points obey $\beta_\lambda < 0.05$ at $M_{\rm Pl}$ while red points obey the more restrictive condition $\beta_\lambda < 0.00005$. The grey bands highlight the SM Higgs mass range.

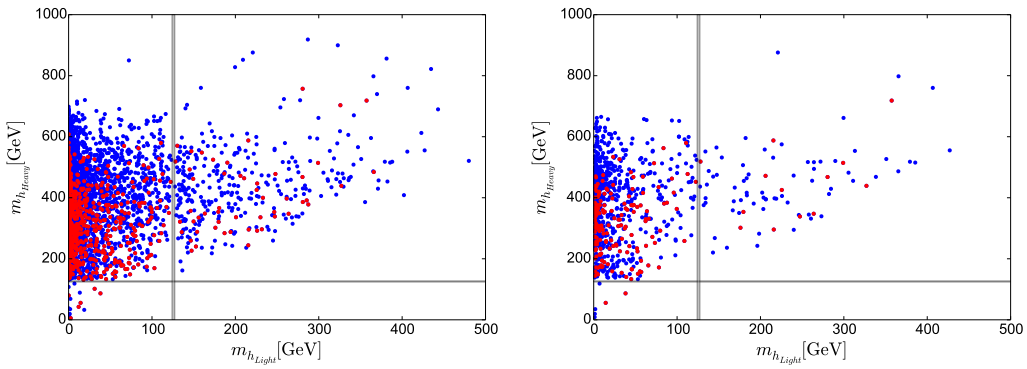

(a) (b)

Figure 7.7: Compatible values of $m_{h_{Light}}$ and $m_{h_{Heavy}}$ in the broken phase with restrictions on β_λ, β_δ and β_{d_2}. **(a)** includes points that are stable and perturbative up to M_{Pl} and include a SM Higgs candidate, whilst **(b)** also enforces all experimental constraints. All points obey $\lambda < 0.067$ at $M_{\rm Pl}$. Blue points obey $\beta_{\lambda,\delta,d_2} < 0.05$ at $M_{\rm Pl}$ while red points obey $\beta_\lambda < 0.0005$, $\beta_\delta < 0.0025$ and $\beta_{d2} < 0.01$. The grey bands highlight the SM Higgs mass range.

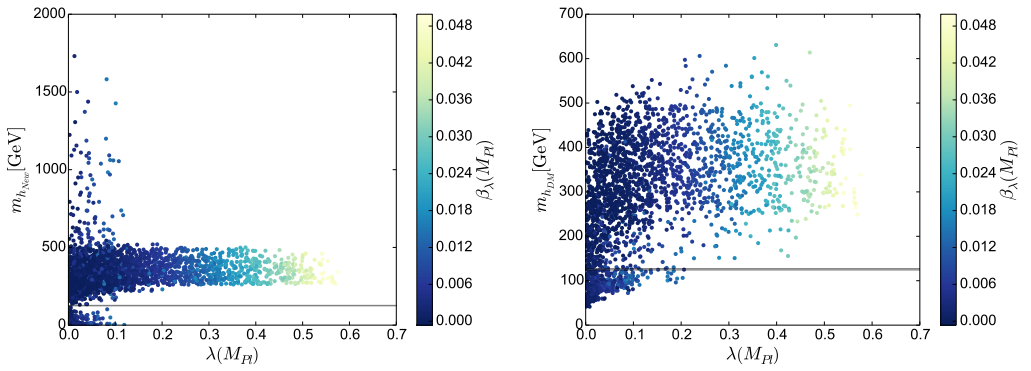

(a) (b)

Figure 7.8: High scale Higgs quartic coupling λ vs. the additional Higgs mass $m_{h_{New}}$ or the DM scalar mass $m_{h_{DM}}$, with values of β_λ. Parameter points pass the theoretical and experimental constraints of Section 7.1, including dark matter relic density and direct detection constraints. The grey band shows the SM Higgs mass range.

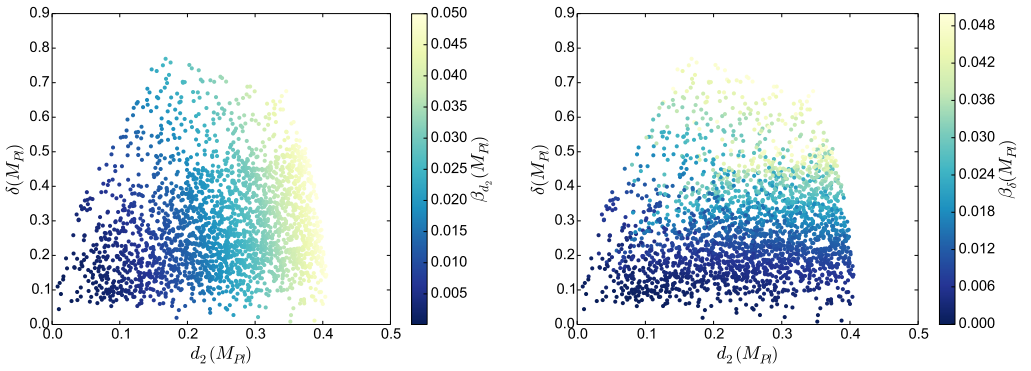

(a) (b)

Figure 7.9: High scale Higgs quartic couplings d_2 and δ with their corresponding β-functions, in the DM phase. Parameter points pass the theoretical and experimental constraints of Section 7.1, including dark matter relic density and direct detection constraints.

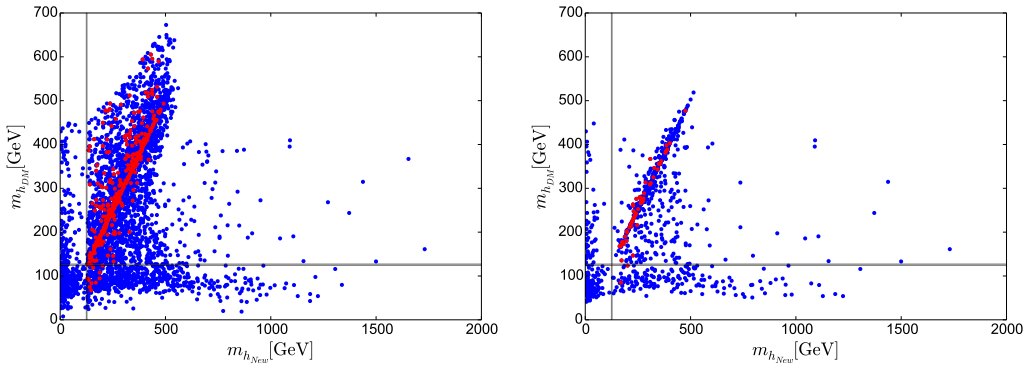

(a) (b)

Figure 7.10: Compatible values of $m_{h_{New}}$ and $m_{h_{DM}}$ in the DM phase for different high scale β_λ constraints. **(a)** includes points that are stable and perturbative up to M_{Pl} and include a SM Higgs candidate, whilst **(b)** also enforces all experimental constraints. All points obey $\lambda < 0.067$ at $M_{\rm Pl}$. Blue points obey $\beta_\lambda < 0.05$ at $M_{\rm Pl}$ while red points obey the more restrictive condition $\beta_\lambda < 0.00005$. The grey bands highlight the SM Higgs mass range.

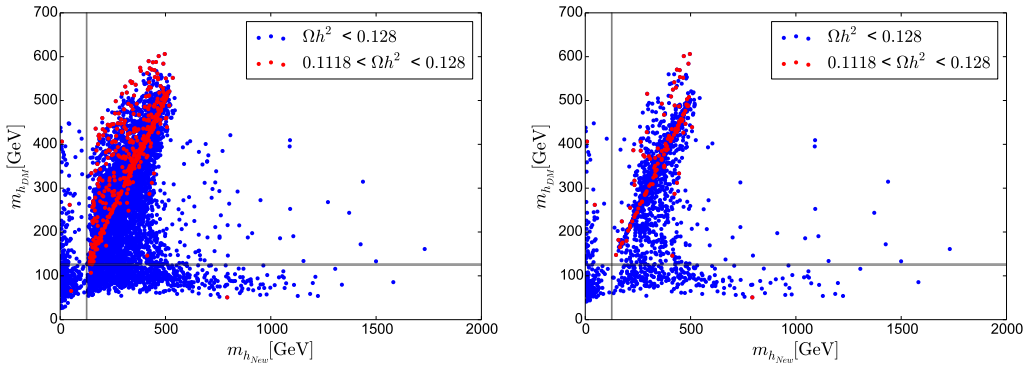

(a) (b)

Figure 7.11: Comparison of dark matter relic density Ωh^2 in the $m_{h_{New}} - m_{h_{DM}}$ plane. Blue points result in $\Omega h^2 < 0.128$ whilst the red points satisfy the stronger constraint $0.1118 < \Omega h^2 < 0.128$. **(a)** includes points that are stable and perturbative up to M_{Pl} and include a SM Higgs candidate, whilst **(b)** also enforces all experimental constraints. The grey band highlights the SM Higgs mass range.

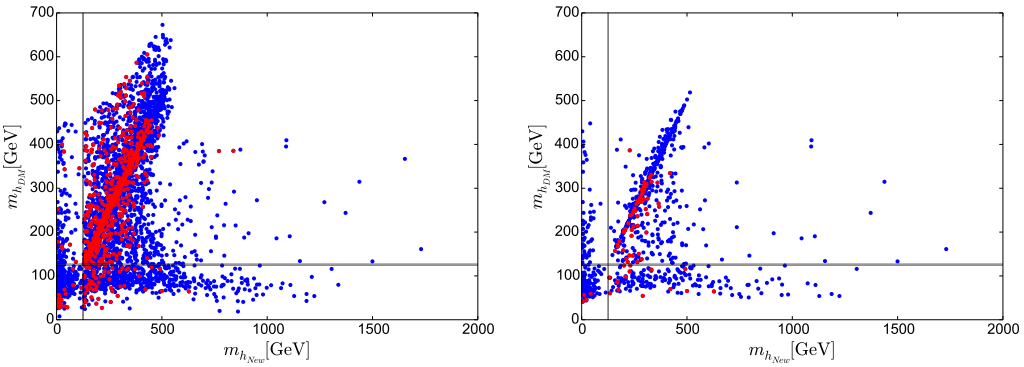

(a) (b)

Figure 7.12: Compatible values of $m_{h_{New}}$ and $m_{h_{DM}}$ in the DM phase with restrictions on β_λ, β_δ and β_{d_2}. **(a)** includes points that are stable and perturbative up to M_{Pl} and include a SM Higgs candidate, whilst **(b)** also enforces all experimental constraints. All points obey $\lambda < 0.067$ at $M_{\rm Pl}$. Blue points obey $\beta_{\lambda,\delta,d_2} < 0.05$ at $M_{\rm Pl}$ while red points obey $\beta_\lambda < 0.0005$, $\beta_\delta < 0.0025$ and $\beta_{d2} < 0.01$. The grey bands highlight the SM Higgs mass range.

Chapter 8

The Two Higgs Doublet Model

Contents

Another simple way to extend the SM is to add a second Higgs doublet. Supersymmetry is the most common motivation for this addition, but SUSY models often require a fine tuning of parameters or non minimal field content to get a Higgs mass that is compatible with the combined ATLAS and CMS result $m_h = 125.09 \pm 0.23\,\text{GeV}$ [8,15,16]. Non-supersymmetric Two Higgs Doublet Models (THDMs) must account for the seemingly very SM-like nature of the Higgs [8,52–54] and must evade strong experimental bounds on its interactions.

The aim of this chapter is to consider whether the Two Higgs Doublet Model (THDM) can exhibit behaviour that is compatible with both the existence of boundary conditions at the Planck scale and curent theoretical and experimental constraints. We will focus on two varieties of the Two Higgs Doublet Model; the Type-II THDM and the Inert Doublet Model (IDM). The addition of a second scalar doublet complicates the resulting scalar spectrum and new scalar sector interactions can alter the high scale behaviour of the scalar potential.

Here we investigate the parameter space of both the Type-II THDM and the IDM, looking for regions that can satisfy the theoretical constraints of pertubativity, vacuum stability, and the existence of a SM Higgs candidate, as well as the

experimental constraints that come from collider and dark matter experiments. We also look at the high scale behaviour and RGE running of the scalar quartic couplings of both models to determine if they are compatible with high scale boundary conditions and whether there are any associated consequences at low energies.

8.1 The Two Higgs Doublet Model

We will investigate the Two Higgs Doublet (THDM), specifically the effects of high scale boundary conditions on its phenomenological viability at low energies. We begin by considering the most general potential of the THDM

$$\begin{aligned} V\left(H_1, H_2\right) \quad &= m_{11}^2 H_1^\dagger H_1 + m_{22}^2 H_2^\dagger H_2 - \left(m_{12}^2 H_1^\dagger H_2 + h.c\right) + \lambda_1 \left(H_1^\dagger H_1\right)^2 \\ &+ \lambda_2 \left(H_2^\dagger H_2\right)^2 + \lambda_3 \left(H_1^\dagger H_1\right)\left(H_2^\dagger H_2\right) + \lambda_4 \left(H_1^\dagger H_2\right)\left(H_2^\dagger H_1\right) \\ &+ \left(\frac{\lambda_5}{2}\left(H_1^\dagger H_2\right)^2 + \lambda_6 \left(H_1^\dagger H_1\right)\left(H_1^\dagger H_2\right) + \lambda_7 \left(H_2^\dagger H_2\right)\left(H_1^\dagger H_2\right) + h.c\right) \end{aligned} \tag{8.1}$$

where

$$H_n = \begin{pmatrix} \chi_n^+ \\ \left(H_n^0 + iA_n^0\right)/\sqrt{2} \end{pmatrix}, \quad n = 1, 2 \tag{8.2}$$

The parameters m_{11}^2, m_{22}^2 and $\lambda_{1,2,3,4}$ are real, whilst m_{12}^2 and $\lambda_{5,6,7}$ can in principle be complex and induce CP violation. During electroweak symmetry breaking the neutral components of the Higgs fields H_n^0 develop vacuum expectation values $\langle H_n \rangle = v_n/\sqrt{2}$. The relationship to the SM vev $v = \sqrt{v_1^2 + v_2^2} = 246\,\text{GeV}$ is determined by the Fermi constant but the ratio of the vevs, $\tan\beta = v_2/v_1$, is a free parameter. The physical scalar sector of the model includes two neutral scalar Higgs h and H, a pseudoscalar Higgs A and the charged Higgs $H^\pm$.

Its clear that the THDM potential is considerably more complicated than its Standard Model counterpart, so it is common to employ additional global symmetries to increase the predictivity of the model. One particularly interesting feature of the THDM scalar potential is that there are only six possible types of global symmetry that have a distinctive effect on the potential [140, 141]. Table 8.1 describes each of these symmetries as well as the associated values of the potential parameters. In this work we implement a $\mathbb{Z}_2$ symmetry to forbid Flavour Changing Neutral Currents (FCNCs) by allowing only one type of fermion to couple to

Symmetry	m_{11}^2	m_{22}^2	m_{12}^2	λ_1	λ_2	λ_3	λ_4	λ_5	λ_6	λ_7
U(2)		m_{11}^2	0		λ_1		$\lambda_1 - \lambda_3$	0	0	0
CP3		m_{11}^2	0		λ_1			$\lambda_1 - \lambda_3 - \lambda_4$	0	0
CP2		m_{11}^2	0		λ_1					$-\lambda_6$
U(1)			0					0	0	0
Z_2			0						0	0
CP1			real					real	real	real

Table 8.1: The six possible symmetries of the scalar potential of the THDM and the corresponding relations between parameters in Eq 8.2.

	u quarks	d quarks	leptons
Type-I	H_2	H_2	H_2
Type-II	H_2	H_1	H_1
Lepton-specific	H_2	H_2	H_1
Flipped	H_1	H_1	H_2

Table 8.2: Possible Yukawa assignments in the $\mathbb{Z}_2$ symmetric THDM.

one Higgs doublet, however we allow the soft $\mathbb{Z}_2$-breaking term m_{12} to be real and non-zero. There are four distinct CP conserving scenarios, summarised in table 8.2, that arise from different $\mathbb{Z}_2$ charge assignments. In this work we will focus on the Type-II case.

For each parameter point the model is described by the bilinear terms m_{11} and m_{22}, which are fixed via the electroweak vacuum minimisation conditions, as well as the input parameters,

$$m_{12}, \quad \tan\beta, \quad \lambda_1(M_{Pl}), \quad \lambda_2(M_{Pl}), \quad \lambda_3(M_{Pl}), \quad \lambda_4(M_{Pl}), \quad \lambda_5(M_{Pl}). \tag{8.3}$$

We also use the top pole mass m_t and the strong coupling constant $\alpha_S(M_Z)$ as input parameters, allowing them to vary between $\pm 3\sigma$ of their central values to account for the effect of their uncertainty on our results. Since we are interested in both the high and low scale behaviour of the potential parameters of the THDM we use SARAH [17] to calculate the two-loop β functions, which are used by FlexibleSUSY [18–21] to run the couplings between M_Z and M_{Pl}.

8.2 The Inert Doublet Model

We can simplify the Two Higgs Doublet Model further by introducing an additional unbroken $\mathbb{Z}_2$ symmetry, under which the new Higgs Doublet has odd parity whilst all other fields have even parity. The scalar sector now consists of the SM Higgs field H and an inert doublet Φ, where Yukawa couplings between the fermions and the inert field are forbidden by the new symmetry. The inert doublet does not gain a vacuum expectation value. The scalar potential is,

$$\begin{aligned} V(H,\Phi) \quad &= m_{11}^2 H^\dagger H + m_{22}^2 \Phi^\dagger \Phi + \lambda_1 \left(H^\dagger H\right)^2 + \lambda_2 \left(\Phi^\dagger \Phi\right)^2 \\ &+ \lambda_3 \left(H^\dagger H\right)\left(\Phi^\dagger \Phi\right) + \lambda_4 \left(H^\dagger \Phi\right)\left(\Phi^\dagger H\right) + \left(\frac{\lambda_5}{2}\left(H^\dagger \Phi\right)^2 + h.c\right). \end{aligned} \tag{8.4}$$

Once again the quartic coupling can have complex values, but in this work we will focus on the real-valued case. During electroweak symmetry breaking the neutral component of the SM Higgs doublet acquires a vacuum expectation value $v \approx 246\,\text{GeV}$. In the Inert doublet case the neutral Higgs h corresponds to the SM Higgs boson whilst H, A and $H^\pm$ are inert scalars. The lightest of these h_{LOP} (Lightest Odd Particle) is stable thanks to the $\mathbb{Z}_2$ symmetry and, assuming h_{LOP} is one of the neutral scalars H or A, it is a potential Dark Matter (DM) candidate.

The tree-level masses for the scalars are given by [142],

$$\begin{aligned} m_h^2 &= m_{11}^2 + 3\lambda_1 v^2 \\ m_H^2 &= m_{22}^2 + \frac{1}{2}\left(\lambda_3 + \lambda_4 + \lambda_5\right) v^2 \\ m_A^2 &= m_{22}^2 + \frac{1}{2}\left(\lambda_3 + \lambda_4 - \lambda_5\right) v^2 \\ m_{H^\pm}^2 &= m_{22}^2 + \frac{1}{2}\lambda_3 v^2. \end{aligned} \tag{8.5}$$

In this model we fix the mass term associated with the SM Higgs doublet m_{11}^2 via the electroweak minimisation conditions. Each point is then described by the remaining input parameters,

$$m_{22}, \quad \lambda_1\left(M_{Pl}\right), \quad \lambda_2\left(M_{Pl}\right), \quad \lambda_3\left(M_{Pl}\right), \quad \lambda_4\left(M_{Pl}\right), \quad \lambda_5\left(M_{Pl}\right). \tag{8.6}$$

As in the Type-II model, we use SARAH and FlexibleSUSY to calculate the mass spectrum and to run couplings between the low and high scales of interest.

Type-II Model Input	
$\lambda_{1,2}\,(M_{Pl})$	$0.0 - 1.0$
$\lambda_{3,4}\,(M_{Pl})$	$-1.0 - 1.0$
$\lambda_{5,6,7}\,(M_{Pl})$	0.0
m_{12}	$0.0 - 2000$ GeV
$\tan\beta$	$2.0 - 50$

Inert Model Input	
$\lambda_{1,2}\,(M_{Pl})$	$0.0 - 1.0$
$\lambda_{3,4}\,(M_{Pl})$	$-1.0 - 1.0$
$\lambda_{5}\,(M_{Pl})$	0.0
m_{22}	$0.0 - 2000$ GeV

Table 8.3: Input parameter ranges for the numerical analysis of the **(left)** Type-II Two Higgs Doublet Model and **(right)** Inert Doublet Model.

8.3 Numerical Analysis and Constraints

The main focus of this work is the possibility and consequences of boundary conditions on all or some of the quartic couplings of the THDM and the IDM and their β functions at the Planck scale,

$$\lambda_i\,(M_{Pl})\,, \beta_{\lambda_i}\,(M_{Pl}) = 0, \quad i = 1\ldots 5. \tag{8.7}$$

We use SARAH 4.12.2 [17] to calculate all of the model parameters, including mass matrices, tadpole equations, vertices and loop corrections, as well as the two-loop β functions for each model. FlexibleSUSY 2.0.1 [18–21] uses this output to calculate the mass spectrum and to run the couplings between M_Z and The Planck scale. Table 8.3 shows the input parameter ranges used in our scans for both the Type-II and Inert models.

Valid points in our parameter space scan must be perturbative up to the Planck scale. For the Higgs quartic couplings this requires them to satisfy $\lambda_i < \sqrt{4\pi}$ up to M_{Pl}. We require points that are bounded from below at all scales up to M_{Pl}. To that end we check if the boundedness conditions [143]

$$\begin{aligned} \lambda_1 &> 0, \\ \lambda_2 &> 0, \\ \lambda_3 &> -2\sqrt{\lambda_1\lambda_2} \\ \lambda_3 + \lambda_4 - |\lambda_5| &> -2\sqrt{\lambda_1\lambda_2} \end{aligned} \tag{8.8}$$

are met at all scales. We also use Vevacious [119] to check if the EWSB minimum is the global minimum. Additionally, we require valid points to provide a SM

Higgs candidate $124.7 \leq m_h \leq 127.1\,\text{GeV}$. This mass range accounts for both the theoretical and experimental uncertainties in the Higgs mass.

Our aim is to find regions of parameter space that are compatible not only with theoretical constraints such as perturbativity, vacuum stability and the SM Higgs mass, but with current experimental constraints. We use 2HDMC 1.7.0 [144] to calculate the relevant branching ratios required by HiggsBounds 4.3.1 [120] to apply 95 % confidence exclusion constraints from LHC Run-I, LEP and the Tevatron. This same input is also used by HiggsSignals 1.4.0 [121] to perform a χ^2 fit to the observed SM signal at the LHC.

In the case of the Inert Doublet Model we apply constraints from analyses of LEP data [142]. Invisible decays of the Z boson are important in the Inert model as the $Z \to HA$ channel is possible. Subsequent decays of the pseudoscalar to a fermion anti-fermion pair $A \to Hf\bar{f}$ and missing energy are in tension with experiment. These decays are required to be small, a constraint that we implemented by requiring [145, 146],

$$M_H + M_A \geq M_Z. \tag{8.9}$$

We also require $\max(M_H, M_A)$ in the inert model to apply limits on the additional neutral Higgs masses from LEP data [147]. Further LEP constraints from searches for charginos and neutralinos are applied to the mass of the charged Higgs by requiring $M_{H^\pm} \geq M_W$. To ensure that our lightest odd particle is a neutral DM candidate we insist on the following relation between the dark sector particles,

$$M_{H^\pm} > \min(M_H, M_A). \tag{8.10}$$

We also look at constraints from electroweak precision observables for both of our models. The S, T and U parameters are calculated using 2HDMC using a reference Higgs mass of $m_h^{ref} = 120\,\text{GeV}$ and the results are checked against the current PDG limits [37],

$$\begin{aligned} S &= 0.05 \pm 0.10 \\ T &= 0.08 \pm 0.12 \\ U &= 0.02 \pm 0.10. \end{aligned} \tag{8.11}$$

Valid points result in values of the precision observables within the $\pm 3\sigma$ range.

In the THDM the existence of the charged Higgs bosons $H^{\pm}$ can affect the calculation of flavour observables. To take this into account we use SuperIso [148–150] to calculate the radiative B meson decay $B \to X_s\gamma$, the leptonic B decays $B_s^0 \to \mu^+\mu^-$, $B_d^0 \to \mu^+\mu^-$, and $B \to \tau\nu$, the leptonic D decays $D \to \mu\nu$, $D_s \to \mu\nu$ and $D_s \to \tau\nu$ as well as the semileptonic decay $B \to D\tau\nu$, the kaon decay $K \to \mu\nu$ and the pion decay $\pi \to \mu\nu$. We then apply 95% confidence level constraints on the branching ratios of these decays.*

In the IDM we use micrOMEGAS [129] to calculate the DM relic density Ωh^2, using the lightest of the neutral scalars H and A as the stable DM candidate. We compare the result to the combined experimental result from the WMAP [123] and Planck [55] experiments,

$$\Omega h^2 = 0.1199 \pm 0.0027. \tag{8.12}$$

We pass points that give a value less than $\Omega h^2 + 3\sigma$ to allow for the possibility that the scalar DM candidate is not the only contribution to the relic density.

Dark matter direct detection experiments place constraints on the spin independent WIMP-nucleon scattering cross-section. The strongest of these comes from LUX [124] which gives constraints that are dependent on the mass of the WIMP DM candidate. We use micrOMEGAS to calculate the scattering cross sections for each of the points in our scan and exclude those that give values greater than the LUX constraints.

8.4 The Multiple Point Principle in the Type-II Two Higgs Doublet Model

We are interested in the high scale behaviour of the quartic couplings and their β functions in Two Higgs Doublet Models which may arise from boundary conditions at the Planck scale. There are a number of possible scenarios that may enforce these conditions. One such scenario is the *Multiple Point Principle* (MPP) [30] which posits that the effective potential has an additional minimum at a high scale such as the Planck scale, degenerate to the electroweak minimum. Applying the MPP in the SM leads to a prediction of the Higgs mass of $m_h = 129 \pm 1.5\,\text{GeV}$ [15], which is not compatible with our current experimental value of m_h but it is close

*Specifically, we use the constraints detailed in Appendix H of the SuperIso manual http://superiso.in2p3.fr/superiso3.4.pdf

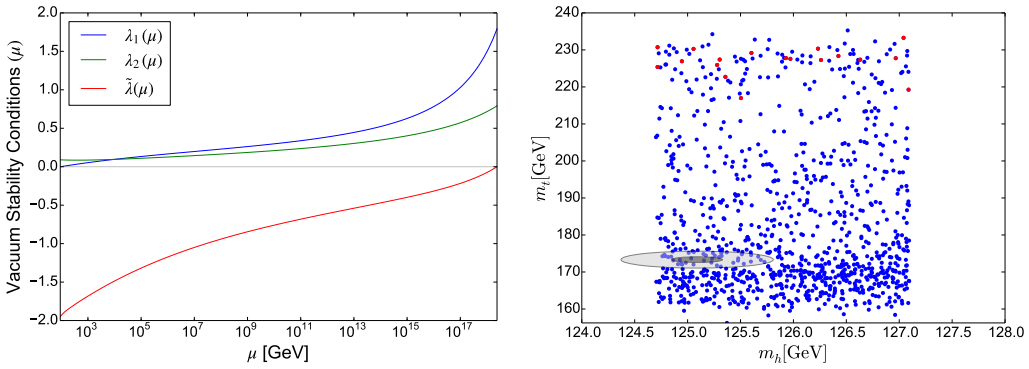

(a) (b)

Figure 8.1: **(a)** Example running of λ_1, λ_2 and $\tilde{\lambda}$ for a point that provides valid masses for the SM Higgs and the top quark in the Type-II Two Higgs Doublet Model. Boundedness from below and vacuum stability requires that all three couplings are positive at all scales. **(b)** Results of our Multiple Point Principle scan in the $m_h - m_t$ plane of the Type-II Two Higgs Doublet Model. The blue points provide valid SM higgs masses whilst the red points also pass the vacuum stability conditions at all scales. The ellipses show the experimentally allowed values of m_t and m_h at $1\,\sigma$ (dark grey) and $3\,\sigma$ (light grey) uncertainty.

enough to have inspired a number of investigations into the MPP in extensions of the SM [69,70,72,151], particularly in the THDM [66–68]. The ideal scenario here would be to have a global minimum at a high scale Λ, degenerate with the electroweak minimum, where all of the quartic couplings are zero at Λ, e.g $\lambda_i = 0, i = 1 \ldots 5$. Unfortunately in this case there is a tension between the renormalisation group running of λ_1 and λ_2 that results in an unstable vacuum configuration [67].

It is possible for degenerate vacua to exist within the THDM if we relax the condition $\lambda_i = 0$. Specifically, by allowing λ_1, λ_2, λ_3 and λ_4 to be non-zero at Λ, then the following conditions are consistent with the implementation of the MPP at Λ;

$$\begin{aligned} \lambda_5(\Lambda) &= 0 \\ \lambda_4(\Lambda) &< 0 \\ \tilde{\lambda}(\Lambda) = \sqrt{\lambda_1\lambda_2} + \lambda_3 + \min(0, \lambda_4) &= 0 \\ \beta_{\tilde{\lambda}}(\Lambda) &= 0. \end{aligned} \tag{8.13}$$

To investigate whether these MPP conditions in the Type-II THDM are consistent with the current experimental constraints on the SM Higgs mass m_h and the top pole mass m_t, we generated points in the parameter space in the manner described in section 8.3, applying the theoretical constraint of vacuum stability at all scales. Figure 8.1a shows an example of the running of λ_1, λ_2 and $\tilde{\lambda}$ for a point that results in experimentally valid values of the SM Higgs mass and the top pole mass, and is also consistent with the MPP conditions 8.14. Vacuum stability requires that all of these couplings remain greater than zero at all scales, but the negative running of $\tilde{\lambda}$ pulls it to negative values. Figure 8.1b shows the results of our investigation in the $m_h - m_t$ plane. The points that satisfy the vacuum stability conditions, highlighted in red, have larger values of the top Yukawa y_t which positively contribute to the running of the quartic couplings. However, the larger y_t corresponds to a top mass in the range $220 \lesssim m_t \lesssim 230\,\text{GeV}$ which is not compatible with current experimental bounds on the top pole mass.

8.5 Asymptotic Safety in the Type-II Two Higgs Doublet Model

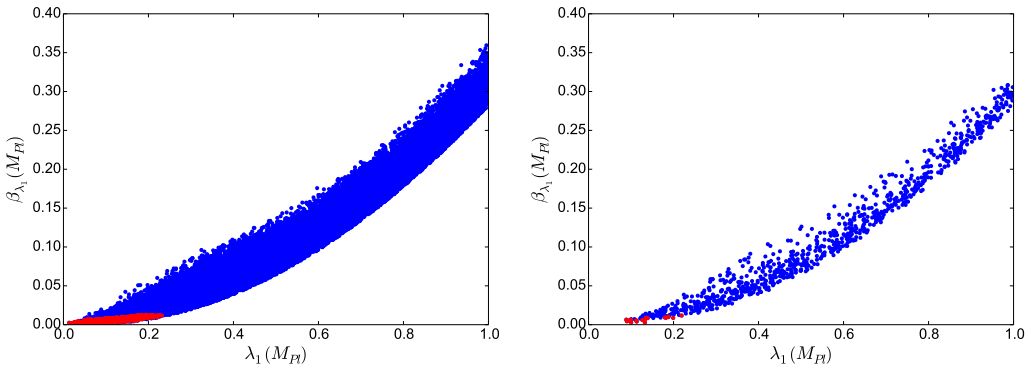

(a) (b)

Figure 8.2: Compatible values of the Higgs quartic coupling $\lambda_1(M_{\text{Pl}})$ against $\beta_{\lambda_1}(M_{\text{Pl}})$ in the Type II Two Higgs Doublet Model. **(a)** includes points that are stable and perturbative up to M_{Pl} and include a SM Higgs candidate, whilst **(b)** also enforces all relevant experimental constraints discussed in section 8.3. Blue points obey $\beta_{\lambda_{1,2,3,4}} < 1.0$ at M_{Pl} whilst red points obey $\beta_{\lambda_1} < 0.0127$, $\beta_{\lambda_2} < 0.0064$, $\beta_{\lambda_3} < 0.0139$, $\beta_{\lambda_4} < 0.0030$ at M_{Pl}.

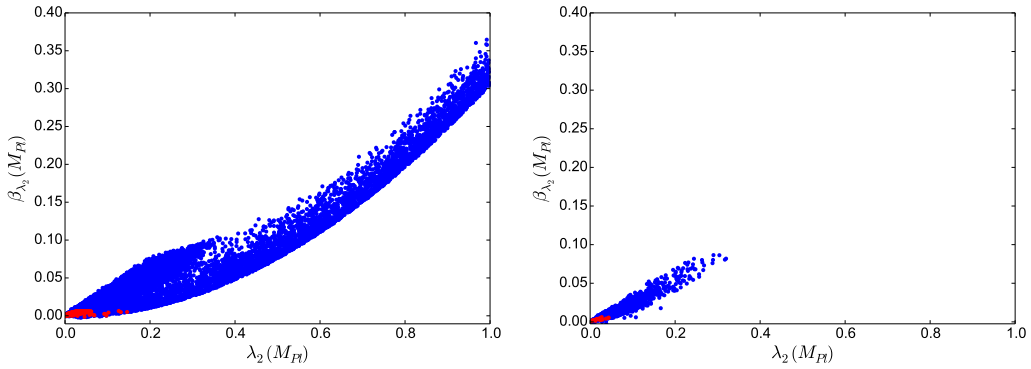

(a) (b)

Figure 8.3: Compatible values of the Higgs quartic coupling $\lambda_2(M_{\rm Pl})$ against $\beta_{\lambda_2}(M_{\rm Pl})$ in the Type II Two Higgs Doublet Model. **(a)** includes points that are stable and perturbative up to M_{Pl} and include a SM Higgs candidate, whilst **(b)** also enforces all relevant experimental constraints discussed in section 8.3. Blue points obey $\beta_{\lambda_{1,2,3,4}} < 1.0$ at M_{Pl} whilst red points obey $\beta_{\lambda_1} < 0.0127$, $\beta_{\lambda_2} < 0.0064$, $\beta_{\lambda_3} < 0.0139$, $\beta_{\lambda_4} < 0.0030$ at M_{Pl}.

Another candidate for the high scale dynamics that enforces high scale boundary conditions is the *Asymptotic Safety* scenario, in which the quartic couplings of the Higgs sector run towards an ultraviolet interacting fixed point [75–82]. This may be caused by gravitational contributions that become significant at very high scales, altering the running of the couplings of the scalar potential [31, 89–92]. In the context of Two Higgs Doublet Models, points in their parameter space that allow for the possibility of a UV fixed point exhibit zero values for the β functions of the Higgs quartic couplings at the Planck scale whilst allowing the couplings themselves to be non-zero. It is important at this stage to be clear on what it means for a β function to be zero. For each of the points in our parameter space scans we perform a perturbative calculation of the RGE evolution of the model couplings, and we accomodate the uncertainty associated with this calculation by allowing for small, non-zero values of the β functions. To estimate this uncertainty in a consistent way we use the difference between parameters at M_{Pl} calculated using one-loop and two-loop RGEs, and we consider a parameter or β function to be zero if it is smaller that this RGE truncation error. In the case of the THDM we calculated the following constraints,

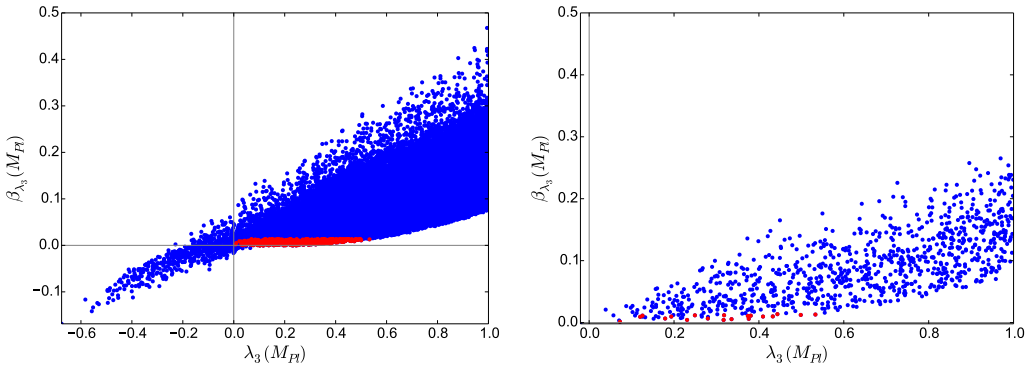

(a) (b)

Figure 8.4: Compatible values of the Higgs quartic coupling $\lambda_3(M_{\rm Pl})$ against $\beta_{\lambda_3}(M_{\rm Pl})$ in the Type II Two Higgs Doublet Model. **(a)** includes points that are stable and perturbative up to M_{Pl} and include a SM Higgs candidate, whilst **(b)** also enforces all relevant experimental constraints discussed in section 8.3. Blue points obey $\beta_{\lambda_{1,2,3,4}} < 1.0$ at M_{Pl} whilst red points obey $\beta_{\lambda_1} < 0.0127$, $\beta_{\lambda_2} < 0.0064$, $\beta_{\lambda_3} < 0.0139$, $\beta_{\lambda_4} < 0.0030$ at M_{Pl}.

$$\begin{aligned} \beta_{\lambda_1}(M_{Pl}) &< 0.0127 \\ \beta_{\lambda_2}(M_{Pl}) &< 0.0064 \\ \beta_{\lambda_3}(M_{Pl}) &< 0.0139 \\ \beta_{\lambda_4}(M_{Pl}) &< 0.0030. \end{aligned} \tag{8.14}$$

We now present the results of our numerical analysis of the Type-II Two Higgs Doublet Model, in which we look for regions of parameter space that are compatible with the high scale boundary conditions that can arise under the asymptotic safety scenario. We apply all of the relevant theoretical and experimental constraints that were described in Section 8.3 as well the $\beta_{\lambda_i} = 0$ constraints shown in Eq. 8.14. Figures 8.2 to 8.5 show the values of the four non-zero quartic Higgs couplings $\lambda_{1,2,3,4}$ and their β functions. The left plots include the theoretical constraints of perturbativity, vacuum stability and a valid SM Higgs candidate, whilst those on the right also include experimental constraints. Points in red provide values of the β functions that are compatible with our asymptotic safety high scale boundary conditions, whilst those in blue do not pass those constraints. Clearly there are regions

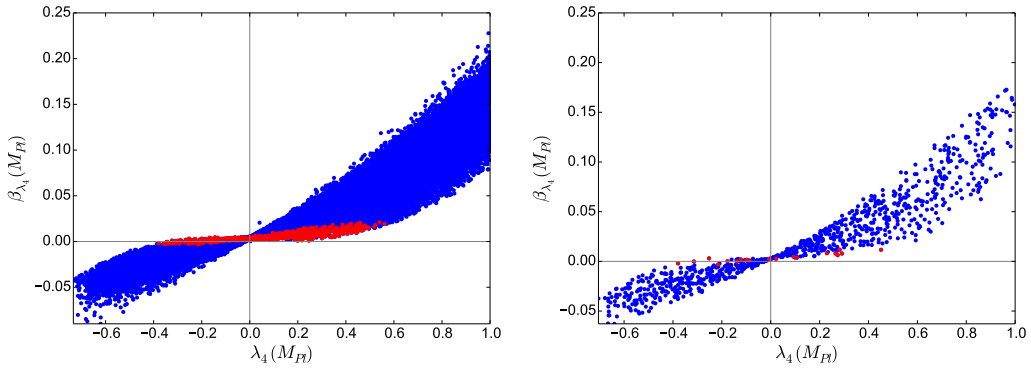

(a) (b)

Figure 8.5: Compatible values of the Higgs quartic coupling $\lambda_4(M_{\rm Pl})$ against $\beta_{\lambda_4}(M_{\rm Pl})$ in the Type II Two Higgs Doublet Model. **(a)** includes points that are stable and perturbative up to M_{Pl} and include a SM Higgs candidate, whilst **(b)** also enforces all relevant experimental constraints discussed in section 8.3. Blue points obey $\beta_{\lambda_{1,2,3,4}} < 1.0$ at M_{Pl} whilst red points obey $\beta_{\lambda_1} < 0.0127$, $\beta_{\lambda_2} < 0.0064$, $\beta_{\lambda_3} < 0.0139$, $\beta_{\lambda_4} < 0.0030$ at M_{Pl}.

of parameter space where all of the β functions of the quartic Higgs couplings are within the truncation errors, even after all of the relevant experimental constraints have been applied. These regions correspond with very small but non-zero values of the quartic couplings at M_{Pl}, which is consistent with a UV interacting fixed point.

Figure 8.6 shows the masses of the heavy neutral scalar m_H against each of the pseudoscalar Higgs mass m_A, whilst Figure 8.7 compares the heavy scalar mass to the charged Higgs mass $m_{H^\pm}$. As the scale associated with the the additional Higgs becomes significantly larger than the electroweak scale, the scalar sector becomes more decoupled and the masses of H, A, and $H^\pm$ become essentially degenerate. A lower limit on the masses of the extra scalars of around $m_{H,A,H^\pm} \approx 330\,\text{GeV}$ is enforced once we apply the collider and flavour constraints. However, the points that are consistent with our high scale β function conditions can have a range of different masses, and those conditions do not seem to apply strong consraints upon the scalar mass spectrum in the Type-II THDM.

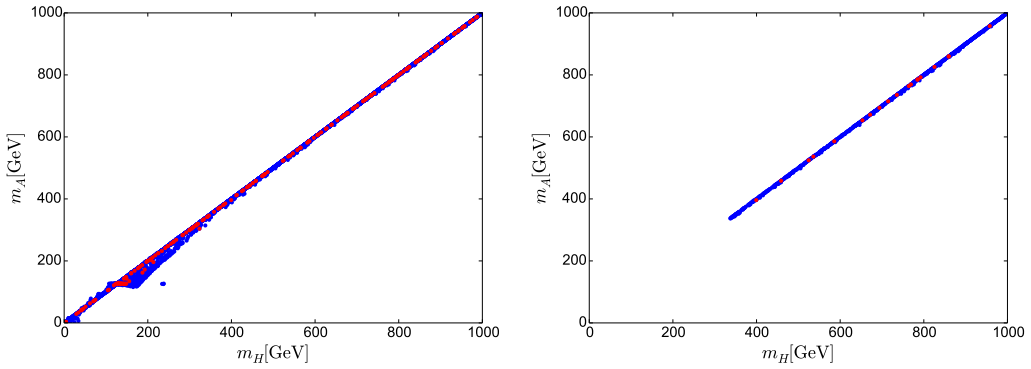

(a) (b)

Figure 8.6: Compatible values of the heavy neutral Higgs mass m_H against the pseudoscalar Higgs m_A in the Type II Two Higgs Doublet Model. **(a)** includes points that are stable and perturbative up to M_{Pl} and include a SM Higgs candidate, whilst **(b)** also enforces all relevant experimental constraints discussed in section 8.3. Blue points obey $\beta_{\lambda_{1,2,3,4}} < 1.0$ at M_{Pl} whilst red points obey $\beta_{\lambda_1} < 0.0127$, $\beta_{\lambda_2} < 0.0064$, $\beta_{\lambda_3} < 0.0139$, $\beta_{\lambda_4} < 0.0030$ at M_{Pl}.

8.6 The Multiple Point Principle in the Inert Doublet Model

In Section 8.4 we discussed the conditions that a THDM parameter point must satisfy to be consistent with the MPP, specifically those detailed in Eq. 8.14. These constraints also apply to the Inert Doublet Model. We performed an IDM parameter space scan in the same way as the Type-II THDM case detailed in Section 8.4. We applied the MPP conditions at M_{Pl} and required valid points to be stable up to the Planck scale and to have a SM Higgs candidate. Figure 8.8 shows the running of the quartic couplings λ_1, λ_2 and $\tilde{\lambda}$ for a point in our scan that provided a valid SM Higgs and top mass. As in the Type-II model, a stable vacuum requires all three of these couplings to be positive at all scales. Clearly this point fails our vacuum stability test, and unfortunately it is representative of the other points in our scan. We found no points that could simultaneously satisfy the constraints of perturbativity, vacuum stability and the requirement of a realistic SM mass spectrum. Specifically, there are points that provide valid SM Higgs and top masses, but all of these points fail under the condition $\tilde{\lambda} > 0$. In fact, we found no points that could satisfy the MPP conditions outlined in Eq. 8.14 that remained stable up to the Planck

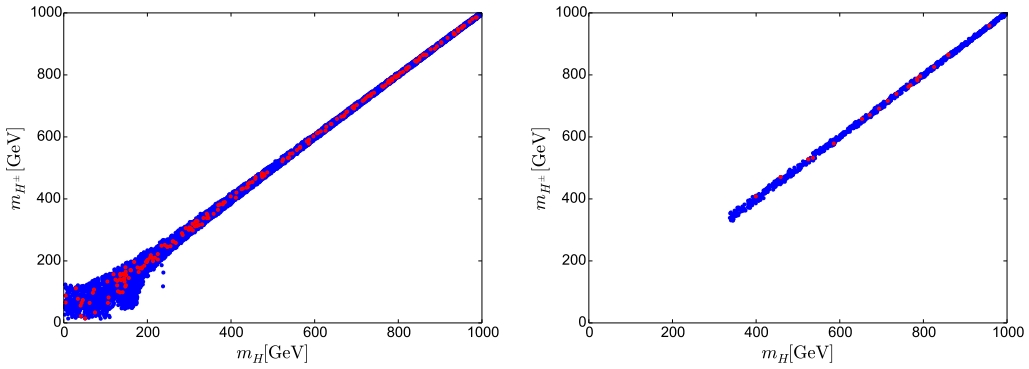

(a) (b)

Figure 8.7: Compatible values of the heavy neutral Higgs mass m_H against the charged Higgs $m_{H^\pm}$ in the Type II Two Higgs Doublet Model. **(a)** includes points that are stable and perturbative up to M_{Pl} and include a SM Higgs candidate, whilst **(b)** also enforces all relevant experimental constraints discussed in section 8.3. Blue points obey $\beta_{\lambda_{1,2,3,4}} < 1.0$ at M_{Pl} whilst red points obey $\beta_{\lambda_1} < 0.0127$, $\beta_{\lambda_2} < 0.0064$, $\beta_{\lambda_3} < 0.0139$, $\beta_{\lambda_4} < 0.0030$ at M_{Pl}.

scale, regardless of their Higgs or top masses. Our results therefore suggest that the multiple point principle cannot be implemented successfully in the Inert Doublet Model.

8.7 Asymptotic Safety in the Inert Doublet Model

We now present the results of our numerical analysis of the Inert Doublet Model. Figures 8.9 to 8.12 show points in the $\lambda_i - \beta_{\lambda_i}$ plane that satisfy both our theoretical and experimental constraints as well as the asymptotic safety high scale boundary conditions of Eq. 8.14. The situation is somewhat similar to the Type-II case discussed in 8.5, inasmuch as there are points in the parameter space that are compatible with the asymptotic safety scenario and that those points have very small values of the quartic couplings.

Figure 8.13 shows the allowed masses of the dark matter candidate m_{LOP} and the charged Higgs mass $m_{H^\pm}$. The requirement that the LOP account for the dark matter relic density and the results from dark matter direct detection experiments places a lower limit on the LOP mass of $m_{LOP} \approx 40\,\text{GeV}$. The relationship between the masses of the additional scalars and the high scale boundary conditions imposed

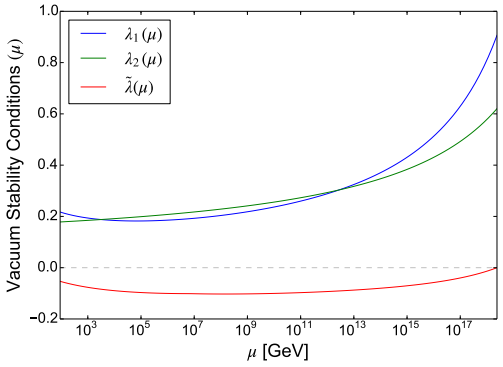

Figure 8.8: Example running of λ_1, λ_2 and $\tilde{\lambda}$ for a point that provides valid masses for the SM Higgs and the top quark in the Inert Doublet Model. Boundedness from below and vacuum stability requires that all three couplings are positive at all scales.

by asymptotic safety is similar to that which we found in the Type-II case, in that those points that meet those constraints were found to have a range of possible masses. It appears from our results that the existence of an interacting UV fixed point for the quartic couplings is valid under both the Type-II model and the Inert model, and that it places constraints on the high scale values of the quartic couplings, however it does not seem to place strong constraints on the possible masses of the new scalars.

8.8 Conclusions

We have investigated the Type-II Two Higgs Doublet Model and the Inert Doublet Model with a focus on possible constraints on the quartic Higgs couplings and their β functions as the Planck scale. These high scale conditions may be a consequence of a second minimum in the potential that is degenerate with the electroweak minimum, as is the case in the Multiple Point Principle, or they may be due to the couplings running towards an interacting UV fixed point at M_{Pl}, as is the case under Aysmptotic Safety. In this work we have examined each of these models for their viability under the constraints that would be evident if either of these scenarios described high scale dynamics in nature. We also checked for their compatibility under the theoretical constraints of perturbativity, vacuum stability, and the necessity of a SM Higgs candidate, as well as experimental constraints such as those from colliders, flavour physics and dark matter experiments.

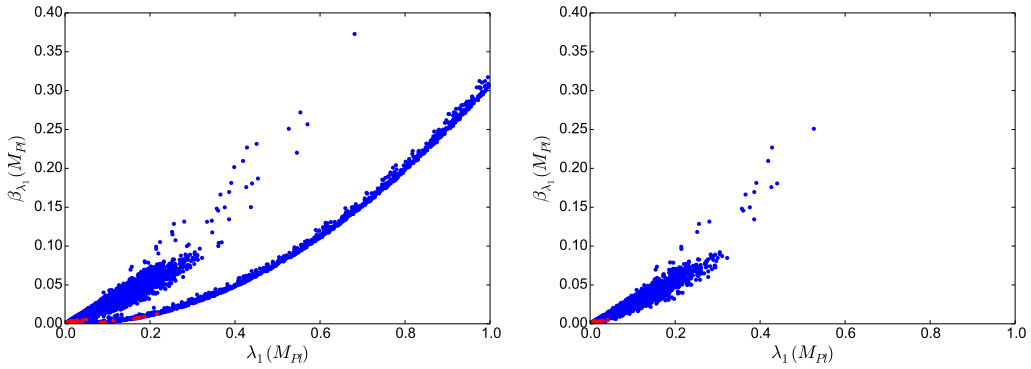

(a) (b)

Figure 8.9: Compatible values of the Higgs quartic coupling $\lambda_1(M_{\rm Pl})$ against $\beta_{\lambda_1}(M_{\rm Pl})$ in the Inert Doublet Model. **(a)** includes points that are stable and perturbative up to M_{Pl} and include a SM Higgs candidate, whilst **(b)** also enforces all relevant experimental constraints discussed in section 8.3. Blue points obey $\beta_{\lambda_{1,2,3,4}} < 1.0$ at M_{Pl} whilst red points obey $\beta_{\lambda_1} < 0.0127$, $\beta_{\lambda_2} < 0.0064$, $\beta_{\lambda_3} < 0.0139$, $\beta_{\lambda_4} < 0.0030$ at M_{Pl}.

Models with a second Higgs doublet have much more flexibility in their scalar potential, which opens up the possibilities for how they can satisfy the boundary conditions that are required by the MPP or by asymptotic safety. However, we found that both the Type-II model and the Inert Doublet Model cannot satisfy the conditions that would be imposed by the degenerate second vacuum at the Planck scale of the MPP scenario. Specifically, we found no points in either model's parameter space that was consistent with the MPP whilst also having a valid SM Higgs, an experimentally acceptable top quark mass, and a stable vacuum. In the Type-II case we found that a stable vacuum would require a top mass on the order of 230 GeV, whilst in the Inert case we found no points at all that could meet our theoretical requirements. The results of our analysis would suggest that the Multiple Point Principle is not compatible with the Two Higgs Doublet Models that we investigated.

The asymptotic safety situation is somewhat better, as our parameter space scans of both models found numerous points that were compatible with theoretical and experimental constraints and also resulted in Planck scale values of the quartic Higgs β functions that were compatible with the high scale condition $\beta_{\lambda_i} = 0$ for $i = 1, \ldots, 5$. These points also have small but non-zero values of the corresponding

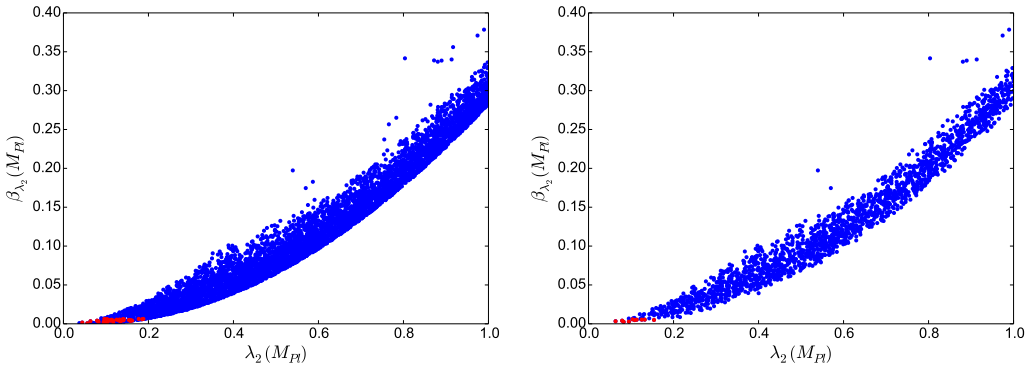

(a) (b)

Figure 8.10: Compatible values of the Higgs quartic coupling $\lambda_2(M_{\rm Pl})$ against $\beta_{\lambda_2}(M_{\rm Pl})$ in the Inert Doublet Model. **(a)** includes points that are stable and perturbative up to M_{Pl} and include a SM Higgs candidate, whilst **(b)** also enforces all relevant experimental constraints discussed in section 8.3. Blue points obey $\beta_{\lambda_{1,2,3,4}} < 1.0$ at M_{Pl} whilst red points obey $\beta_{\lambda_1} < 0.0127$, $\beta_{\lambda_2} < 0.0064$, $\beta_{\lambda_3} < 0.0139$, $\beta_{\lambda_4} < 0.0030$ at M_{Pl}.

quartic couplings, which is entirely in keeping with the existence of an interacting UV fixed point. The type-II case has a lower limit on the masses of the additional scalars of $m_{H,A,H^\pm} \approx 330\,\text{GeV}$ imposed by experimental constraints. In the Inert model the dark matter relic density and direct detectioon experiments place contraints on the mass of the model's dark matter candidate of $m_{LOP} \approx 40\,\text{GeV}$. Although our investigation found regions of parameter space that are compatible with all of our constraints, they correspond to a range of masses for the extra Higgs, with no apparent restriction on those masses coming from the high scale boundary conditions.

Here we have discussed two minimal examples of the Two Higgs Doublet Model class, and a logical next step would be to investigate models that expand upon them. For example, would the situation regarding the Multiple Point Principle be changed if we introduced field content, such as scalar singlets or vector-like fermions?

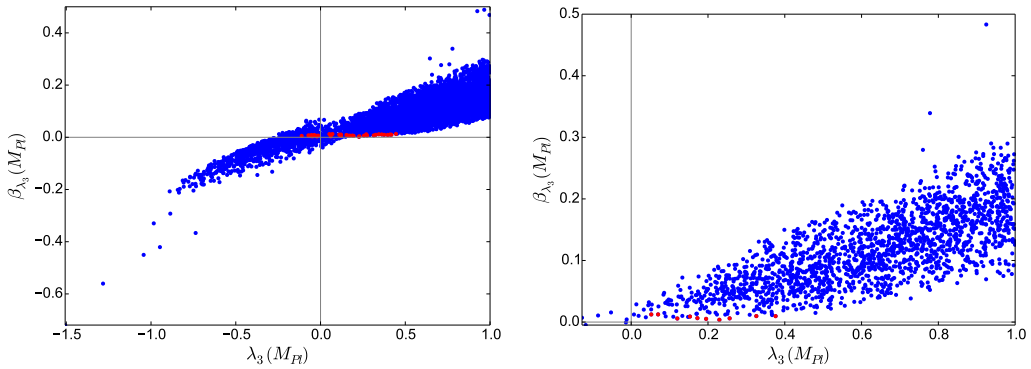

(a) (b)

Figure 8.11: Compatible values of the Higgs quartic coupling $\lambda_3(M_{\rm Pl})$ against $\beta_{\lambda_3}(M_{\rm Pl})$ in the Inert Doublet Model. **(a)** includes points that are stable and perturbative up to M_{Pl} and include a SM Higgs candidate, whilst **(b)** also enforces all relevant experimental constraints discussed in section 8.3. Blue points obey $\beta_{\lambda_{1,2,3,4}} < 1.0$ at M_{Pl} whilst red points obey $\beta_{\lambda_1} < 0.0127$, $\beta_{\lambda_2} < 0.0064$, $\beta_{\lambda_3} < 0.0139$, $\beta_{\lambda_4} < 0.0030$ at M_{Pl}.

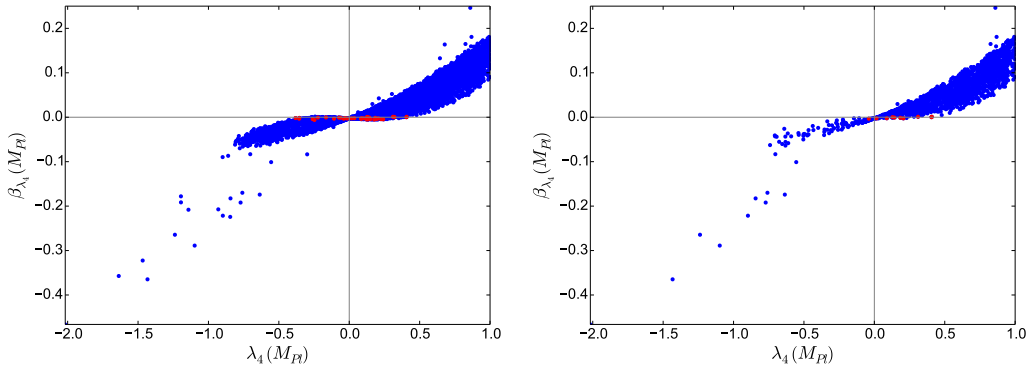

(a) (b)

Figure 8.12: Compatible values of the Higgs quartic coupling $\lambda_4(M_{\rm Pl})$ against $\beta_{\lambda_4}(M_{\rm Pl})$ in the Inert Doublet Model. **(a)** includes points that are stable and perturbative up to M_{Pl} and include a SM Higgs candidate, whilst **(b)** also enforces all relevant experimental constraints discussed in section 8.3. Blue points obey $\beta_{\lambda_{1,2,3,4}} < 1.0$ at M_{Pl} whilst red points obey $\beta_{\lambda_1} < 0.0127$, $\beta_{\lambda_2} < 0.0064$, $\beta_{\lambda_3} < 0.0139$, $\beta_{\lambda_4} < 0.0030$ at M_{Pl}.

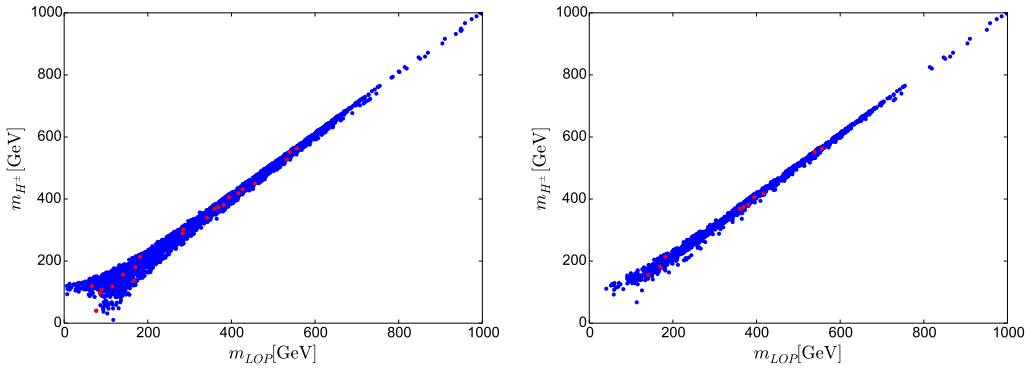

(a) (b)

Figure 8.13: Compatible values of the Lightest Odd Particle mass m_{LOP} against the charged Higgs mass $m_{H^\pm}$ in the Inert Doublet Model. **(a)** includes points that are stable and perturbative up to M_{Pl} and include a SM Higgs candidate, whilst **(b)** also enforces all relevant experimental constraints discussed in section 8.3. Blue points obey $\beta_{\lambda_{1,2,3,4}} < 1.0$ at M_{Pl} whilst red points obey $\beta_{\lambda_1} < 0.0127$, $\beta_{\lambda_2} < 0.0064$, $\beta_{\lambda_3} < 0.0139$, $\beta_{\lambda_4} < 0.0030$ at M_{Pl}.

Chapter 9

Summary and Conclusions

In this thesis we investigated the possibility and consequences of high scale boundary conditions in extensions of the Standard Model. The focus was on what, if any, signatures that new dynamics at the UV scale would leave at energy scales that can be probed by current experiments. We were motivated by the very small value of the Higgs quartic coupling λ in the SM at scales nearing M_{Pl} and by its renormalisation group running, which flattens outs at around the same high scale. These signs could arise due to the existence of a second minimum at M_{Pl}, degenerate with the electroweak minimum, as is predicted by the Multiple Point Principle, or it could be due to an interacting UV fixed point, as in the Asymptotic Safety scenario. We looked at a number of extensions of the SM, specifically the Real Singlet model the Complex Singlet model, the Two Higgs Doublet Model and the Inert Doublet Model. On top of the high scale boundary constraints we also applied a number of model specific theoretical constraints, as well as experimental constraints including collider and dark matter experiments. Here we will summarise our main results.

Real Singlet Model

We studied the possibility of high scale boundary conditions in the broken phase of the real singlet extension of the SM under the following additional constraints: pertubativity, global vacuum stability, the requirement of a SM-like Higgs in the scalar mass spectrum, and collider constraints from the LHC, LEP and the Tevatron. In the dark matter phase of the model we also applied relic density constraints from the combined Planck and WMAP measurements, and direct detection constraints on the spin independent cross section of the DM candidate on nucleons from the LUX experiment. We found that the conditions that are consistent with asymptotic safety, $\beta_\lambda(M_{Pl}) = \beta_{\lambda_S}(M_{Pl}) = \beta_{k_2}(M_{Pl}) = 0$, can be satisfied in both the broken phase and dark matter phases of the model. In the broken phase of the model, in which both scalars are free to mix, we found that the region of parameter space that met all of our constraints corresponded to an additional Higgs mass within the range

$200 \lesssim m_H \lesssim 1000\,\text{GeV}$. There were fewer points in the valid parameter space of the DM phase, with masses between the SM Higgs mass and approximately 500 GeV. This upper limit increases to 1000 GeV if we loosen our β function constraints to account for effects from unknown UV physics.

Complex Singlet Model

As in the real singlet case, the complex singlet model exhibits a broken phase if both the real and imaginary parts of the field gain a vev and the three scalars of the model can mix, as well as a DM phase in which the imaginary part of the complex field is a potential WIMP dark matter candidate. Our investigation found regions of parameter space in both phases that are compatible with theoretical and experimental constraints, as well as our high scale conditions. In the broken phase we found that the majority of valid points had one scalar that was lighter than the SM Higgs and one that was heavier. The majority of valid points in the DM phase have both additional scalars that are heavier than the SM Higgs. The condition $\lambda = \beta_\lambda = 0$ results in upper limits of the heavy Higgs of about 600 GeV in the broken phase and 500 GeV in the DM phase. Scenarios in which all of the quartic couplings and their β functions run to exactly zero at M_{Pl} were found not to be possible because setting the Higgs portal coupling δ to zero at this scale does not allow it to regenerate at lower scales. We found valid regions of parameter space by allowing for small, non-zero values of the quartic β functions to account for uncertainties in the high scale calculation.

Two Higgs Doublet Model

Our investigation of the Type-II Two Higgs Doublet Model included the theoretical constraints of perturbativity, vacuum stability and a SM Higgs, as well as the collider constraints from the LHC, LEP and Tevatron, electroweak precision observable constraints, and those from flavour observables such as $B \to X_s\gamma$. The results of our scan suggested that the potentials of both the Type-II THDM and the Inert Doublet Model cannot accomodate the conditions required by the degenerate minimum at M_{Pl} that is a hallmark of the Multiple Point Principle whilst also providing valid SM Higgs and top quark masses. On the other hand, we found that both models could satisfy the $\beta_{\lambda_i}(M_{Pl}) = 0$ conditions of Asymptotic Safety alongside all of the other constriants. However, while the experimental constraints gave a lower limit on the additional scalars of the Higgs sector of $m_{H,A,H^\pm} \approx 330\,\text{GeV}$, the high scale

boundary conditions appeared not to impose any limits on the scalar mass spectrum.

Further Questions

In this thesis we have focused on models that introduce a somewhat minimal number of extra fields into the scalar sector of the SM, with an eye on their implications for high scale boundary conditions. One could expand upon this work by looking at models with more complicated field content, such as those that contain a larger scalar sector with both singlet and doublet fields, or those with new vector-like fermions. These additions could affect the outlook for both the new UV physics scenarios that were at the centre of our investigations by significantly altering the running of the quartic and Yukawa couplings of the scalar potential. It would also be interesting to look at whether these high scale conditions can be simultaneously reconciled with others, such as gauge coupling unification, or with intermediate scales between the low scale and M_{Pl} that introduce new gauge symmetries. If we could find models that can incorporate these various different concepts it could be used as a stepping stone towards Grand Unifcation Theories that are also compatible with the Multiple Point Principle or Aysmptotic Safety.

Appendix A

The $SU(5)$ Gell-Mann Matrices

$$\lambda_1 = \begin{pmatrix} 0 & 1 & 0 & 0 & 0 \\ 1 & 0 & 0 & 0 & 0 \\ 0 & 0 & 0 & 0 & 0 \\ 0 & 0 & 0 & 0 & 0 \\ 0 & 0 & 0 & 0 & 0 \end{pmatrix}, \quad \lambda_2 = \begin{pmatrix} 0 & -i & 0 & 0 & 0 \\ i & 0 & 0 & 0 & 0 \\ 0 & 0 & 0 & 0 & 0 \\ 0 & 0 & 0 & 0 & 0 \\ 0 & 0 & 0 & 0 & 0 \end{pmatrix}, \quad \lambda_3 = \begin{pmatrix} 1 & 0 & 0 & 0 & 0 \\ 0 & -1 & 0 & 0 & 0 \\ 0 & 0 & 0 & 0 & 0 \\ 0 & 0 & 0 & 0 & 0 \\ 0 & 0 & 0 & 0 & 0 \end{pmatrix}, \tag{A.1}$$

$$\lambda_4 = \begin{pmatrix} 0 & 0 & 1 & 0 & 0 \\ 0 & 0 & 0 & 0 & 0 \\ 1 & 0 & 0 & 0 & 0 \\ 0 & 0 & 0 & 0 & 0 \\ 0 & 0 & 0 & 0 & 0 \end{pmatrix}, \quad \lambda_5 = \begin{pmatrix} 0 & 0 & -i & 0 & 0 \\ 0 & 0 & 0 & 0 & 0 \\ i & 0 & 0 & 0 & 0 \\ 0 & 0 & 0 & 0 & 0 \\ 0 & 0 & 0 & 0 & 0 \end{pmatrix}, \quad \lambda_6 = \begin{pmatrix} 0 & 0 & 0 & 0 & 0 \\ 0 & 0 & 1 & 0 & 0 \\ 0 & 1 & 0 & 0 & 0 \\ 0 & 0 & 0 & 0 & 0 \\ 0 & 0 & 0 & 0 & 0 \end{pmatrix}, \tag{A.2}$$

$$\lambda_7 = \begin{pmatrix} 0 & 0 & 0 & 0 & 0 \\ 0 & 0 & -i & 0 & 0 \\ 0 & i & 0 & 0 & 0 \\ 0 & 0 & 0 & 0 & 0 \\ 0 & 0 & 0 & 0 & 0 \end{pmatrix}, \quad \lambda_8 = \frac{1}{\sqrt{3}} \begin{pmatrix} 1 & 0 & 0 & 0 & 0 \\ 0 & 1 & 0 & 0 & 0 \\ 0 & 0 & -2 & 0 & 0 \\ 0 & 0 & 0 & 0 & 0 \\ 0 & 0 & 0 & 0 & 0 \end{pmatrix}, \quad \lambda_9 = \begin{pmatrix} 0 & 0 & 0 & 1 & 0 \\ 0 & 0 & 0 & 0 & 0 \\ 0 & 0 & 0 & 0 & 0 \\ 1 & 0 & 0 & 0 & 0 \\ 0 & 0 & 0 & 0 & 0 \end{pmatrix}, \tag{A.3}$$

$$\lambda_{10} = \begin{pmatrix} 0 & 0 & 0 & -i & 0 \\ 0 & 0 & 0 & 0 & 0 \\ 0 & 0 & 0 & 0 & 0 \\ i & 0 & 0 & 0 & 0 \\ 0 & 0 & 0 & 0 & 0 \end{pmatrix}, \quad \lambda_{11} = \begin{pmatrix} 0 & 0 & 0 & 0 & 0 \\ 0 & 0 & 0 & 1 & 0 \\ 0 & 0 & 0 & 0 & 0 \\ 0 & 1 & 0 & 0 & 0 \\ 0 & 0 & 0 & 0 & 0 \end{pmatrix}, \quad \lambda_{12} = \begin{pmatrix} 0 & 0 & 0 & 0 & 0 \\ 0 & 0 & 0 & -i & 0 \\ 0 & 0 & 0 & 0 & 0 \\ 0 & i & 0 & 0 & 0 \\ 0 & 0 & 0 & 0 & 0 \end{pmatrix}, \tag{A.4}$$

$$\lambda_{13} = \begin{pmatrix} 0 & 0 & 0 & 0 & 0 \\ 0 & 0 & 0 & 0 & 0 \\ 0 & 0 & 0 & 1 & 0 \\ 0 & 0 & 1 & 0 & 0 \\ 0 & 0 & 0 & 0 & 0 \end{pmatrix}, \quad \lambda_{14} = \begin{pmatrix} 0 & 0 & 0 & 0 & 0 \\ 0 & 0 & 0 & 0 & 0 \\ 0 & 0 & 0 & -i & 0 \\ 0 & 0 & i & 0 & 0 \\ 0 & 0 & 0 & 0 & 0 \end{pmatrix}, \quad \lambda_{15} = \frac{1}{\sqrt{6}} \begin{pmatrix} 1 & 0 & 0 & 0 & 0 \\ 0 & 1 & 0 & 0 & 0 \\ 0 & 0 & 1 & 0 & 0 \\ 0 & 0 & 0 & -3 & 0 \\ 0 & 0 & 0 & 0 & 0 \end{pmatrix}, \tag{A.5}$$

$$\lambda_{16} = \begin{pmatrix} 0 & 0 & 0 & 0 & 1 \\ 0 & 0 & 0 & 0 & 0 \\ 0 & 0 & 0 & 0 & 0 \\ 0 & 0 & 0 & 0 & 0 \\ 1 & 0 & 0 & 0 & 0 \end{pmatrix}, \quad \lambda_{17} = \begin{pmatrix} 0 & 0 & 0 & 0 & -i \\ 0 & 0 & 0 & 0 & 0 \\ 0 & 0 & 0 & 0 & 0 \\ 0 & 0 & 0 & 0 & 0 \\ i & 0 & 0 & 0 & 0 \end{pmatrix}, \quad \lambda_{18} = \begin{pmatrix} 0 & 0 & 0 & 0 & 0 \\ 0 & 0 & 0 & 0 & 1 \\ 0 & 0 & 0 & 0 & 0 \\ 0 & 0 & 0 & 0 & 0 \\ 0 & 1 & 0 & 0 & 0 \end{pmatrix}, \tag{A.6}$$

$$\lambda_{19} = \begin{pmatrix} 0 & 0 & 0 & 0 & 0 \\ 0 & 0 & 0 & 0 & -i \\ 0 & 0 & 0 & 0 & 0 \\ 0 & 0 & 0 & 0 & 0 \\ 0 & i & 0 & 0 & 0 \end{pmatrix}, \quad \lambda_{20} = \begin{pmatrix} 0 & 0 & 0 & 0 & 0 \\ 0 & 0 & 0 & 0 & 0 \\ 0 & 0 & 0 & 0 & 1 \\ 0 & 0 & 0 & 0 & 0 \\ 0 & 0 & 1 & 0 & 0 \end{pmatrix}, \quad \lambda_{21} = \begin{pmatrix} 0 & 0 & 0 & 0 & 0 \\ 0 & 0 & 0 & 0 & 0 \\ 0 & 0 & 0 & 0 & -i \\ 0 & 0 & 0 & 0 & 0 \\ 0 & 0 & i & 0 & 0 \end{pmatrix}, \tag{A.7}$$

$$\lambda_{22} = \begin{pmatrix} 0 & 0 & 0 & 0 & 0 \\ 0 & 0 & 0 & 0 & 0 \\ 0 & 0 & 0 & 0 & 0 \\ 0 & 0 & 0 & 0 & 1 \\ 0 & 0 & 0 & 1 & 0 \end{pmatrix}, \quad \lambda_{23} = \begin{pmatrix} 0 & 0 & 0 & 0 & 0 \\ 0 & 0 & 0 & 0 & 0 \\ 0 & 0 & 0 & 0 & 0 \\ 0 & 0 & 0 & 0 & -i \\ 0 & 0 & 0 & i & 0 \end{pmatrix}, \quad \lambda_{24} = \frac{1}{\sqrt{10}} \begin{pmatrix} 1 & 0 & 0 & 0 & 0 \\ 0 & 1 & 0 & 0 & 0 \\ 0 & 0 & 1 & 0 & 0 \\ 0 & 0 & 0 & 1 & 0 \\ 0 & 0 & 0 & 0 & -4 \end{pmatrix}. \tag{A.8}$$

Appendix B

Renormalisation Group Equations of the Standard Model at Two Loops

---

The β functions of the Standard Model for number of fermions $n_f = 6$, defined for a coupling g as,

$$\beta_g^{(i)} = \frac{\partial g}{\partial \log \mu}, \tag{B.1}$$

where $i = 1, 2, \ldots$ is the loop level, encode how a coupling's value with energy μ. Here we provide the two-loop β functions for all of the SM's dimensionless couplings [56–59].

B.1 Gauge Couplings

$$\beta_{g_1}^{(1)} = \frac{41}{10} g_1^3 \tag{B.2}$$

$$\beta_{g_1}^{(2)} = \frac{1}{50} g_1^3 \Big(135 g_2^2 + 199 g_1^2 - 25 \mathrm{Tr}\Big(Y_d Y_d^\dagger\Big) + 440 g_3^2 - 75 \mathrm{Tr}\Big(Y_e Y_e^\dagger\Big) - 85 \mathrm{Tr}\Big(Y_u Y_u^\dagger\Big) \Big) \tag{B.3}$$

$$\beta_{g_2}^{(1)} = -\frac{19}{6} g_2^3 \tag{B.4}$$

$$\beta_{g_2}^{(2)} = \frac{1}{30} g_2^3 \Big(-15 \mathrm{Tr}\Big(Y_e Y_e^\dagger\Big) + 175 g_2^2 + 27 g_1^2 + 360 g_3^2 - 45 \mathrm{Tr}\Big(Y_d Y_d^\dagger\Big) - 45 \mathrm{Tr}\Big(Y_u Y_u^\dagger\Big) \Big) \tag{B.5}$$

$$\beta_{g_3}^{(1)} = -7 g_3^3 \tag{B.6}$$

$$\beta_{g_3}^{(2)} = -\frac{1}{10} g_3^3 \Big(-11 g_1^2 + 20 \mathrm{Tr}\Big(Y_d Y_d^\dagger\Big) + 20 \mathrm{Tr}\Big(Y_u Y_u^\dagger\Big) + 260 g_3^2 - 45 g_2^2 \Big) \tag{B.7}$$

B.2 Quartic scalar couplings

$$\begin{aligned}\beta_\lambda^{(1)} &= +\frac{27}{100}g_1^4 + \frac{9}{10}g_1^2g_2^2 + \frac{9}{4}g_2^4 - \frac{9}{5}g_1^2\lambda - 9g_2^2\lambda + 12\lambda^2 + 12\lambda\mathrm{Tr}\Big(Y_dY_d^\dagger\Big) + 4\lambda\mathrm{Tr}\Big(Y_eY_e^\dagger\Big) \\ &\quad + 12\lambda\mathrm{Tr}\Big(Y_uY_u^\dagger\Big) - 12\mathrm{Tr}\Big(Y_dY_d^\dagger Y_dY_d^\dagger\Big) - 4\mathrm{Tr}\Big(Y_eY_e^\dagger Y_eY_e^\dagger\Big) - 12\mathrm{Tr}\Big(Y_uY_u^\dagger Y_uY_u^\dagger\Big) \qquad \text{(B.8)}\end{aligned}$$

$$\begin{aligned}\beta_\lambda^{(2)} &= -\frac{3411}{1000}g_1^6 - \frac{1677}{200}g_1^4g_2^2 - \frac{289}{40}g_1^2g_2^4 + \frac{305}{8}g_2^6 + \frac{1887}{200}g_1^4\lambda + \frac{117}{20}g_1^2g_2^2\lambda - \frac{73}{8}g_2^4\lambda + \frac{54}{5}g_1^2\lambda^2 + 54g_2^2\lambda^2 \\ &\quad - 78\lambda^3 + \frac{1}{10}\Big(225g_2^2\lambda - 45g_2^4 + 80\Big(10g_3^2 - 9\lambda\Big)\lambda + 9g_1^4 + g_1^2\Big(25\lambda + 54g_2^2\Big)\Big)\mathrm{Tr}\Big(Y_dY_d^\dagger\Big) \\ &\quad - \frac{3}{10}\Big(15g_1^4 + 5\Big(16\lambda^2 - 5g_2^2\lambda + g_2^4\Big) - g_1^2\Big(22g_2^2 + 25\lambda\Big)\Big)\mathrm{Tr}\Big(Y_eY_e^\dagger\Big) - \frac{171}{50}g_1^4\mathrm{Tr}\Big(Y_uY_u^\dagger\Big) \\ &\quad + \frac{63}{5}g_1^2g_2^2\mathrm{Tr}\Big(Y_uY_u^\dagger\Big) - \frac{9}{2}g_2^4\mathrm{Tr}\Big(Y_uY_u^\dagger\Big) + \frac{17}{2}g_1^2\lambda\mathrm{Tr}\Big(Y_uY_u^\dagger\Big) + \frac{45}{2}g_2^2\lambda\mathrm{Tr}\Big(Y_uY_u^\dagger\Big) \\ &\quad + 80g_3^2\lambda\mathrm{Tr}\Big(Y_uY_u^\dagger\Big) - 72\lambda^2\mathrm{Tr}\Big(Y_uY_u^\dagger\Big) + \frac{8}{5}g_1^2\mathrm{Tr}\Big(Y_dY_d^\dagger Y_dY_d^\dagger\Big) - 64g_3^2\mathrm{Tr}\Big(Y_dY_d^\dagger Y_dY_d^\dagger\Big) \\ &\quad - 3\lambda\mathrm{Tr}\Big(Y_dY_d^\dagger Y_dY_d^\dagger\Big) - 42\lambda\mathrm{Tr}\Big(Y_dY_u^\dagger Y_uY_d^\dagger\Big) - \frac{24}{5}g_1^2\mathrm{Tr}\Big(Y_eY_e^\dagger Y_eY_e^\dagger\Big) - \lambda\mathrm{Tr}\Big(Y_eY_e^\dagger Y_eY_e^\dagger\Big) \\ &\quad - \frac{16}{5}g_1^2\mathrm{Tr}\Big(Y_uY_u^\dagger Y_uY_u^\dagger\Big) - 64g_3^2\mathrm{Tr}\Big(Y_uY_u^\dagger Y_uY_u^\dagger\Big) - 3\lambda\mathrm{Tr}\Big(Y_uY_u^\dagger Y_uY_u^\dagger\Big) + 60\mathrm{Tr}\Big(Y_dY_d^\dagger Y_dY_d^\dagger Y_dY_d^\dagger\Big) \\ &\quad - 24\mathrm{Tr}\Big(Y_dY_d^\dagger Y_dY_u^\dagger Y_uY_d^\dagger\Big) + 12\mathrm{Tr}\Big(Y_dY_u^\dagger Y_uY_d^\dagger Y_dY_d^\dagger\Big) - 12\mathrm{Tr}\Big(Y_dY_u^\dagger Y_uY_u^\dagger Y_uY_d^\dagger\Big) \\ &\quad + 20\mathrm{Tr}\Big(Y_eY_e^\dagger Y_eY_e^\dagger Y_eY_e^\dagger\Big) + 60\mathrm{Tr}\Big(Y_uY_u^\dagger Y_uY_u^\dagger Y_uY_u^\dagger\Big) \qquad \text{(B.9)}\end{aligned}$$

B.3 Yukawa Couplings

$$\begin{aligned}\beta_{Y_u}^{(1)} &= -\frac{3}{2}\Big(-Y_uY_u^\dagger Y_u + Y_uY_d^\dagger Y_d\Big) \\ &\quad + Y_u\Big(3\mathrm{Tr}\Big(Y_dY_d^\dagger\Big) + 3\mathrm{Tr}\Big(Y_uY_u^\dagger\Big) - 8g_3^2 - \frac{17}{20}g_1^2 - \frac{9}{4}g_2^2 + \mathrm{Tr}\Big(Y_eY_e^\dagger\Big)\Big) \qquad \text{(B.10)} \\ \beta_{Y_u}^{(2)} &= +\frac{1}{80}\Big(20\Big(11Y_uY_d^\dagger Y_dY_d^\dagger Y_d - 4Y_uY_u^\dagger Y_uY_d^\dagger Y_d + 6Y_uY_u^\dagger Y_uY_u^\dagger Y_u - Y_uY_d^\dagger Y_dY_u^\dagger Y_u\Big) \\ &\quad + Y_uY_u^\dagger Y_u\Big(1280g_3^2 - 180\mathrm{Tr}\Big(Y_eY_e^\dagger\Big) + 223g_1^2 - 480\lambda - 540\mathrm{Tr}\Big(Y_dY_d^\dagger\Big) - 540\mathrm{Tr}\Big(Y_uY_u^\dagger\Big) + 675g_2^2\Big) \\ &\quad + Y_uY_d^\dagger Y_d\Big(100\mathrm{Tr}\Big(Y_eY_e^\dagger\Big) - 1280g_3^2 + 300\mathrm{Tr}\Big(Y_dY_d^\dagger\Big) + 300\mathrm{Tr}\Big(Y_uY_u^\dagger\Big) - 43g_1^2 + 45g_2^2\Big)\Big) \\ &\quad + \frac{1}{600}Y_u\Big(1187g_1^4 - 270g_1^2g_2^2 - 3450g_2^4 + 760g_1^2g_3^2 + 5400g_2^2g_3^2 - 64800g_3^4 + 900\lambda^2 \\ &\quad + 375\Big(32g_3^2 + 9g_2^2 + g_1^2\Big)\mathrm{Tr}\Big(Y_dY_d^\dagger\Big) + 1125\Big(g_1^2 + g_2^2\Big)\mathrm{Tr}\Big(Y_eY_e^\dagger\Big) + 1275g_1^2\mathrm{Tr}\Big(Y_uY_u^\dagger\Big) \\ &\quad + 3375g_2^2\mathrm{Tr}\Big(Y_uY_u^\dagger\Big) + 12000g_3^2\mathrm{Tr}\Big(Y_uY_u^\dagger\Big) - 4050\mathrm{Tr}\Big(Y_dY_d^\dagger Y_dY_d^\dagger\Big) + 900\mathrm{Tr}\Big(Y_dY_u^\dagger Y_uY_d^\dagger\Big) \\ &\quad - 1350\mathrm{Tr}\Big(Y_eY_e^\dagger Y_eY_e^\dagger\Big) - 4050\mathrm{Tr}\Big(Y_uY_u^\dagger Y_uY_u^\dagger\Big)\Big) \qquad \text{(B.11)}\end{aligned}$$

$$\beta_{Y_d}^{(1)} = \frac{1}{4}\Big(6\Big(- Y_d Y_u^\dagger Y_u + Y_d Y_d^\dagger Y_d\Big) - Y_d\Big(- 12\mathrm{Tr}\Big(Y_d Y_d^\dagger\Big) - 12\mathrm{Tr}\Big(Y_u Y_u^\dagger\Big) + 32 g_3^2 - 4\mathrm{Tr}\Big(Y_e Y_e^\dagger\Big) + 9 g_2^2 + g_1^2\Big)\Big) \tag{B.12}$$

$$\begin{aligned}\beta_{Y_d}^{(2)} = &+\frac{1}{80}\Big(20\Big(11 Y_d Y_u^\dagger Y_u Y_u^\dagger Y_u - 4 Y_d Y_d^\dagger Y_d Y_u^\dagger Y_u + 6 Y_d Y_d^\dagger Y_d Y_d^\dagger Y_d - Y_d Y_u^\dagger Y_u Y_d^\dagger Y_d\Big) \\ &+ Y_d Y_d^\dagger Y_d\Big(1280 g_3^2 - 180\mathrm{Tr}\Big(Y_e Y_e^\dagger\Big) + 187 g_1^2 - 480\lambda - 540\mathrm{Tr}\Big(Y_d Y_d^\dagger\Big) - 540\mathrm{Tr}\Big(Y_u Y_u^\dagger\Big) + 675 g_2^2\Big) \\ &+ Y_d Y_u^\dagger Y_u\Big(100\mathrm{Tr}\Big(Y_e Y_e^\dagger\Big) - 1280 g_3^2 + 300\mathrm{Tr}\Big(Y_d Y_d^\dagger\Big) + 300\mathrm{Tr}\Big(Y_u Y_u^\dagger\Big) + 45 g_2^2 - 79 g_1^2\Big)\Big) \\ &+ Y_d\Big(- \frac{127}{600} g_1^4 - \frac{27}{20} g_1^2 g_2^2 - \frac{23}{4} g_2^4 + \frac{31}{15} g_1^2 g_3^2 + 9 g_2^2 g_3^2 - 108 g_3^4 + \frac{3}{2}\lambda^2 \\ &+ \frac{5}{8}\Big(32 g_3^2 + 9 g_2^2 + g_1^2\Big)\mathrm{Tr}\Big(Y_d Y_d^\dagger\Big) + \frac{15}{8}\Big(g_1^2 + g_2^2\Big)\mathrm{Tr}\Big(Y_e Y_e^\dagger\Big) + \frac{17}{8} g_1^2\mathrm{Tr}\Big(Y_u Y_u^\dagger\Big) + \frac{45}{8} g_2^2\mathrm{Tr}\Big(Y_u Y_u^\dagger\Big) \\ &+ 20 g_3^2\mathrm{Tr}\Big(Y_u Y_u^\dagger\Big) - \frac{27}{4}\mathrm{Tr}\Big(Y_d Y_d^\dagger Y_d Y_d^\dagger\Big) + \frac{3}{2}\mathrm{Tr}\Big(Y_d Y_u^\dagger Y_u Y_d^\dagger\Big) - \frac{9}{4}\mathrm{Tr}\Big(Y_e Y_e^\dagger Y_e Y_e^\dagger\Big) - \frac{27}{4}\mathrm{Tr}\Big(Y_u Y_u^\dagger Y_u Y_u^\dagger\Big)\end{aligned} \tag{B.13}$$

$$\beta_{Y_e}^{(1)} = \frac{3}{2} Y_e Y_e^\dagger Y_e + Y_e\Big(3\mathrm{Tr}\Big(Y_d Y_d^\dagger\Big) + 3\mathrm{Tr}\Big(Y_u Y_u^\dagger\Big) - \frac{9}{4} g_1^2 - \frac{9}{4} g_2^2 + \mathrm{Tr}\Big(Y_e Y_e^\dagger\Big)\Big) \tag{B.14}$$

$$\begin{aligned}\beta_{Y_e}^{(2)} = &\frac{1}{400}\Big(15\Big(40 Y_e Y_e^\dagger Y_e Y_e^\dagger Y_e \\ &+ Y_e Y_e^\dagger Y_e\Big(129 g_1^2 - 160\lambda - 180\mathrm{Tr}\Big(Y_d Y_d^\dagger\Big) - 180\mathrm{Tr}\Big(Y_u Y_u^\dagger\Big) + 225 g_2^2 - 60\mathrm{Tr}\Big(Y_e Y_e^\dagger\Big)\Big)\Big) \\ &+ Y_e\Big(2742 g_1^4 + 540 g_1^2 g_2^2 - 2300 g_2^4 + 600\lambda^2 + 250\Big(32 g_3^2 + 9 g_2^2 + g_1^2\Big)\mathrm{Tr}\Big(Y_d Y_d^\dagger\Big) \\ &+ 750\Big(g_1^2 + g_2^2\Big)\mathrm{Tr}\Big(Y_e Y_e^\dagger\Big) + 850 g_1^2\mathrm{Tr}\Big(Y_u Y_u^\dagger\Big) + 2250 g_2^2\mathrm{Tr}\Big(Y_u Y_u^\dagger\Big) + 8000 g_3^2\mathrm{Tr}\Big(Y_u Y_u^\dagger\Big) \\ &- 2700\mathrm{Tr}\Big(Y_d Y_d^\dagger Y_d Y_d^\dagger\Big) + 600\mathrm{Tr}\Big(Y_d Y_u^\dagger Y_u Y_d^\dagger\Big) - 900\mathrm{Tr}\Big(Y_e Y_e^\dagger Y_e Y_e^\dagger\Big) - 2700\mathrm{Tr}\Big(Y_u Y_u^\dagger Y_u Y_u^\dagger\Big)\Big)\Big)\end{aligned} \tag{B.15}$$

Appendix C

Renormalisation Group Equations of the Real Singlet Model at Two Loops

Here we provide the two-loop β functions for all of the Real Singlet Model's dimensionless couplings, with $n_f = 6$ [56–59].

C.1 Gauge Couplings

$$\beta_{g_1}^{(1)} = \frac{41}{10} g_1^3 \tag{C.1}$$

$$\beta_{g_1}^{(2)} = \frac{1}{50} g_1^3 \Big(135 g_2^2 + 199 g_1^2 - 25 \mathrm{Tr}\Big(Y_d Y_d^\dagger \Big) + 440 g_3^2 - 75 \mathrm{Tr}\Big(Y_e Y_e^\dagger \Big) - 85 \mathrm{Tr}\Big(Y_u Y_u^\dagger \Big) \Big) \tag{C.2}$$

$$\beta_{g_2}^{(1)} = -\frac{19}{6} g_2^3 \tag{C.3}$$

$$\beta_{g_2}^{(2)} = \frac{1}{30} g_2^3 \Big(-15 \mathrm{Tr}\Big(Y_e Y_e^\dagger \Big) + 175 g_2^2 + 27 g_1^2 + 360 g_3^2 - 45 \mathrm{Tr}\Big(Y_d Y_d^\dagger \Big) - 45 \mathrm{Tr}\Big(Y_u Y_u^\dagger \Big) \Big) \tag{C.4}$$

$$\beta_{g_3}^{(1)} = -7 g_3^3 \tag{C.5}$$

$$\beta_{g_3}^{(2)} = -\frac{1}{10} g_3^3 \Big(-11 g_1^2 + 20 \mathrm{Tr}\Big(Y_d Y_d^\dagger \Big) + 20 \mathrm{Tr}\Big(Y_u Y_u^\dagger \Big) + 260 g_3^2 - 45 g_2^2 \Big) \tag{C.6}$$

C.2 Quartic scalar couplings

$$\beta_{\lambda_S}^{(1)} = 36 \lambda_S^2 + \kappa_2^2 \tag{C.7}$$

$$\beta_{\lambda_S}^{(2)} = +\frac{6}{5} g_1^2 \kappa_2^2 + 6 g_2^2 \kappa_2^2 - 4 \kappa_2^3 - 20 \kappa_2^2 \lambda_S - 816 \lambda_S^3 - 6 \kappa_2^2 \mathrm{Tr}\Big(Y_d Y_d^\dagger \Big) - 2 \kappa_2^2 \mathrm{Tr}\Big(Y_e Y_e^\dagger \Big) - 6 \kappa_2^2 \mathrm{Tr}\Big(Y_u Y_u^\dagger \Big) \tag{C.8}$$

$$\beta_{\kappa_2}^{(1)} = \frac{1}{10}\kappa_2\Big(120\lambda_S + 20\mathrm{Tr}\Big(Y_eY_e^\dagger\Big) + 40\kappa_2 - 45g_2^2 + 60\lambda + 60\mathrm{Tr}\Big(Y_dY_d^\dagger\Big) + 60\mathrm{Tr}\Big(Y_uY_u^\dagger\Big) - 9g_1^2\Big) \tag{C.9}$$

$$\begin{aligned}\beta_{\kappa_2}^{(2)} = &+\frac{1671}{400}g_1^4\kappa_2 + \frac{9}{8}g_1^2g_2^2\kappa_2 - \frac{145}{16}g_2^4\kappa_2 + \frac{3}{5}g_1^2\kappa_2^2 + 3g_2^2\kappa_2^2 - \frac{21}{2}\kappa_2^3 - 72\kappa_2^2\lambda_S - 120\kappa_2\lambda_S^2\\
&+ \frac{36}{5}g_1^2\kappa_2\lambda + 36g_2^2\kappa_2\lambda - 36\kappa_2^2\lambda - 15\kappa_2\lambda^2\\
&+ \frac{1}{4}\kappa_2\Big(16\Big(10g_3^2 - 3\kappa_2 - 9\lambda\Big) + 45g_2^2 + 5g_1^2\Big)\mathrm{Tr}\Big(Y_dY_d^\dagger\Big) + \frac{1}{4}\kappa_2\Big(15g_1^2 + 15g_2^2 - 16\Big(3\lambda + \kappa_2\Big)\Big)\mathrm{Tr}\Big(Y_eY_e^\dagger\Big)\\
&+ \frac{17}{4}g_1^2\kappa_2\mathrm{Tr}\Big(Y_uY_u^\dagger\Big) + \frac{45}{4}g_2^2\kappa_2\mathrm{Tr}\Big(Y_uY_u^\dagger\Big) + 40g_3^2\kappa_2\mathrm{Tr}\Big(Y_uY_u^\dagger\Big) - 12\kappa_2^2\mathrm{Tr}\Big(Y_uY_u^\dagger\Big)\\
&- 36\kappa_2\lambda\mathrm{Tr}\Big(Y_uY_u^\dagger\Big) - \frac{27}{2}\kappa_2\mathrm{Tr}\Big(Y_dY_d^\dagger Y_dY_d^\dagger\Big) - 21\kappa_2\mathrm{Tr}\Big(Y_dY_u^\dagger Y_uY_d^\dagger\Big) - \frac{9}{2}\kappa_2\mathrm{Tr}\Big(Y_eY_e^\dagger Y_eY_e^\dagger\Big)\\
&- \frac{27}{2}\kappa_2\mathrm{Tr}\Big(Y_uY_u^\dagger Y_uY_u^\dagger\Big)\end{aligned} \tag{C.10}$$

$$\begin{aligned}\beta_\lambda^{(1)} = &+\frac{27}{100}g_1^4 + \frac{9}{10}g_1^2g_2^2 + \frac{9}{4}g_2^4 + \kappa_2^2 - \frac{9}{5}g_1^2\lambda - 9g_2^2\lambda + 12\lambda^2 + 12\lambda\mathrm{Tr}\Big(Y_dY_d^\dagger\Big) + 4\lambda\mathrm{Tr}\Big(Y_eY_e^\dagger\Big)\\
&+ 12\lambda\mathrm{Tr}\Big(Y_uY_u^\dagger\Big) - 12\mathrm{Tr}\Big(Y_dY_d^\dagger Y_dY_d^\dagger\Big) - 4\mathrm{Tr}\Big(Y_eY_e^\dagger Y_eY_e^\dagger\Big) - 12\mathrm{Tr}\Big(Y_uY_u^\dagger Y_uY_u^\dagger\Big)\end{aligned} \tag{C.11}$$

$$\begin{aligned}\beta_\lambda^{(2)} = &-\frac{3411}{1000}g_1^6 - \frac{1677}{200}g_1^4g_2^2 - \frac{289}{40}g_1^2g_2^4 + \frac{305}{8}g_2^6 - 4\kappa_2^3 + \frac{1887}{200}g_1^4\lambda + \frac{117}{20}g_1^2g_2^2\lambda - \frac{73}{8}g_2^4\lambda - 5\kappa_2^2\lambda\\
&+ \frac{54}{5}g_1^2\lambda^2 + 54g_2^2\lambda^2 - 78\lambda^3\\
&+ \frac{1}{10}\Big(225g_2^2\lambda - 45g_2^4 + 80\Big(10g_3^2 - 9\lambda\Big)\lambda + 9g_1^4 + g_1^2\Big(25\lambda + 54g_2^2\Big)\Big)\mathrm{Tr}\Big(Y_dY_d^\dagger\Big)\\
&- \frac{3}{10}\Big(15g_1^4 + 5\Big(16\lambda^2 - 5g_2^2\lambda + g_2^4\Big) - g_1^2\Big(22g_2^2 + 25\lambda\Big)\Big)\mathrm{Tr}\Big(Y_eY_e^\dagger\Big) - \frac{171}{50}g_1^4\mathrm{Tr}\Big(Y_uY_u^\dagger\Big)\\
&+ \frac{63}{5}g_1^2g_2^2\mathrm{Tr}\Big(Y_uY_u^\dagger\Big) - \frac{9}{2}g_2^4\mathrm{Tr}\Big(Y_uY_u^\dagger\Big) + \frac{17}{2}g_1^2\lambda\mathrm{Tr}\Big(Y_uY_u^\dagger\Big) + \frac{45}{2}g_2^2\lambda\mathrm{Tr}\Big(Y_uY_u^\dagger\Big)\\
&+ 80g_3^2\lambda\mathrm{Tr}\Big(Y_uY_u^\dagger\Big) - 72\lambda^2\mathrm{Tr}\Big(Y_uY_u^\dagger\Big) + \frac{8}{5}g_1^2\mathrm{Tr}\Big(Y_dY_d^\dagger Y_dY_d^\dagger\Big) - 64g_3^2\mathrm{Tr}\Big(Y_dY_d^\dagger Y_dY_d^\dagger\Big)\\
&- 3\lambda\mathrm{Tr}\Big(Y_dY_d^\dagger Y_dY_d^\dagger\Big) - 42\lambda\mathrm{Tr}\Big(Y_dY_u^\dagger Y_uY_d^\dagger\Big) - \frac{24}{5}g_1^2\mathrm{Tr}\Big(Y_eY_e^\dagger Y_eY_e^\dagger\Big) - \lambda\mathrm{Tr}\Big(Y_eY_e^\dagger Y_eY_e^\dagger\Big)\\
&- \frac{16}{5}g_1^2\mathrm{Tr}\Big(Y_uY_u^\dagger Y_uY_u^\dagger\Big) - 64g_3^2\mathrm{Tr}\Big(Y_uY_u^\dagger Y_uY_u^\dagger\Big) - 3\lambda\mathrm{Tr}\Big(Y_uY_u^\dagger Y_uY_u^\dagger\Big) + 60\mathrm{Tr}\Big(Y_dY_d^\dagger Y_dY_d^\dagger Y_dY_d^\dagger\Big)\\
&- 24\mathrm{Tr}\Big(Y_dY_d^\dagger Y_dY_u^\dagger Y_uY_d^\dagger\Big) + 12\mathrm{Tr}\Big(Y_dY_u^\dagger Y_uY_d^\dagger Y_dY_d^\dagger\Big) - 12\mathrm{Tr}\Big(Y_dY_u^\dagger Y_uY_u^\dagger Y_uY_d^\dagger\Big)\\
&+ 20\mathrm{Tr}\Big(Y_eY_e^\dagger Y_eY_e^\dagger Y_eY_e^\dagger\Big) + 60\mathrm{Tr}\Big(Y_uY_u^\dagger Y_uY_u^\dagger Y_uY_u^\dagger\Big)\end{aligned} \tag{C.12}$$

C.3 Trilinear Scalar couplings

$$\beta_\kappa^{(1)} = 6\Big(6\lambda_S\kappa + \kappa_1\kappa_2\Big) \tag{C.13}$$

$$\beta_{\kappa}^{(2)} = +\frac{36}{5}g_1^2\kappa_1\kappa_2 + 36g_2^2\kappa_1\kappa_2 - 24\kappa_1\kappa_2^2 - 72\kappa_1\kappa_2\lambda_S - 9\kappa_2^2\kappa - 828\lambda_S^2\kappa - 36\kappa_1\kappa_2\mathrm{Tr}\Big(Y_dY_d^\dagger\Big)$$
$$- 12\kappa_1\kappa_2\mathrm{Tr}\Big(Y_eY_e^\dagger\Big) - 36\kappa_1\kappa_2\mathrm{Tr}\Big(Y_uY_u^\dagger\Big) \tag{C.14}$$

$$\beta_{\kappa_1}^{(1)} = 2\kappa_1\mathrm{Tr}\Big(Y_eY_e^\dagger\Big) + 2\kappa_2\kappa + 4\kappa_1\kappa_2 + 6\kappa_1\lambda + 6\kappa_1\mathrm{Tr}\Big(Y_dY_d^\dagger\Big) + 6\kappa_1\mathrm{Tr}\Big(Y_uY_u^\dagger\Big) - \frac{9}{10}g_1^2\kappa_1 - \frac{9}{2}g_2^2\kappa_1 \tag{C.15}$$

$$\beta_{\kappa_1}^{(2)} = +\frac{1671}{400}g_1^4\kappa_1 + \frac{9}{8}g_1^2g_2^2\kappa_1 - \frac{145}{16}g_2^4\kappa_1 + \frac{3}{5}g_1^2\kappa_1\kappa_2 + 3g_2^2\kappa_1\kappa_2 - \frac{23}{2}\kappa_1\kappa_2^2 - 24\kappa_1\kappa_2\lambda_S + 12\kappa_1\lambda_S^2$$
$$- 8\kappa_2^2\kappa - 24\kappa_2\lambda_S\kappa + \frac{36}{5}g_1^2\kappa_1\lambda + 36g_2^2\kappa_1\lambda - 36\kappa_1\kappa_2\lambda - 15\kappa_1\lambda^2$$
$$+ \frac{1}{4}\kappa_1\Big(16\Big(10g_3^2 - 3\kappa_2 - 9\lambda\Big) + 45g_2^2 + 5g_1^2\Big)\mathrm{Tr}\Big(Y_dY_d^\dagger\Big) + \frac{1}{4}\kappa_1\Big(15g_1^2 + 15g_2^2$$
$$- 16\Big(3\lambda + \kappa_2\Big)\Big)\mathrm{Tr}\Big(Y_eY_e^\dagger\Big) + \frac{17}{4}g_1^2\kappa_1\mathrm{Tr}\Big(Y_uY_u^\dagger\Big)$$
$$+ \frac{45}{4}g_2^2\kappa_1\mathrm{Tr}\Big(Y_uY_u^\dagger\Big) + 40g_3^2\kappa_1\mathrm{Tr}\Big(Y_uY_u^\dagger\Big) - 12\kappa_1\kappa_2\mathrm{Tr}\Big(Y_uY_u^\dagger\Big)$$
$$- 36\kappa_1\lambda\mathrm{Tr}\Big(Y_uY_u^\dagger\Big) - \frac{27}{2}\kappa_1\mathrm{Tr}\Big(Y_dY_d^\dagger Y_dY_d^\dagger\Big) - 21\kappa_1\mathrm{Tr}\Big(Y_dY_u^\dagger Y_uY_d^\dagger\Big) - \frac{9}{2}\kappa_1\mathrm{Tr}\Big(Y_eY_e^\dagger Y_eY_e^\dagger\Big)$$
$$- \frac{27}{2}\kappa_1\mathrm{Tr}\Big(Y_uY_u^\dagger Y_uY_u^\dagger\Big) \tag{C.16}$$

C.4 Yukawa Couplings

$$\beta_{Y_u}^{(1)} = -\frac{3}{2}\Big(-Y_uY_u^\dagger Y_u + Y_uY_d^\dagger Y_d\Big)$$
$$+ Y_u\Big(3\mathrm{Tr}\Big(Y_dY_d^\dagger\Big) + 3\mathrm{Tr}\Big(Y_uY_u^\dagger\Big) - 8g_3^2 - \frac{17}{20}g_1^2 - \frac{9}{4}g_2^2 + \mathrm{Tr}\Big(Y_eY_e^\dagger\Big)\Big) \tag{C.17}$$

$$\beta_{Y_u}^{(2)} = +\frac{1}{80}\Big(20\Big(11Y_uY_d^\dagger Y_dY_d^\dagger Y_d - 4Y_uY_u^\dagger Y_uY_d^\dagger Y_d + 6Y_uY_u^\dagger Y_uY_u^\dagger Y_u - Y_uY_d^\dagger Y_dY_u^\dagger Y_u\Big)$$
$$+ Y_uY_u^\dagger Y_u\Big(1280g_3^2 - 180\mathrm{Tr}\Big(Y_eY_e^\dagger\Big) + 223g_1^2 - 480\lambda - 540\mathrm{Tr}\Big(Y_dY_d^\dagger\Big) - 540\mathrm{Tr}\Big(Y_uY_u^\dagger\Big) + 675g_2^2\Big)$$
$$+ Y_uY_d^\dagger Y_d\Big(100\mathrm{Tr}\Big(Y_eY_e^\dagger\Big) - 1280g_3^2 + 300\mathrm{Tr}\Big(Y_dY_d^\dagger\Big) + 300\mathrm{Tr}\Big(Y_uY_u^\dagger\Big) - 43g_1^2 + 45g_2^2\Big)\Big)$$
$$+ \frac{1}{600}Y_u\Big(1187g_1^4 - 270g_1^2g_2^2 - 3450g_2^4 + 760g_1^2g_3^2 + 5400g_2^2g_3^2 - 64800g_3^4 + 150\kappa_2^2 + 900\lambda^2$$
$$+ 375\Big(32g_3^2 + 9g_2^2 + g_1^2\Big)\mathrm{Tr}\Big(Y_dY_d^\dagger\Big) + 1125\Big(g_1^2 + g_2^2\Big)\mathrm{Tr}\Big(Y_eY_e^\dagger\Big) + 1275g_1^2\mathrm{Tr}\Big(Y_uY_u^\dagger\Big)$$
$$+ 3375g_2^2\mathrm{Tr}\Big(Y_uY_u^\dagger\Big) + 12000g_3^2\mathrm{Tr}\Big(Y_uY_u^\dagger\Big) - 4050\mathrm{Tr}\Big(Y_dY_d^\dagger Y_dY_d^\dagger\Big) + 900\mathrm{Tr}\Big(Y_dY_u^\dagger Y_uY_d^\dagger\Big)$$
$$- 1350\mathrm{Tr}\Big(Y_eY_e^\dagger Y_eY_e^\dagger\Big) - 4050\mathrm{Tr}\Big(Y_uY_u^\dagger Y_uY_u^\dagger\Big)\Big) \tag{C.18}$$

$$\beta_{Y_d}^{(1)} = \frac{1}{4}\Big(6\Big(-Y_dY_u^\dagger Y_u + Y_dY_d^\dagger Y_d\Big)$$

$$- Y_d\Big(- 12\mathrm{Tr}\Big(Y_dY_d^\dagger\Big) - 12\mathrm{Tr}\Big(Y_uY_u^\dagger\Big) + 32g_3^2 - 4\mathrm{Tr}\Big(Y_eY_e^\dagger\Big) + 9g_2^2 + g_1^2\Big)\Big) \tag{C.19}$$

$$\begin{aligned}\beta_{Y_d}^{(2)} = &+\frac{1}{80}\Big(20\Big(11Y_dY_u^\dagger Y_uY_u^\dagger Y_u - 4Y_dY_d^\dagger Y_dY_u^\dagger Y_u + 6Y_dY_d^\dagger Y_dY_d^\dagger Y_d - Y_dY_u^\dagger Y_uY_d^\dagger Y_d\Big)\\
&+ Y_dY_d^\dagger Y_d\Big(1280g_3^2 - 180\mathrm{Tr}\Big(Y_eY_e^\dagger\Big) + 187g_1^2 - 480\lambda - 540\mathrm{Tr}\Big(Y_dY_d^\dagger\Big) - 540\mathrm{Tr}\Big(Y_uY_u^\dagger\Big) + 675g_2^2\Big)\\
&+ Y_dY_u^\dagger Y_u\Big(100\mathrm{Tr}\Big(Y_eY_e^\dagger\Big) - 1280g_3^2 + 300\mathrm{Tr}\Big(Y_dY_d^\dagger\Big) + 300\mathrm{Tr}\Big(Y_uY_u^\dagger\Big) + 45g_2^2 - 79g_1^2\Big)\Big)\\
&+ Y_d\Big(- \frac{127}{600}g_1^4 - \frac{27}{20}g_1^2g_2^2 - \frac{23}{4}g_2^4 + \frac{31}{15}g_1^2g_3^2 + 9g_2^2g_3^2 - 108g_3^4 + \frac{1}{4}\kappa_2^2 + \frac{3}{2}\lambda^2\\
&+ \frac{5}{8}\Big(32g_3^2 + 9g_2^2 + g_1^2\Big)\mathrm{Tr}\Big(Y_dY_d^\dagger\Big) + \frac{15}{8}\Big(g_1^2 + g_2^2\Big)\mathrm{Tr}\Big(Y_eY_e^\dagger\Big) + \frac{17}{8}g_1^2\mathrm{Tr}\Big(Y_uY_u^\dagger\Big) + \frac{45}{8}g_2^2\mathrm{Tr}\Big(Y_uY_u^\dagger\Big)\\
&+ 20g_3^2\mathrm{Tr}\Big(Y_uY_u^\dagger\Big) - \frac{27}{4}\mathrm{Tr}\Big(Y_dY_d^\dagger Y_dY_d^\dagger\Big) + \frac{3}{2}\mathrm{Tr}\Big(Y_dY_u^\dagger Y_uY_d^\dagger\Big) - \frac{9}{4}\mathrm{Tr}\Big(Y_eY_e^\dagger Y_eY_e^\dagger\Big) - \frac{27}{4}\mathrm{Tr}\Big(Y_uY_u^\dagger Y_uY_u^\dagger\Big)\Big)\end{aligned} \tag{C.20}$$

$$\beta_{Y_e}^{(1)} = \frac{3}{2}Y_eY_e^\dagger Y_e + Y_e\Big(3\mathrm{Tr}\Big(Y_dY_d^\dagger\Big) + 3\mathrm{Tr}\Big(Y_uY_u^\dagger\Big) - \frac{9}{4}g_1^2 - \frac{9}{4}g_2^2 + \mathrm{Tr}\Big(Y_eY_e^\dagger\Big)\Big) \tag{C.21}$$

$$\begin{aligned}\beta_{Y_e}^{(2)} = &\frac{1}{400}\Big(15\Big(40Y_eY_e^\dagger Y_eY_e^\dagger Y_e\\
&+ Y_eY_e^\dagger Y_e\Big(129g_1^2 - 160\lambda - 180\mathrm{Tr}\Big(Y_dY_d^\dagger\Big) - 180\mathrm{Tr}\Big(Y_uY_u^\dagger\Big) + 225g_2^2 - 60\mathrm{Tr}\Big(Y_eY_e^\dagger\Big)\Big)\Big)\\
&+ 2Y_e\Big(1371g_1^4 + 270g_1^2g_2^2 - 1150g_2^4 + 50\kappa_2^2 + 300\lambda^2 + 125\Big(32g_3^2 + 9g_2^2 + g_1^2\Big)\mathrm{Tr}\Big(Y_dY_d^\dagger\Big)\\
&+ 375\Big(g_1^2 + g_2^2\Big)\mathrm{Tr}\Big(Y_eY_e^\dagger\Big) + 425g_1^2\mathrm{Tr}\Big(Y_uY_u^\dagger\Big) + 1125g_2^2\mathrm{Tr}\Big(Y_uY_u^\dagger\Big) + 4000g_3^2\mathrm{Tr}\Big(Y_uY_u^\dagger\Big)\\
&- 1350\mathrm{Tr}\Big(Y_dY_d^\dagger Y_dY_d^\dagger\Big) + 300\mathrm{Tr}\Big(Y_dY_u^\dagger Y_uY_d^\dagger\Big) - 450\mathrm{Tr}\Big(Y_eY_e^\dagger Y_eY_e^\dagger\Big) - 1350\mathrm{Tr}\Big(Y_uY_u^\dagger Y_uY_u^\dagger\Big)\Big)\Big)\end{aligned} \tag{C.22}$$

Appendix D

Renormalisation Group Equations of the Complex Singlet Model at Two Loops

Here we provide the two-loop β functions for all of the Complex Singlet Model's dimensionless couplings, with $n_f = 6$ [56–59].

D.1 Gauge Couplings

$$\beta_{g_1}^{(1)} = \frac{41}{10} g_1^3 \tag{D.1}$$

$$\beta_{g_1}^{(2)} = \frac{1}{50} g_1^3 \Big(135 g_2^2 + 199 g_1^2 - 25 \mathrm{Tr}\Big(Y_d Y_d^\dagger \Big) + 440 g_3^2 - 75 \mathrm{Tr}\Big(Y_e Y_e^\dagger \Big) - 85 \mathrm{Tr}\Big(Y_u Y_u^\dagger \Big) \Big) \tag{D.2}$$

$$\beta_{g_2}^{(1)} = -\frac{19}{6} g_2^3 \tag{D.3}$$

$$\beta_{g_2}^{(2)} = \frac{1}{30} g_2^3 \Big(-15 \mathrm{Tr}\Big(Y_e Y_e^\dagger \Big) + 175 g_2^2 + 27 g_1^2 + 360 g_3^2 - 45 \mathrm{Tr}\Big(Y_d Y_d^\dagger \Big) - 45 \mathrm{Tr}\Big(Y_u Y_u^\dagger \Big) \Big) \tag{D.4}$$

$$\beta_{g_3}^{(1)} = -7 g_3^3 \tag{D.5}$$

$$\beta_{g_3}^{(2)} = -\frac{1}{10} g_3^3 \Big(-11 g_1^2 + 20 \mathrm{Tr}\Big(Y_d Y_d^\dagger \Big) + 20 \mathrm{Tr}\Big(Y_u Y_u^\dagger \Big) + 260 g_3^2 - 45 g_2^2 \Big) \tag{D.6}$$

D.2 Quartic scalar couplings

$$\beta_{d_2}^{(1)} = 2 \Big(10 d_2^2 + \delta^2 \Big) \tag{D.7}$$

$$\beta_{d_2}^{(2)} = -\frac{4}{5} \Big(300 d_2^3 + 25 d_2 \delta^2 - 3 g_1^2 \delta^2 - 15 g_2^2 \delta^2 + 10 \delta^3 + 15 \delta^2 \mathrm{Tr}\Big(Y_d Y_d^\dagger \Big) + 5 \delta^2 \mathrm{Tr}\Big(Y_e Y_e^\dagger \Big)$$

$$+ 15\delta^2 \mathrm{Tr}\Big(Y_u Y_u^\dagger\Big)\Big) \tag{D.8}$$

$$\beta_{d_2}^{(1)} = 2\Big(10 d_2^2 + \delta^2\Big) \tag{D.9}$$

$$\beta_{d_2}^{(2)} = -\frac{4}{5}\Big(300 d_2^3 + 25 d_2 \delta^2 - 3 g_1^2 \delta^2 - 15 g_2^2 \delta^2 + 10\delta^3 + 15\delta^2 \mathrm{Tr}\Big(Y_d Y_d^\dagger\Big) + 5\delta^2 \mathrm{Tr}\Big(Y_e Y_e^\dagger\Big) + 15\delta^2 \mathrm{Tr}\Big(Y_u Y_u^\dagger\Big)\Big) \tag{D.10}$$

$$\beta_{d_2}^{(1)} = 2\Big(10 d_2^2 + \delta^2\Big) \tag{D.11}$$

$$\beta_{d_2}^{(2)} = -\frac{4}{5}\Big(300 d_2^3 + 25 d_2 \delta^2 - 3 g_1^2 \delta^2 - 15 g_2^2 \delta^2 + 10\delta^3 + 15\delta^2 \mathrm{Tr}\Big(Y_d Y_d^\dagger\Big) + 5\delta^2 \mathrm{Tr}\Big(Y_e Y_e^\dagger\Big) + 15\delta^2 \mathrm{Tr}\Big(Y_u Y_u^\dagger\Big)\Big) \tag{D.12}$$

$$\beta_{\delta}^{(1)} = \frac{1}{10}\delta\Big(20\mathrm{Tr}\Big(Y_e Y_e^\dagger\Big) + 40\delta - 45 g_2^2 + 60\lambda + 60\mathrm{Tr}\Big(Y_d Y_d^\dagger\Big) + 60\mathrm{Tr}\Big(Y_u Y_u^\dagger\Big) + 80 d_2 - 9 g_1^2\Big) \tag{D.13}$$

$$\begin{aligned}\beta_{\delta}^{(2)} = {} & -40 d_2^2 \delta + \frac{1671}{400} g_1^4 \delta + \frac{9}{8} g_1^2 g_2^2 \delta - \frac{145}{16} g_2^4 \delta - 48 d_2 \delta^2 + \frac{3}{5} g_1^2 \delta^2 + 3 g_2^2 \delta^2 - 11\delta^3 + \frac{36}{5} g_1^2 \delta\lambda \\ & + 36 g_2^2 \delta\lambda - 36\delta^2\lambda - 15\delta\lambda^2 + \frac{1}{4}\delta\Big(16\Big(10 g_3^2 - 3\delta - 9\lambda\Big) + 45 g_2^2 + 5 g_1^2\Big)\mathrm{Tr}\Big(Y_d Y_d^\dagger\Big) \\ & + \frac{1}{4}\delta\Big(15 g_1^2 + 15 g_2^2 - 16\Big(3\lambda + \delta\Big)\Big)\mathrm{Tr}\Big(Y_e Y_e^\dagger\Big) + \frac{17}{4} g_1^2 \delta \mathrm{Tr}\Big(Y_u Y_u^\dagger\Big) + \frac{45}{4} g_2^2 \delta \mathrm{Tr}\Big(Y_u Y_u^\dagger\Big) \\ & + 40 g_3^2 \delta \mathrm{Tr}\Big(Y_u Y_u^\dagger\Big) - 12\delta^2 \mathrm{Tr}\Big(Y_u Y_u^\dagger\Big) - 36\delta\lambda \mathrm{Tr}\Big(Y_u Y_u^\dagger\Big) - \frac{27}{2}\delta \mathrm{Tr}\Big(Y_d Y_d^\dagger Y_d Y_d^\dagger\Big) \\ & - 21\delta \mathrm{Tr}\Big(Y_d Y_u^\dagger Y_u Y_d^\dagger\Big) - \frac{9}{2}\delta \mathrm{Tr}\Big(Y_e Y_e^\dagger Y_e Y_e^\dagger\Big) - \frac{27}{2}\delta \mathrm{Tr}\Big(Y_u Y_u^\dagger Y_u Y_u^\dagger\Big)\end{aligned} \tag{D.14}$$

$$\beta_{\delta}^{(1)} = \frac{1}{10}\delta\Big(20\mathrm{Tr}\Big(Y_e Y_e^\dagger\Big) + 40\delta - 45 g_2^2 + 60\lambda + 60\mathrm{Tr}\Big(Y_d Y_d^\dagger\Big) + 60\mathrm{Tr}\Big(Y_u Y_u^\dagger\Big) + 80 d_2 - 9 g_1^2\Big) \tag{D.15}$$

$$\begin{aligned}\beta_{\delta}^{(2)} = {} & -40 d_2^2 \delta + \frac{1671}{400} g_1^4 \delta + \frac{9}{8} g_1^2 g_2^2 \delta - \frac{145}{16} g_2^4 \delta - 48 d_2 \delta^2 + \frac{3}{5} g_1^2 \delta^2 + 3 g_2^2 \delta^2 - 11\delta^3 + \frac{36}{5} g_1^2 \delta\lambda \\ & + 36 g_2^2 \delta\lambda - 36\delta^2\lambda - 15\delta\lambda^2 + \frac{1}{4}\delta\Big(16\Big(10 g_3^2 - 3\delta - 9\lambda\Big) + 45 g_2^2 + 5 g_1^2\Big)\mathrm{Tr}\Big(Y_d Y_d^\dagger\Big) \\ & + \frac{1}{4}\delta\Big(15 g_1^2 + 15 g_2^2 - 16\Big(3\lambda + \delta\Big)\Big)\mathrm{Tr}\Big(Y_e Y_e^\dagger\Big) + \frac{17}{4} g_1^2 \delta \mathrm{Tr}\Big(Y_u Y_u^\dagger\Big) + \frac{45}{4} g_2^2 \delta \mathrm{Tr}\Big(Y_u Y_u^\dagger\Big) \\ & + 40 g_3^2 \delta \mathrm{Tr}\Big(Y_u Y_u^\dagger\Big) - 12\delta^2 \mathrm{Tr}\Big(Y_u Y_u^\dagger\Big) - 36\delta\lambda \mathrm{Tr}\Big(Y_u Y_u^\dagger\Big) - \frac{27}{2}\delta \mathrm{Tr}\Big(Y_d Y_d^\dagger Y_d Y_d^\dagger\Big) \\ & - 21\delta \mathrm{Tr}\Big(Y_d Y_u^\dagger Y_u Y_d^\dagger\Big) - \frac{9}{2}\delta \mathrm{Tr}\Big(Y_e Y_e^\dagger Y_e Y_e^\dagger\Big) - \frac{27}{2}\delta \mathrm{Tr}\Big(Y_u Y_u^\dagger Y_u Y_u^\dagger\Big)\end{aligned} \tag{D.16}$$

$$\begin{aligned}\beta_{\lambda}^{(1)} = {} & +\frac{27}{100} g_1^4 + \frac{9}{10} g_1^2 g_2^2 + \frac{9}{4} g_2^4 + 2\delta^2 - \frac{9}{5} g_1^2 \lambda - 9 g_2^2 \lambda + 12\lambda^2 + 12\lambda \mathrm{Tr}\Big(Y_d Y_d^\dagger\Big) + 4\lambda \mathrm{Tr}\Big(Y_e Y_e^\dagger\Big) \\ & + 12\lambda \mathrm{Tr}\Big(Y_u Y_u^\dagger\Big) - 12\mathrm{Tr}\Big(Y_d Y_d^\dagger Y_d Y_d^\dagger\Big) - 4\mathrm{Tr}\Big(Y_e Y_e^\dagger Y_e Y_e^\dagger\Big) - 12\mathrm{Tr}\Big(Y_u Y_u^\dagger Y_u Y_u^\dagger\Big)\end{aligned} \tag{D.17}$$

$$\beta_{\lambda}^{(2)} = -\frac{3411}{1000} g_1^6 - \frac{1677}{200} g_1^4 g_2^2 - \frac{289}{40} g_1^2 g_2^4 + \frac{305}{8} g_2^6 - 8\delta^3 + \frac{1887}{200} g_1^4 \lambda + \frac{117}{20} g_1^2 g_2^2 \lambda - \frac{73}{8} g_2^4 \lambda - 10\delta^2 \lambda$$

$$
\begin{aligned}
&+\frac{54}{5}g_1^2\lambda^2+54g_2^2\lambda^2-78\lambda^3\\
&+\frac{1}{10}\Big(225g_2^2\lambda-45g_2^4+80\Big(10g_3^2-9\lambda\Big)\lambda+9g_1^4+g_1^2\Big(25\lambda+54g_2^2\Big)\Big)\mathrm{Tr}\Big(Y_dY_d^\dagger\Big)\\
&-\frac{3}{10}\Big(15g_1^4+5\Big(16\lambda^2-5g_2^2\lambda+g_2^4\Big)-g_1^2\Big(22g_2^2+25\lambda\Big)\Big)\mathrm{Tr}\Big(Y_eY_e^\dagger\Big)-\frac{171}{50}g_1^4\mathrm{Tr}\Big(Y_uY_u^\dagger\Big)\\
&+\frac{63}{5}g_1^2g_2^2\mathrm{Tr}\Big(Y_uY_u^\dagger\Big)-\frac{9}{2}g_2^4\mathrm{Tr}\Big(Y_uY_u^\dagger\Big)+\frac{17}{2}g_1^2\lambda\mathrm{Tr}\Big(Y_uY_u^\dagger\Big)+\frac{45}{2}g_2^2\lambda\mathrm{Tr}\Big(Y_uY_u^\dagger\Big)\\
&+80g_3^2\lambda\mathrm{Tr}\Big(Y_uY_u^\dagger\Big)-72\lambda^2\mathrm{Tr}\Big(Y_uY_u^\dagger\Big)+\frac{8}{5}g_1^2\mathrm{Tr}\Big(Y_dY_d^\dagger Y_dY_d^\dagger\Big)-64g_3^2\mathrm{Tr}\Big(Y_dY_d^\dagger Y_dY_d^\dagger\Big)\\
&-3\lambda\mathrm{Tr}\Big(Y_dY_d^\dagger Y_dY_d^\dagger\Big)-42\lambda\mathrm{Tr}\Big(Y_dY_u^\dagger Y_uY_d^\dagger\Big)-\frac{24}{5}g_1^2\mathrm{Tr}\Big(Y_eY_e^\dagger Y_eY_e^\dagger\Big)-\lambda\mathrm{Tr}\Big(Y_eY_e^\dagger Y_eY_e^\dagger\Big)\\
&-\frac{16}{5}g_1^2\mathrm{Tr}\Big(Y_uY_u^\dagger Y_uY_u^\dagger\Big)-64g_3^2\mathrm{Tr}\Big(Y_uY_u^\dagger Y_uY_u^\dagger\Big)-3\lambda\mathrm{Tr}\Big(Y_uY_u^\dagger Y_uY_u^\dagger\Big)+60\mathrm{Tr}\Big(Y_dY_d^\dagger Y_dY_d^\dagger Y_dY_d^\dagger\Big)\\
&-24\mathrm{Tr}\Big(Y_dY_d^\dagger Y_dY_u^\dagger Y_uY_d^\dagger\Big)+12\mathrm{Tr}\Big(Y_dY_u^\dagger Y_uY_d^\dagger Y_dY_d^\dagger\Big)-12\mathrm{Tr}\Big(Y_dY_u^\dagger Y_uY_u^\dagger Y_uY_d^\dagger\Big)\\
&+20\mathrm{Tr}\Big(Y_eY_e^\dagger Y_eY_e^\dagger Y_eY_e^\dagger\Big)+60\mathrm{Tr}\Big(Y_uY_u^\dagger Y_uY_u^\dagger Y_uY_u^\dagger\Big)
\end{aligned}
\tag{D.18}
$$

D.3 Yukawa Couplings

$$
\begin{aligned}
\beta_{Y_u}^{(1)}=&-\frac{3}{2}\Big(-Y_uY_u^\dagger Y_u+Y_uY_d^\dagger Y_d\Big)\\
&+Y_u\Big(3\mathrm{Tr}\Big(Y_dY_d^\dagger\Big)+3\mathrm{Tr}\Big(Y_uY_u^\dagger\Big)-8g_3^2-\frac{17}{20}g_1^2-\frac{9}{4}g_2^2+\mathrm{Tr}\Big(Y_eY_e^\dagger\Big)\Big)
\end{aligned}
\tag{D.19}
$$

$$
\begin{aligned}
\beta_{Y_u}^{(2)}=&+\frac{1}{80}\Big(20\Big(11Y_uY_d^\dagger Y_dY_d^\dagger Y_d-4Y_uY_u^\dagger Y_uY_d^\dagger Y_d+6Y_uY_u^\dagger Y_uY_u^\dagger Y_u-Y_uY_d^\dagger Y_dY_u^\dagger Y_u\Big)\\
&+Y_uY_u^\dagger Y_u\Big(1280g_3^2-180\mathrm{Tr}\Big(Y_eY_e^\dagger\Big)+223g_1^2-480\lambda-540\mathrm{Tr}\Big(Y_dY_d^\dagger\Big)-540\mathrm{Tr}\Big(Y_uY_u^\dagger\Big)+675g_2^2\Big)\\
&+Y_uY_d^\dagger Y_d\Big(100\mathrm{Tr}\Big(Y_eY_e^\dagger\Big)-1280g_3^2+300\mathrm{Tr}\Big(Y_dY_d^\dagger\Big)+300\mathrm{Tr}\Big(Y_uY_u^\dagger\Big)-43g_1^2+45g_2^2\Big)\Big)\\
&+\frac{1}{600}Y_u\Big(1187g_1^4-270g_1^2g_2^2-3450g_2^4+760g_1^2g_3^2+5400g_2^2g_3^2-64800g_3^4+300\delta^2+900\lambda^2\\
&+375\Big(32g_3^2+9g_2^2+g_1^2\Big)\mathrm{Tr}\Big(Y_dY_d^\dagger\Big)+1125\Big(g_1^2+g_2^2\Big)\mathrm{Tr}\Big(Y_eY_e^\dagger\Big)+1275g_1^2\mathrm{Tr}\Big(Y_uY_u^\dagger\Big)\\
&+3375g_2^2\mathrm{Tr}\Big(Y_uY_u^\dagger\Big)+12000g_3^2\mathrm{Tr}\Big(Y_uY_u^\dagger\Big)-4050\mathrm{Tr}\Big(Y_dY_d^\dagger Y_dY_d^\dagger\Big)+900\mathrm{Tr}\Big(Y_dY_u^\dagger Y_uY_d^\dagger\Big)\\
&-1350\mathrm{Tr}\Big(Y_eY_e^\dagger Y_eY_e^\dagger\Big)-4050\mathrm{Tr}\Big(Y_uY_u^\dagger Y_uY_u^\dagger\Big)\Big)
\end{aligned}
\tag{D.20}
$$

$$
\begin{aligned}
\beta_{Y_d}^{(1)}=&\frac{1}{4}\Big(6\Big(-Y_dY_u^\dagger Y_u+Y_dY_d^\dagger Y_d\Big)\\
&-Y_d\Big(-12\mathrm{Tr}\Big(Y_dY_d^\dagger\Big)-12\mathrm{Tr}\Big(Y_uY_u^\dagger\Big)+32g_3^2-4\mathrm{Tr}\Big(Y_eY_e^\dagger\Big)+9g_2^2+g_1^2\Big)\Big)
\end{aligned}
\tag{D.21}
$$

$$
\beta_{Y_d}^{(2)}=+\frac{1}{80}\Big(20\Big(11Y_dY_u^\dagger Y_uY_u^\dagger Y_u-4Y_dY_d^\dagger Y_dY_u^\dagger Y_u+6Y_dY_d^\dagger Y_dY_d^\dagger Y_d-Y_dY_u^\dagger Y_uY_d^\dagger Y_d\Big)
$$

$$
\begin{aligned}
&+ Y_d Y_d^\dagger Y_d \Big(1280 g_3^2 - 180 \mathrm{Tr}\Big(Y_e Y_e^\dagger\Big) + 187 g_1^2 - 480\lambda - 540 \mathrm{Tr}\Big(Y_d Y_d^\dagger\Big) - 540 \mathrm{Tr}\Big(Y_u Y_u^\dagger\Big) + 675 g_2^2\Big) \\
&+ Y_d Y_u^\dagger Y_u \Big(100 \mathrm{Tr}\Big(Y_e Y_e^\dagger\Big) - 1280 g_3^2 + 300 \mathrm{Tr}\Big(Y_d Y_d^\dagger\Big) + 300 \mathrm{Tr}\Big(Y_u Y_u^\dagger\Big) + 45 g_2^2 - 79 g_1^2\Big)\Big) \\
&+ Y_d\Big(- \frac{127}{600} g_1^4 - \frac{27}{20} g_1^2 g_2^2 - \frac{23}{4} g_2^4 + \frac{31}{15} g_1^2 g_3^2 + 9 g_2^2 g_3^2 - 108 g_3^4 + \frac{1}{2}\delta^2 + \frac{3}{2}\lambda^2 \\
&+ \frac{5}{8}\Big(32 g_3^2 + 9 g_2^2 + g_1^2\Big) \mathrm{Tr}\Big(Y_d Y_d^\dagger\Big) + \frac{15}{8}\Big(g_1^2 + g_2^2\Big) \mathrm{Tr}\Big(Y_e Y_e^\dagger\Big) + \frac{17}{8} g_1^2 \mathrm{Tr}\Big(Y_u Y_u^\dagger\Big) + \frac{45}{8} g_2^2 \mathrm{Tr}\Big(Y_u Y_u^\dagger\Big) \\
&+ 20 g_3^2 \mathrm{Tr}\Big(Y_u Y_u^\dagger\Big) - \frac{27}{4} \mathrm{Tr}\Big(Y_d Y_d^\dagger Y_d Y_d^\dagger\Big) + \frac{3}{2} \mathrm{Tr}\Big(Y_d Y_u^\dagger Y_u Y_d^\dagger\Big) - \frac{9}{4} \mathrm{Tr}\Big(Y_e Y_e^\dagger Y_e Y_e^\dagger\Big) - \frac{27}{4} \mathrm{Tr}\Big(Y_u Y_u^\dagger Y_u Y_u^\dagger\Big)\Big)
\end{aligned}
\tag{D.22}
$$

$$
\beta_{Y_e}^{(1)} = \frac{3}{2} Y_e Y_e^\dagger Y_e + Y_e\Big(3 \mathrm{Tr}\Big(Y_d Y_d^\dagger\Big) + 3 \mathrm{Tr}\Big(Y_u Y_u^\dagger\Big) - \frac{9}{4} g_1^2 - \frac{9}{4} g_2^2 + \mathrm{Tr}\Big(Y_e Y_e^\dagger\Big)\Big)
\tag{D.23}
$$

$$
\begin{aligned}
\beta_{Y_e}^{(2)} = \frac{1}{400}\Big(&15\Big(40 Y_e Y_e^\dagger Y_e Y_e^\dagger Y_e \\
&+ Y_e Y_e^\dagger Y_e \Big(129 g_1^2 - 160\lambda - 180 \mathrm{Tr}\Big(Y_d Y_d^\dagger\Big) - 180 \mathrm{Tr}\Big(Y_u Y_u^\dagger\Big) + 225 g_2^2 - 60 \mathrm{Tr}\Big(Y_e Y_e^\dagger\Big)\Big)\Big) \\
&+ Y_e\Big(2742 g_1^4 + 540 g_1^2 g_2^2 - 2300 g_2^4 + 200\delta^2 + 600\lambda^2 + 250\Big(32 g_3^2 + 9 g_2^2 + g_1^2\Big) \mathrm{Tr}\Big(Y_d Y_d^\dagger\Big) \\
&+ 750\Big(g_1^2 + g_2^2\Big) \mathrm{Tr}\Big(Y_e Y_e^\dagger\Big) + 850 g_1^2 \mathrm{Tr}\Big(Y_u Y_u^\dagger\Big) + 2250 g_2^2 \mathrm{Tr}\Big(Y_u Y_u^\dagger\Big) + 8000 g_3^2 \mathrm{Tr}\Big(Y_u Y_u^\dagger\Big) \\
&- 2700 \mathrm{Tr}\Big(Y_d Y_d^\dagger Y_d Y_d^\dagger\Big) + 600 \mathrm{Tr}\Big(Y_d Y_u^\dagger Y_u Y_d^\dagger\Big) - 900 \mathrm{Tr}\Big(Y_e Y_e^\dagger Y_e Y_e^\dagger\Big) - 2700 \mathrm{Tr}\Big(Y_u Y_u^\dagger Y_u Y_u^\dagger\Big)\Big)\Big)
\end{aligned}
\tag{D.24}
$$

Appendix E

Renormalisation Group Equations of the Type-II Two Higgs Doublet Model at Two Loops

Here we provide the two-loop β functions for all of the Complex Singlet Model's dimensionless couplings, with $n_f = 6$ [56–59].

E.1 Gauge Couplings

$$\beta_{g_1}^{(1)} = \frac{21}{5} g_1^3 \tag{E.1}$$

$$\beta_{g_1}^{(2)} = \frac{1}{50} g_1^3 \Big(180 g_2^2 + 208 g_1^2 - 25 \mathrm{Tr}\Big(Y_d Y_d^\dagger \Big) + 440 g_3^2 - 75 \mathrm{Tr}\Big(Y_e Y_e^\dagger \Big) - 85 \mathrm{Tr}\Big(Y_u Y_u^\dagger \Big) \Big) \tag{E.2}$$

$$\beta_{g_2}^{(1)} = -3 g_2^3 \tag{E.3}$$

$$\beta_{g_2}^{(2)} = \frac{1}{10} g_2^3 \Big(120 g_3^2 + 12 g_1^2 - 15 \mathrm{Tr}\Big(Y_d Y_d^\dagger \Big) - 15 \mathrm{Tr}\Big(Y_u Y_u^\dagger \Big) - 5 \mathrm{Tr}\Big(Y_e Y_e^\dagger \Big) + 80 g_2^2 \Big) \tag{E.4}$$

$$\beta_{g_3}^{(1)} = -7 g_3^3 \tag{E.5}$$

$$\beta_{g_3}^{(2)} = -\frac{1}{10} g_3^3 \Big(-11 g_1^2 + 20 \mathrm{Tr}\Big(Y_d Y_d^\dagger \Big) + 20 \mathrm{Tr}\Big(Y_u Y_u^\dagger \Big) + 260 g_3^2 - 45 g_2^2 \Big) \tag{E.6}$$

E.2 Quartic scalar couplings

$$\begin{aligned} \beta_{\lambda_6}^{(1)} = & -\frac{9}{5} g_1^2 \lambda_6 - 9 g_2^2 \lambda_6 + 24 \lambda_1 \lambda_6 + 6 \lambda_3 \lambda_6 + 8 \lambda_4 \lambda_6 + 10 \lambda_5 \lambda_6 + 6 \lambda_3 \lambda_7 + 4 \lambda_4 \lambda_7 + 2 \lambda_5 \lambda_7 \\ & + 9 \lambda_6 \mathrm{Tr}\Big(Y_d Y_d^\dagger \Big) + 3 \lambda_6 \mathrm{Tr}\Big(Y_e Y_e^\dagger \Big) + 3 \lambda_6 \mathrm{Tr}\Big(Y_u Y_u^\dagger \Big) \end{aligned} \tag{E.7}$$

$$\beta_{\lambda_6}^{(2)} = +\frac{1683}{200} g_1^4 \lambda_6 + \frac{87}{20} g_1^2 g_2^2 \lambda_6 - \frac{141}{8} g_2^4 \lambda_6 + \frac{108}{5} g_1^2 \lambda_1 \lambda_6 + 108 g_2^2 \lambda_1 \lambda_6 - 318 \lambda_1^2 \lambda_6 + 6 \lambda_2^2 \lambda_6$$

$$
\begin{aligned}
&+\frac{18}{5}g_1^2\lambda_3\lambda_6+18g_2^2\lambda_3\lambda_6-132\lambda_1\lambda_3\lambda_6-36\lambda_2\lambda_3\lambda_6-32\lambda_3^2\lambda_6+6g_1^2\lambda_4\lambda_6+36g_2^2\lambda_4\lambda_6\\
&-140\lambda_1\lambda_4\lambda_6-28\lambda_2\lambda_4\lambda_6-68\lambda_3\lambda_4\lambda_6-34\lambda_4^2\lambda_6+12g_1^2\lambda_5\lambda_6+54g_2^2\lambda_5\lambda_6-148\lambda_1\lambda_5\lambda_6\\
&-20\lambda_2\lambda_5\lambda_6-72\lambda_3\lambda_5\lambda_6-76\lambda_4\lambda_5\lambda_6-36\lambda_5^2\lambda_6-111\lambda_6^3+\frac{27}{20}g_1^4\lambda_7+\frac{3}{2}g_1^2g_2^2\lambda_7+\frac{45}{4}g_2^4\lambda_7\\
&+\frac{36}{5}g_1^2\lambda_3\lambda_7+36g_2^2\lambda_3\lambda_7-36\lambda_1\lambda_3\lambda_7-36\lambda_2\lambda_3\lambda_7-36\lambda_3^2\lambda_7+\frac{24}{5}g_1^2\lambda_4\lambda_7+18g_2^2\lambda_4\lambda_7\\
&-28\lambda_1\lambda_4\lambda_7-28\lambda_2\lambda_4\lambda_7-56\lambda_3\lambda_4\lambda_7-34\lambda_4^2\lambda_7-\frac{6}{5}g_1^2\lambda_5\lambda_7-20\lambda_1\lambda_5\lambda_7-20\lambda_2\lambda_5\lambda_7\\
&-40\lambda_3\lambda_5\lambda_7-44\lambda_4\lambda_5\lambda_7-42\lambda_5^2\lambda_7-126\lambda_6^2\lambda_7-33\lambda_6\lambda_7^2-42\lambda_7^3\\
&+\frac{3}{8}\Big(16\Big(10g_3^2-24\lambda_1-3\lambda_3-4\lambda_4-5\lambda_5\Big)+45g_2^2+5g_1^2\Big)\lambda_6\mathrm{Tr}\Big(Y_dY_d^\dagger\Big)\\
&+\frac{1}{8}\Big(-16\Big(24\lambda_1+3\lambda_3+4\lambda_4+5\lambda_5\Big)+45g_1^2+45g_2^2\Big)\lambda_6\mathrm{Tr}\Big(Y_eY_e^\dagger\Big)+\frac{17}{8}g_1^2\lambda_6\mathrm{Tr}\Big(Y_uY_u^\dagger\Big)\\
&+\frac{45}{8}g_2^2\lambda_6\mathrm{Tr}\Big(Y_uY_u^\dagger\Big)+20g_3^2\lambda_6\mathrm{Tr}\Big(Y_uY_u^\dagger\Big)-18\lambda_3\lambda_6\mathrm{Tr}\Big(Y_uY_u^\dagger\Big)-24\lambda_4\lambda_6\mathrm{Tr}\Big(Y_uY_u^\dagger\Big)\\
&-30\lambda_5\lambda_6\mathrm{Tr}\Big(Y_uY_u^\dagger\Big)-36\lambda_3\lambda_7\mathrm{Tr}\Big(Y_uY_u^\dagger\Big)-24\lambda_4\lambda_7\mathrm{Tr}\Big(Y_uY_u^\dagger\Big)-12\lambda_5\lambda_7\mathrm{Tr}\Big(Y_uY_u^\dagger\Big)\\
&-\frac{33}{4}\lambda_6\mathrm{Tr}\Big(Y_dY_d^\dagger Y_dY_d^\dagger\Big)-21\lambda_6\mathrm{Tr}\Big(Y_dY_u^\dagger Y_uY_d^\dagger\Big)-\frac{11}{4}\lambda_6\mathrm{Tr}\Big(Y_eY_e^\dagger Y_eY_e^\dagger\Big)-\frac{27}{4}\lambda_6\mathrm{Tr}\Big(Y_uY_u^\dagger Y_uY_u^\dagger\Big)
\end{aligned}
\tag{E.8}
$$

$$
\begin{aligned}
\beta_{\lambda_5}^{(1)}=&-\frac{9}{5}g_1^2\lambda_5-9g_2^2\lambda_5+4\lambda_1\lambda_5+4\lambda_2\lambda_5+8\lambda_3\lambda_5+12\lambda_4\lambda_5+10\lambda_6^2+4\lambda_6\lambda_7+10\lambda_7^2+6\lambda_5\mathrm{Tr}\Big(Y_dY_d^\dagger\Big)\\
&+2\lambda_5\mathrm{Tr}\Big(Y_eY_e^\dagger\Big)+6\lambda_5\mathrm{Tr}\Big(Y_uY_u^\dagger\Big)
\end{aligned}
\tag{E.9}
$$

$$
\begin{aligned}
\beta_{\lambda_5}^{(2)}=&+\frac{1413}{200}g_1^4\lambda_5+\frac{57}{20}g_1^2g_2^2\lambda_5-\frac{231}{8}g_2^4\lambda_5-\frac{12}{5}g_1^2\lambda_1\lambda_5-28\lambda_1^2\lambda_5-\frac{12}{5}g_1^2\lambda_2\lambda_5-28\lambda_2^2\lambda_5\\
&+\frac{48}{5}g_1^2\lambda_3\lambda_5+36g_2^2\lambda_3\lambda_5-80\lambda_1\lambda_3\lambda_5-80\lambda_2\lambda_3\lambda_5-28\lambda_3^2\lambda_5+\frac{72}{5}g_1^2\lambda_4\lambda_5+72g_2^2\lambda_4\lambda_5\\
&-88\lambda_1\lambda_4\lambda_5-88\lambda_2\lambda_4\lambda_5-76\lambda_3\lambda_4\lambda_5-32\lambda_4^2\lambda_5+6\lambda_5^3+12g_1^2\lambda_6^2+54g_2^2\lambda_6^2-148\lambda_1\lambda_6^2\\
&-20\lambda_2\lambda_6^2-72\lambda_3\lambda_6^2-76\lambda_4\lambda_6^2-72\lambda_5\lambda_6^2-\frac{12}{5}g_1^2\lambda_6\lambda_7-40\lambda_1\lambda_6\lambda_7-40\lambda_2\lambda_6\lambda_7\\
&-80\lambda_3\lambda_6\lambda_7-88\lambda_4\lambda_6\lambda_7-168\lambda_5\lambda_6\lambda_7+12g_1^2\lambda_7^2+54g_2^2\lambda_7^2-20\lambda_1\lambda_7^2-148\lambda_2\lambda_7^2\\
&-72\lambda_3\lambda_7^2-76\lambda_4\lambda_7^2-72\lambda_5\lambda_7^2\\
&+\frac{1}{4}\Big(16\Big(10g_3^2\lambda_5-3\Big(2\lambda_1\lambda_5+2\lambda_3\lambda_5+3\lambda_4\lambda_5+5\lambda_6^2+\lambda_6\lambda_7\Big)\Big)+45g_2^2\lambda_5+5g_1^2\lambda_5\Big)\mathrm{Tr}\Big(Y_dY_d^\dagger\Big)\\
&+\frac{1}{4}\Big(15g_1^2\lambda_5+15g_2^2\lambda_5-16\Big(2\lambda_1\lambda_5+2\lambda_3\lambda_5+3\lambda_4\lambda_5+5\lambda_6^2+\lambda_6\lambda_7\Big)\Big)\mathrm{Tr}\Big(Y_eY_e^\dagger\Big)\\
&+\frac{17}{4}g_1^2\lambda_5\mathrm{Tr}\Big(Y_uY_u^\dagger\Big)+\frac{45}{4}g_2^2\lambda_5\mathrm{Tr}\Big(Y_uY_u^\dagger\Big)+40g_3^2\lambda_5\mathrm{Tr}\Big(Y_uY_u^\dagger\Big)-24\lambda_2\lambda_5\mathrm{Tr}\Big(Y_uY_u^\dagger\Big)\\
&-24\lambda_3\lambda_5\mathrm{Tr}\Big(Y_uY_u^\dagger\Big)-36\lambda_4\lambda_5\mathrm{Tr}\Big(Y_uY_u^\dagger\Big)-12\lambda_6\lambda_7\mathrm{Tr}\Big(Y_uY_u^\dagger\Big)-60\lambda_7^2\mathrm{Tr}\Big(Y_uY_u^\dagger\Big)\\
&-\frac{3}{2}\lambda_5\mathrm{Tr}\Big(Y_dY_d^\dagger Y_dY_d^\dagger\Big)-33\lambda_5\mathrm{Tr}\Big(Y_dY_u^\dagger Y_uY_d^\dagger\Big)-\frac{1}{2}\lambda_5\mathrm{Tr}\Big(Y_eY_e^\dagger Y_eY_e^\dagger\Big)-\frac{3}{2}\lambda_5\mathrm{Tr}\Big(Y_uY_u^\dagger Y_uY_u^\dagger\Big)
\end{aligned}
\tag{E.10}
$$

$$\beta^{(1)}_{\lambda_7} = +6\lambda_3\lambda_6 + 4\lambda_4\lambda_6 + 2\lambda_5\lambda_6 - \frac{9}{5}g_1^2\lambda_7 - 9g_2^2\lambda_7 + 24\lambda_2\lambda_7 + 6\lambda_3\lambda_7 + 8\lambda_4\lambda_7 + 10\lambda_5\lambda_7$$
$$+ 3\lambda_7\mathrm{Tr}\Big(Y_dY_d^\dagger\Big) + \lambda_7\mathrm{Tr}\Big(Y_eY_e^\dagger\Big) + 9\lambda_7\mathrm{Tr}\Big(Y_uY_u^\dagger\Big) \tag{E.11}$$

$$\beta^{(2)}_{\lambda_7} = +\frac{27}{20}g_1^4\lambda_6 + \frac{3}{2}g_1^2g_2^2\lambda_6 + \frac{45}{4}g_2^4\lambda_6 + \frac{36}{5}g_1^2\lambda_3\lambda_6 + 36g_2^2\lambda_3\lambda_6 - 36\lambda_1\lambda_3\lambda_6 - 36\lambda_2\lambda_3\lambda_6$$
$$- 36\lambda_3^2\lambda_6 + \frac{24}{5}g_1^2\lambda_4\lambda_6 + 18g_2^2\lambda_4\lambda_6 - 28\lambda_1\lambda_4\lambda_6 - 28\lambda_2\lambda_4\lambda_6 - 56\lambda_3\lambda_4\lambda_6 - 34\lambda_4^2\lambda_6$$
$$- \frac{6}{5}g_1^2\lambda_5\lambda_6 - 20\lambda_1\lambda_5\lambda_6 - 20\lambda_2\lambda_5\lambda_6 - 40\lambda_3\lambda_5\lambda_6 - 44\lambda_4\lambda_5\lambda_6 - 42\lambda_5^2\lambda_6 - 42\lambda_6^3 + \frac{1683}{200}g_1^4\lambda_7$$
$$+ \frac{87}{20}g_1^2g_2^2\lambda_7 - \frac{141}{8}g_2^4\lambda_7 + 6\lambda_1^2\lambda_7 + \frac{108}{5}g_1^2\lambda_2\lambda_7 + 108g_2^2\lambda_2\lambda_7 - 318\lambda_2^2\lambda_7 + \frac{18}{5}g_1^2\lambda_3\lambda_7$$
$$+ 18g_2^2\lambda_3\lambda_7 - 36\lambda_1\lambda_3\lambda_7 - 132\lambda_2\lambda_3\lambda_7 - 32\lambda_3^2\lambda_7 + 6g_1^2\lambda_4\lambda_7 + 36g_2^2\lambda_4\lambda_7 - 28\lambda_1\lambda_4\lambda_7$$
$$- 140\lambda_2\lambda_4\lambda_7 - 68\lambda_3\lambda_4\lambda_7 - 34\lambda_4^2\lambda_7 + 12g_1^2\lambda_5\lambda_7 + 54g_2^2\lambda_5\lambda_7 - 20\lambda_1\lambda_5\lambda_7 - 148\lambda_2\lambda_5\lambda_7$$
$$- 72\lambda_3\lambda_5\lambda_7 - 76\lambda_4\lambda_5\lambda_7 - 36\lambda_5^2\lambda_7 - 33\lambda_6^2\lambda_7 - 126\lambda_6\lambda_7^2 - 111\lambda_7^3 - \frac{1}{8}\Big(144\lambda_3\Big(2\lambda_6 + \lambda_7\Big)$$
$$- 160g_3^2\lambda_7 + 192\lambda_4\Big(\lambda_6 + \lambda_7\Big) + 240\lambda_5\lambda_7 - 45g_2^2\lambda_7 - 5g_1^2\lambda_7 + 96\lambda_5\lambda_6\Big)\mathrm{Tr}\Big(Y_dY_d^\dagger\Big)$$
$$- \frac{1}{8}\Big(- 15g_1^2\lambda_7 - 15g_2^2\lambda_7 + 32\lambda_5\lambda_6 + 48\lambda_3\Big(2\lambda_6 + \lambda_7\Big) + 64\lambda_4\Big(\lambda_6 + \lambda_7\Big) + 80\lambda_5\lambda_7\Big)\mathrm{Tr}\Big(Y_eY_e^\dagger\Big)$$
$$+ \frac{51}{8}g_1^2\lambda_7\mathrm{Tr}\Big(Y_uY_u^\dagger\Big) + \frac{135}{8}g_2^2\lambda_7\mathrm{Tr}\Big(Y_uY_u^\dagger\Big) + 60g_3^2\lambda_7\mathrm{Tr}\Big(Y_uY_u^\dagger\Big) - 144\lambda_2\lambda_7\mathrm{Tr}\Big(Y_uY_u^\dagger\Big)$$
$$- 18\lambda_3\lambda_7\mathrm{Tr}\Big(Y_uY_u^\dagger\Big) - 24\lambda_4\lambda_7\mathrm{Tr}\Big(Y_uY_u^\dagger\Big) - 30\lambda_5\lambda_7\mathrm{Tr}\Big(Y_uY_u^\dagger\Big) - \frac{27}{4}\lambda_7\mathrm{Tr}\Big(Y_dY_d^\dagger Y_dY_d^\dagger\Big)$$
$$- 21\lambda_7\mathrm{Tr}\Big(Y_dY_u^\dagger Y_uY_d^\dagger\Big) - \frac{9}{4}\lambda_7\mathrm{Tr}\Big(Y_eY_e^\dagger Y_eY_e^\dagger\Big) - \frac{33}{4}\lambda_7\mathrm{Tr}\Big(Y_uY_u^\dagger Y_uY_u^\dagger\Big) \tag{E.12}$$

$$\beta^{(1)}_{\lambda_1} = +\frac{27}{200}g_1^4 + \frac{9}{20}g_1^2g_2^2 + \frac{9}{8}g_2^4 - \frac{9}{5}g_1^2\lambda_1 - 9g_2^2\lambda_1 + 24\lambda_1^2 + 2\lambda_3^2 + 2\lambda_3\lambda_4 + \lambda_4^2 + \lambda_5^2 + 12\lambda_6^2$$
$$+ 12\lambda_1\mathrm{Tr}\Big(Y_dY_d^\dagger\Big) + 4\lambda_1\mathrm{Tr}\Big(Y_eY_e^\dagger\Big) - 6\mathrm{Tr}\Big(Y_dY_d^\dagger Y_dY_d^\dagger\Big) - 2\mathrm{Tr}\Big(Y_eY_e^\dagger Y_eY_e^\dagger\Big) \tag{E.13}$$

$$\beta^{(2)}_{\lambda_1} = -\frac{3537}{2000}g_1^6 - \frac{1719}{400}g_1^4g_2^2 - \frac{303}{80}g_1^2g_2^4 + \frac{291}{16}g_2^6 + \frac{1953}{200}g_1^4\lambda_1 + \frac{117}{20}g_1^2g_2^2\lambda_1 - \frac{51}{8}g_2^4\lambda_1 + \frac{108}{5}g_1^2\lambda_1^2$$
$$+ 108g_2^2\lambda_1^2 - 312\lambda_1^3 + \frac{9}{10}g_1^4\lambda_3 + \frac{15}{2}g_2^4\lambda_3 + \frac{12}{5}g_1^2\lambda_3^2 + 12g_2^2\lambda_3^2 - 20\lambda_1\lambda_3^2 - 8\lambda_3^3 + \frac{9}{20}g_1^4\lambda_4$$
$$+ \frac{3}{2}g_1^2g_2^2\lambda_4 + \frac{15}{4}g_2^4\lambda_4 + \frac{12}{5}g_1^2\lambda_3\lambda_4 + 12g_2^2\lambda_3\lambda_4 - 20\lambda_1\lambda_3\lambda_4 - 12\lambda_3^2\lambda_4 + \frac{6}{5}g_1^2\lambda_4^2$$
$$+ 3g_2^2\lambda_4^2 - 12\lambda_1\lambda_4^2 - 16\lambda_3\lambda_4^2 - 6\lambda_4^3 - \frac{3}{5}g_1^2\lambda_5^2 - 14\lambda_1\lambda_5^2 - 20\lambda_3\lambda_5^2 - 22\lambda_4\lambda_5^2$$
$$+ \frac{54}{5}g_1^2\lambda_6^2 + 54g_2^2\lambda_6^2 - 318\lambda_1\lambda_6^2 - 66\lambda_3\lambda_6^2 - 70\lambda_4\lambda_6^2 - 74\lambda_5\lambda_6^2 - 36\lambda_3\lambda_6\lambda_7 - 28\lambda_4\lambda_6\lambda_7$$
$$- 20\lambda_5\lambda_6\lambda_7 + 6\lambda_1\lambda_7^2 - 18\lambda_3\lambda_7^2 - 14\lambda_4\lambda_7^2 - 10\lambda_5\lambda_7^2$$
$$+ \frac{1}{20}\Big(- 5\Big(144\lambda_6^2 - 320g_3^2\lambda_1 + 576\lambda_1^2 - 90g_2^2\lambda_1 + 9g_2^4\Big) + 9g_1^4 + g_1^2\Big(50\lambda_1 + 54g_2^2\Big)\Big)\mathrm{Tr}\Big(Y_dY_d^\dagger\Big)$$
$$- \frac{3}{20}\Big(15g_1^4 - 2g_1^2\Big(11g_2^2 + 25\lambda_1\Big) + 5\Big(- 10g_2^2\lambda_1 + 16\lambda_6^2 + 64\lambda_1^2 + g_2^4\Big)\Big)\mathrm{Tr}\Big(Y_eY_e^\dagger\Big)$$

$$
\begin{aligned}
&- 12\lambda_3^2\mathrm{Tr}\Big(Y_uY_u^\dagger\Big) - 12\lambda_3\lambda_4\mathrm{Tr}\Big(Y_uY_u^\dagger\Big) - 6\lambda_4^2\mathrm{Tr}\Big(Y_uY_u^\dagger\Big) - 6\lambda_5^2\mathrm{Tr}\Big(Y_uY_u^\dagger\Big) - 36\lambda_6^2\mathrm{Tr}\Big(Y_uY_u^\dagger\Big)\\
&+ \frac{4}{5}g_1^2\mathrm{Tr}\Big(Y_dY_d^\dagger Y_dY_d^\dagger\Big) - 32g_3^2\mathrm{Tr}\Big(Y_dY_d^\dagger Y_dY_d^\dagger\Big) - 3\lambda_1\mathrm{Tr}\Big(Y_dY_d^\dagger Y_dY_d^\dagger\Big) - 9\lambda_1\mathrm{Tr}\Big(Y_dY_u^\dagger Y_uY_d^\dagger\Big)\\
&- \frac{12}{5}g_1^2\mathrm{Tr}\Big(Y_eY_e^\dagger Y_eY_e^\dagger\Big) - \lambda_1\mathrm{Tr}\Big(Y_eY_e^\dagger Y_eY_e^\dagger\Big) + 30\mathrm{Tr}\Big(Y_dY_d^\dagger Y_dY_d^\dagger Y_dY_d^\dagger\Big) + 6\mathrm{Tr}\Big(Y_dY_u^\dagger Y_uY_d^\dagger Y_dY_d^\dagger\Big)\\
&+ 10\mathrm{Tr}\Big(Y_eY_e^\dagger Y_eY_e^\dagger Y_eY_e^\dagger\Big) \qquad \text{(E.14)}\\
\beta_{\lambda_4}^{(1)} &= +\frac{9}{5}g_1^2g_2^2 - \frac{9}{5}g_1^2\lambda_4 - 9g_2^2\lambda_4 + 4\lambda_1\lambda_4 + 4\lambda_2\lambda_4 + 8\lambda_3\lambda_4 + 4\lambda_4^2 + 8\lambda_5^2 + 10\lambda_6^2 + 4\lambda_6\lambda_7 + 10\lambda_7^2\\
&+ 6\lambda_4\mathrm{Tr}\Big(Y_dY_d^\dagger\Big) + 2\lambda_4\mathrm{Tr}\Big(Y_eY_e^\dagger\Big) + 6\lambda_4\mathrm{Tr}\Big(Y_uY_u^\dagger\Big) + 12\mathrm{Tr}\Big(Y_dY_u^\dagger Y_uY_d^\dagger\Big) \qquad \text{(E.15)}\\
\beta_{\lambda_4}^{(2)} &= -\frac{657}{50}g_1^4g_2^2 - \frac{42}{5}g_1^2g_2^4 + 6g_1^2g_2^2\lambda_1 + 6g_1^2g_2^2\lambda_2 + \frac{6}{5}g_1^2g_2^2\lambda_3 + \frac{1413}{200}g_1^4\lambda_4 + \frac{153}{20}g_1^2g_2^2\lambda_4\\
&- \frac{231}{8}g_2^4\lambda_4 + \frac{24}{5}g_1^2\lambda_1\lambda_4 - 28\lambda_1^2\lambda_4 + \frac{24}{5}g_1^2\lambda_2\lambda_4 - 28\lambda_2^2\lambda_4 + \frac{12}{5}g_1^2\lambda_3\lambda_4 + 36g_2^2\lambda_3\lambda_4\\
&- 80\lambda_1\lambda_3\lambda_4 - 80\lambda_2\lambda_3\lambda_4 - 28\lambda_3^2\lambda_4 + \frac{24}{5}g_1^2\lambda_4^2 + 18g_2^2\lambda_4^2 - 40\lambda_1\lambda_4^2 - 40\lambda_2\lambda_4^2 - 28\lambda_3\lambda_4^2\\
&+ \frac{48}{5}g_1^2\lambda_5^2 + 54g_2^2\lambda_5^2 - 48\lambda_1\lambda_5^2 - 48\lambda_2\lambda_5^2 - 48\lambda_3\lambda_5^2 - 26\lambda_4\lambda_5^2 + \frac{42}{5}g_1^2\lambda_6^2 + 54g_2^2\lambda_6^2\\
&- 148\lambda_1\lambda_6^2 - 20\lambda_2\lambda_6^2 - 72\lambda_3\lambda_6^2 - 68\lambda_4\lambda_6^2 - 80\lambda_5\lambda_6^2 + \frac{24}{5}g_1^2\lambda_6\lambda_7 - 40\lambda_1\lambda_6\lambda_7 - 40\lambda_2\lambda_6\lambda_7\\
&- 80\lambda_3\lambda_6\lambda_7 - 160\lambda_4\lambda_6\lambda_7 - 96\lambda_5\lambda_6\lambda_7 + \frac{42}{5}g_1^2\lambda_7^2 + 54g_2^2\lambda_7^2 - 20\lambda_1\lambda_7^2 - 148\lambda_2\lambda_7^2\\
&- 72\lambda_3\lambda_7^2 - 68\lambda_4\lambda_7^2 - 80\lambda_5\lambda_7^2 + \frac{1}{20}\Big(5\Big(16\Big(10g_3^2\lambda_4\\
&- 3\Big(2\lambda_1\lambda_4 + 2\lambda_3\lambda_4 + 2\lambda_5^2 + 5\lambda_6^2 + \lambda_6\lambda_7 + \lambda_4^2\Big)\Big) + 45g_2^2\lambda_4\Big) + g_1^2\Big(108g_2^2 + 25\lambda_4\Big)\Big)\mathrm{Tr}\Big(Y_dY_d^\dagger\Big)\\
&+ \frac{1}{20}\Big(3g_1^2\Big(25\lambda_4 + 44g_2^2\Big) + 5\Big(15g_2^2\lambda_4 - 16\Big(2\lambda_1\lambda_4 + 2\lambda_3\lambda_4 + 2\lambda_5^2 + 5\lambda_6^2 + \lambda_6\lambda_7 + \lambda_4^2\Big)\Big)\Big)\mathrm{Tr}\Big(Y_eY_e^\dagger\Big)\\
&+ \frac{63}{5}g_1^2g_2^2\mathrm{Tr}\Big(Y_uY_u^\dagger\Big) + \frac{17}{4}g_1^2\lambda_4\mathrm{Tr}\Big(Y_uY_u^\dagger\Big) + \frac{45}{4}g_2^2\lambda_4\mathrm{Tr}\Big(Y_uY_u^\dagger\Big) + 40g_3^2\lambda_4\mathrm{Tr}\Big(Y_uY_u^\dagger\Big)\\
&- 24\lambda_2\lambda_4\mathrm{Tr}\Big(Y_uY_u^\dagger\Big) - 24\lambda_3\lambda_4\mathrm{Tr}\Big(Y_uY_u^\dagger\Big) - 12\lambda_4^2\mathrm{Tr}\Big(Y_uY_u^\dagger\Big) - 24\lambda_5^2\mathrm{Tr}\Big(Y_uY_u^\dagger\Big)\\
&- 12\lambda_6\lambda_7\mathrm{Tr}\Big(Y_uY_u^\dagger\Big) - 60\lambda_7^2\mathrm{Tr}\Big(Y_uY_u^\dagger\Big) - \frac{27}{2}\lambda_4\mathrm{Tr}\Big(Y_dY_d^\dagger Y_dY_d^\dagger\Big) + \frac{4}{5}g_1^2\mathrm{Tr}\Big(Y_dY_u^\dagger Y_uY_d^\dagger\Big)\\
&+ 64g_3^2\mathrm{Tr}\Big(Y_dY_u^\dagger Y_uY_d^\dagger\Big) - 24\lambda_3\mathrm{Tr}\Big(Y_dY_u^\dagger Y_uY_d^\dagger\Big) - 33\lambda_4\mathrm{Tr}\Big(Y_dY_u^\dagger Y_uY_d^\dagger\Big)\\
&- \frac{9}{2}\lambda_4\mathrm{Tr}\Big(Y_eY_e^\dagger Y_eY_e^\dagger\Big) - \frac{27}{2}\lambda_4\mathrm{Tr}\Big(Y_uY_u^\dagger Y_uY_u^\dagger\Big) - 12\mathrm{Tr}\Big(Y_dY_d^\dagger Y_dY_u^\dagger Y_uY_d^\dagger\Big) - 12\mathrm{Tr}\Big(Y_dY_u^\dagger Y_uY_d^\dagger Y_dY_d^\dagger\Big)\\
&- 24\mathrm{Tr}\Big(Y_dY_u^\dagger Y_uY_u^\dagger Y_uY_d^\dagger\Big) \qquad \text{(E.16)}\\
\beta_{\lambda_3}^{(1)} &= +\frac{27}{100}g_1^4 - \frac{9}{10}g_1^2g_2^2 + \frac{9}{4}g_2^4 - \frac{9}{5}g_1^2\lambda_3 - 9g_2^2\lambda_3 + 12\lambda_1\lambda_3 + 12\lambda_2\lambda_3 + 4\lambda_3^2 + 4\lambda_1\lambda_4 + 4\lambda_2\lambda_4 + 2\lambda_4^2\\
&+ 2\lambda_5^2 + 4\lambda_6^2 + 16\lambda_6\lambda_7 + 4\lambda_7^2 + 6\lambda_3\mathrm{Tr}\Big(Y_dY_d^\dagger\Big) + 2\lambda_3\mathrm{Tr}\Big(Y_eY_e^\dagger\Big) + 6\lambda_3\mathrm{Tr}\Big(Y_uY_u^\dagger\Big)\\
&- 12\mathrm{Tr}\Big(Y_dY_u^\dagger Y_uY_d^\dagger\Big) \qquad \text{(E.17)}\\
\beta_{\lambda_3}^{(2)} &= -\frac{3537}{1000}g_1^6 + \frac{909}{200}g_1^4g_2^2 + \frac{33}{40}g_1^2g_2^4 + \frac{291}{8}g_2^6 + \frac{27}{10}g_1^4\lambda_1 - 3g_1^2g_2^2\lambda_1 + \frac{45}{2}g_2^4\lambda_1 + \frac{27}{10}g_1^4\lambda_2
\end{aligned}
$$

$$
\begin{aligned}
&- 3g_1^2g_2^2\lambda_2 + \frac{45}{2}g_2^4\lambda_2 + \frac{1773}{200}g_1^4\lambda_3 + \frac{33}{20}g_1^2g_2^2\lambda_3 - \frac{111}{8}g_2^4\lambda_3 + \frac{72}{5}g_1^2\lambda_1\lambda_3 + 72g_2^2\lambda_1\lambda_3 \\
&- 60\lambda_1^2\lambda_3 + \frac{72}{5}g_1^2\lambda_2\lambda_3 + 72g_2^2\lambda_2\lambda_3 - 60\lambda_2^2\lambda_3 + \frac{6}{5}g_1^2\lambda_3^2 + 6g_2^2\lambda_3^2 - 72\lambda_1\lambda_3^2 - 72\lambda_2\lambda_3^2 \\
&- 12\lambda_3^3 + \frac{9}{10}g_1^4\lambda_4 - \frac{9}{5}g_1^2g_2^2\lambda_4 + \frac{15}{2}g_2^4\lambda_4 + \frac{24}{5}g_1^2\lambda_1\lambda_4 + 36g_2^2\lambda_1\lambda_4 - 16\lambda_1^2\lambda_4 + \frac{24}{5}g_1^2\lambda_2\lambda_4 \\
&+ 36g_2^2\lambda_2\lambda_4 - 16\lambda_2^2\lambda_4 - 12g_2^2\lambda_3\lambda_4 - 32\lambda_1\lambda_3\lambda_4 - 32\lambda_2\lambda_3\lambda_4 - 4\lambda_3^2\lambda_4 - \frac{6}{5}g_1^2\lambda_4^2 \\
&+ 6g_2^2\lambda_4^2 - 28\lambda_1\lambda_4^2 - 28\lambda_2\lambda_4^2 - 16\lambda_3\lambda_4^2 - 12\lambda_4^3 + \frac{12}{5}g_1^2\lambda_5^2 - 36\lambda_1\lambda_5^2 - 36\lambda_2\lambda_5^2 \\
&- 18\lambda_3\lambda_5^2 - 44\lambda_4\lambda_5^2 + \frac{6}{5}g_1^2\lambda_6^2 - 124\lambda_1\lambda_6^2 - 44\lambda_2\lambda_6^2 - 60\lambda_3\lambda_6^2 - 68\lambda_4\lambda_6^2 - 68\lambda_5\lambda_6^2 \\
&+ \frac{96}{5}g_1^2\lambda_6\lambda_7 + 108g_2^2\lambda_6\lambda_7 - 88\lambda_1\lambda_6\lambda_7 - 88\lambda_2\lambda_6\lambda_7 - 176\lambda_3\lambda_6\lambda_7 - 88\lambda_4\lambda_6\lambda_7 - 72\lambda_5\lambda_6\lambda_7 \\
&+ \frac{6}{5}g_1^2\lambda_7^2 - 44\lambda_1\lambda_7^2 - 124\lambda_2\lambda_7^2 - 60\lambda_3\lambda_7^2 - 68\lambda_4\lambda_7^2 - 68\lambda_5\lambda_7^2 \\
&+ \frac{1}{20}\Big(9g_1^4 + g_1^2\Big(25\lambda_3 - 54g_2^2\Big) - 5\Big(- 45g_2^2\lambda_3 + 8\Big(- 20g_3^2\lambda_3 + 3\Big(2\lambda_3^2 + 4\lambda_1\Big(3\lambda_3 + \lambda_4\Big) \\
&+ 4\lambda_6^2 + 8\lambda_6\lambda_7 + \lambda_4^2 + \lambda_5^2\Big)\Big) + 9g_2^4\Big)\Big)\mathrm{Tr}\Big(Y_dY_d^\dagger\Big) - \frac{1}{20}\Big(45g_1^4 + 5\Big(- 15g_2^2\lambda_3 \\
&+ 3g_2^4 + 8\Big(2\lambda_3^2 + 4\lambda_1\Big(3\lambda_3 + \lambda_4\Big) + 4\lambda_6^2 + 8\lambda_6\lambda_7 + \lambda_4^2 + \lambda_5^2\Big)\Big) + g_1^2\Big(66g_2^2 - 75\lambda_3\Big)\Big)\mathrm{Tr}\Big(Y_eY_e^\dagger\Big) \\
&- \frac{171}{100}g_1^4\mathrm{Tr}\Big(Y_uY_u^\dagger\Big) - \frac{63}{10}g_1^2g_2^2\mathrm{Tr}\Big(Y_uY_u^\dagger\Big) - \frac{9}{4}g_2^4\mathrm{Tr}\Big(Y_uY_u^\dagger\Big) + \frac{17}{4}g_1^2\lambda_3\mathrm{Tr}\Big(Y_uY_u^\dagger\Big) \\
&+ \frac{45}{4}g_2^2\lambda_3\mathrm{Tr}\Big(Y_uY_u^\dagger\Big) + 40g_3^2\lambda_3\mathrm{Tr}\Big(Y_uY_u^\dagger\Big) - 72\lambda_2\lambda_3\mathrm{Tr}\Big(Y_uY_u^\dagger\Big) - 12\lambda_3^2\mathrm{Tr}\Big(Y_uY_u^\dagger\Big) \\
&- 24\lambda_2\lambda_4\mathrm{Tr}\Big(Y_uY_u^\dagger\Big) - 6\lambda_4^2\mathrm{Tr}\Big(Y_uY_u^\dagger\Big) - 6\lambda_5^2\mathrm{Tr}\Big(Y_uY_u^\dagger\Big) - 48\lambda_6\lambda_7\mathrm{Tr}\Big(Y_uY_u^\dagger\Big) \\
&- 24\lambda_7^2\mathrm{Tr}\Big(Y_uY_u^\dagger\Big) - \frac{27}{2}\lambda_3\mathrm{Tr}\Big(Y_dY_d^\dagger Y_dY_d^\dagger\Big) - \frac{4}{5}g_1^2\mathrm{Tr}\Big(Y_dY_u^\dagger Y_uY_d^\dagger\Big) \\
&- 64g_3^2\mathrm{Tr}\Big(Y_dY_u^\dagger Y_uY_d^\dagger\Big) + 15\lambda_3\mathrm{Tr}\Big(Y_dY_u^\dagger Y_uY_d^\dagger\Big) - \frac{9}{2}\lambda_3\mathrm{Tr}\Big(Y_eY_e^\dagger Y_eY_e^\dagger\Big) \\
&- \frac{27}{2}\lambda_3\mathrm{Tr}\Big(Y_uY_u^\dagger Y_uY_u^\dagger\Big) + 12\mathrm{Tr}\Big(Y_dY_d^\dagger Y_dY_u^\dagger Y_uY_d^\dagger\Big) + 24\mathrm{Tr}\Big(Y_dY_u^\dagger Y_uY_d^\dagger Y_dY_d^\dagger\Big) \\
&+ 36\mathrm{Tr}\Big(Y_dY_u^\dagger Y_uY_u^\dagger Y_uY_d^\dagger\Big) \qquad \text{(E.18)}
\end{aligned}
$$

$$
\begin{aligned}
\beta_{\lambda_2}^{(1)} = &+\frac{27}{200}g_1^4 + \frac{9}{20}g_1^2g_2^2 + \frac{9}{8}g_2^4 - \frac{9}{5}g_1^2\lambda_2 - 9g_2^2\lambda_2 + 24\lambda_2^2 + 2\lambda_3^2 + 2\lambda_3\lambda_4 + \lambda_4^2 + \lambda_5^2 + 12\lambda_7^2 \\
&+ 12\lambda_2\mathrm{Tr}\Big(Y_uY_u^\dagger\Big) - 6\mathrm{Tr}\Big(Y_uY_u^\dagger Y_uY_u^\dagger\Big) \qquad \text{(E.19)}
\end{aligned}
$$

$$
\begin{aligned}
\beta_{\lambda_2}^{(2)} = &-\frac{3537}{2000}g_1^6 - \frac{1719}{400}g_1^4g_2^2 - \frac{303}{80}g_1^2g_2^4 + \frac{291}{16}g_2^6 + \frac{1953}{200}g_1^4\lambda_2 + \frac{117}{20}g_1^2g_2^2\lambda_2 - \frac{51}{8}g_2^4\lambda_2 + \frac{108}{5}g_1^2\lambda_2^2 \\
&+ 108g_2^2\lambda_2^2 - 312\lambda_2^3 + \frac{9}{10}g_1^4\lambda_3 + \frac{15}{2}g_2^4\lambda_3 + \frac{12}{5}g_1^2\lambda_3^2 + 12g_2^2\lambda_3^2 - 20\lambda_2\lambda_3^2 - 8\lambda_3^3 + \frac{9}{20}g_1^4\lambda_4 \\
&+ \frac{3}{2}g_1^2g_2^2\lambda_4 + \frac{15}{4}g_2^4\lambda_4 + \frac{12}{5}g_1^2\lambda_3\lambda_4 + 12g_2^2\lambda_3\lambda_4 - 20\lambda_2\lambda_3\lambda_4 - 12\lambda_3^2\lambda_4 + \frac{6}{5}g_1^2\lambda_4^2 \\
&+ 3g_2^2\lambda_4^2 - 12\lambda_2\lambda_4^2 - 16\lambda_3\lambda_4^2 - 6\lambda_4^3 - \frac{3}{5}g_1^2\lambda_5^2 - 14\lambda_2\lambda_5^2 - 20\lambda_3\lambda_5^2 - 22\lambda_4\lambda_5^2 + 6\lambda_2\lambda_6^2
\end{aligned}
$$

$$
\begin{aligned}
&- 18\lambda_3\lambda_6^2 - 14\lambda_4\lambda_6^2 - 10\lambda_5\lambda_6^2 - 36\lambda_3\lambda_6\lambda_7 - 28\lambda_4\lambda_6\lambda_7 - 20\lambda_5\lambda_6\lambda_7 + \frac{54}{5}g_1^2\lambda_7^2 + 54g_2^2\lambda_7^2 \\
&- 318\lambda_2\lambda_7^2 - 66\lambda_3\lambda_7^2 - 70\lambda_4\lambda_7^2 - 74\lambda_5\lambda_7^2 - 6\Big(2\lambda_3^2 + 2\lambda_3\lambda_4 + 6\lambda_7^2 + \lambda_4^2 + \lambda_5^2\Big)\mathrm{Tr}\Big(Y_dY_d^\dagger\Big) \\
&- 2\Big(2\lambda_3^2 + 2\lambda_3\lambda_4 + 6\lambda_7^2 + \lambda_4^2 + \lambda_5^2\Big)\mathrm{Tr}\Big(Y_eY_e^\dagger\Big) - \frac{171}{100}g_1^4\mathrm{Tr}\Big(Y_uY_u^\dagger\Big) + \frac{63}{10}g_1^2g_2^2\mathrm{Tr}\Big(Y_uY_u^\dagger\Big) \\
&- \frac{9}{4}g_2^4\mathrm{Tr}\Big(Y_uY_u^\dagger\Big) + \frac{17}{2}g_1^2\lambda_2\mathrm{Tr}\Big(Y_uY_u^\dagger\Big) + \frac{45}{2}g_2^2\lambda_2\mathrm{Tr}\Big(Y_uY_u^\dagger\Big) + 80g_3^2\lambda_2\mathrm{Tr}\Big(Y_uY_u^\dagger\Big) \\
&- 144\lambda_2^2\mathrm{Tr}\Big(Y_uY_u^\dagger\Big) - 36\lambda_7^2\mathrm{Tr}\Big(Y_uY_u^\dagger\Big) - 9\lambda_2\mathrm{Tr}\Big(Y_dY_u^\dagger Y_uY_d^\dagger\Big) - \frac{8}{5}g_1^2\mathrm{Tr}\Big(Y_uY_u^\dagger Y_uY_u^\dagger\Big) \\
&- 32g_3^2\mathrm{Tr}\Big(Y_uY_u^\dagger Y_uY_u^\dagger\Big) - 3\lambda_2\mathrm{Tr}\Big(Y_uY_u^\dagger Y_uY_u^\dagger\Big) + 6\mathrm{Tr}\Big(Y_dY_u^\dagger Y_uY_u^\dagger Y_uY_d^\dagger\Big) + 30\mathrm{Tr}\Big(Y_uY_u^\dagger Y_uY_u^\dagger Y_uY_u^\dagger\Big)
\end{aligned}
\tag{E.20}
$$

E.3 Yukawa Couplings

$$\beta_{Y_u}^{(1)} = \frac{1}{2}\Big(3Y_uY_u^\dagger Y_u + Y_uY_d^\dagger Y_d\Big) + Y_u\Big(3\mathrm{Tr}\Big(Y_uY_u^\dagger\Big) - 8g_3^2 - \frac{17}{20}g_1^2 - \frac{9}{4}g_2^2\Big) \tag{E.21}$$

$$
\begin{aligned}
\beta_{Y_u}^{(2)} = {}& +Y_uY_d^\dagger Y_d\Big(- 2\lambda_3 + 2\lambda_4 + \frac{16}{3}g_3^2 + \frac{33}{16}g_2^2 - \frac{3}{4}\mathrm{Tr}\Big(Y_eY_e^\dagger\Big) - \frac{41}{240}g_1^2 - \frac{9}{4}\mathrm{Tr}\Big(Y_dY_d^\dagger\Big)\Big) \\
&+ \frac{1}{80}\Big(- 20\Big(- 6Y_uY_u^\dagger Y_uY_u^\dagger Y_u + Y_uY_d^\dagger Y_dY_d^\dagger Y_d + Y_uY_d^\dagger Y_dY_u^\dagger Y_u\Big) \\
&+ Y_uY_u^\dagger Y_u\Big(1280g_3^2 + 223g_1^2 - 540\mathrm{Tr}\Big(Y_uY_u^\dagger\Big) + 675g_2^2 - 960\lambda_2\Big)\Big) \\
&+ Y_u\Big(\frac{1267}{600}g_1^4 - \frac{9}{20}g_1^2g_2^2 - \frac{21}{4}g_2^4 + \frac{19}{15}g_1^2g_3^2 + 9g_2^2g_3^2 - 108g_3^4 + 6\lambda_2^2 + \lambda_3^2 + \lambda_3\lambda_4 + \lambda_4^2 + \frac{3}{2}\lambda_5^2 + \frac{3}{2}\lambda_6^2 \\
&+ \frac{9}{2}\lambda_7^2 + \frac{1}{8}\Big(160g_3^2 + 17g_1^2 + 45g_2^2\Big)\mathrm{Tr}\Big(Y_uY_u^\dagger\Big) - \frac{9}{4}\mathrm{Tr}\Big(Y_dY_u^\dagger Y_uY_d^\dagger\Big) - \frac{27}{4}\mathrm{Tr}\Big(Y_uY_u^\dagger Y_uY_u^\dagger\Big)\Big)
\end{aligned}
\tag{E.22}
$$

$$\beta_{Y_d}^{(1)} = \frac{1}{4}\Big(2\Big(3Y_dY_d^\dagger Y_d + Y_dY_u^\dagger Y_u\Big) - Y_d\Big(- 12\mathrm{Tr}\Big(Y_dY_d^\dagger\Big) + 32g_3^2 - 4\mathrm{Tr}\Big(Y_eY_e^\dagger\Big) + 9g_2^2 + g_1^2\Big)\Big) \tag{E.23}$$

$$
\begin{aligned}
\beta_{Y_d}^{(2)} = {}& +\frac{1}{240}\Big(60\Big(6Y_dY_d^\dagger Y_dY_d^\dagger Y_d - Y_dY_u^\dagger Y_uY_d^\dagger Y_d - Y_dY_u^\dagger Y_uY_u^\dagger Y_u\Big) \\
&+ 3Y_dY_d^\dagger Y_d\Big(1280g_3^2 - 180\mathrm{Tr}\Big(Y_eY_e^\dagger\Big) + 187g_1^2 - 540\mathrm{Tr}\Big(Y_dY_d^\dagger\Big) + 675g_2^2 - 960\lambda_1\Big) \\
&+ Y_dY_u^\dagger Y_u\Big(5\Big(256g_3^2 - 96\lambda_3 + 96\lambda_4 + 99g_2^2\Big) - 53g_1^2 - 540\mathrm{Tr}\Big(Y_uY_u^\dagger\Big)\Big)\Big) \\
&+ Y_d\Big(- \frac{113}{600}g_1^4 - \frac{27}{20}g_1^2g_2^2 - \frac{21}{4}g_2^4 + \frac{31}{15}g_1^2g_3^2 + 9g_2^2g_3^2 - 108g_3^4 + 6\lambda_1^2 + \lambda_3^2 + \lambda_3\lambda_4 + \lambda_4^2 + \frac{3}{2}\lambda_5^2 + \frac{9}{2}\lambda_6^2 \\
&+ \frac{3}{2}\lambda_7^2 + \frac{5}{8}\Big(32g_3^2 + 9g_2^2 + g_1^2\Big)\mathrm{Tr}\Big(Y_dY_d^\dagger\Big) + \frac{15}{8}\Big(g_1^2 + g_2^2\Big)\mathrm{Tr}\Big(Y_eY_e^\dagger\Big) - \frac{27}{4}\mathrm{Tr}\Big(Y_dY_d^\dagger Y_dY_d^\dagger\Big) \\
&- \frac{9}{4}\mathrm{Tr}\Big(Y_dY_u^\dagger Y_uY_d^\dagger\Big) - \frac{9}{4}\mathrm{Tr}\Big(Y_eY_e^\dagger Y_eY_e^\dagger\Big)\Big)
\end{aligned}
\tag{E.24}
$$

$$\beta_{Y_e}^{(1)} = \frac{1}{4}\Big(6Y_eY_e^\dagger Y_e + Y_e\Big(12\mathrm{Tr}\Big(Y_dY_d^\dagger\Big) + 4\mathrm{Tr}\Big(Y_eY_e^\dagger\Big) - 9\Big(g_1^2 + g_2^2\Big)\Big)\Big) \tag{E.25}$$

$$\begin{aligned}\beta_{Y_e}^{(2)} = &+\frac{3}{80}\Big(40Y_eY_e^\dagger Y_eY_e^\dagger Y_e + Y_eY_e^\dagger Y_e\Big(129g_1^2 - 180\mathrm{Tr}\Big(Y_dY_d^\dagger\Big) + 225g_2^2 - 320\lambda_1 - 60\mathrm{Tr}\Big(Y_eY_e^\dagger\Big)\Big)\Big)\\ &+ Y_e\Big(\frac{1449}{200}g_1^4 + \frac{27}{20}g_1^2g_2^2 - \frac{21}{4}g_2^4 + 6\lambda_1^2 + \lambda_3^2 + \lambda_3\lambda_4 + \lambda_4^2 + \frac{3}{2}\lambda_5^2 + \frac{9}{2}\lambda_6^2 + \frac{3}{2}\lambda_7^2\\ &+ \frac{5}{8}\Big(32g_3^2 + 9g_2^2 + g_1^2\Big)\mathrm{Tr}\Big(Y_dY_d^\dagger\Big) + \frac{15}{8}\Big(g_1^2 + g_2^2\Big)\mathrm{Tr}\Big(Y_eY_e^\dagger\Big) - \frac{27}{4}\mathrm{Tr}\Big(Y_dY_d^\dagger Y_dY_d^\dagger\Big)\\ &- \frac{9}{4}\mathrm{Tr}\Big(Y_dY_u^\dagger Y_uY_d^\dagger\Big) - \frac{9}{4}\mathrm{Tr}\Big(Y_eY_e^\dagger Y_eY_e^\dagger\Big)\Big)\end{aligned} \tag{E.26}$$

List of Figures

List of Tables

Bibliography

[1] J. McDowall and D. J. Miller, *High scale boundary conditions with an additional complex singlet*, arXiv:1802.02391. (Cited on page 5.)

[2] J. McDowall and D. J. Miller, *High Scale Boundary Conditions in Models with Two Higgs Doublets*, arXiv:1810.04518. (Cited on page 5.)

[3] S. L. Glashow, *Partial Symmetries of Weak Interactions*, *Nucl. Phys.* **22** (1961) 579–588. (Cited on page 1.)

[4] S. Weinberg, *A Model of Leptons*, *Phys. Rev. Lett.* **19** (1967) 1264–1266. (Cited on page 1.)

[5] A. Salam, *Weak and Electromagnetic Interactions*, *Conf. Proc.* **C680519** (1968) 367–377. (Cited on page 1.)

[6] **ATLAS** Collaboration, G. Aad et al., *Observation of a new particle in the search for the Standard Model Higgs boson with the ATLAS detector at the LHC*, *Phys. Lett.* **B716** (2012) 1–29, [arXiv:1207.7214]. (Cited on page 1.)

[7] **CMS** Collaboration, S. Chatrchyan et al., *Observation of a new boson at a mass of 125 GeV with the CMS experiment at the LHC*, *Phys. Lett.* **B716** (2012) 30–61, [arXiv:1207.7235]. (Cited on page 1.)

[8] **ATLAS, CMS** Collaboration, G. Aad et al., *Combined Measurement of the Higgs Boson Mass in pp Collisions at $\sqrt{s} = 7$ and 8 TeV with the ATLAS and CMS Experiments*, *Phys. Rev. Lett.* **114** (2015) 191803, [arXiv:1503.07589]. (Cited on pages 1, 24 and 93.)

[9] K. G. Wilson, *Renormalization group and strong interactions*, *Phys. Rev. D* **3** (Apr, 1971) 1818–1846. (Cited on page 1.)

[10] E. Gildener, *Gauge-symmetry hierarchies*, *Phys. Rev. D* **14** (Sep, 1976) 1667–1672. (Cited on page 1.)

[11] E. Gildener and S. Weinberg, *Symmetry breaking and scalar bosons*, *Phys. Rev. D* **13** (Jun, 1976) 3333–3341. (Cited on page 1.)

[12] I. J. Aitchison, *Supersymmetry and the MSSM: An Elementary introduction*, hep-ph/0505105. (Cited on pages 1 and 20.)

[13] J. L. Feng, *Naturalness and the Status of Supersymmetry*, *Ann.Rev.Nucl.Part.Sci.* **63** (2013) 351–382, [arXiv:1302.6587]. (Cited on page 1.)

[14] G. G. Ross, K. Schmidt-Hoberg, and F. Staub, *Revisiting fine-tuning in the MSSM*, *JHEP* **03** (2017) 021, [arXiv:1701.03480]. (Cited on pages 1, 2 and 21.)

[15] D. Buttazzo, G. Degrassi, P. P. Giardino, G. F. Giudice, F. Sala, A. Salvio, and A. Strumia, *Investigating the near-criticality of the Higgs boson*, *JHEP* **12** (2013) 089, [arXiv:1307.3536]. (Cited on pages 2, 3, 21, 23, 24, 30, 93, 99 and 139.)

[16] N. Craig, *The State of Supersymmetry after Run I of the LHC*, arXiv:1309.0528. (Cited on pages 2, 21 and 93.)

[17] F. Staub, *SARAH 4 : A tool for (not only SUSY) model builders*, *Comput. Phys. Commun.* **185** (2014) 1773–1790, [arXiv:1309.7223]. (Cited on pages 2, 26, 52, 60, 76, 95, 97 and 139.)

[18] P. Athron, J.-h. Park, D. Stockinger, and A. Voigt, *FlexibleSUSY - A spectrum generator generator for supersymmetric models*, *Comput. Phys. Commun.* **190** (2015) 139–172, [arXiv:1406.2319]. (Cited on pages 2, 26, 52, 60, 76, 95, 97 and 139.)

[19] P. Athron, M. Bach, D. Harries, T. Kwasnitza, J.-h. Park, D. Stöckinger, A. Voigt, and J. Ziebell, *FlexibleSUSY 2.0: Extensions to investigate the phenomenology of SUSY and non-SUSY models*, arXiv:1710.03760. (Cited on pages 2, 26, 52, 60, 95, 97 and 139.)

[20] B. C. Allanach, *SOFTSUSY: a program for calculating supersymmetric spectra*, *Comput. Phys. Commun.* **143** (2002) 305–331, [hep-ph/0104145]. (Cited on pages 2, 26, 52, 60, 95, 97 and 139.)

[21] B. C. Allanach, P. Athron, L. C. Tunstall, A. Voigt, and A. G. Williams, *Next-to-Minimal SOFTSUSY*, *Comput. Phys. Commun.* **185** (2014) 2322–2339, [arXiv:1311.7659]. (Cited on pages 2, 26, 52, 60, 95, 97 and 139.)

[22] J. R. Espinosa, G. F. Giudice, E. Morgante, A. Riotto, L. Senatore, A. Strumia, and N. Tetradis, *The cosmological Higgstory of the vacuum instability*, *JHEP* **09** (2015) 174, [arXiv:1505.04825]. (Cited on page 2.)

[23] G. Degrassi, S. Di Vita, J. Elias-Miro, J. R. Espinosa, G. F. Giudice, G. Isidori, and A. Strumia, *Higgs mass and vacuum stability in the Standard Model at NNLO*, *JHEP* **08** (2012) 098, [arXiv:1205.6497]. (Cited on pages 3, 25 and 26.)

[24] M. Holthausen, K. S. Lim, and M. Lindner, *Planck scale Boundary Conditions and the Higgs Mass*, *JHEP* **02** (2012) 037, [arXiv:1112.2415]. (Cited on pages 3 and 25.)

[25] G. Iacobellis and I. Masina, *Stationary configurations of the Standard Model Higgs potential: electroweak stability and rising inflection point*, arXiv:1604.06046. (Cited on pages 3 and 25.)

[26] N. Haba, K. Kaneta, and R. Takahashi, *Planck scale boundary conditions in the standard model with singlet scalar dark matter*, *JHEP* **04** (2014) 029, [arXiv:1312.2089]. (Cited on pages 3 and 25.)

[27] A. Eichhorn and M. M. Scherer, *Planck scale, Higgs mass, and scalar dark matter*, *Phys. Rev.* **D90** (2014), no. 2 025023, [arXiv:1404.5962]. (Cited on pages 3 and 25.)

[28] N. Khan and S. Rakshit, *Study of electroweak vacuum metastability with a singlet scalar dark matter*, *Phys. Rev.* **D90** (2014), no. 11 113008, [arXiv:1407.6015]. (Cited on pages 3 and 25.)

[29] A. J. Helmboldt, P. Humbert, M. Lindner, and J. Smirnov, *Minimal conformal extensions of the Higgs sector*, *JHEP* **07** (2017) 113, [arXiv:1603.03603]. (Cited on pages 3 and 25.)

[30] C. D. Froggatt and H. B. Nielsen, *Standard model criticality prediction: Top mass 173 +- 5-GeV and Higgs mass 135 +- 9-GeV*, *Phys. Lett.* **B368** (1996) 96–102, [hep-ph/9511371]. (Cited on pages 3, 28, 29, 30 and 99.)

[31] M. Shaposhnikov and C. Wetterich, *Asymptotic safety of gravity and the Higgs boson mass*, *Phys. Lett.* **B683** (2010) 196–200, [arXiv:0912.0208]. (Cited on pages 3, 32 and 102.)

[32] H. Georgi and S. L. Glashow, *Unity of All Elementary Particle Forces*, *Phys. Rev. Lett.* **32** (1974) 438–441. (Cited on pages 3 and 39.)

[33] R. N. Mohapatra and G. Senjanovic, *Neutrino Masses and Mixings in Gauge Models with Spontaneous Parity Violation*, *Phys. Rev.* **D23** (1981) 165. (Cited on page 4.)

[34] S. Bertolini, M. Frigerio, and M. Malinsky, *Fermion masses in SUSY SO(10) with type II seesaw: A Non-minimal predictive scenario*, *Phys.Rev.* **D70** (2004) 095002, [hep-ph/0406117]. (Cited on pages 4 and 47.)

[35] G. 't Hooft, *Magnetic Monopoles in Unified Gauge Theories*, *Nucl. Phys.* **B79** (1974) 276–284. [,291(1974)]. (Cited on page 4.)

[36] M. Gell-Mann, P. Ramond, and R. Slansky, *Complex Spinors and Unified Theories*, *Conf. Proc.* **C790927** (1979) 315–321, [arXiv:1306.4669]. (Cited on page 4.)

[37] **Particle Data Group** Collaboration, C. Patrignani et al., *Review of Particle Physics*, *Chin. Phys.* **C40** (2016), no. 10 100001. (Cited on pages 13, 19, 98 and 149.)

[38] P. W. Higgs, *Broken symmetries, massless particles and gauge fields*, *Phys. Lett.* **12** (1964) 132–133. (Cited on page 13.)

[39] F. Englert and R. Brout, *Broken Symmetry and the Mass of Gauge Vector Mesons*, *Phys. Rev. Lett.* **13** (1964) 321–323. [,157(1964)]. (Cited on page 13.)

[40] G. S. Guralnik, C. R. Hagen, and T. W. B. Kibble, *Global Conservation Laws and Massless Particles*, *Phys. Rev. Lett.* **13** (1964) 585–587. [,162(1964)]. (Cited on page 13.)

[41] N. Cabibbo, *Unitary Symmetry and Leptonic Decays*, *Phys. Rev. Lett.* **10** (1963) 531–533. [,648(1963)]. (Cited on page 15.)

[42] M. Kobayashi and T. Maskawa, *CP Violation in the Renormalizable Theory of Weak Interaction*, *Prog. Theor. Phys.* **49** (1973) 652–657. (Cited on page 15.)

[43] C. G. Callan, Jr., *Broken scale invariance in scalar field theory*, *Phys. Rev.* **D2** (1970) 1541–1547. (Cited on page 17.)

[44] S. P. Martin, *A Supersymmetry primer*, *Adv.Ser.Direct.High Energy Phys.* **21** (2010) 1–153, [hep-ph/9709356]. (Cited on page 20.)

[45] Y. Golfand and E. Likhtman, *Extension of the Algebra of Poincare Group Generators and Violation of p Invariance*, *JETP Lett.* **13** (1971) 323–326. (Cited on page 21.)

[46] **Super-Kamiokande** Collaboration, Y. Fukuda et al., *Evidence for oscillation of atmospheric neutrinos*, *Phys. Rev. Lett.* **81** (1998) 1562–1567, [hep-ex/9807003]. (Cited on page 21.)

[47] **SNO** Collaboration, Q. R. Ahmad et al., *Measurement of the rate of $\nu_e + d \to p + p + e^-$ interactions produced by ^8B solar neutrinos at the Sudbury Neutrino Observatory*, *Phys. Rev. Lett.* **87** (2001) 071301, [nucl-ex/0106015]. (Cited on page 21.)

[48] **RENO** Collaboration, J. K. Ahn et al., *Observation of Reactor Electron Antineutrino Disappearance in the RENO Experiment*, *Phys. Rev. Lett.* **108** (2012) 191802, [arXiv:1204.0626]. (Cited on page 21.)

[49] **Particle Data Group** Collaboration, M. Tanabashi et al., *Review of Particle Physics*, *Phys. Rev.* **D98** (2018), no. 3 030001. (Cited on page 22.)

[50] L. Canetti, M. Drewes, and M. Shaposhnikov, *Matter and Antimatter in the Universe*, *New J. Phys.* **14** (2012) 095012, [arXiv:1204.4186]. (Cited on page 22.)

[51] A. D. Sakharov, *Violation of CP Invariance, C asymmetry, and baryon asymmetry of the universe*, *Pisma Zh. Eksp. Teor. Fiz.* **5** (1967) 32–35. [Usp. Fiz. Nauk161,no.5,61(1991)]. (Cited on page 22.)

[52] **CMS** Collaboration, V. Khachatryan et al., *Constraints on the spin-parity and anomalous HVV couplings of the Higgs boson in proton collisions at 7 and 8 TeV*, *Phys. Rev.* **D92** (2015), no. 1 012004, [arXiv:1411.3441]. (Cited on pages 24 and 93.)

[53] **CMS** Collaboration, V. Khachatryan et al., *Precise determination of the mass of the Higgs boson and tests of compatibility of its couplings with the standard model predictions using proton collisions at 7 and 8 TeV*, *Eur. Phys. J.* **C75** (2015), no. 5 212, [arXiv:1412.8662]. (Cited on pages 24 and 93.)

[54] **ATLAS** Collaboration, G. Aad et al., *Measurements of the Higgs boson production and decay rates and coupling strengths using pp collision data at $\sqrt{s} = 7$ and 8 TeV in the ATLAS experiment*, *Eur. Phys. J.* **C76** (2016), no. 1 6, [arXiv:1507.04548]. (Cited on pages 24 and 93.)

[55] **Planck** Collaboration, P. A. R. Ade et al., *Planck 2015 results. XIII. Cosmological parameters*, *Astron. Astrophys.* **594** (2016) A13, [arXiv:1502.01589]. (Cited on pages 24, 55, 61, 78 and 99.)

[56] M. E. Machacek and M. T. Vaughn, *Two Loop Renormalization Group Equations in a General Quantum Field Theory. 2. Yukawa Couplings*, *Nucl.Phys.* **B236** (1984) 221. (Cited on pages 25, 119, 123, 127 and 131.)

[57] M. E. Machacek and M. T. Vaughn, *Two Loop Renormalization Group Equations in a General Quantum Field Theory. 1. Wave Function Renormalization*, *Nucl.Phys.* **B222** (1983) 83. (Cited on pages 25, 35, 119, 123, 127 and 131.)

[58] M. E. Machacek and M. T. Vaughn, *Two Loop Renormalization Group Equations in a General Quantum Field Theory. 3. Scalar Quartic Couplings*, *Nucl.Phys.* **B249** (1985) 70. (Cited on pages 25, 35, 119, 123, 127 and 131.)

[59] M.-x. Luo, H.-w. Wang, and Y. Xiao, *Two loop renormalization group equations in general gauge field theories*, *Phys. Rev.* **D67** (2003) 065019, [hep-ph/0211440]. (Cited on pages 25, 119, 123, 127 and 131.)

[60] S. Bethke, G. Dissertori, and G. Salam, *"particle data group review on quantum chromodynamics, http://pdg.lbl.gov/2015/reviews/rpp2015-rev-qcd.pdf "*, . (Cited on page 26.)

[61] P. H. Ginsparg, *Gauge and Gravitational Couplings in Four-Dimensional String Theories*, *Phys. Lett.* **B197** (1987) 139–143. (Cited on page 27.)

[62] E. Witten, *Strong coupling expansion of Calabi-Yau compactification*, *Nucl. Phys.* **B471** (1996) 135–158, [hep-th/9602070]. (Cited on page 27.)

[63] S. R. Coleman and E. J. Weinberg, *Radiative Corrections as the Origin of Spontaneous Symmetry Breaking*, *Phys. Rev.* **D7** (1973) 1888–1910. (Cited on page 27.)

[64] J. A. Casas, J. R. Espinosa, M. Quiros, and A. Riotto, *The Lightest Higgs boson mass in the minimal supersymmetric standard model*, *Nucl. Phys.* **B436** (1995) 3–29, [hep-ph/9407389]. [Erratum: Nucl. Phys.B439,466(1995)]. (Cited on page 27.)

[65] F. Jegerlehner, M. Yu. Kalmykov, and B. A. Kniehl, *Self-consistence of the Standard Model via the renormalization group analysis*, *J. Phys. Conf. Ser.* **608** (2015), no. 1 012074, [arXiv:1412.4215]. (Cited on pages 27, 28 and 140.)

[66] C. D. Froggatt, L. V. Laperashvili, R. B. Nevzorov, H. B. Nielsen, and M. Sher, *The Two Higgs doublet model and the multiple point principle*, *Bled Workshops Phys.* **5** (2004), no. 2 28–39, [hep-ph/0412333]. (Cited on pages 30 and 100.)

[67] C. D. Froggatt, L. Laperashvili, R. Nevzorov, H. B. Nielsen, and M. Sher, *Implementation of the multiple point principle in the two-Higgs doublet model of type II*, *Phys. Rev.* **D73** (2006) 095005, [hep-ph/0602054]. (Cited on pages 30 and 100.)

[68] C. D. Froggatt, R. Nevzorov, H. B. Nielsen, and D. Thompson, *Fixed point scenario in the Two Higgs Doublet Model inspired by degenerate vacua*, *Phys. Lett.* **B657** (2007) 95–102, [arXiv:0708.2903]. (Cited on pages 30 and 100.)

[69] N. Haba, H. Ishida, N. Okada, and Y. Yamaguchi, *Multiple-point principle with a scalar singlet extension of the Standard Model*, *PTEP* **2017** (2017), no. 1 013B03, [arXiv:1608.00087]. (Cited on pages 30 and 100.)

[70] K. Kawana, *Multiple Point Principle of the Standard Model with Scalar Singlet Dark Matter and Right Handed Neutrinos*, *PTEP* **2015** (2015) 023B04, [arXiv:1411.2097]. (Cited on pages 30 and 100.)

[71] N. Haba, H. Ishida, K. Kaneta, and R. Takahashi, *Vanishing Higgs potential at the Planck scale in a singlet extension of the standard model*, *Phys. Rev.* **D90** (2014) 036006, [arXiv:1406.0158]. (Cited on page 30.)

[72] Y. Hamada, H. Kawai, and K.-y. Oda, *Predictions on mass of Higgs portal scalar dark matter from Higgs inflation and flat potential*, *JHEP* **07** (2014) 026, [arXiv:1404.6141]. (Cited on pages 30 and 100.)

[73] K. G. Wilson, *Renormalization group and critical phenomena. 1. Renormalization group and the Kadanoff scaling picture*, *Phys. Rev.* **B4** (1971) 3174–3183. (Cited on page 30.)

[74] S. Weinberg, *Ultraviolet divergences in quantum theories of gravitation, in General Relativity: an Einstein Centenary Survey, Hawking, S. and Israel, W*, pp. 790–831. Mar., 2010. (Cited on page 30.)

[75] D. F. Litim and F. Sannino, *Asymptotic safety guaranteed*, *JHEP* **12** (2014) 178, [arXiv:1406.2337]. (Cited on pages 30 and 102.)

[76] D. F. Litim, M. Mojaza, and F. Sannino, *Vacuum stability of asymptotically safe gauge-Yukawa theories*, *JHEP* **01** (2016) 081, [arXiv:1501.03061]. (Cited on pages 30 and 102.)

[77] A. D. Bond and D. F. Litim, *Theorems for Asymptotic Safety of Gauge Theories*, arXiv:1608.00519. (Cited on pages 30, 31 and 102.)

[78] A. D. Bond, G. Hiller, K. Kowalska, and D. F. Litim, *Directions for model building from asymptotic safety*, arXiv:1702.01727. (Cited on pages 30, 31 and 102.)

[79] F. Sannino and I. M. Shoemaker, *Asymptotically Safe Dark Matter*, *Phys. Rev.* **D92** (2015), no. 4 043518, [arXiv:1412.8034]. (Cited on pages 30 and 102.)

[80] B. Bajc and F. Sannino, *Asymptotically Safe Grand Unification*, *JHEP* **12** (2016) 141, [arXiv:1610.09681]. (Cited on pages 30 and 102.)

[81] G. M. Pelaggi, F. Sannino, A. Strumia, and E. Vigiani, *Naturalness of asymptotically safe Higgs*, arXiv:1701.01453. (Cited on pages 30 and 102.)

[82] G. M. Pelaggi, A. D. Plascencia, A. Salvio, F. Sannino, J. Smirnov, and A. Strumia, *Asymptotically Safe Standard Model Extensions*, arXiv:1708.00437. (Cited on pages 30 and 102.)

[83] G. F. Giudice, G. Isidori, A. Salvio, and A. Strumia, *Softened Gravity and the Extension of the Standard Model up to Infinite Energy*, *JHEP* **02** (2015) 137, [arXiv:1412.2769]. (Cited on page 31.)

[84] M. B. Einhorn and D. R. T. Jones, *Asymptotic freedom in certain $SO(N)$ and $SU(N)$ models*, *Phys. Rev.* **D96** (2017), no. 5 055035, [arXiv:1705.00751]. (Cited on page 31.)

[85] B. Holdom, J. Ren, and C. Zhang, *Stable Asymptotically Free Extensions (SAFEs) of the Standard Model*, *JHEP* **03** (2015) 028, [arXiv:1412.5540]. (Cited on page 31.)

[86] H. Gies and L. Zambelli, *Asymptotically free scaling solutions in non-Abelian Higgs models*, *Phys. Rev.* **D92** (2015), no. 2 025016, [arXiv:1502.05907]. (Cited on page 31.)

[87] W. E. Caswell, *Asymptotic Behavior of Nonabelian Gauge Theories to Two Loop Order*, *Phys. Rev. Lett.* **33** (1974) 244. (Cited on page 31.)

[88] T. Banks and A. Zaks, *On the Phase Structure of Vector-Like Gauge Theories with Massless Fermions*, *Nucl. Phys.* **B196** (1982) 189–204. (Cited on page 31.)

[89] C. Wetterich, *Where to look for solving the gauge hierarchy problem?*, *Phys. Lett.* **B718** (2012) 573–576, [arXiv:1112.2910]. (Cited on pages 32 and 102.)

[90] A. Eichhorn, S. Lippoldt, and V. Skrinjar, *Nonminimal hints for asymptotic safety*, *Phys. Rev.* **D97** (2018), no. 2 026002, [arXiv:1710.03005]. (Cited on pages 32 and 102.)

[91] A. Eichhorn and F. Versteegen, *Upper bound on the Abelian gauge coupling from asymptotic safety*, *JHEP* **01** (2018) 030, [arXiv:1709.07252]. (Cited on pages 32 and 102.)

[92] A. Eichhorn and A. Held, *Top mass from asymptotic safety*, *Phys. Lett.* **B777** (2018) 217–221, [arXiv:1707.01107]. (Cited on pages 32 and 102.)

[93] S. A. R. Ellis and J. D. Wells, *Visualizing gauge unification with high-scale thresholds*, arXiv:1502.01362. (Cited on page 35.)

[94] L. J. Hall, *Grand Unification of Effective Gauge Theories*, *Nucl.Phys.* **B178** (1981) 75. (Cited on page 35.)

[95] R. Feger and T. W. Kephart, *LieART—A Mathematica application for Lie algebras and representation theory*, *Comput. Phys. Commun.* **192** (2015) 166–195, [arXiv:1206.6379]. (Cited on page 37.)

[96] Y. Aoki, T. Izubuchi, E. Shintani, and A. Soni, *Improved lattice computation of proton decay matrix elements*, *Phys. Rev.* **D96** (2017), no. 1 014506, [arXiv:1705.01338]. (Cited on page 45.)

[97] R. P. Feynman and M. Gell-Mann, *Theory of the fermi interaction*, *Phys. Rev.* **109** (Jan, 1958) 193–198. (Cited on page 45.)

[98] **Super-Kamiokande** Collaboration, K. Abe et al., *Search for proton decay via $p \to e^+\pi^0$ and $p \to \mu^+\pi^0$ in 0.31 megaton years exposure of the Super-Kamiokande water Cherenkov detector*, *Phys. Rev.* **D95** (2017), no. 1 012004, [arXiv:1610.03597]. (Cited on page 45.)

[99] E. Witten, *Mass Hierarchies in Supersymmetric Theories*, *Phys. Lett.* **105B** (1981) 267. (Cited on page 45.)

[100] A. Masiero, D. V. Nanopoulos, K. Tamvakis, and T. Yanagida, *Naturally Massless Higgs Doublets in Supersymmetric SU(5)*, *Phys. Lett.* **115B** (1982) 380–384. (Cited on page 45.)

[101] D. V. Nanopoulos and K. Tamvakis, *SUSY GUTS: 4 - GUTS: 3*, *Phys. Lett.* **113B** (1982) 151–158. (Cited on page 45.)

[102] S. Dimopoulos and H. Georgi, *Solution of the Gauge Hierarchy Problem*, *Phys. Lett.* **117B** (1982) 287–290. (Cited on page 45.)

[103] B. Grinstein, *A Supersymmetric SU(5) Gauge Theory with No Gauge Hierarchy Problem*, *Nucl. Phys.* **B206** (1982) 387. (Cited on page 45.)

[104] H. Georgi and C. Jarlskog, *A New Lepton - Quark Mass Relation in a Unified Theory*, *Phys. Lett.* **86B** (1979) 297–300. (Cited on page 46.)

[105] I. Dorsner and P. Fileviez Perez, *Unification without supersymmetry: Neutrino mass, proton decay and light leptoquarks*, *Nucl. Phys.* **B723** (2005) 53–76, [hep-ph/0504276]. (Cited on page 46.)

[106] K. S. Babu and S. Khan, *Minimal nonsupersymmetric $SO(10)$ model: Gauge coupling unification, proton decay, and fermion masses*, *Phys. Rev.* **D92** (2015), no. 7 075018, [arXiv:1507.06712]. (Cited on pages 46 and 140.)

[107] H. Fritzsch and P. Minkowski, *Unified Interactions of Leptons and Hadrons*, *Annals Phys.* **93** (1975) 193–266. (Cited on page 46.)

[108] R. Mohapatra, *Neutrino mass and grand unification*, *Phys.Scripta* **T121** (2005) 185–191, [hep-ph/0412050]. (Cited on page 47.)

[109] C. S. Aulakh and S. K. Garg, *MSGUT : From bloom to doom*, *Nucl.Phys.* **B757** (2006) 47–78, [hep-ph/0512224]. (Cited on page 47.)

[110] B. Bajc, I. Dorsner, and M. Nemevsek, *Minimal SO(10) splits supersymmetry*, *JHEP* **0811** (2008) 007, [arXiv:0809.1069]. (Cited on page 47.)

[111] J. C. Pati and A. Salam, *Lepton Number as the Fourth Color*, *Phys.Rev.* **D10** (1974) 275–289. (Cited on page 47.)

[112] F. F. Deppisch, N. Desai, and T. E. Gonzalo, *Compressed and Split Spectra in Minimal SUSY SO(10)*, *Front.in Phys.* **2** (2014) 27, [arXiv:1403.2312]. (Cited on pages 47, 48 and 140.)

[113] G. Altarelli and D. Meloni, *A non supersymmetric SO(10) grand unified model for all the physics below M_{GUT}*, *JHEP* **1308** (2013) 021, [arXiv:1305.1001]. (Cited on page 48.)

[114] B. Bajc, A. Melfo, G. Senjanovic, and F. Vissani, *Yukawa sector in non-supersymmetric renormalizable SO(10)*, *Phys.Rev.* **D73** (2006) 055001, [hep-ph/0510139]. (Cited on page 48.)

[115] R. Peccei and H. R. Quinn, *CP Conservation in the Presence of Instantons*, *Phys.Rev.Lett.* **38** (1977) 1440–1443. (Cited on page 48.)

[116] R. Holman, G. Lazarides, and Q. Shafi, *Axions and the Dark Matter of the Universe*, *Phys.Rev.* **D27** (1983) 995. (Cited on page 48.)

[117] S. Bertolini, L. Di Luzio, and M. Malinsky, *Intermediate mass scales in the non-supersymmetric SO(10) grand unification: A Reappraisal*, *Phys.Rev.* **D80** (2009) 015013, [arXiv:0903.4049]. (Cited on page 49.)

[118] P. Z. Skands et al., *SUSY Les Houches accord: Interfacing SUSY spectrum calculators, decay packages, and event generators*, *JHEP* **07** (2004) 036, [hep-ph/0311123]. (Cited on page 53.)

[119] J. E. Camargo-Molina, B. O'Leary, W. Porod, and F. Staub, **Vevacious***: A Tool For Finding The Global Minima Of One-Loop Effective Potentials With Many Scalars*, *Eur. Phys. J.* **C73** (2013), no. 10 2588, [arXiv:1307.1477]. (Cited on pages 54, 60, 77 and 97.)

[120] P. Bechtle, O. Brein, S. Heinemeyer, O. Stal, T. Stefaniak, G. Weiglein, and K. E. Williams, HiggsBounds – 4*: Improved Tests of Extended Higgs Sectors against Exclusion Bounds from LEP, the Tevatron and the LHC*, *Eur. Phys. J.* **C74** (2014), no. 3 2693, [arXiv:1311.0055]. (Cited on pages 54, 60, 77 and 98.)

[121] P. Bechtle, S. Heinemeyer, O. Stal, T. Stefaniak, and G. Weiglein, *HiggsSignals: Confronting arbitrary Higgs sectors with measurements at the Tevatron and the LHC*, *Eur. Phys. J.* **C74** (2014), no. 2 2711, [arXiv:1305.1933]. (Cited on pages 54, 60, 77 and 98.)

[122] A. Pukhov, *CalcHEP 2.3: MSSM, structure functions, event generation, batchs, and generation of matrix elements for other packages*, hep-ph/0412191. (Cited on page 55.)

[123] **WMAP** Collaboration, G. Hinshaw et al., *Nine-Year Wilkinson Microwave Anisotropy Probe (WMAP) Observations: Cosmological Parameter Results*, *Astrophys. J. Suppl.* **208** (2013) 19, [arXiv:1212.5226]. (Cited on pages 55, 61, 78 and 99.)

[124] **LUX** Collaboration, D. S. Akerib et al., *Results from a search for dark matter in the complete LUX exposure*, *Phys. Rev. Lett.* **118** (2017), no. 2 021303, [arXiv:1608.07648]. (Cited on pages 55, 62, 78 and 99.)

[125] T. Robens and T. Stefaniak, *Status of the Higgs Singlet Extension of the Standard Model after LHC Run 1*, *Eur. Phys. J.* **C75** (2015) 104, [arXiv:1501.02234]. (Cited on pages 58 and 61.)

[126] R. Costa, M. Mühlleitner, M. O. P. Sampaio, and R. Santos, *Singlet Extensions of the Standard Model at LHC Run 2: Benchmarks and Comparison with the NMSSM*, *JHEP* **06** (2016) 034, [arXiv:1512.05355]. (Cited on pages 61 and 77.)

[127] R. Coimbra, M. O. P. Sampaio, and R. Santos, *ScannerS: Constraining the phase diagram of a complex scalar singlet at the LHC*, *Eur. Phys. J.* **C73** (2013) 2428, [arXiv:1301.2599]. (Cited on pages 61, 73, 77 and 83.)

[128] J. M. Butterworth et al., *THE TOOLS AND MONTE CARLO WORKING GROUP Summary Report from the Les Houches 2009 Workshop on TeV Colliders*, in *Physics at TeV colliders. Proceedings, 6th Workshop, dedicated to Thomas Binoth, Les Houches, France, June 8-26, 2009*, 2010. arXiv:1003.1643. (Cited on pages 61 and 77.)

[129] G. Bélanger, F. Boudjema, A. Pukhov, and A. Semenov, *micrOMEGAs4.1: two dark matter candidates*, *Comput. Phys. Commun.* **192** (2015) 322–329, [arXiv:1407.6129]. (Cited on pages 61, 78 and 99.)

[130] R. Costa, A. P. Morais, M. O. P. Sampaio, and R. Santos, *Two-loop stability of a complex singlet extended Standard Model*, *Phys. Rev.* **D92** (2015) 025024, [arXiv:1411.4048]. (Cited on pages 73, 82 and 84.)

[131] M. Muhlleitner, M. O. P. Sampaio, R. Santos, and J. Wittbrodt, *Phenomenological Comparison of Models with Extended Higgs Sectors*, arXiv:1703.07750. (Cited on page 73.)

[132] V. Barger, P. Langacker, M. McCaskey, M. Ramsey-Musolf, and G. Shaughnessy, *Complex Singlet Extension of the Standard Model*, *Phys. Rev.* **D79** (2009) 015018, [arXiv:0811.0393]. (Cited on page 73.)

[133] A. Djouadi, J. Kalinowski, and M. Spira, *HDECAY: A Program for Higgs boson decays in the standard model and its supersymmetric extension*, *Comput. Phys. Commun.* **108** (1998) 56–74, [hep-ph/9704448]. (Cited on page 77.)

[134] S. Dawson and M. Sullivan, *Enhanced di-Higgs boson production in the complex Higgs singlet model*, *Phys. Rev.* **D97** (2018), no. 1 015022, [arXiv:1711.06683]. (Cited on page 78.)

[135] V. Barger, M. McCaskey, and G. Shaughnessy, *Complex Scalar Dark Matter vis-à-vis CoGeNT, DAMA/LIBRA and XENON100*, *Phys. Rev.* **D82** (2010) 035019, [arXiv:1005.3328]. (Cited on page 78.)

[136] J. R. Ellis, A. Ferstl, and K. A. Olive, *Reevaluation of the elastic scattering of supersymmetric dark matter*, *Phys. Lett.* **B481** (2000) 304–314, [hep-ph/0001005]. (Cited on page 79.)

[137] M. J. Baker et al., *The Coannihilation Codex*, *JHEP* **12** (2015) 120, [arXiv:1510.03434]. (Cited on page 83.)

[138] K. Ghorbani and H. Ghorbani, *Scalar split WIMPs in future direct detection experiments*, *Phys. Rev.* **D93** (2016), no. 5 055012, [arXiv:1501.00206]. (Cited on page 83.)

[139] W.-F. Chang, T. Modak, and J. N. Ng, *Signal for a light singlet scalar at the LHC*, arXiv:1711.05722. (Cited on page 84.)

[140] I. P. Ivanov, *Minkowski space structure of the Higgs potential in 2HDM*, *Phys. Rev.* **D75** (2007) 035001, [hep-ph/0609018]. [Erratum: Phys. Rev.D76,039902(2007)]. (Cited on page 94.)

[141] P. Ferreira, H. E. Haber, and E. Santos, *Preserving the validity of the Two-Higgs Doublet Model up to the Planck scale*, *Phys. Rev.* **D92** (2015) 033003, [arXiv:1505.04001]. (Cited on page 94.)

[142] A. Goudelis, B. Herrmann, and O. Stål, *Dark matter in the inert doublet model after the discovery of a Higgs- like boson at the LHC*, *Journal of High Energy Physics* **2013** (Sept., 2013) 106, [arXiv:1303.3010]. (Cited on pages 96 and 98.)

[143] G. C. Branco, P. M. Ferreira, L. Lavoura, M. N. Rebelo, M. Sher, and J. P. Silva, *Theory and phenomenology of two-Higgs-doublet models*, *Phys. Rept.* **516** (2012) 1–102, [arXiv:1106.0034]. (Cited on page 97.)

[144] D. Eriksson, J. Rathsman, and O. Stal, *2HDMC: Two-Higgs-Doublet Model Calculator Physics and Manual*, *Comput. Phys. Commun.* **181** (2010) 189–205, [arXiv:0902.0851]. (Cited on page 98.)

[145] M. Gustafsson, E. Lundstrom, L. Bergstrom, and J. Edsjo, *Significant Gamma Lines from Inert Higgs Dark Matter*, *Phys. Rev. Lett.* **99** (2007) 041301, [astro-ph/0703512]. (Cited on page 98.)

[146] Q.-H. Cao, E. Ma, and G. Rajasekaran, *Observing the Dark Scalar Doublet and its Impact on the Standard-Model Higgs Boson at Colliders*, *Phys. Rev.* **D76** (2007) 095011, [arXiv:0708.2939]. (Cited on page 98.)

[147] E. Lundstrom, M. Gustafsson, and J. Edsjo, *The Inert Doublet Model and LEP II Limits*, *Phys. Rev.* **D79** (2009) 035013, [arXiv:0810.3924]. (Cited on page 98.)

[148] F. Mahmoudi, *SuperIso: A Program for calculating the isospin asymmetry of B —> K* gamma in the MSSM*, *Comput. Phys. Commun.* **178** (2008) 745–754, [arXiv:0710.2067]. (Cited on page 99.)

[149] F. Mahmoudi, *SuperIso v2.3: A Program for calculating flavor physics observables in Supersymmetry*, *Comput. Phys. Commun.* **180** (2009) 1579–1613, [arXiv:0808.3144]. (Cited on page 99.)

[150] F. Mahmoudi, *SuperIso v3.0, flavor physics observables calculations: Extension to NMSSM*, *Comput. Phys. Commun.* **180** (2009) 1718–1719. (Cited on page 99.)

[151] H. F. B. Nielsen, D. L. Bennett, C. R. Das, C. D. Froggatt, and L. V. Laperashvili, *F(750), We Miss You as a Bound State of 6 Top and 6 Antitop Quarks, Multiple Point Principle*, *PoS* **CORFU2016** (2017) 050, [arXiv:1705.10749]. (Cited on page 100.)